A Fundamental Model Methodology

For the Analysis, Design and Fabrication of

A Narrow Transparency Window in a Bulk Meta-Material

by

Shahriar Alam

A Dissertation Presented in Partial Fulfillment
of the Requirements for the Degree
Doctor of Philosophy

Approved October 2017 by the
Graduate Supervisory Committee:

Rodolfo Diaz, Chair
Stephen Krause
Fernando Ponce

ARIZONA STATE UNIVERSITY

December 2017

ABSTRACT

The optical valley of water, where water is transparent only in the visible range, is a fascinating phenomenon and cannot be modeled by conventional dielectric material modeling. While dielectric properties of materials can be modeled as a sum of Lorentz or Debye simple harmonic oscillators, water is the exception. In 1992 Diaz and Alexopoulos published a causal and passive circuit model that predicted the window of water by adding a "zero shunt" circuit in parallel with every Debye and Lorentz circuit branch. Other than the Diaz model, extensive literature survey yielded no *universal* dielectric material model that included water or offered an explanation for this window phenomenon. A hybrid phenomenological model of water, proposed by Shubitidze and Osterberg, was the only model other than the Diaz-Alexopoulos model that tried to predict and match the optical valley of water. However, we show that when we apply the requirement that the permittivity function must be a complex analytic function, it fails our test of *causality* and the model terms lack physical meaning, exhibiting various mathematical and physical contradictions. Left with only the Diaz proposed fundamental model as the only casual model, this dissertation explores its physical implications. Specifically, the theoretical prescription of Kyriazidou et al for creating artificial dielectric materials with a narrow band transparency is experimentally demonstrated for the first time at radiofrequencies. It is proposed that the most general component of the model of the frequency dependent permittivity of materials is not the simple harmonic oscillator but rather the harmonic oscillator augmented by the presence of a zero shunt circuit. The experimental demonstration illustrates the synthesis and design of a new generation of window materials based on that model. Physically realizable Lorentz coatings and RF Debye "molecules" for creating the desired windows material are

designed using the full physics computational electromagnetic code. The prescribed material is then implemented in printed circuit board technology combined with composite manufacturing to successfully fabricate a lab demonstrator that exhibits a narrow RF window at a preselected frequency of interest. Demonstrator test data shows good agreement with HFSS predictions.

DEDICATION

In memory of my grandfather, Muhammad Hussein, who taught me that serenity and joy come from clear intention, persistent industry and a zest for living,

For my father Dr. Muhammad Shamsul Alam, my first teacher, Renaissance man, and consummate engineer, whose standards of excellence I still strive to emulate

For my amazing daughter, Dr. Urusa Shahriar Alaan, the love of my life, who has been on this journey with me, completing her own PhD in Material Science and Engineering two months before her mother

For my family and extended family – I have learned something from each and everyone

And for the truth seekers who strive to open windows into the mysteries of the Universe…

ACKNOWLEDGMENTS

I am eternally grateful to Dr. Rodolfo Diaz, my amazing advisor, mentor, manager and director for this opportunity to carry out his vision. His genius and generosity, guidance and grace have been so humbling, that in his presence, I think I can hear the angels sing. *None of this would be possible without him.*

I am so very thankful to Dr. Stephan Krause for inspiring me in my first Material Science course, and helping me enroll into the Material Science and Engineering master's program.

I am indebted to Dr. Fernando Ponce for teaching me materials physics and his incredible patience and humility in answering all my questions without ever making me feel foolish.

Thanks to my colleagues, Ryan Wilhelm, for his help with MathCAD and being a great resource, and Ray Sundar and Brandon Dowd for their help with MATLAB.

I am totally indebted to Dr. Mahkamehossodat Mostafavi for teaching me HFSS from ground zero and supporting me in any way she could; often acting like our post doc.

I want to thank Dr. Rodolfo Diaz and Jeff Peebles for testing my demonstrator article.

Also thanks to Rogers Corporation for supplying the Duroid materials, Amy Boyd at the Diab Corporation for supplying foam, and Southwest Exhibits for machining materials.

Thanks to Dr. James Aberle and Dr. James Adams for our discussions. I am indebted to James Eason at Sunstone for his sense of urgency and attention to detail that made the board a success and Screaming Circuits for their assembly expertise.

Finally I am blessed by the encouragement and support of my father, my daughter, and my dear friends, Caroline Boles, Marina Cleary, Marcy Diaz and Michael Miller.

TABLE OF CONTENTS

Page

CHAPTER Page

CHAPTER Page

APPENDIX Page

LIST OF TABLES

LIST OF FIGURES

Figure Page

Figure Page

CHAPTER 1

INTRODUCTION

It is generally agreed that all dielectric materials can be modeled as a sum of Lorentz (simple harmonic oscillators) or Debye (over-damped harmonic oscillators) terms. The only exception is water. Such traditional methods of modeling permittivity, cannot predict the extreme transparency of the optical valley of water, at a frequency of $10^{14.73}$ hertz, where, water is transmissive, and exhibits nearly no loss. Although water behaves like a Debye material at low frequencies Hasted (Hasted 1973) claims that to correctly model the high frequency properties, this Debye term must be expressed as a Lorentz term bringing it in line with the infrared absorption lines. However, making this change does not fix the problem. It is easy to show that the out of band behavior of all the harmonic oscillator Lorentz terms would combine to add so much loss that the optical valley should be obscured (Diaz 1992). After a discussion of the unique properties of the water substance in chapter 2, these conventional methods for modeling dielectric materials are reviewed in chapter 3.

The only dielectric model of water, that predicts the optical valley, using causal and passive circuit elements, was published in 1992, by Diaz and Alexopoulos. Diaz adds a "zero shunt" circuit in parallel with every Lorentz and Debye circuit branch which cancels the Lorentz and Debye tails (the out of band behavior) in the band of interest, while maintaining causality and preserving passive individual circuit elements.

If the "zero shunt" circuit elements are not used, this generalized model of permittivity, we call the Fundamental model, simplifies to material models that do not exhibit windows. In other words, the Lorentz model is a special case of the generalized Fundamental model when there is no window, just like the Debye model is a special case of the Lorentz model when there is excess damping. The Diaz-Alexopoulos work is discussed in chapter 4.

A thorough literature search outlined in chapter 5, determined there are many models of water available, especially in the infrared, and the ultra-violet regimes; but everyone avoids explaining or predicting the optical valley. Only one alternative hypothesis offered by Shubitidze and Osterberg, claimed improvement over the Diaz-Alexopoulos model. However, exhaustive analysis proves, in addition to many mathematical contradictions, and physical anomalies the model is not causal, and therefore cannot be universally applied to any material. Rigorous causality analysis of this work by Shubitidze and Osterberg is offered in chapter 6.

As such the only *causal* model of water that predicts the optical valley, the Fundamental electric circuit model proposed by Diaz- Alexopoulos, is explored to understand the material wave interactions that create this window phenomenon. Based on this work and the work of Kyriazidou, Diaz, and Alexopoulos, which offers a theoretical approach to creating artificial dielectric materials (made of resonant Lorentz coated particles) exhibiting a pair of narrow-band transparencies, we develop an understanding of the physics of a material window in chapter 7.

Due to the absence of natural dielectric Lorentz materials at radio frequencies (RF), our frequency band of interest for a laboratory demonstrator, a "Lorentz coating" must be manufactured by implementing microscopic antenna elements or other frequency selective (FS) microstructures. We propose that a composite material that consists of an array of material structures (antennas) tightly coupled to this "Lorentz coating" can artificially emulate the key elements that create the optical valley in water. This is shown in chapter 8. Optimal material designs with the desired properties and behavior are down-selected to construct a candidate material with a transparent window based on ANSOFT (ANSYS) HFSS simulations in chapter 9. This artificial window material fabricated using Printed Circuit Board techniques, is tested, and validated against HFSS predictions in chapter 10. Chapter 11 discusses our conclusions based on the demonstrator analysis and results and recaps the work done; chapter 12 compares our meta-material with Rasorbers. Chapter 13 recommends future work.

This dissertation offers analysis, design, synthesis and method of making of an artificial bulk meta-material, where the material is transparent in the tuned RF frequency band of interest but opaque or reflective outside this band just like water.

CHAPTER 2

MOTIVATION

Water is ubiquitous. It makes up more than two thirds of the earth and our bodies. The unique properties of water are not only unusual; but have significant consequences and benefits to life on earth. There is a lot we can learn from understanding the material properties of water. If we truly understand these properties and can imitate them or engineer them into an artificial material all sorts of useful devices could result.

2.1 BACKGROUND: Why Study the Dielectric Properties of Water?

Water exhibits many unique properties. We elucidate a few examples from Figure 2-1 below.

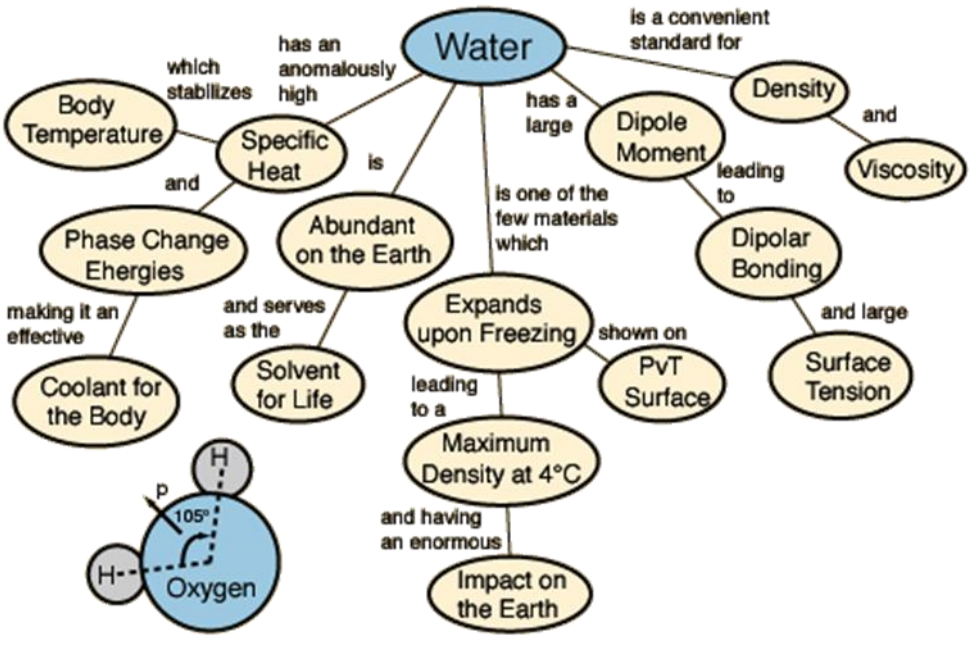

Figure 2-1. The Unique Properties of Water (Hyperphysics n.d.).

The boiling points of hydrides typically decrease with decreasing molecular size. Water has unusually high boiling and freezing points for a small molecule of its size. Water's extremely high heat of vaporization is primarily due to the difficulty in breaking the hydrogen bonds, and gaining kinetic energy, makes it an endothermic reaction (Corinne Yee (UCD) 2015). Water also has a very high heat of fusion, and requires a lot of energy before it changes temperature or states. Water's high heat capacity, coupled with its moderate pH buffering capabilities, ensures our lakes and oceans remain resistant to drastic changes in the environment, especially protecting aquatic life (Biology n.d.).

Again, due to its hydrogen bonding, water has very strong intermolecular forces which give rise to its high viscosity – much higher viscosity compared to other substances of similar structure. Greater intermolecular forces correlate inversely to vapor pressure – water exhibits much lower vapor pressure than larger molecules (Corinne Yee (UCD) 2015).
It is also very rare for inorganic materials to be a liquid at room temperature – water is an exception and therefore can move more freely and pack more closely. Other than mercury, water has the highest surface tension of any known liquid, which allows good cohesion to itself, enabling objects to float on water (Biology n.d.).

The water molecule is a strong dipole, and its polarity enables it to be the universal solvent and carrier of most nutrients and chemicals, required for plant and organism growth and sustenance. Frozen water is less dense than liquid water and has 9% greater volume due to the formation of hexagonal crystalline structures where the hydrogen bonds are held

farther apart (Biology n.d.). Water's expansion in the solid state, allows ice to float, enabling the flora and fauna below frozen lakes and rivers to survive and thrive, making life possible (Corinne Yee (UCD) 2015). One of most important unique properties of water is its behavior at optical frequencies.

2.1.1 The Optical Valley of Water

Unlike any other material known at this time, water has a sharp, narrow, window where it is transparent in the visible spectrum (390 - 700 nm), while being strongly absorbing and opaque in the rest of the wavelengths in the electromagnetic spectrum, including the adjacent infrared and ultraviolet regimes. Coincidentally, the optical valley of water corresponds to the range of frequencies where the rods and cones in our retinas can detect light and of course also to the region in the spectrum of peak emitted intensity by a black body radiator at 6000K (equivalent to the output radiation of our sun.) This enables penetration of the sun's energy through the water vapor in our atmosphere enabling life in the oceans and the earth. Yet the absorption in the UV range increases by nine orders of magnitude in water, providing protection from harmful UV rays as shown in Figure 2-2. (Physics n.d.)

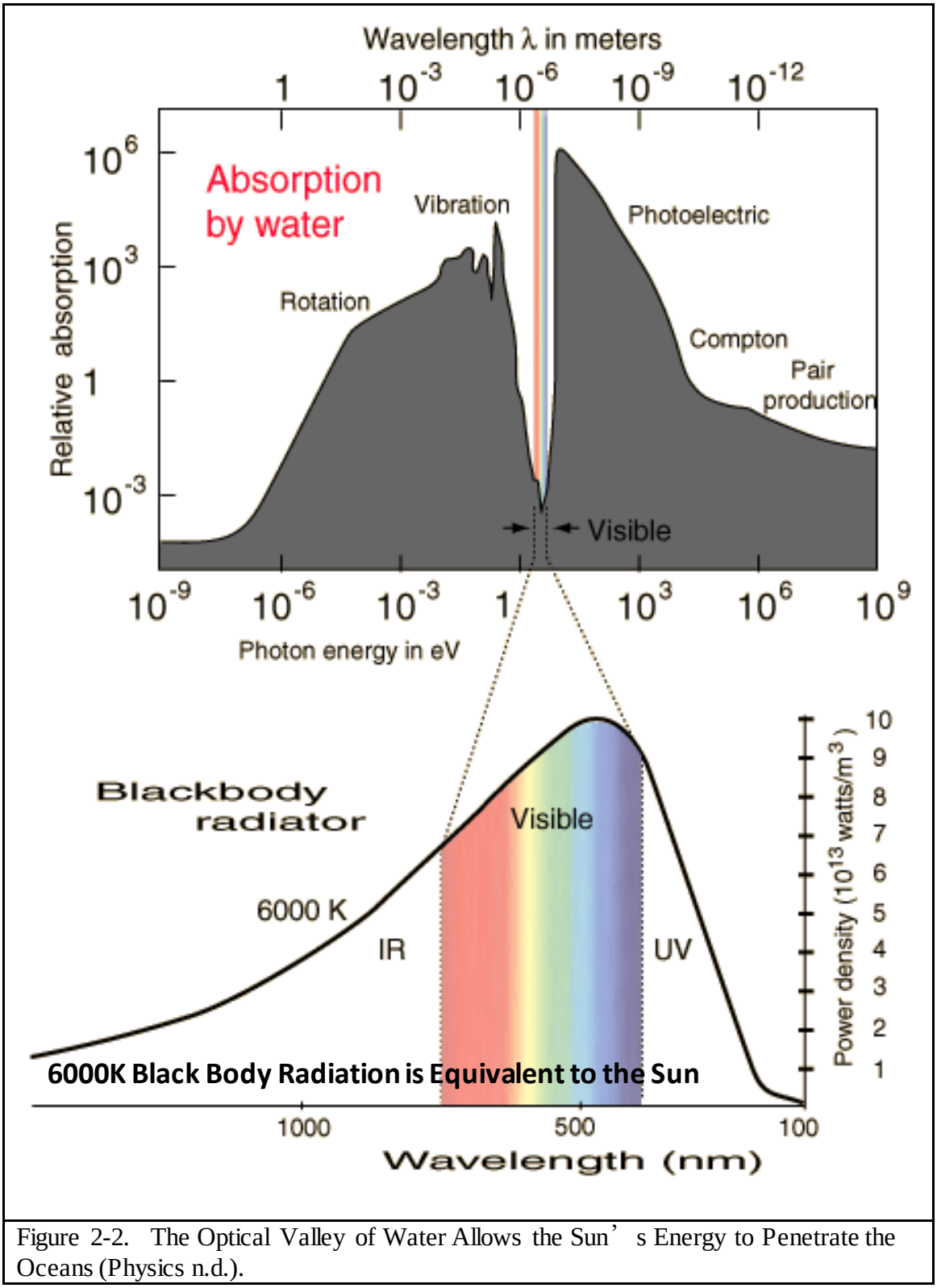

Figure 2-2. The Optical Valley of Water Allows the Sun's Energy to Penetrate the Oceans (Physics n.d.).

2.1.2 The Material Science Consequences of the Optical Valley of Water

The optical valley of water is also an interesting problem from a material science and engineering perspective because conventional material modeling methods for permittivity cannot predict the optical valley of water. Frequency dependent dielectric properties of materials are usually modeled as a sum of Lorentz and/or Debye terms, simple harmonic oscillators. These models, described in chapter 3, are often represented physically using the classical spring, mass, and dashpot model or the electric circuit model as a parallel sum of series LRC (inductor, resistor, capacitor) circuit branches. Both the mechanical and electrical models are analogous to a sum of simple harmonic oscillators. Although most materials can be modeled in this way, the exception is water. Traditional harmonic oscillators used to model any material, cannot predict the sharp optical valley of water, where the imaginary permittivity drops eight orders of magnitude at a frequency of $10^{14.73}$ hertz, where water exhibits no loss.

Water behaves like a Debye material at low frequencies; but at high frequencies, water, like other materials in the infrared range, appears Lorentz like. But this model has to be incomplete because the tails (out of band behavior) of the Debye and Lorentz harmonic oscillators would additively obscure the optical valley. Therefore the full spectrum permittivity of water cannot be exclusively modeled as a sum of Lorentz and Debye oscillators. This suggests that there must be a more complete, or generalized, model of the permittivity function that also includes water. As described in Chapter 4, this model must be analytic

to ensure *causality* and therefore ensure that the model then can be universally applied to all materials.

As discussed in Chapter 4 a modified harmonic oscillator, modeled as an electric circuit by Diaz and Alexopoulos is able to explain the optical valley of water. Diaz and Alexopoulos require their electric circuit model to be causal and passive. Causality means there is no violation of time reversal, i.e., the effect follows the cause, and passivity means that the laws of thermodynamics are obeyed, conservation of energy. The sum total of the material model has to be causal and passive because natural materials are causal and passive. Beyond requiring the *total* model to be causal, they also require the *individual* circuit elements to be causal and passive. Since causality is inherent in all passive circuit models, this additional condition of passivity for all circuit elements ensure we obey the laws of thermodynamics in the micro-scale as well as the macro-scale. This makes their model completely physically realizable and therefore meaningful in the realm of the universe we live in.

Although it is mathematically conceivable to create a model that in the sum total appears passive and causal and yet uses individual components that are not, such a model would raise questions about the meaningfulness of the assumed components. Furthermore, if any of the assumed components are unphysical then there would be no way to construct in the laboratory as an equivalent model system to study.

From this basis of understanding, we use causality and passivity as our litmus test for analyzing all future dielectric models and their components, because only such a model could be applied to all materials and only such a model could be manufactured in the real world, which is ultimately the objective of this dissertation.

2.2 Objective

Since water exists, it demands we ask the question whether there is a more generalized universal model of material permittivity than the current models, which although explaining most materials, fail to include water. Because water physically exists, and the transmissive property data is irrefutable in the visible range, the conventional dielectric models of materials cannot be universal or complete. The objective of this dissertation is to understand how this window occurs in nature, so a universal model can be developed, analyzed and demonstrated to be the superset that includes the complex permittivity of water. The second objective is to use this understanding to design an artificial bulk material (effective medium: unit cell size is much less than the wavelength) that exhibits this same behavior, in a frequency band of our choice, independent of angle of incidence. Mimicking nature we can develop a new generation of novel synthetic materials that have custom windows that are tunable at a frequency band of interest, that have neither been discovered nor abundant in nature.

2.3 Applications of Narrow Windows in Bulk Materials

By understanding and manipulating this generalized permittivity model that explains the window in water, where a precipitous drop in the imaginary permittivity can exist in a frequency range while high absorption occurs in the adjacent frequencies, we can create artificial materials with a narrow band window where we choose which frequencies can pass through and which do not. Essentially these would be materials with intrinsic engineered filter properties. There are many applications that could benefit from materials that block or absorb a wide range of frequencies, while allowing a selective frequency band through. More possibilities will grow over time as we innovate new ways to exploit these narrow window materials. The few concepts mentioned below are based on creating a material that is lossy - absorbing at all bands except a narrow transparency window.

For instance, a bulk material with such a window could be used as a radome, transmitting and receiving in the frequency range of interest but blocking all other frequencies. Since (as will be shown in chapter 8) the window frequency is closely related to the resonant frequency of the Lorentz coating around the elements in an artificial dielectric medium and since these elements can vary in shape and size and can have different Lorentz coatings with different, resonant frequencies, there could be more than one transmissive window designed into the system. This way windows with separate functions could be created, where incoming and outgoing signal wavelengths may be different. The key feature is that narrow operating windows give the designer a new tool with which to reduce interference and cross talk between antennas.

This concept is not limited to application in radomes but could be applied to any type of enclosure that could use a narrow window at the wireless communication frequency of interest like a cell phone to block interference from any other frequency source.

What is done with the out of band energy depends on the design: the radiation could be absorbed by making the bulk material lossy or reflected if it is a highly conductive material depending on the functionality intentionally designed into the system.

Unlike a two dimensional frequency selective surfaces used in present day radomes and multi-chroic scatterers, this frequency selective resonant bulk material is three dimensional and has more degrees of functionality that can be used to guide or scatter waves. We will discuss this in chapter 12.

In addition, other frequency selective microwave devices could be constructed with this material including antennas, frequency converters, and very narrowband filters and couplers. (Diaz, Frequency Selective Microwave Devices Using Narrowband Metal Materials 2002)

CHAPTER 3

MODELING THE COMPLEX DIELECTRIC PROPERTIES OF MATERIALS

All realistic materials are dispersive, that is, their constitutive properties vary with frequency and represent both energy storage and energy dissipation phenomena.

In chapter two, in the motivation, we defined the optical valley of water, where there is an eight order of magnitude drop in the imaginary part of the refractive index at $10^{14.73}$hertz. Since the complex refractive index is the square root of the complex permittivity of a material, this means the imaginary permittivity has no loss in the optical valley, making water completely transparent in this regime.

$n^* = \sqrt{\varepsilon^*}$, where n^* is the complex refractive index and $\varepsilon^*$is the complex permittivity

$n^2 - k^2 = \varepsilon_R$, the real part of the complex permittivity and n is the real part of and k is the imaginary part of the index of refraction

2nk= ε_I the imaginary part of the complex permittivity (ocw.mit.edu/courses n.d.)

In order to grasp this uniqueness of water and why this optical valley is so difficult to explain, we must understand the permittivity function and how the dielectric properties of a material are modeled. How does the interaction of waves with molecular charges give us the index of refraction or the permittivity function?

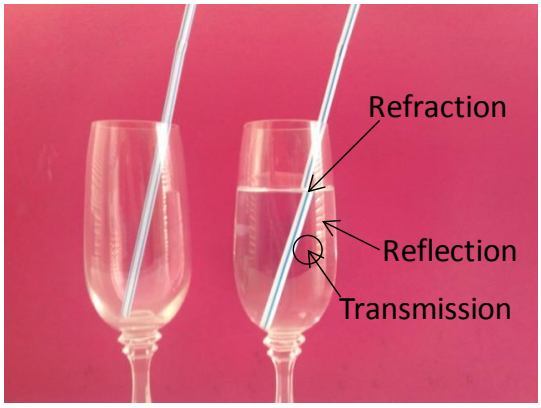

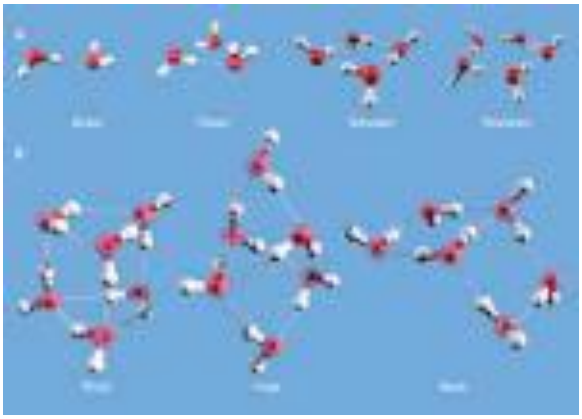

Figure 3-1. Wave Molecular Interactions Give Rise to Permittivity

https://www.youtube.com/watch?feature=player_detailpage&v=XbPmqnnr0jU

Thermodynamically speaking, some level of dielectric loss is present in all materials and therefore dispersion and absorption are inherent to all dielectric materials. Consequently permittivity has to be frequency dependent and consistently coexist with all other material properties (Kao 2004). When an electromagnetic wave propagates through a material, it undergoes a variety of interactions during transmission. These include reflection, refraction, and attenuation. In general these interactions are frequency dependent, in other words, the dielectric function, permittivity, ε, is dispersive in a material.

For a linear, homogeneous, isotropic materials, the electric field **E**, (V/m), reorganizes the electric charges and dipoles to produce a net displacement field **D**, (C/m^2) where $\mathbf{D} = \varepsilon\mathbf{E}$ by definition. For an anisotropic material ε, is a second order tensor, and, for non-linear

systems, the permittivity may depend on the strength of the electric field. The permittivity ε, (F/m), is related to the unitless susceptibility which is the ability of an **E**-field to polarize a dielectric material.

Where

$$\varepsilon = \varepsilon_r \varepsilon_0 = (1 + \chi)\varepsilon_0$$

$$\varepsilon_0 = the\ permittivity\ of\ free\ space\ = 8.855x10^{-12}\frac{F}{m}$$

$$\epsilon_r = the\ relative\ permittivity\ \varepsilon/\varepsilon_0$$

(Permittivity n.d.)

And the polarization of the material is defined by

$$\boldsymbol{P} = \varepsilon_0 \chi \boldsymbol{E}$$

$$\boldsymbol{P} = the\ polarization\ density$$

$$\boldsymbol{E} = the\ external\ electric\ field.$$

The permittivity of the material is the susceptibility of the material plus the background of the material, the environment it is in (in most cases free space).

The electric displacement field, **D**, can also be written using the polarization density and the susceptibility.

$$\boldsymbol{D} = \varepsilon \boldsymbol{E} = \boldsymbol{\varepsilon_0}(\chi + 1)\boldsymbol{E}$$

$$= \boldsymbol{\varepsilon_0 E}\chi + \varepsilon_0 \boldsymbol{E}$$

$$= \boldsymbol{P} + \boldsymbol{\varepsilon_0 E}$$

(Griffith 2007)

Because there is a response time associated with the application of a field, the time dependent general form of the electrical displacement according to J. S. Toll is given by

$$\boldsymbol{D}(t) = \boldsymbol{E}(t) + (2\pi)^{-1/2} \int_{-\infty}^{+\infty} \boldsymbol{T}(t\text{-}t')\boldsymbol{E}(t')dt'$$

Where **T (t)**, the second term, is the response to a Dirac delta function at t=0. Taking a Fourier transform, according to the laws of the convolution theorem, in the frequency domain, the integral becomes a simple product where

$$\boldsymbol{D}(\omega) = \varepsilon(\omega)\boldsymbol{E}(\omega) = \varepsilon_0\boldsymbol{E}(\omega) + \varepsilon_0(\varepsilon_r(\omega) - 1)\boldsymbol{E}(\omega)$$

$$\boldsymbol{D}(\omega) = \varepsilon(\omega)\boldsymbol{E}(\omega) = \varepsilon_0\boldsymbol{E}(\omega) + \varepsilon_0\chi(\omega))\boldsymbol{E}(\omega)$$

$$\boldsymbol{D}(\omega) = \boldsymbol{E}(\omega) + \boldsymbol{P}(\omega)$$

And the $\mathbf{E}(\omega)$, and $\mathbf{P}(\omega)$ are the frequency dependent electric field and polarization respectively, which in turn defines the frequency dependent complex permittivity function.

Thus the complex permittivity is defined as

$$\varepsilon(\omega) = 1 + \int_0^{\infty} T(\tau)e^{i\omega\tau}\,d\tau$$

$$\varepsilon^*(\omega) = \varepsilon'(\omega) + i\varepsilon''(\omega)$$

(Toll 1956)

(This last result is written in what is called the Physics convention. In Electrical Engineering the convention is to write

$$\varepsilon^*(\omega) = \varepsilon'(\omega) - j\varepsilon''(\omega)$$

because time harmonic solutions are written in terms of $e^{+j\omega t}$ and passivity is guaranteed by $\varepsilon'' > 0$.)

Now that we know what gives rise to the complex frequency dependent permittivity function, we need to understand how the dielectric function is modeled. Our way of understanding how material behaves can be facilitated by creating mechanistic or electrical models that physically illustrate the microscopic or macroscopic phenomena of interest. From a historical perspective, in the whole discussion of materials, the permittivity function is considered a Debye or a Lorentz material, which have been classically modeled as a sum of simple harmonic oscillators.

What is a Simple Harmonic Oscillator?

The mathematics of a simple harmonic oscillator is used as a mechanistic model to describe many different types of physical phenomena. These include but are not limited to the oscillation of a spring with a mass, a pendulum, the classical spring/mass and dashpot, and even vibrations in molecules. This motion can be described as a sinusoidal displacement in time. The period contains an oscillatory displacement from an equilibrium position to a restored position that is directly opposite to that displacement. Since this motion is repeated in a regular time interval it is called simple harmonic motion (Wikipedia n.d.).

The classical permittivity function can be understood from at least three different viewpoints outlined below.

3.1 Classical Models of the Dielectric Function

The most fundamental physical model of the dielectric function is the mechanical Mass on a Spring with Dashpot Model.

The Mass on a Spring with a Dashpot (friction) is a physical model, based on a mechanis-

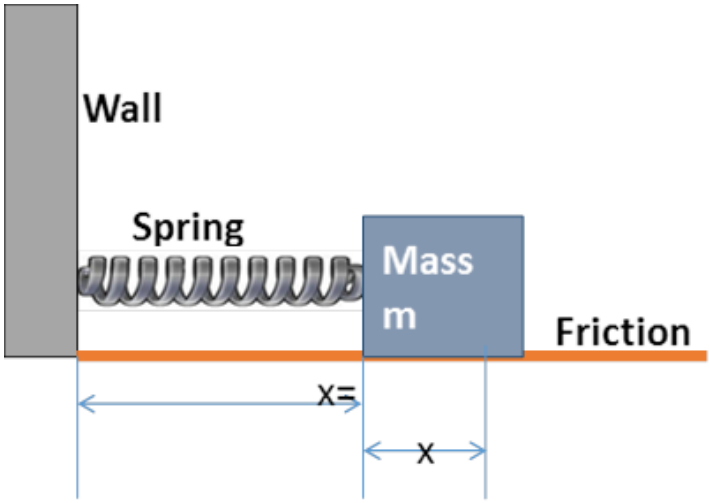

Figure 3-2. Spring Mass Dashpot.

tic picture of a simple harmonic oscillator.

In order to demonstrate the simple harmonic oscillator we consider a mass connected to a fixed wall with a spring, where the displacement x = 0 at the equilibrium position at time t = 0, and x (t) will be the displacement from this position at any time t.

According to Newton's second law **F**=ma, the acceleration of an object due to an applied force is in the direction of the force and inversely proportional to the mass of the object. In one dimension the acceleration force takes the following form.

$$\boldsymbol{F_{net}} = m\ddot{x}$$

The restorative force in the opposite direction is proportional to k, the spring constant per Hooke's law is given by

$$\boldsymbol{F_H} = -kx$$

And the friction force, which is assumed to be proportional to the velocity of the mass that opposes the motion is given by

$$\boldsymbol{F_F} = -c\dot{x}$$

If we do a force balance, and assume there are no other forces acting on the system we obtain

$$\sum \mathbf{F_{net}} = \mathbf{F_H} + \mathbf{F_F}$$

$$m\ddot{x}(t) + c\dot{x}(t) + kx(t) = 0$$

This is known as a simple harmonic oscillator or the classical Spring-Mass-Dashpot. The general solution to this second order differential equation is

$$x(t) = Acos(\omega_0 t) + Bsin(\omega_0 t) = Ae^{-i\omega_0 t}$$

where

$$\omega_0 = \sqrt{\frac{k}{m}} = \sqrt{\frac{elasticity}{inertia}}$$

All physical systems subject to forces, acceleration and friction can be cast in the form of these equations.

3.1.1 Classical Theory of Dielectric Materials: The Lorentz or Simple Harmonic Oscillator

Materials

The physical model of the kinematics of the dynamics of a simple harmonic oscillator can effectively describe the Lorentz and (when over-damped) Debye models of permittivity.

The Lorentz Model

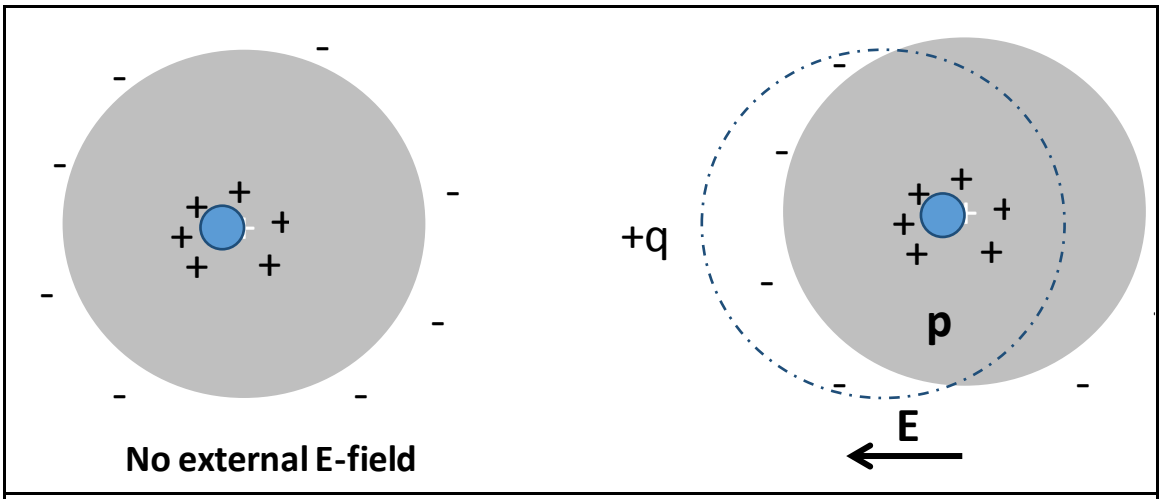

Figure 3-3. Small Amount of Charge Moved by E-Field.

The Lorentz model is shown in Figure 3-3.

Before the age of quantum mechanics, Hendrik Lorentz described those atom field interactions in terms of classical mechanics and electro-magnetic theory. Lorentz formulated that the electrons are quasi-elastically bound to their nuclei, very much like a mass is attached to a spring in our simple harmonic oscillator example. The presence of an electric field would cause the positively charged nucleus and negatively charged electron cloud to be displaced relative to each other. He postulated the force binding the atom and electron could also be described by Hooke's law, $F(x) = -kx$ like the spring example (Hummel 2011, 238). Under the influence of an oscillating field of an electromagnetic wave, the electron will be forced to vibrate. These electron vibrations can be described by the same mathematics of the simple harmonic oscillators discussed before.

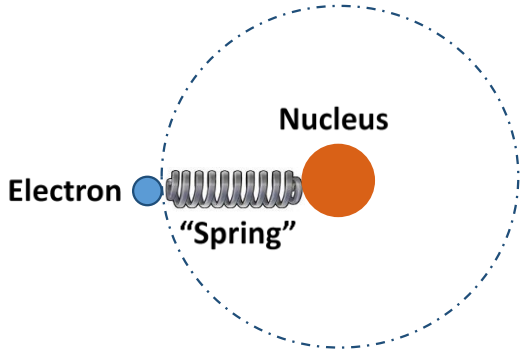

Figure 3-4. The Lorentz Model.

Performing a force balance we change the simple harmonic oscillator mass to the mass of the electron obeying Newton's second law, the restoring force of the spring is now binding the electron to the nucleus, obeying Hooke's law, we add the driving force of the electric field **E** and subtract the frictional force we will now call damping (OpenCourseWare 2011).

$$m\ddot{x}(t) = kx(t) + q\boldsymbol{E_x} - c\dot{x}(t)$$

$$m = electron\ mass$$

$$kx(t) = restoring\ force\ binding\ electron\ and\ nucleus, where$$

$$k = m\omega_0^2$$

$$q\boldsymbol{E_x} = \boldsymbol{E} = eE_0e^{-i\omega t/m} = E - field\ force$$

$$c\dot{x}(t) = the\ damping\ force\ due\ to\ electron$$

$$-electron\ and\ \ electron - lattice\ collisions\ and$$

$$c{=}m\gamma\ where\ \gamma\ is\ the\ damping\ factor\ and\ m\gamma\ is\ the\ damping\ coefficient$$

(Often this equation is divided by mass and we are left with γ)

Since the magnetic field is much less than the electric field it is therefore neglected.

How does the complex frequency dependent permittivity function arise from the mathematics of the simple harmonic oscillator? Given the classical model that electrons bound to their nuclei, under the influence of an applied electric field, will oscillate about their equilibrium position in the manner described by the second order differential equation above it is immediately derived. Using the general solution for the simple harmonic oscillator, we assume,

$$x(t) = Ae^{-i\omega_0 t}$$

Substituting this into the differential equation, we obtain

$$A = \frac{eE_0}{m} \frac{1}{\omega_0^2 \quad - \omega^2 \quad - i\gamma\omega}$$

And

$$x(t) = \frac{eE_0}{m} \frac{e^{-i\omega_0 t}}{\omega_0^2 \quad - \omega^2 \quad - i\gamma\omega}$$

Remembering that e_x is the polarization of one oscillator, we calculate the total polarization per unit volume as

$$\mathbf{P} = N_0 ex(t) = \frac{N_0\, e^2 E_0}{m} \frac{e^{-i\omega_0 t}}{\omega_0^2 \quad -\omega^2 \quad -i\gamma\omega} = \frac{\omega_p^2}{\omega_0^2 - \omega^2 \quad -i\gamma\omega}$$

Where

$$\omega_p^2 = \frac{N_0 e^2}{m\varepsilon_0}$$

As defined before, the polarization is $\boldsymbol{P} = \varepsilon_0 \chi \boldsymbol{E}$, so solving for χ, we obtain

$$\chi = \frac{\omega_p^2}{\omega_0^2 \quad - \omega^2 \quad - i\gamma\omega}$$

And

$$\varepsilon_r = 1 + \chi = 1 + \frac{\omega_p^2}{\omega_0^2 - \omega^2 - i\gamma\omega} = \varepsilon_r' + j\varepsilon_r''$$

The real and imaginary Lorentz permittivity can be separated as $\varepsilon_R = \varepsilon_r'$ and $\varepsilon_I = \varepsilon''_r$ respectively.

$$\varepsilon_R = 1 + \frac{\omega_p^2(\omega_0^2 - \omega^2)}{(\omega_0^2 - \omega^2)^2 - \gamma^2\omega^2}$$

$$\varepsilon_I = 1 + \frac{\omega_p^2\gamma\omega}{(\omega_0^2 - \omega^2)^2 - \gamma^2\omega^2}$$

We stated before that most materials can be modeled as a sum of simple harmonic oscillators where classically speaking ω_0 is the resonant frequency of the simple harmonic oscillator. For the sum of many oscillators we write the permittivity as

$$\varepsilon_r = 1 + \sum_j \frac{\omega_{pj}^2}{\omega_{0j}^2 - \omega^2 - i\gamma_j\omega}$$

Quantum mechanically speaking the ω_0 is the energy difference between the final and initial states (OpenCourseWare 2011).

3.1.2 Classical Theory of Dielectric Materials: The Drüde Permittivity Model

The Drüde model is important for the understanding of the optical properties of noble metals and plasmas. Electrons are considered free for metals so there is no "spring" attaching electrons to the nucleus. So if we remove the spring, the spring constant k becomes zero and therefore

$\omega_0 = \sqrt{\frac{k}{m}} = \sqrt{\frac{elasticity}{inertia}} = 0$, the permittivity equation becomes

$$\varepsilon_r = 1 - \frac{\omega_p^2}{\omega^2 - i\gamma\omega}$$

Then the real and imaginary parts are

$$\varepsilon_R = 1 + \frac{\omega_p^2}{\omega^2 + \gamma^2}$$

$$\varepsilon_I = 1 + \frac{\omega_p^2 \gamma}{\omega(\omega^2 + \gamma^2)}$$

Generally $\omega_p > \gamma$. So if $\omega >> \omega_p$, then $\varepsilon_I > 0$, and this means there is no absorption and at these frequencies, the metal becomes transparent. A Lorentz material, in its sharp conductive band can be very highly conductive and behave like a metal. (OpenCourseWare 2011).

3.1.3 Classical Theory of Dielectric Materials: The Debye Permittivity Model

Although a Debye model is equivalent to an over-damped Lorentz model, the original Debye model dealt with the properties of fluids consisting of permanently polarized molecules. Unlike dipoles induced by an electric field, described for the Lorentz type materials, Debye materials already possess permanent dipoles that are randomly oriented as in water molecules. Under the presence of an electromagnetic field, these dipoles will align with the field. But when the field is turned off there is no restoring force (i.e. "spring") to return the dipoles to their equilibrium position. The only available restoring force is random thermal motion which will not align the dipole in any specific orientation. This random orientation is called the Debye relaxation. The process is described as

$$P_d(t) = P_d(0)e^{-t/\tau}$$

Where $\tau =$ the relaxation time constant

For spheres of radius d, in a fluid of viscosity, μ, the relaxation time is

$$\tau = \frac{\pi \mu d^3}{2\kappa_B T}$$

The resulting frequency domain expression for the Debye permittivity is

$$\varepsilon^* = 1 + \chi_v = \frac{\chi_D - \chi_v}{1 - i\omega\tau}$$

Where χ_v is the electrical susceptibility at high frequencies, and χ_D is the electric susceptibility at the low frequencies. But a more rigorous derivation is required to understand that the Debye model of permittivity arises from the physical description of the kinematics of the dynamics of the simple harmonic oscillator. Jackson offers the following derivation.

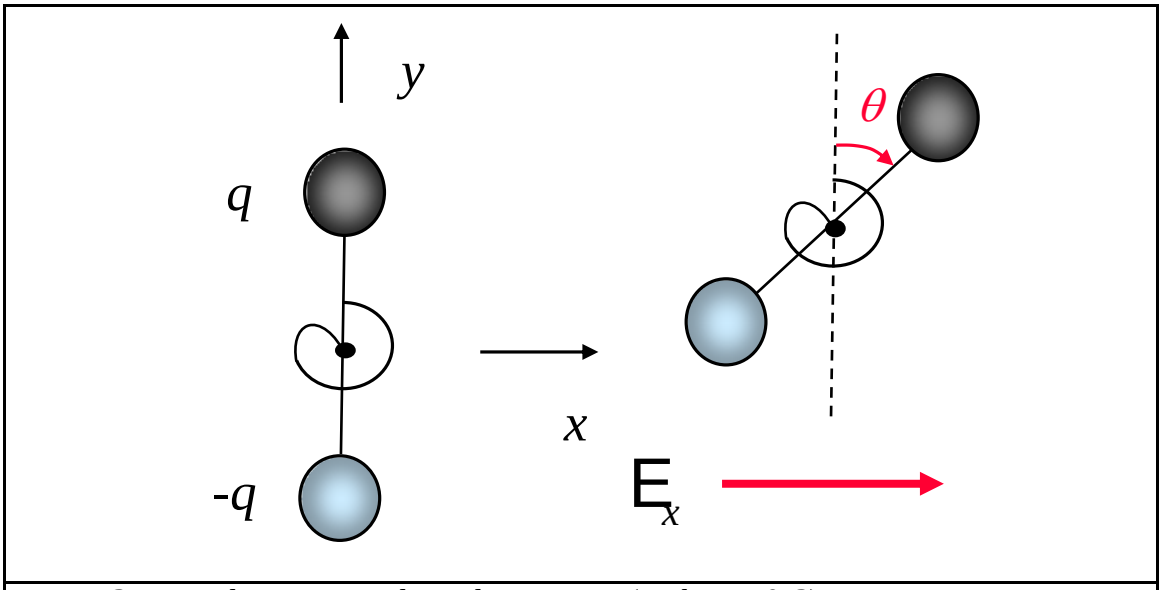

Figure 3-5. Dipole at Rest and Dipole Rotating (Jackson 2013).

Consider an electric field applied on a single molecule in the x-direction where $p_x = 0$ when the molecule is at rest and when $p_x > 0$, when the field is applied. Adopting a rotational and harmonic motion, and performing a torque balance, we obtain T which is in the z-direction. Then

$$T = I\frac{d^2\theta}{dt^2} = T_E + T_S + T_F$$

$$\boldsymbol{T_E} = (qr^+ - qr^-) \times \boldsymbol{E} = \boldsymbol{q}(\tilde{\boldsymbol{p}}\, d) \times \boldsymbol{E} = \boldsymbol{p} \times \boldsymbol{E}$$

where the cross product of the dipole with the electric field is

$$\boldsymbol{T_E} = -zp\grave{E}_x \sin\left(\frac{\pi}{2} - \theta\right)$$

$$\boldsymbol{T_E} = qdE_x cos\theta = \textit{the driving force}$$

$$\boldsymbol{T_S} = -s\theta = rotational\ spring\ force$$

$$\boldsymbol{T_F} = -c\frac{d\theta}{dt} = rotational\ friction\ force$$

Then the total torque becomes

$$I\frac{d^2\theta}{dt^2} = qdE_x cos\theta - s\theta - c\frac{d\theta}{dt}$$

$$Assuming\ \theta \ll 1, cos\theta \approx 1\ which\ means\ small\ fields$$

$$Then\ qdE_x \approx s\theta + c\frac{d\theta}{dt} + I\frac{d^2\theta}{dt^2}$$

$$For\ small\ angles\ p_x = qdsin\theta \approx qd\theta$$

$$\theta \approx \frac{p_x}{qd}$$

Inserting this back into the torque balance we obtain

$$qdE_x \approx s\frac{p_x}{qd} + c\frac{1}{qd}\frac{dp_x}{dt} + I\frac{1}{qd}\frac{d^2p_x}{dt^2}$$

$$Or\ (qd)^2E_x = sp_x + c\frac{dp_x}{dt} + I\frac{d^2p_x}{dt^2}$$

Assuming sinusoidal steady state

$$(qd)^2E_x = sp_x + j\omega cp_x - \omega^2 Ip_x$$

Solving for $p_x = E_x\left(\frac{(qd)^2}{s - \omega^2 + j\omega cI}\right)$

$$N_m = \frac{number\ of\ molecules}{m^3}$$

Then we have the total dipole moment per unit volume for M molecules

$$P_x^M = N_m p_x$$

We know for a linear material, using the molecular susceptibility χ_E^M

$$P_x^M = \varepsilon_0 \chi_E^M E_x$$

$$\chi_E^M = \frac{P_x^M}{N_m p_x} = \frac{N_m p_x}{\varepsilon_0 E_x}$$

$$\chi_E^M = \frac{N_m}{\varepsilon_0}(qd)^2\left(\frac{1}{s - \omega^2 + j\omega cI}\right)$$

Assuming that the frequency is much lower than the resonance of the of the molecule – millimeter wave frequencies or lower $\omega^2 I \ll s$ then

$$\chi_E^M = \frac{N_m}{\varepsilon_0}(qd)^2\frac{1}{s}\left(\frac{1}{1 - \omega^2 + j\omega\frac{c}{s}}\right)$$

Where the relaxation constant

$$\tau = \frac{c}{s}$$

At the zero frequency

$$\chi_E^M(0) = \frac{N_m}{\varepsilon_0}(qd)^2\frac{1}{s}$$

We can write the molecular susceptibility as

$$\chi_E^M = \frac{\chi_E^M(0)}{1 + j\omega\tau}$$

Or the permittivity function is

$$\varepsilon_r = 1 + \frac{\chi_E^M(0)}{1 + j\omega\tau}$$

At high frequencies the molecules cannot respond to the field, so the relative permittivity tends to be one. At high frequency the atomic effects dominate. If we include both the molecule and atomic effects, we obtain

$$P_x = P_x^M + P_x^A$$

$$= \varepsilon_0 \chi_E^M E_x + \varepsilon_0 \chi_E^A E_x$$

$$= \varepsilon_0 \chi_E E_x$$

The atomic susceptibility is almost constant because atoms respond much faster to a field than molecules as long as we are not in THz frequency regime, then

$$\chi_E = \chi_E^M + \chi_E^A$$

$$= \frac{\chi_E^M(0)}{1 + j\omega\tau} + \chi_E^A$$

$$\varepsilon_r = 1 + \chi_E^A + \frac{\chi_E^M(0)}{1 + j\omega\tau}$$

$$= a + \frac{b}{1 + j\omega\tau}$$

Where

$$a = 1 + \chi_E^A$$

$$b = \chi_E^M(0)$$

Since

$$\varepsilon_r(0) = a + b$$

$$\varepsilon_r(\infty) = a$$

Which means

$$b = \varepsilon_r(0) - \varepsilon_r(\infty)$$

Therefore

$$\varepsilon_r = \varepsilon_r(\infty) + \frac{\varepsilon_r(0) - \varepsilon_r(\infty)}{1 + j\omega\tau}$$

The real part is

$$\varepsilon_R = \varepsilon_r(\infty) + \frac{\varepsilon_r(0) - \varepsilon_r(\infty)}{1 + (\omega\tau)^2}$$

The imaginary part is

$$\varepsilon_I = \omega\tau \frac{\varepsilon_r(0) - \varepsilon_r(\infty)}{1 + (\omega\tau)^2}$$

(Jackson 2013)

3.2 Quantum Models of the Permittivity function: The Quantum Two-level System Representation of the Simple Harmonic Oscillator

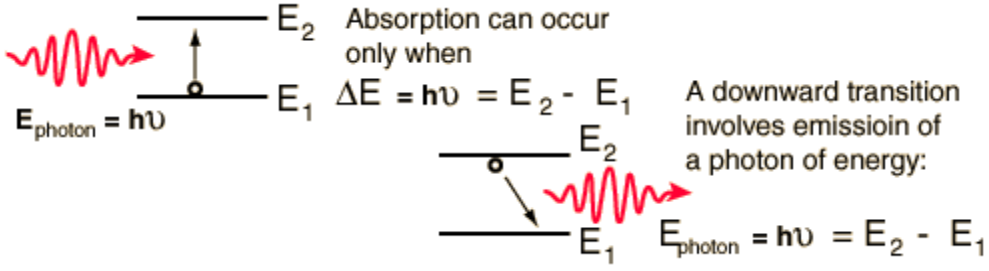

Figure 3-6. Atomic Transitions Which Emit or Absorb Visible Light Are Generally Electronic Transitions, Which Can Be Pictured in Terms of Electron Jumps Between Quantized Atomic Energy Levels (Hyperphysics, Quantum Properties of Light n.d.).

Following Shimoda (Shimoda, Introduction to Laser Physics 1984), absorption and emission of light are invariably accompanied by dispersion. In the case of lasers, these processes for transition between two energy levels of an atom, could be treated as we did earlier, as a classical oscillating dipole. If we consider a medium with numerous atoms, the

differential equation describing the electric dipole has the same mathematical form as before.

$$\frac{d^2x}{dt^2} + 2\gamma\frac{dx}{dt} + \omega_0^2 x = \frac{F}{m}$$

Where x is the amplitude of the oscillator with frequency, ω_0, and a damping constant, γ, and F is the driving force F, with m as the mass of the oscillator. If the driving force is the electric field of the incident light $E(\omega)\exp(i\omega t)$, with charge e, the above equation becomes

$$\frac{d^2x}{dt^2} + 2\gamma\frac{dx}{dt} + \omega_0^2 x = -\frac{e}{m}E(\omega)e^{jwt}$$

Substituting the steady state solution,

$$x = x(\omega)e^{jwt}$$

We get

$$x(\omega) = \frac{e}{2m\omega_0}\frac{E(\omega)}{\omega^2 - 2j\gamma\omega - \omega_0^2}$$

If $\omega_0 \cong \omega$, then we can approximate this equation to be

$$x(\omega) = \frac{e}{2m\omega_0}\frac{E(\omega)}{(\omega - \omega_0 - j\gamma)}$$

If $\gamma \ll \omega$.

And also if we assume there are N_U atoms per unit volume in the upper level and N_L atoms per unit volume in the lower level, the polarization, $P(\omega)e^{jwt}$ of the medium is given by

$$P(\omega) = -ex(\omega)(N_L - N_U)$$

And as we defined before, since

$$P(\omega) = \varepsilon_0 \chi(\omega) E(\omega)$$

Combining the two equations we obtain

$$\chi(\omega) = \frac{-ex(\omega)(N_L - N_U)}{\varepsilon_0 E(\omega)}$$

$$= \frac{-e^2 E(\omega)(N_L - N_U)}{2m\omega_0(\omega - \omega_0 - j\gamma)\varepsilon_0 E(\omega)}$$

$$= \frac{-e^2(N_L - N_U)}{2m\varepsilon_0\omega_0(\omega - \omega_0 - j\gamma)}$$

Separating the real $\chi'(\omega)$ and the imaginary part $\chi^{"}(\omega)$, we obtain

$$\chi'(\omega) = -\frac{(N_L - N_U)e^2}{2m\varepsilon_0\omega_0} \cdot \frac{\omega - \omega_0}{(\omega - \omega_0)^2 + \gamma^2}$$

$$\chi^{"}(\omega) = -\frac{(N_L - N_U)e^2}{2m\varepsilon_0\omega_0} \cdot \frac{\gamma}{(\omega - \omega_0)^2 + \gamma^2}$$

(Shimoda, Introductions to Lasers 1984)

And as seen before

$$\varepsilon(\omega) = \varepsilon_0[1 + \chi(\omega)].$$

In order to derive the complex susceptibility we assumed that the medium was an ensemble of classical oscillators, where the magnitudes of the atomic dipoles were determined from dipole radiation. A quantum mechanical derivation of the susceptibility begins with the same differential equation of motion but the acceleration given by F/m must be expressed in quantum mechanical terms. Shimoda states that this term is $\frac{2\omega|\mu_{UL}|^2}{3\hbar}$ which replaces $\frac{e^2}{m}$, where μ_{UL} is the non zero off diagonal elements of the dipole moment when the symmetries of the upper and lower states are different and they represent the probability amplitude

of transition. Remembering that $\omega_0 \cong \omega$ and inserting this quantum mechanical term into our susceptibility equations, the 2 and ω cancel and we are left with.

$$\chi'(\omega) = -\frac{(N_L - N_U)e^2|\mu_{UL}|^2}{3\mathcal{E}_0\hbar} \cdot \frac{\omega - \omega_0}{(\omega - \omega_0)^2 + \gamma^2}$$

$$\chi''(\omega) = -\frac{(N_L - N_U)e^2|\mu_{UL}|^2}{3\mathcal{E}_0\hbar} \cdot \frac{\gamma}{(\omega - \omega_0)^2 + \gamma^2}$$

(Shimoda, Introductions to Lasers 1984)

Thus in this semi classical model the transition of an atom or molecule from one level to another is mediated by the monochromatic light. The transition itself can be thought of as the superposition of the two Eigen state probability functions coupled by an almost resonant source. The probability amplitude distribution of this mixed state is that of an oscillating electric dipole moment exactly as described in the classical models. In the Quantum Mechanical description this dipole transition results in a dielectric susceptibility based on energy levels and the electric dipole of the molecule.

Beyond the semi classical approach, a more formal derivation is given in chapter 2 on dipole transitions in the book Fundamentals of Quantum Electronics by Pantell and Puthoff. They have a rigorous and detailed development of the electric dipole transition for lasers as do many books. In summary they chose an assumed interaction Hamiltonian of interest, they form expectation values of relevant observables, a set of derivatives of the expectation values leading to the equation of motion for an isotropic medium. Only the results will be presented here.

$$\ddot{\boldsymbol{P}} + \frac{2}{T_2}\dot{\boldsymbol{P}} + \Omega^2\mathbf{P} = \frac{2\Omega}{\hbar}\mathrm{L}\frac{|\mu_{UL}|^2}{3}(N_L - N_U)$$

Where $\boldsymbol{P}$ is the polarization associated with the transition of interest, $1/T_2$ is the damping constant, Ω is the oscillator frequency, often called the Rabi frequency, L is the Lorentz correction factor and μ_{UL} is the dipole operator. As before ω doesn't deviate much from the transition frequency Ω, so the solution is in the form

$$\widetilde{\boldsymbol{P}} = \frac{1}{2} P e^{j\omega t - kz)} + complex\ conjugate$$

for plane wave propagation in the z-direction and similarly for $\widetilde{\boldsymbol{E}}$. We obtain

$$\widetilde{\boldsymbol{P}} = \frac{1}{\hbar} L \frac{|\mu_{UL}|^2}{3} (N_L - N_U) \frac{1}{(\Omega - \omega) + j\,{}^{1}/_{T_2}} \widetilde{\boldsymbol{E}}$$

Assuming that $(N_L - N_U)$ is time independent and recalling

$$\widetilde{\boldsymbol{P}} = \varepsilon_0\, \chi(\omega) \widetilde{\boldsymbol{E}},$$

Then the susceptibility derived by Pantell and Puthoff takes the same form as Shimoda where

$$\chi(\omega) = \frac{\pi}{\hbar \varepsilon_0} L \frac{|\mu_{UL}|^2}{3} (N_L - N_U) \widetilde{g_L}(\omega, \Omega)$$

And where $\widetilde{g_L}(\omega, \Omega)$ is the frequency dependent line-shape factor referred to as a complex Lorentzian function

$$\widetilde{g_L}(\omega, \Omega) = \frac{1}{\pi} \frac{1}{(\Omega - \omega) + j\,{}^{1}/_{T_2}}$$

$$= \frac{1}{\pi} \frac{(\Omega - \omega)}{(\Omega - \omega)^2 + ({}^{1}/_{T_2})^2} - j \frac{1}{\pi} \frac{1/T_2}{(\Omega - \omega)^2 + ({}^{1}/_{T_2})^2}$$

(Puthoff 1969, 56-57)

Thus we find the mathematical model of the simple harmonic oscillator can be used to describe the physical behavior of not only a mass spring dashpot, but also dielectric properties of Lorentz or Debye materials as a sum of simple harmonic oscillators and even quantum multi-level systems. The key point here is that these are physical models –they are not phenomenological. They are modeling a dynamic, whether it is classical or quantum mechanical, they are purely physical models derived from the equations of motion that describe the dielectric function.

This equivalency is a reflection of a deeper symmetry that exists in Physics that allows us to seamlessly transition between systems that share the same differential equations. Brillouin formally exploits this equivalency in his analysis of systems consisting of <u>interconnected</u> elements which is clearly the most fundamental model of a material (mechanically and electrically.)

3.3 The One Dimensional (Linear) Material Model

Brillouin in chapter 3 of his book on Wave Propagation in Period Structures similarly develops the equations of motion for a one dimensional lattice of infinite identical particles of mass M; each connected with its nearest neighbor with a spring at distance d in the x axis. If the particles are numbered such that the origin is 0 and the particle to the right is 1 and the displacement of the nth particle is y_n, so that x_n the coordinate of particle n is given by

$$x_n = nd + y_n,$$

the distance between two particles n, and $n+m$, is given by

$$r_{n,n+m} = x_{n+m} - x_n = md + y_{n+m} - y_n.$$

The energy of interaction between the two particles are given by

$$U(r) = U(|x_{n+m} - x_n|)$$

and the total potential energy of the lattice is given by

$$U = \sum_n \sum_{m>0} U(|x_{n+m} - x_n|).$$

If we only pick m>0, and assume that the displacement y_n, is much smaller than the distance d, and we expand U in a Taylor series we obtain:

$$U(x_{n+m} - x_n) = U(md) + (y_{n+m} - y_n)U'(md) + \frac{1}{2}(y_{n+m} - y_n)^2 U''(md) + \cdots$$

Substituting the Taylor expansion and ignoring terms greater than 2nd order we obtain

$$U = Constant + \sum_n \sum_{m>0} \left[+(y_{n+m} - y_n)U'(md) + \frac{1}{2}(y_{n+m} - y_n)^2 U''(md) \right]$$

where the

$$Constant = \sum_n \sum_{m>0} U(md) = n \sum_{m>0} U(md)$$

The force F_p, the force acting on the pth particle, is obtained by taking the negative derivative of the potential energy with respect to the displacement of this particle. All variables not containing y_p, drop out leaving $n = p$, and $n + m = p$

$$F_p = -\frac{\partial U}{\partial y_p} = -\frac{\partial U}{\partial y_p} \sum_n \sum_{m>0} (y_{n+m} - y_n)\, U'(md) + \frac{1}{2}(y_{n+m} - y_n)^2 U''(md)$$

$$= \frac{\partial}{\partial y_p} \sum_{m>0} \left(y_{p+m} - y_p\right) U'(md) + \frac{1}{2}\left(y_{p+m} - y_p\right)^2 U^{"}(md)$$

$$+ (y_p - y_{p=m}) U'(md) + \frac{1}{2}\left(y_p - y_{p-m}\right)^2 U^{"}(md)$$

$$= \sum_{m>0} - U'(md) + \left(y_{p+m} - y_p\right) \quad U^{"}(md) + U'(md) + \left(y_p - y_{p-m}\right)^2 U^{"}(md)$$

If $U^{"}(md) = U_m^{"}$

$$F_p = M \frac{d^2 y_p}{dt^2} = U_m^{"}(y_{p+m} + y_{p-m} - 2y_p)$$

By differentiating the potential energy Brillouin gets the same equation of motion on the left side of the equation ***F = ma is where*** a ***continuous second order derivative in time and the right side of the equation is a second derivative in space for a discrete ensemble***. The mass behaves the same way as a simple harmonic oscillator as a wave travels through the medium.

Every element of the material medium is acted upon by the same kind of dynamic equation that we saw before for an individual element. ***Therefore the derivations of the permittivity of an atom or molecule derived in the previous sections also holds true for interconnected ensemble of atoms or molecules.***

3.3.1 Equivalency of Mechanical and Electrical Systems

Brillouin also derives the same equation for a low pass filter where there are equal self-inductances, L and equal capacitors, C, shown in the diagram below, in order to demonstrate mechanical and electrical equivalency.

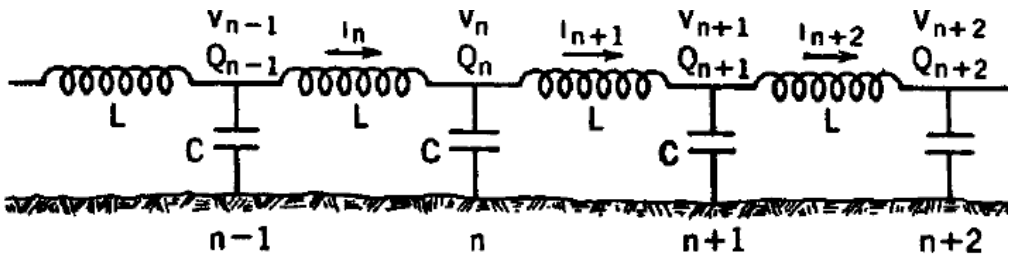

Figure 3-7. Mechanical Low Pass Filter (Brillouin 1953).

If Q_n, is the charge and V_n, is the potential on the capacitor n, and i_n is the current flowing between n-1 and n. Then

$$L\frac{di_n}{dt} = V_n - V_n = \frac{Q_{n-1}}{C} - \frac{Q_n}{C}$$

$$i_n - i_{n+1} = \frac{dQ_n}{dt}$$

$$V_n = \frac{Q_n}{C}$$

Differentiating the above equation we obtain the following flow of current, based on the potential differences and the charges on the capacitor plates.

$$L\frac{d^2 i_n}{dt^2} = \frac{1}{C}\left(\frac{dQ_{n-1}}{dt} - \frac{Q_n}{dt}\right) = \frac{1}{C}(i_{n-1} + i_{n+1} - 2i_n)$$

Brillouin points out that this equation is identical to the equation of motion for the one dimensional lattice with nearest neighbor interactions shown above. The mass is equivalent to L as the left side of the equation is the force due to acceleration of the mass and 1/C is the spring constant as the right side of the equation which is the restoring force. This is the classical approach to associate electromagnetic energy with kinetic energy and electrostatic energy with potential energy which means *1/C* is associated with *U*, and *L* with *M*. The resistance in the wire is not considered here for simplicity and to illustrate the mechanical

and electric analogue. Since the equation of propagation of electric waves along a low pass electric line was exactly of the same form as the propagation of an elastic wave along a low pass mechanical lattices the electric and mechanical systems may be considered analogous Figure 3-8 (Brillouin 1953). For the purposes of this dissertation the classical electric circuit model which has been shown to be analogous to the mechanical system will be adopted.

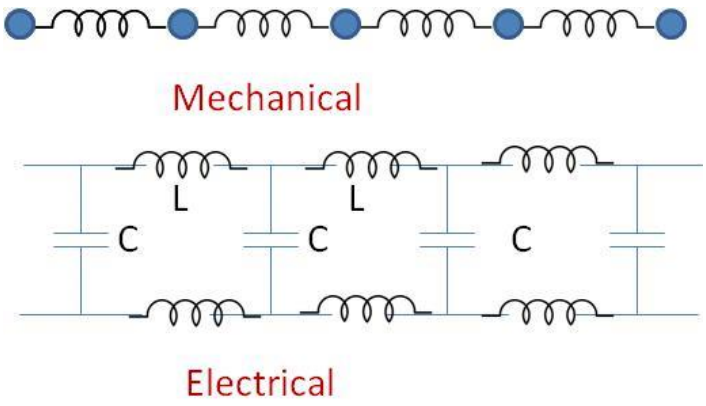

Figure 3-8. Mechanical and Electrical Systems Are Analogous (Brillouin 1953).

Now that we have established that the symmetry between mechanical and electrical systems and that they obey the same mathematics and equations of motion we formalize the representation of dielectrics by lumped circuit equivalents in the next section.

3.4 Representation of Dielectrics by Lumped Circuit Equivalents

Von Hippel broaches the concept of complex permittivity and complex permeability by analyzing the current and voltage signatures of a capacitor and inductor. He introduces

these concepts in field theory and illustrates the field and matter interactions and its macroscopic consequences. He points out that it is often convenient to treat field phenomena by an equivalence approach, where the electrical and magnetic fields are considered the voltages and currents in an electric circuit. He exploits this symmetry by formally representing the dielectrics as lumped equivalent circuits.

The most simple of such a circuit representation would be an ideal capacitor and resistor in series or parallel shown in Figure 3-9. Von Hippel states that the integrity of the circuit simulation to predict actual dielectric behavior is compared to observed dielectric response behavior.

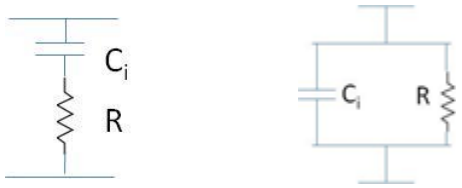

Figure 3-9. The Ideal Resistive Material (DC Conductive like Carbon).

In the series representation the applied sinusoidal voltage is the sum of the voltage drop across the resistor and the capacitor whereas in the parallel scenario the total current is equal to sum of currents passing the circuit elements C and R.

Series Arrangement

$$v = IR + \int \frac{Idt}{C_i} = I\left(R + \frac{1}{j\omega C_i}\right)$$

$$Z = \frac{v}{I} = R + \frac{1}{j\omega C_i}$$

Parallel Arrangement

$$I = \frac{v}{R} + C_i \frac{dv}{dt} = v\left(\frac{1}{R} + j\omega C_i\right)$$

$$Y = \frac{I}{v} = \frac{1}{R} + j\omega C_i$$

A capacitor C_0 has the admittance

$$Y = \frac{1}{Z} = (\varepsilon^{"} + j\varepsilon')\frac{\omega}{C_0}$$

By equating this expression to impedance and admittance we obtain

Series Arrangement

$$\varepsilon_r = \frac{\varepsilon'}{\varepsilon_0} = \frac{C_i}{C_0[1 + (\omega R C_i)^2]}$$

$$\varepsilon_I = \frac{\varepsilon^{"}}{\varepsilon_0} = \frac{\omega R {C_i}^2}{C_0[1 + (\omega R C_i)^2]}$$

Parallel Arrangement

$$\varepsilon_r = \frac{\varepsilon'}{\varepsilon_0} = \frac{C_i}{C_0}$$

$$\varepsilon_r = \frac{\varepsilon^{"}}{\varepsilon_0} = \frac{1}{\omega R C_0}$$

The frequency dependence of these two circuits are very different and therefore combinations of these circuits would yield very different circuit responses and may fit and represent measured data where neither of the circuits alone could provide an adequate fit (Hippel 1995).

A dielectric spectrum that is the same response as a network combination of an RC circuit is called relaxation spectra. The simplest form is shown in Figure 3-10.

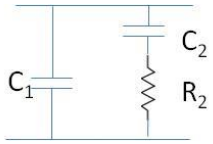

Figure 3-10. Network Representing the Simplest Type of Relaxation Spectrum of a Polar Material.

In this case

$$Y = (j\omega C_i + \frac{1}{Z_2})$$

where

$$Z_2 = R_2 + \frac{1}{j\omega C_2}$$

By introducing the relaxation time constant $\tau_2 = R_2 C_2$ and separating the real and imaginary parts we obtain

$$Y = \frac{\omega^2 C_2 \tau_2}{1 + \omega^2 \tau_2^2} + j\omega C_1 + \frac{j\omega C_2}{1 + \omega^2 \tau_2^2}$$

By equating the above expression to the geometric capacitance Y in terms of complex permittivity, we obtain the relative dielectric constant for the equivalent circuit.

$$\varepsilon_r = \frac{C_1}{C_0} + \frac{C_2}{C_0} \frac{1}{1 + \omega^2 \tau_2^2}$$

$$\varepsilon_I = \frac{C_2}{C_0} \frac{1}{1 + \omega^2 \tau_2^2}$$

This represents the Debye function we modeled before (Hippel 1995).

For an RLC circuit which represents a Lorentz material, we can derive the dielectric function in a similar manner.

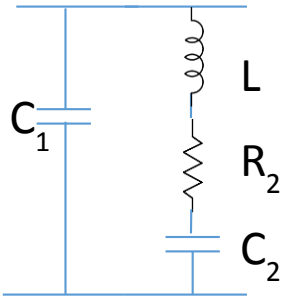

Figure 3-11. A Lorentz Material.

A voltage balance gives us the following differential equation

$$L\frac{dI}{dt} + RI + \frac{1}{C}\int Idt = v$$

The steady state solution for the current is

$$I = \frac{v}{R + j\omega L + \frac{1}{j\omega C}} = vY$$

The current is maximum when the two reactances cancel each other.

$$\omega_0 = 1/\sqrt{LC}$$

For zero voltage the equation transforms into a transient equation of a series resonant circuit. If the change Q is the current we obtain

$$L\frac{d^2Q}{dt^2} + R\frac{dQ}{dt} + \frac{1}{C}Q = 0$$

This is the same equation of motion as we have solved many times.

$$Y = j\omega C_1 + \frac{1}{Z_2}$$

where

$$Z_2 = j\omega L + R + \frac{1}{j\omega C_2}$$

$$Y = j\omega C_1 + \frac{j\omega C_2}{j\omega L j\omega C_2 + j\omega C_2 R + 1}$$

By equating the above expression to the geometric capacitance Y in terms of complex permittivity, we obtain

$$Y = j\omega C_{eff}$$

$$C_{eff} = \frac{Y}{j\omega}$$

$$C_{eff} = C_1 + \frac{C_2}{1 - \omega^2 L C_2 + jRC_2\omega}$$

And since

$\tau_C = RC$ the capacitative time constant

$\tau_L = \frac{L}{R}$ the inductive time constant

$\omega_0 = \frac{1}{\sqrt{LC}}$ the resonant frequency

We can rewrite this equation in terms of then standard Debye equation of permittivity, where

$$C_{eff} = C_1 + \frac{C_2}{1 - \omega^2 L C_2 + jRC_2\omega \times \frac{\omega_0}{\omega_0}}$$

$$C_{eff} = C_1 + \frac{C_2}{1 - \frac{\omega^2}{\omega_0{}^2} + jRC_2\omega_0 \times \frac{\omega}{\omega_0}}$$

$$C_{eff} = C_1 + \frac{C_2}{1 - \left(\frac{\omega}{\omega_0}\right)^2 + j\left(\frac{\omega}{\omega_0}\right)\frac{RC_2}{\sqrt{LC_2}}}$$

$$C_{eff} = C_1 + \frac{C_2}{1 - \left(\frac{\omega}{\omega_0}\right)^2 + j\left(\frac{\omega}{\omega_0}\right)\sqrt{\frac{R^2C^2}{LC}}}$$

$$C_{eff} = C_1 + \frac{C_2}{1 - \left(\frac{\omega}{\omega_0}\right)^2 + j\left(\frac{\omega}{\omega_0}\right)\sqrt{\frac{RC}{\frac{L}{R}}}}$$

$$C_{eff} = C_1 + \frac{C_2}{1 - \left(\frac{\omega}{\omega_0}\right)^2 + j\left(\frac{\omega}{\omega_0}\right)\sqrt{\frac{\tau_C}{\tau_L}}}$$

And the quantity $\frac{1}{X} = \sqrt{\frac{\tau_C}{\tau_L}}$ controls the sharpness of the resonance.

This behavior is typical of resonant materials that we will use for the Lorentz coatings in fabrication of our meta-material.

CHAPTER 4

FUNDAMENTAL DIAZ MODEL

Again why is the window in water interesting? Another reason why water is interesting is because the optical window behavior, according to the Diaz and Alexopoulos paper, is a unique behavior which is distinct from the classic classification of Debye and Lorentz. Most books on material science and permittivity, tell us that there are only Debyes and Lorentzes. Or most books about conductivity tell us, we have a sum of simple harmonic oscillators, so how many ways can we explain the permittivity?

Some say, like Von Hippel, that there are Debye models and there are Lorentz models. And these two categories historically came from the physics of these two models as we discussed earlier. A Debye is a molecule that is already polarized, like water, and electric field tends to rotate the molecule. It doesn't increase the polarization of the molecule but tends to rotate it, to align it with the field. But when there is such a huge ensemble of such dipoles, and we apply a field, they arrange themselves into the least energy configuration possible. When a field is applied all the dipoles don't turn towards the field. They are fighting each other; there is interaction, so one obtains a net polarization. Also there is a very small fraction of the permanent dipole moment. This is historically important because there are catastrophes that can occur. When people were developing these models of dielectric constants, there were catastrophes associated with permanent dipoles. Originally people thought dipoles rotated, or electrons attached to an atom, like a spring constant oscillated like a Debye and a Lorentz. These are the oldest models. They were motivated by

a physical picture. Later scientists, who wanted to generalize, or favor quantum mechanics, stated these were simple harmonic oscillators. They are an arbitrary sum of simple harmonic oscillators. This allowed people to say, that we can have that picture, whether it is mechanical, a mechanistic picture of actual oscillation of electron clouds; or we can have states; we can have a potential well with states. And the transition from one state to the other is a simple harmonic oscillator. They have Lorentzian line widths. As we saw earlier the mathematics of a simple harmonic oscillator, which is a classical mechanistic object, consisting of a spring with a mass, when replicated with the quantum mechanics model – it is completely analogous mathematically. This allowed people to postulate all sorts of theories. They could worry about how many states there were. So this is another viewpoint of the permittivity.

The first view is that we have permittivity as a simple harmonic oscillator. The second view is a physical, molecular one that we view permittivity as a Debye or a Lorentz. This is important because people thought that those two models were completely different – and physically they are. A molecule either rotates or vibrates, - a rotation is not the same thing as we saw in chapter 3. The mathematicians say we can take any Lorentz and add damping until it becomes a Debye. Although a Debye rotates, mathematically, if we take a Lorentz and damp it the equation of motion looks like a Debye. This viewpoint says we don't look at individual molecules, we focus on what does the dielectric constant behave like.

The oil in the dashpot, mass, spring constant model holds here. So mathematically it is clear that we can mimic any Debye, by starting from a Lorentz and then over damping it.

The window is a behavior that no one had tried to explain until the Diaz dissertation; there has been no attempt at explaining why there should be a window. And what is important about the window is that it is not a low loss region; *but there is a complete absence of loss*. This dissertation also explains why the window is unusual. According to Diaz one cannot make a window out of a sum of simple harmonic oscillators; one has to modify all the oscillators with an additional circuit. It is still causal because all circuits are causal. So Diaz to preserve causality stated that the most general circuit is not a pure simple harmonic oscillator. It is a pure simple harmonic oscillator - with another oscillator shunting it. The Diaz statement is that there is something more fundamental.

Back in the days when they would look at dielectrics, they would say this is good enough to explain everything - it was a Debye or a Lorentz. Diaz says because water is a Lorentz, Hasted (Hasted 1973) knows from classical physics; the inductance, L, maps to the mass; C, capacitance maps to the spring constant, and R, the resistance is the damping. So when Hasted chose his model of water, he makes a comment that the Debye relaxation, of water, cannot possibly be a Debye relaxation. He says this for two reasons. One reason is everything has mass. So his argument is there is never a perfect Debye. If we are modeling actual motion dynamics, we couldn't possibly have a Debye because that would imply the absence of mass (inertia): because there is no inductor – there is the damping, R and there is a spring constant C only. How can there be a physical process where there is no mass? What could we apply it to? Diaz states Hasted knew this Debye, would obscure the optical valley. If we believe that to be a Debye and everyone knows what the parameters of that Debye are – we can quickly calculate what the loss would be at the optical valley, and the

result is that light could not penetrate water. So Hasted just makes the comment, that it is obviously missing inertia. But he doesn't bother to do the calculations to show that even if this was a Lorentz, it would still obscure the valley. Because the shape of the peak limits what inductor we could ever assume for it, we are not free to assign an arbitrary inductor to a Debye.

The Debye loses its shape if we add too much inductance. If we add a little bit it doesn't look like it changes very much. But if we took a Debye, and start adding an inductor (Diaz thesis) how does this change? When we add very little inductance, we know that this starts going up a little, in magnitude, and this starts shifting back a little -but not too much. At a glance when we look at it, it still looks like a Debye. As we keep adding inductance, the real part starts getting really flat, and starts changing shape. Eventually it becomes a Lorentz which is sharp. There is region between zero damping and zero mass and some mass, where it sort of looks like a weird Debye. We can't tell it is a Lorentz. Diaz states that given the faithful data of water in this range, everyone fits it with a Debye, if we say, it has some Lorentz – i.e. some inductance, but we couldn't add enough inductance to make it match. Because it would get too deformed - we couldn't maintain it. But Hasted doesn't go into that in much detail. Diaz deduced that Hasted states that the absence of inertia makes the Debye models wrong because of the optical valley of water. But even if this statement was granted, Hasted missed the fact that the out of band "tails" of the infrared Lorentz terms, which by definition have mass, would also obscure the valley.

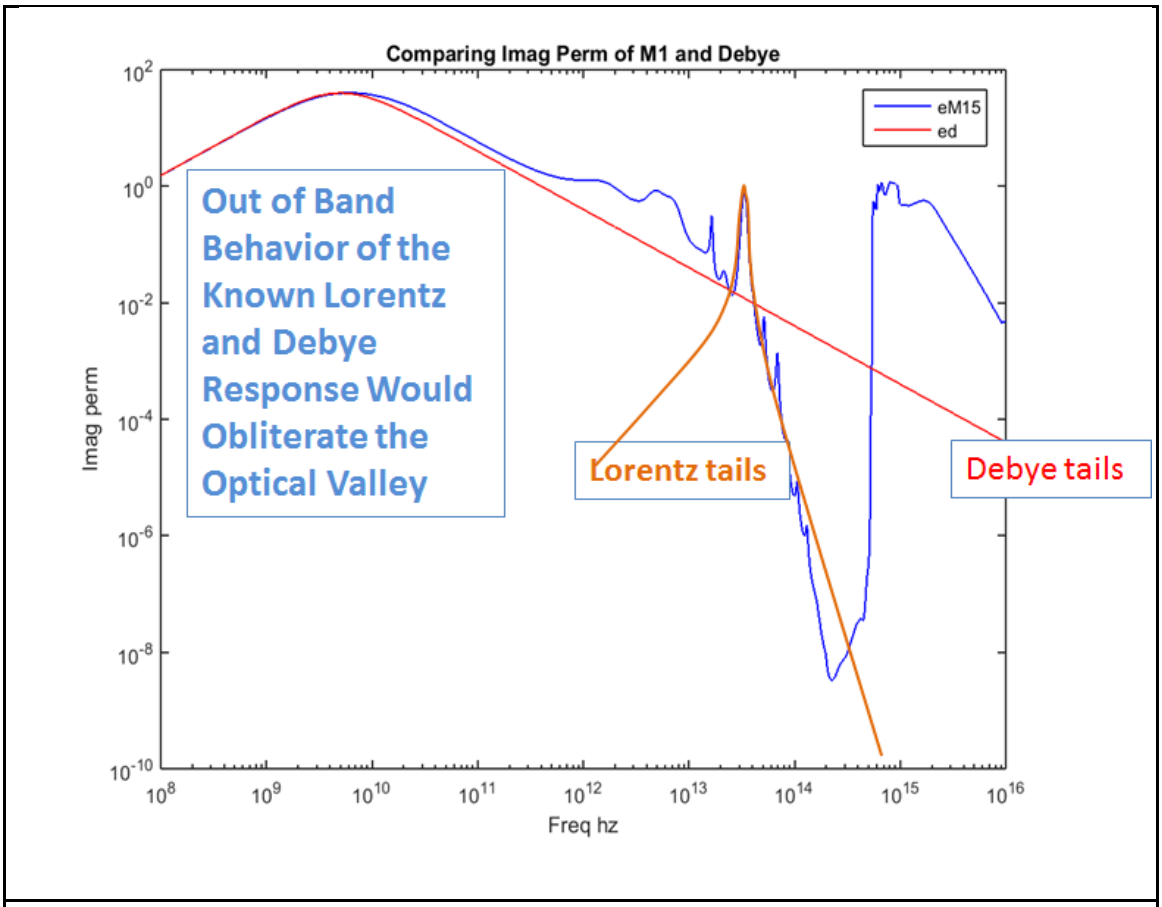

Figure 4-1. The Out-of-Band Behavior of Known Lorentz and Debye-like Responses of Water Would Obscure the Optical Valley.

The Debye is a special case of the Lorentz. So that's why the physicists say no its all quantum mechanics, it's all energy levels, it's all simple harmonic oscillators, every physicist will agree. But there is an important point. We know that the summation of n = 1 to n = N for many LRC circuits (oscillators) represent the dielectric property of a material. (R = q > 0, L = m > 0, C = k > 0). But this is not the fundamental model because it cannot represent water.

Initially Dr. Diaz tried to model the permittivity of water using a parallel sum of LRC circuits, the procedure outlined in his dissertation. The attenuation did not match the permittivity of water at the window frequency of $10^{\wedge 14.73}$GHz, where it becomes exceedingly small. He points out that changing the values of the circuit branches to match the attenuation still would not yield results matching the window because in order to match the infrared peaks that have associated Lorentz tails of $1/\omega^2$ would still be present in the optical valley.

Dr. Diaz postulates that there may be one or more zeros at the lower half plane and that the window of water is due to more zeros of the permittivity function in very close proximity to the real axis at the window frequency. In order for the optical valley to be so deep every Lorentz tail would have to be eliminated so he pointed out that this meant that all the conductivities of every LRC branch would have to be bypassed. Diaz achieves this by providing an alternative path for every single branch with what he calls a zero circuit, an LRC circuit in shunt with each branch. The idea was at the optical frequency this zero circuit path was the preferred path that bypassed all the conductances of each branch thereby eliminating the problem of the Lorentz tails. The Diaz circuit model is shown below in Figure 4-2 and Figure 4-3. We see that using this zero circuit model Diaz was able to match the dielectric properties of water as shown in Figure 4-4. The dashed lines is the model and the solid lines are the measured properties of water.

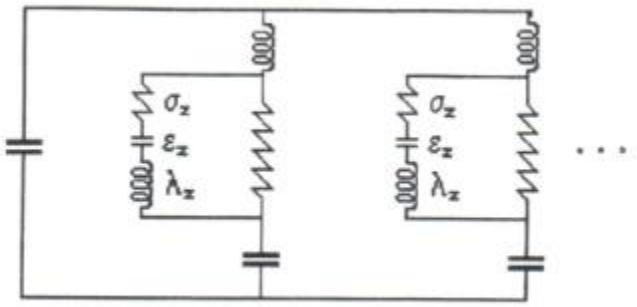

Figure 4-2. The Inclusion of a Zero Circuit in the Analytic Model by Diaz.

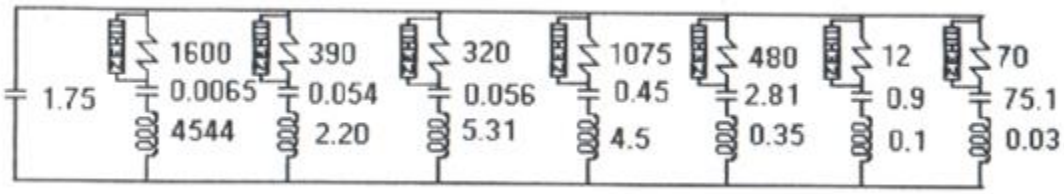

Figure 4-3. The Inclusion of the Zero Circuit in the Analytic Model by Diaz Models the Optical Valley of Water from DC to Daylight.

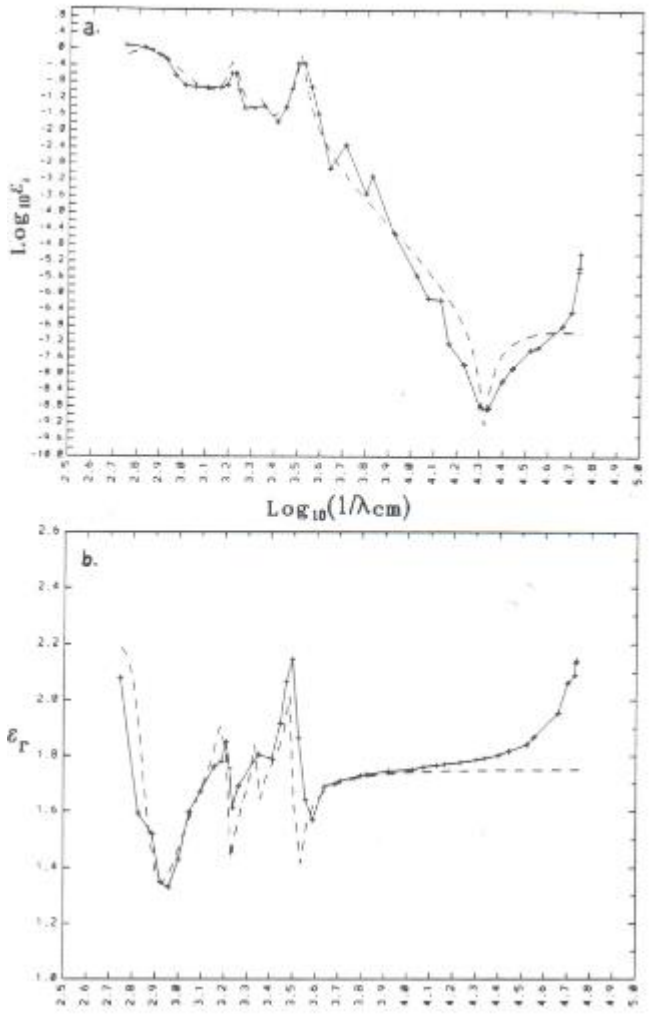

Figure 4-4. Log of the Imaginary Permittivity and Real Permittivity as a Function of Log 1/(λ (cm) for Water.

The fundamental model is therefore the LRC circuit with a zero shunt circuit (another LRC). This is the generalized function required to model a material. The Lorentz is a special case of the Fundamental and the Debye is a special case of the Lorentz.

Luckily the Diaz model is circuit based and we know circuits are causal. Not only is it mathematically sounds and physically sound; but also it gives us a mathematical tool to design materials.

They say every harmonic oscillator in water can be represented as a circuit branch. With every harmonic oscillator there is another oscillator in shunt with a loss term. And Diaz claims it is equivalent to saying that every water molecule behaves as if there were a conductive layer coating it which is represented by that shunt circuit.

So what does this circuit mean and how does it work? At optical frequencies at resonance $\omega_0 = 1/\sqrt{LC}$ this becomes a short circuit. Since the shunt resistor is much much less than the branch resistor, the current bypasses the large resistor here and takes the path of least resistance. It takes the shunt path. The Diaz model works by putting this shunt circuit on every resistor of the model and so at that frequency range you wipe out the loss. This is the only way you can hide each of these circuits. Without the shunt, the molecule vibrates as long as it sees an electric field. The only way you can hide every mode is to shield it. And that shunt is equivalent to this layer over water that hides every mode of water at the visual frequency. It is like frequency selective shield. A soon as you put a shield all the modes become irresponsive. The only way to shield an electric field is a metal. This shield is highly conductive and the field runs over the surface. This shunt circuit does exactly that due to its very low resistance. At the shunt circuit resonance, the shunt circuit becomes a short circuit and it is then is equivalent to having a conductive layer (Figure 4-5). The

water molecule behaves as if there was a sphere around it which at the optical valley becomes suddenly highly conducting. This completely eliminates the dissipation. Dissipation comes from motion – interaction with the electric field. This is the only way we can prevent dissipation since the motion is driven by the E field. The only way we can wipe out the motion is if we eliminate the E- field. We can eliminates the E-field if we surround the water molecule by a conductive shield.

The Diaz calculations showed how it could create the valley. This was the only physical mechanism that can be considered that eliminates all the loss due to every Lorentz tail.

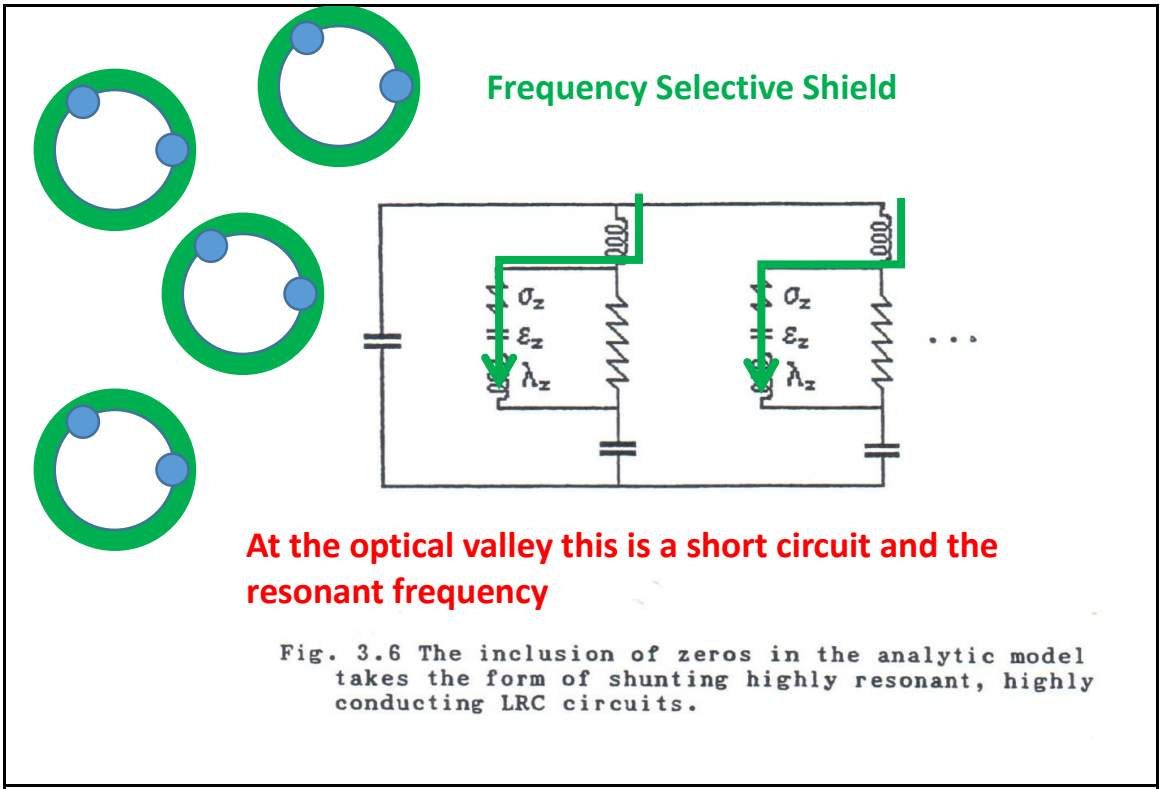

Figure 4-5. At the Optical Valley This Is a Short Circuit at the Resonant Frequency.

Diaz could come up with this because he insists when the simple harmonic oscillators, are expressed as an LRC branch; where L= mass, R= damping constant, and C = spring constant, all these terms must be positive. No physicist in their right mind would assume there is such a thing as a negative mass for a simple harmonic oscillator, or a negative spring constant because then it would create a force of its own. This is an energy argument. If we look at the definition of the potential energy of a spring, definition of a gravitational potential energy with mass, inertia; kinetic energy goes as mv^2. If m is negative than we get negative kinetic energy. This statement, R = q > 0, L = m > 0, C = k > 0, means we are assuming R > 0, C > 0, L > 0 for the overall circuit model and individual circuit branches. So every individual term of the Diaz expansion is passive and causal. Passive means there is no gain – no energy is generated. Passive means we can only lose energy. Energy can be conserved or lost; but thermodynamics dictates that energy is lost. Thermodynamics says we must always have an R that is positive.

Therefore what is important in the Diaz dissertation, is that there is no way a sum of simple harmonic oscillators can give us the window in water. This is intuitively obvious. In order to subtract loss, one would have to force the RLC branches into a form where we are going to have some terms that have to have negative resistances. How else can we erase loss? There is no absorption in the optical valley of water - it is totally transparent. And water is a real Lorentz and the only way to cancel it is to add a negative Lorentz.

The reason we are going through all this explanation is because people who are mathematically inclined might want to tell us that this is really a polynomial ratio of zeros and poles.

Suppose we had a polynomial of zeros and poles. Any material can be represented as a sum of simple harmonic oscillators and such a sum can be expressed as a polynomial. The Diaz dissertation makes a physical argument that the denominator of such a polynomial expression, must be larger than the numerator. That is to say it has to be a meromorphic function. The whole argument is that mathematicians may say it is okay to write it this way. But the physicists say it's okay for the mathematician write it this way, ***as long as when we see that the individual circuit elements RLC, are positive.*** Otherwise these terms have no physical meaning. It may be a mathematical artifice, a trick, but it ceases to have physical meaning.

By making RLC positive we make the system passive and causal. It is causal because inductances and capacitances have to be positive to be a causal circuit. If we ever see a true negative capacitance in a circuit - this is not causal. We have to spend energy to create negative capacitance. Something else is happening if there is gain – we are somehow putting energy into the system. Our goal here is to model real materials.

The Diaz- Alexopoulos fundamental model has great implications. And the key is that Diaz has established certain rules for including these "zero shunt" components, the RLCs have to be positive. So we could add this circuit to all other material models and we would still get what we are getting as long as we turn off the zero circuit or the shunting. Turning off the zero means that the capacitor of the zero shunt is too small, it's an open circuit, the resistor in the circuit is too high, and doesn't let current flow. The resistor tells us the conductivity of the path.

At the end of the dissertation Diaz points out that a physical model of the zero shunt circuit can be conceived: Water behaves like it has a layer around it which is not only resonant at the optical valley frequency, its effective conductivity is enormous. In order to have a valley that deep, the effective conductivity of that layer has to be enormous. It is as if at the optical valley, each mode of water is covered by a highly conductive Lorentz shell. This is the model that Diaz proposes in his dissertation (Diaz, The Analytic Continuation Method for the analysis and Design of dispersive Materials 1992).

CHAPTER 5

LITERATURE SURVEY FOR A MODEL OF THE OPTICAL VALLEY OF WATER

An in depth survey of the literature was performed to determine if there were any broad-band phenomenological models developed to fit the complex permittivity data of water from RF to optical frequencies where the $10^{\wedge-8}$ order imaginary permittivity drop prediction matched the optical valley of water observed at $10^{\wedge 14.73}$ Hz. Almost all models surveyed do not predict or discuss this optical valley. Often there is no information on the optical valley. If there is information on the optical valley and there is a drop; it is not typically in the $10^{\wedge 8}$ order of magnitude. It appears that when one tries to macroscopically model water some special "tricks" must be employed to obtain this deep valley of water. Furthermore, if the model correctly or closely predicts this behavior it is not clear which components of the model or their interaction are responsible for the optical valley.

We found many approaches to solve this problem; but they do not explain the optical valley. Explanations include "It doesn't absorb in the wavelength range of visible light, at roughly 400-700 nm, because there is no physical mechanism which produces transitions in that region - it is too energetic for the vibrations of the water molecule and below the energies needed to cause electronic transitions". (Hyperphysics, Physical Properties of Water n.d.)

Overall approaches are outlined below.

1. **DFT** Ab initio calculations using quantum mechanics in the IR range was used for most of the work surveyed. For example in a paper by Martin French, and Ronald Redmer (Universitat Rostock, Institut fur Physik. D-18051 Rostock, Germany, Physics of Plasmas published online April 20 2011) they calculated the dielectric properties of water with density functional theory and the Kubo-Greenwood formula using the Vienna ab initio simulation package. The exchange and correlation terms were approximated by either the functional of PBE or HSE and the results were compared to the experimental data from Hayashi et al. The real and imaginary dielectric functions of water under ambient conditions with 27 to 54 molecules in the simulation box resulted in distributions around the Hayashi data but the imaginary part of the Hayashi data was around 0.75 for the water at the window frequency. Also the authors point out that they do not achieve good agreement with any of the exchange terms for the full spectrum using DFT.

2. **Classical Molecular Dynamics** There are many molecular dynamic simulations of water in the literature. In a paper titled *A Systematic Study of Water Models for Molecular Simulation*: Derivation of water models optimized for use with a reaction field by David van der Spoel, Paul J van Maaren, and Herman J. C. Berendesen (Biosen Research Institue and Laboratory of Biophysical Chemistry, University of Gronimgen, Nijenborgh 4, 9747 AG Groninjen was noted. The Netherlands Journal of Chemical Physics Volume 108 Number 24 22 June 1998) investigated four of the most popular models of water. They were simple point charge (SPC), extended simple point charge (SPC/E), and the three point (TIP3P) and the

four point (TIP4P) transferable intermolecular potentials. The frequency dependence of the dielectric constant from an 820 molecule simulation with a 1.2 nm cut off radii where SPC/E gave the closest values of the dielectric properties of water. But the frequency range was from 1 to 1000 GHz or up to 1 THz much lower than the frequency range of water's optical valley.

3. **Diaz Circuit Model** In his dissertation *The Analytic Continuation Method for the Analysis and Design of Dispersive Materials* (UCLA 1992) models the full broad band spectrum of water using pure circuit model and is associated mathematical manipulation.

4. **Shubitidze and Osterberg Phenomenological Model** Fridon Shubitidze and Ulf Osterberg' s paper titled *Phenomenological model to fit the complex permittivity of water from radio frequencies to optical frequencies* (Physical Review E 75 046608 2007) proposes a hybrid phenomenological model using rational polynomials, Lorentz and Debye terms and some physical traits fit Segelstien's water data.

5. **Water Measurements based Segelstein Dissertation** D. Segelstein completed a broadband collection of dielectric data for his Master's thesis titled *The Complete Refractive Index of water* (1992) that was found to be a rich data set that included the optical valley given that the data were measured values and not a model.

6. **Other Models** There were other model that were not greater than 1THz and therefore not in the optical valley regime. *A model for the complex permittivity of water at frequencies below 1 THz* by Hans J. Liebe, Geroge A. Hufford, and Takashe Manabe (Journal of Infrared and Millimeter Waves July 1991, Volume 12 Issue 7, pp 659-675) is another example where they used experimental data of liquid water from the literature to employ their strategy of non-linear least square fitting. At low frequencies their expression was made up of two Debye terms whereas at high frequencies the two Debye terms collapsed to one Debye term but adding two resonances or Lorentzian terms. With the maximum frequency extension the model could be used up to 30 THz. Water's valley being at 537 THz does not go up to such high frequencies and therefore this valley was again avoided.

Finally there were many combinations of density functional theory and molecular dynamics papers out there but none were in the optical valley regime that we were interested in observing.

We found only two papers attempt to explain the optical valley in the imaginary permittivity of water. These were Diaz and Alexopoulos circuit mode that we discussed in chapter 4 and the Shubitidze and Osterberg phenomenological model that will be discussed in detail in the following chapter (6).

CHAPTER 6

THE SHUBITIDZE & OSTERBERG ALTERNATE HYPOTHESIS

The Shubitidze and Osterberg paper claims improvement of the Diaz-Alexopoulos model and will be analyzed in the next section.

6.1 Summary of the Shubitidze and Osterberg Paper

Shubitidze and Osterberg offer a phenomenological model of the dielectric constant of water in the desired range of $10^8 - 10^{16}$Hz. Like the Diaz-Alexopoulos model they use general factorized form of the dielectric function. This combined with fractional model-based parameter estimation method; they provide the real and imaginary permittivitys of water, which at first glance appear to match the measured dielectric water data. The model is derived from a microscopic frequency dependent rational function for adjusting zeros and poles of the dielectric dispersion together with the macroscopic statistical Fermi-Dirac distribution that allows the drastic reduction of the imaginary permittivity of water in the optical valley region. They claim the following meromorphic function *automatically* fulfills the necessary causality conditions.

$$\varepsilon = \frac{\prod_{m=1}^{M} \omega - Z_m}{\prod_{n=1}^{N} \omega - P_n}$$

Where $M < N - 1$ and Z_m are the zeros and P_n are the poles. Shubitidze and Osterberg claim building on the success of the Diaz-Alexopoulos rational function approach in two ways. First they use many more terms in the rational function expansion that they try to relate to the vibrational and electronic resonances noted in water. Second they use the

Fermi-Dirac distribution to model what they call the "reduced density of states" in the optical valley. The kinetic energy is calculated by assuming that all the kinetic energy comes from the rotating water molecule; and the potential energy terms for this distribution comes from the Lennard Jones Potential. The frequency dependent radius (distance between adjacent oxygen atoms) in these equations is allowed to vary as yet another fitting parameter. Their complex formula for the permittivity of water was derived using a fitting algorithm described below.

Shubitidze and Osterberg then define the complex refractive in a non-orthodox manner:

$$n_r(\omega) = Re[a(\omega)]Re[b(\omega)]$$

$$n_r(\omega) = Im[a(\omega)]Im[b(\omega)]$$

Where $a(\omega)$ and $b(\omega)$ are the microscopic and macroscopic phenomena respectively where $a(\omega)$ is described as a sum of resonant and non-resonant parts.

$$a_j = a_{j,res}(\omega) + a_{j,nres}(\omega)$$

where j refers to a particular resonance.

$$a_{j,res}(\omega) = \sum_{m=1}^{M} \frac{R_{j,m}}{\omega - \omega_{j,m}}$$

Where $\omega_{j,m}$ is a complex resonance and the non-resonant part is in the range of 0 to P complex frequencies:

$$a_{j,nres}(\omega) = \sum_{p=0}^{P} C_{j,p}\,\omega^p$$

Combining the resonant and non-resonant function a rational function representation of $a(\omega)$ is given by:

$$a(\omega) = \sum_{i=1}^{M} \frac{N_j(\omega)}{D_j(\omega)}$$

where

$$N_j(\omega) = \sum_{l=0}^{n_j} N_j^l \, \omega^l$$

$$D_j(\omega) = \sum_{l=0}^{d_j} D_j^l \, \omega^l$$

The unknown coefficients N_j^l and D_j^l are determined by fitting $a(\omega)$ against measured data of water found in Segelstein's thesis. However using the pole-zero series of the $a(\omega)$, Shubitidze and Osterberg were not able to obtain the eight orders of magnitude decrease in the imaginary permittivity of water in the visible region any better than Diaz-Alexopoulos. In order to solve this problem, the authors use a statistical approach as if this region is a band gap with reduced density of states by introducing the function $b(\omega)$, where

$$b(\omega) = D(\omega) + L(\omega)$$

Where $D(\omega)$ and $L(\omega)$ are the Debye one-pole (Frohlic Distribution) and Lorentz double-pole relaxation models multiplied by the Fermi-Dirac distribution $F(\omega)$ respectively.

$$D(\omega) = \sqrt{\chi_0 \left[1 - \frac{1}{lnln(\frac{\tau_1}{\tau_2})}\right] ln \frac{i\omega\tau_2 + 1}{i\omega\tau_1 + 1} F(\omega)}$$

$$L(\omega) = \sqrt{\varepsilon_\infty - \frac{\omega_0^2(\varepsilon_s - \varepsilon_\infty)}{\omega^2 - 2i\gamma\omega - \omega_0^2} F(\omega)}$$

Where χ_0 and $\varepsilon_\infty$are the low and high frequency responses for the Debye and Lorentz distributions, $\hbar$ is Plank's constant, k is the Boltzmann constant, Ep is the Leonard-Jones potential energy and T is the temperature.

$$F(\omega) = \frac{1}{1 + e^{(\hbar\omega/(3/2kT) - Ep)}}$$

Only the intra-molecular O-O interaction is considered, and it assumed that all the kinetic energy is coming from the rotation of the water molecule such that

$$\frac{1}{2} m\omega^2 r(\omega) = \hbar\omega$$

This $r(\omega)$ function here is inserted into the Lennard-Jones potential to yield the following $b(\omega)$ function.

$$E_p = \left(\frac{A}{r}\right)^6 + \left(\frac{B}{r}\right)^{12}$$

$$b(\omega) = \sqrt{\frac{\chi_0}{1+e^{(\hbar\omega/(3/2kT) - Ep)}}\left[1 - \left[\frac{1}{ln(\tau\_1/\tau\_2)}\right]\right] ln\frac{i\omega\tau_2+1}{i\omega\tau_1+1}} +$$

$$\sqrt{\varepsilon_\infty - \frac{\omega_0^2(\varepsilon_S - \varepsilon_\infty)}{\omega^2 - 2i\gamma\omega - \omega_0^2}\frac{1}{1+e^{(\hbar\omega/(3/2kT) - Ep)}}}$$

Where

$$E_p(\omega) = \left(\frac{2\hbar}{m\omega}\right)^6 + B^{12}\left(\frac{2\hbar}{m\omega}\right)^6 - A^6$$

Introducing the statistical $b(\omega)$ function and fitting parameter $r(\omega)$, radius between adjacent oxygen atoms, Shubitidze and Osterberg appear to reasonably fit the water data where the n_i coefficient terms range from 1-5 and the d_i coefficient ranged from 6-14

depending on the speed at which different resonances converged. The results are as follows where the double sum terms ended up to be M=15 terms. Their MATLAB program used to be on their website and is too complex to illustrate here but has been inserted in the Appendix 6 for further reference. Figure 6-1 and Figure 6-2 compare their algorithm predictions versus compiled data by Segelstein. At first glance their algorithm appears to be a good fit on a log-log plot.

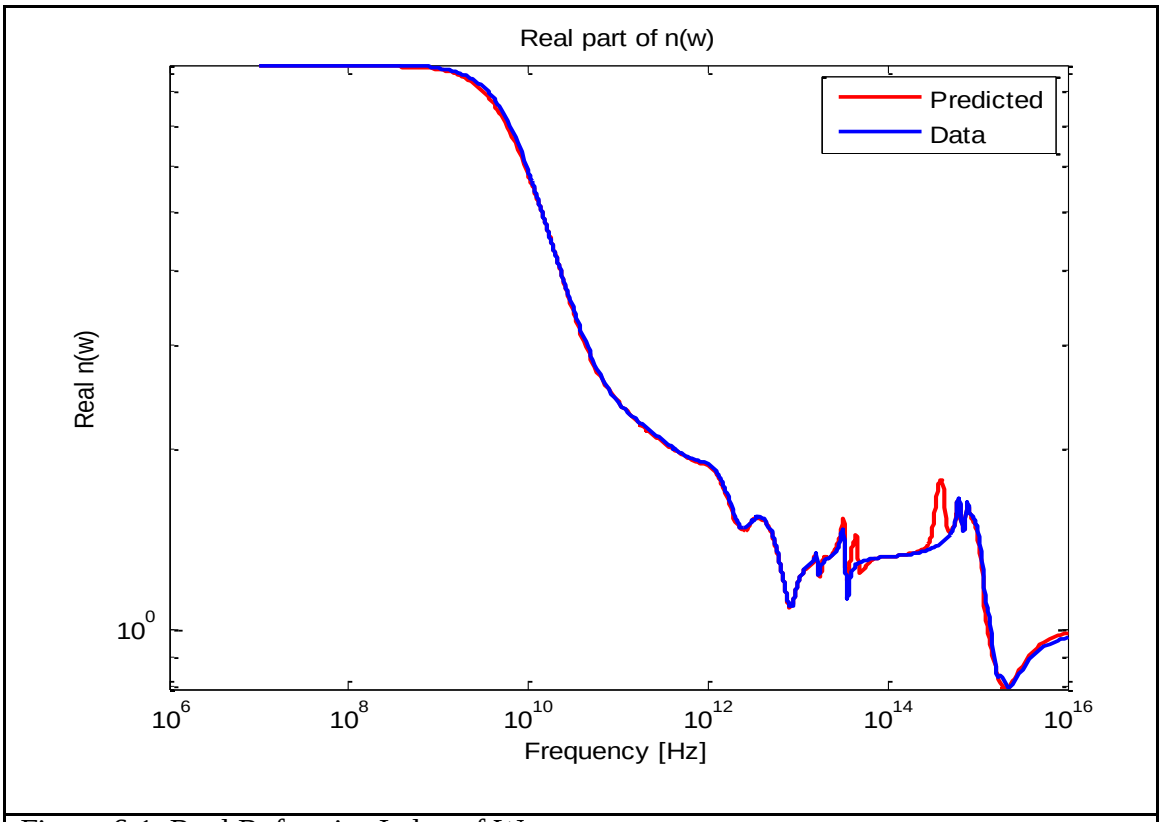

Figure 6-1. Real Refractive Index of Water.

This MATLAB output matches their paper data.

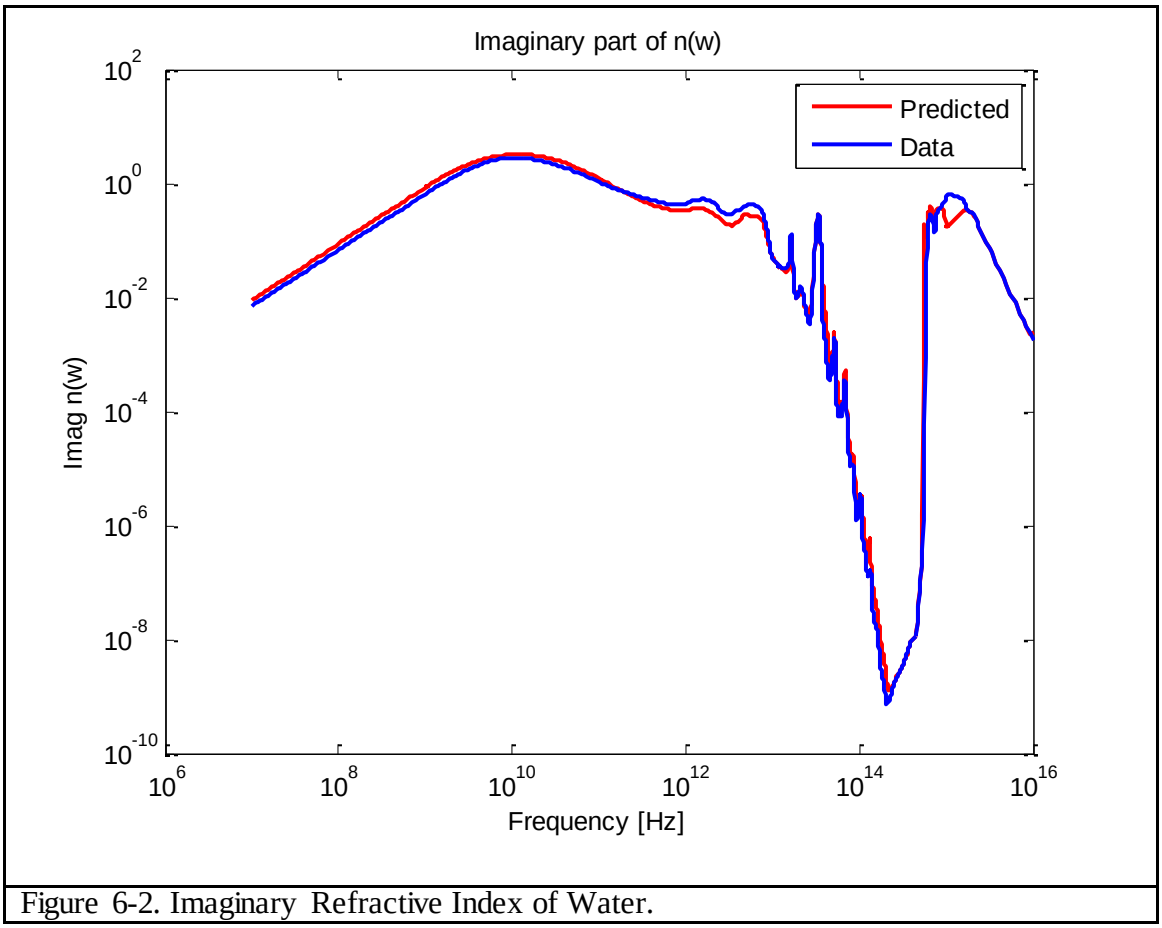

Figure 6-2. Imaginary Refractive Index of Water.

6.2 Mathematical Problems

There are many typos and discrepancies between the Shubitidze and Osterberg's paper and their MATLAB program that can be found in APPENDIX A. But a more fundamental problem is their definition of the refractive index. Permittivity is defined as the square root of the refractive index (Chapter 3). We explore Shubitidze and Osterberg's (S&O) definition of their refractive index below.

6.2.1 Definition of the Refractive Index

The definition of refractive index in the paper appears inconsistent with the classical definition of refractive index especially as it relates to the permittivity. They define the refractive index in two parts, the real part of the function a times the real part of function b, is the real part of the refractive index; and the imaginary part of the function a, times the imaginary part of the function b is the imaginary part of the refractive index.

$$n_r = Re(a) \cdot Re(b)$$

$$n_i = Im(a) \cdot Im(b)$$

If this definition is valid in general then we should be able to define the function a as a single Debye and define the function b as a single Lorentz and obtain a valid refractive index per the definition of the paper. We know that the Lorentz and Debye permittivities are analytic functions and therefore causal. We can perform Hilbert transforms of these functions to illustrate causality. The Hilbert transform of the imaginary part of the permittivity from this refractive index should give us the real part of the original function and vice versa. This bi-directional mathematical relationship is called the Kramers-Krönig relationship (Johnson 1975). Given a function like susceptibility discussed in chapter 3, we obtain

$$\chi(\omega) = \chi_1 - i\chi_2(\omega)$$

If is $\chi(\omega)$ is a complex function in the upper half plane that is analytic, and ω is a complex variable and $\chi_1$and χ_2 are real then the Kramers-Krönig relationship is given by

$$\chi_1 = \frac{1}{\pi} \mathrm{P} \int_{-\infty}^{+\infty} \frac{\chi_2(\omega')}{\omega' - \omega} d\omega'$$

$$\chi_2 = \frac{1}{\pi} \mathrm{P} \int_{-\infty}^{+\infty} \frac{\chi_{21}(\omega')}{\omega' - \omega} d\omega'$$

where P denotes the Cauchy principle value. So the real and imaginary parts of such a function are not independent of each other (Wikipedia, Kramers-Kronig Relations 2015).

However, when we perform the Hilbert transform (via the FFT algorithm) using the S&O prescription, the real part does not give the imaginary Hilbert transform. The IFFT method used to perform the Hilbert transform has been used by many including Fannin et al. (Fannin, Mlina and Charles 1993). Please see details of the Hilbert transform performed using MATHCAD in APPENDIX B.

We first define a permittivity function by adding a Debye and a Lorentz permittivity function plus 1 for the permittivity of free space. The function is described in the following plot, Figure 6-3.

$$\varepsilon_T = 1 + \varepsilon_D + \varepsilon_L$$

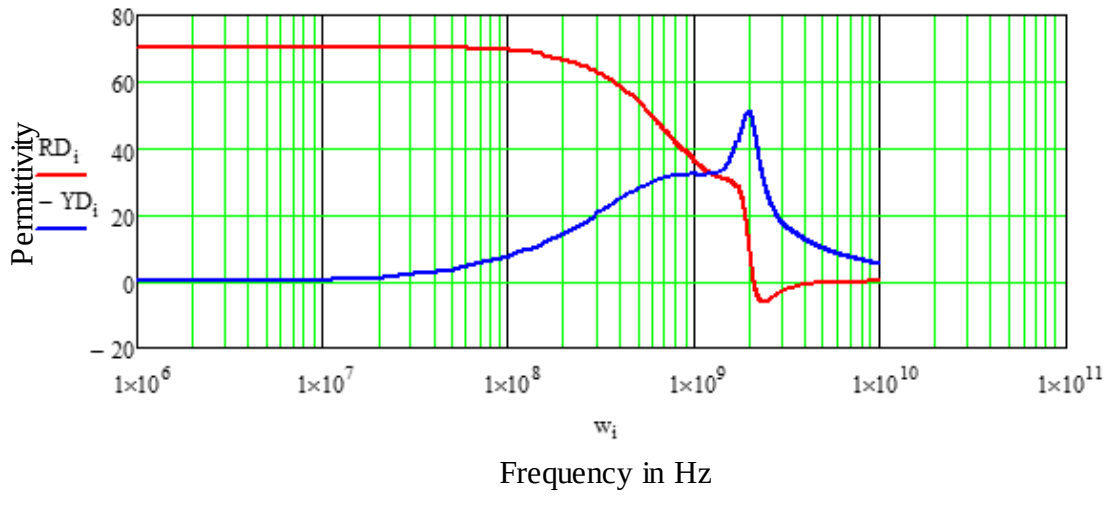

Figure 6-3. Permittivity Function That Is a Sum of a Debye and Lorentz.

We then take the same Debye function and Lorentz function and determine the refractive index based on the operation of the paper.

$$n_{r\,paper} = Re(D) \cdot Re(L)$$

$$n_{ipaper} = Im(D) \cdot Im(L)$$

$$n_{paper} = n_{rpaper} + n_{ipaper}$$

$$\varepsilon_{paper} = {n_{paper}}^2$$

We take the square of the refractive index to determine the permittivity that corresponds to this refractive index, according to the paper. The function does not look like the above function in Figure 6-4 and is not equivalent. Performing the Hilbert transform on the real part of ε_{paper} (efake in MATHCAD program in the Appendix for chapter 6) we were not able to recover the imaginary part of the original function from the real part as shown in the Figure 6-5 below.

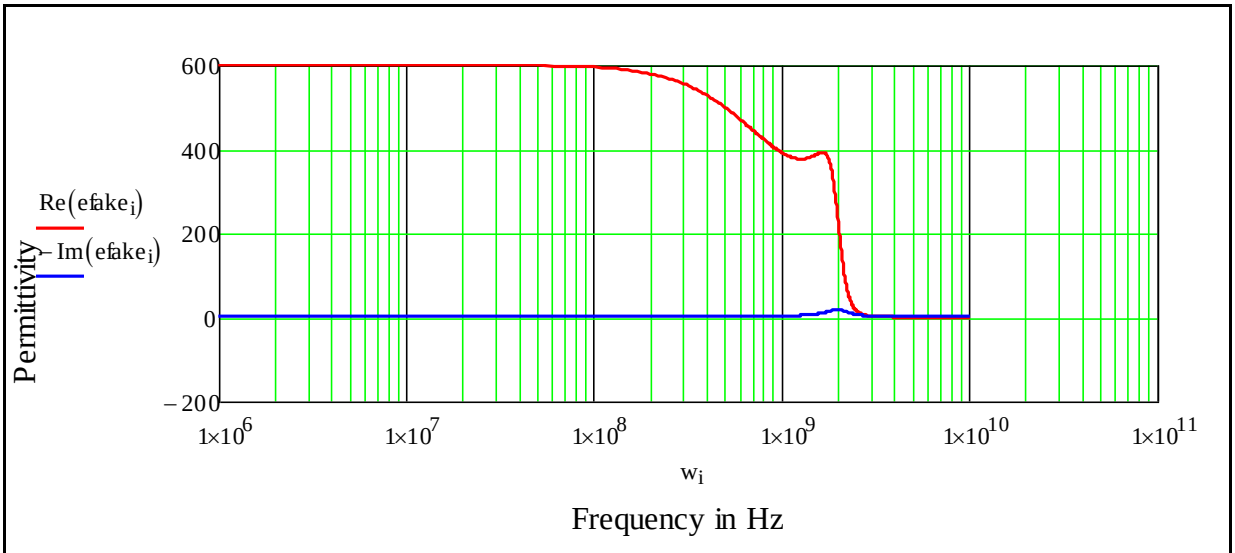

Figure 6-4. Permittivity Function That Is the Square of the Sum of a Debye and Square Root of a Lorentz Using S&O Refractive Index Formula.

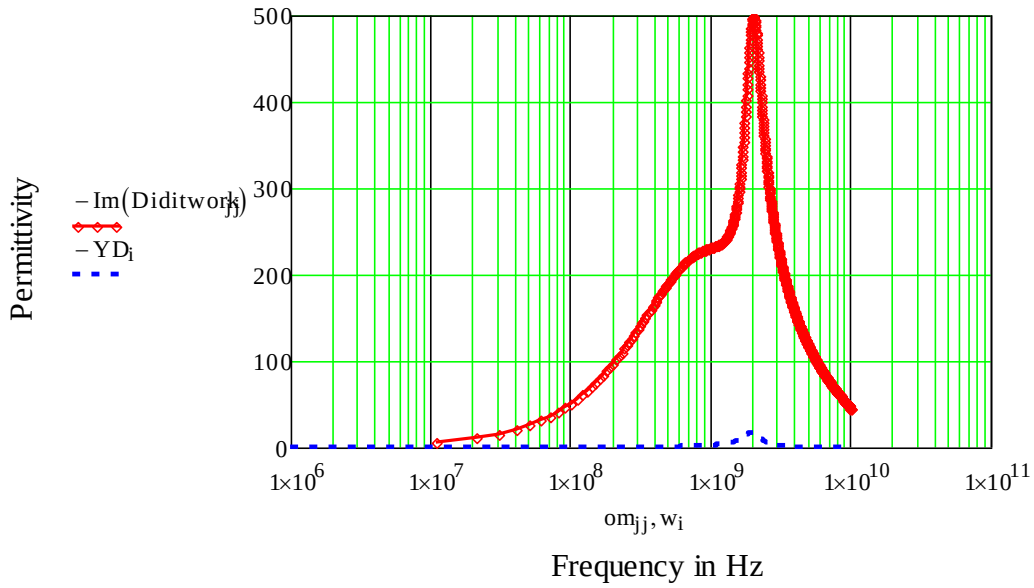

Figure 6-5. Hilbert Transform of the Real Part of the Permittivity Function Using S&O Refractive Index (Red) Does Not Yield the Original Imaginary Part (Blue).

Since there are a lot of typos in the paper and we know that the permittivity is the square of the refractive index; we assumed that perhaps S&O meant to use refractive indices throughout. So we will take the square root of the Lorentz and Debye function prior to applying the definition of the refractive index per Shubitidze and Osterberg to determine if this version yields a permittivity that is causal.

$$n_{r\,paper} = Re(\sqrt{D}) \cdot Re(\sqrt{L})$$

$$n_{ipaper} = Im(\sqrt{D}) \cdot Im(\sqrt{L})$$

$$n_{paper} = n_{rpaper} + n_{ipaper}$$

$$\varepsilon_{paper} = n_{paper}{}^2$$

But again it fails our test for causality. Taking the Hilbert transform of the real part of this function we are not able to recover the imaginary function. Please see results below in Figure 6-6 and Figure 6-7.

Original function

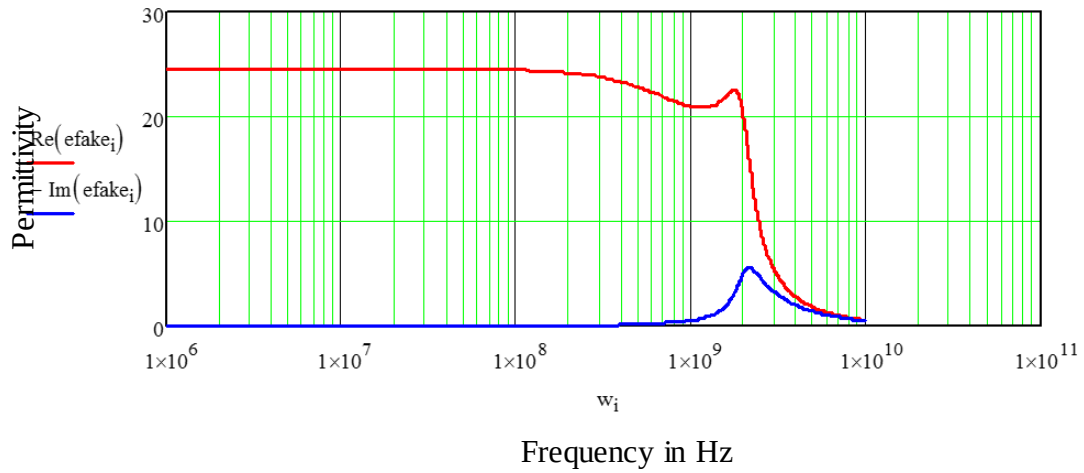

Figure 6-6. Permittivity Function That Is a Sum of the Square Root of a Debye and Square Root of a Lorentz Function Using S&O Refractive Index Definition.

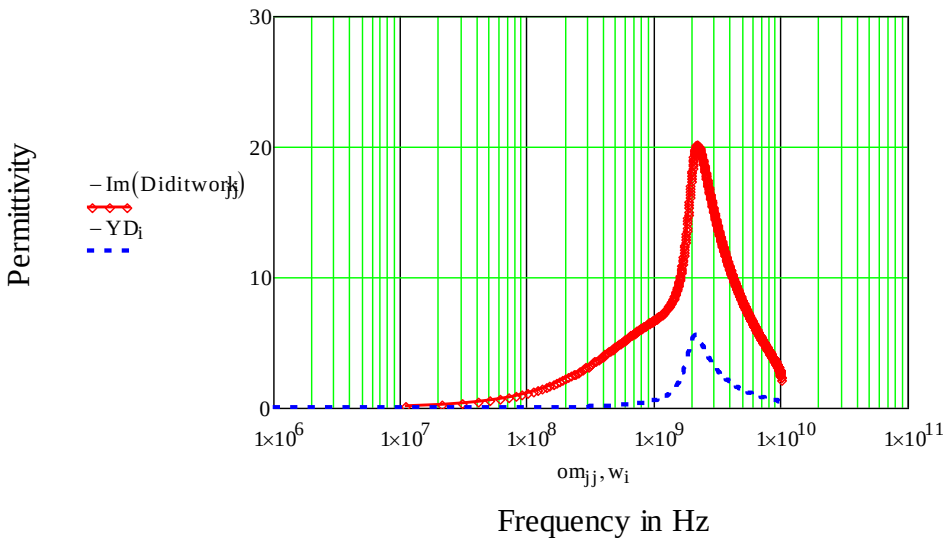

Figure 6-7. Hilbert Transform on the Real Part of the Permittivity Function That Is a Sum of a Debye and Lorentz Using S&O Refractive Index Definition Does Not Yield the Imaginary Part.

Again the discrepancy is very high. Therefore the definition of their refractive index isn't consistent with normal definition of refractive index, and the resulting permittivity is not causal because it does not have the Hilbert transform properties required by the Kramers-Krönig relation.

6.2.2 Adding Indices

The only special case where the Shubitidze and Osterberg definition of the refractive index may work is if one of the functions either *a* or *b* is essentially equal to 1. It depends on what the definition of *a* and *b* are. In the paper, it is difficult to determine whether the various functions assumed to be expressible as rational polynomials are meant to be permittivities or refractive indices. The only statement given is that *a*, is a Debye, and written

as a rational polynomial. The authors never take the square root of the function a. However b is more clearly defined as the square root of a Lorentz added to a square root of a Debye. But this creates another illegal operation.

Since Lorentz and Debye functions represent permittivities (not refractive indices), the paper appears to be adding refractive indices to create a refractive index. However, we can only add the permittivity function, since it is equivalent to adding capacitors in parallel, a clearly valid operation. The square root of a capacitor does not add in parallel to the square root of another capacitor. So even this definition where b is defined as the sum of a square root of a Lorentz and a square root of a Debye, which is adding indices and not permittivities, should be considered illegal.

If we model the material as a sum of simple harmonic oscillators, each one having a resonance, then, we can show that the effect is the same as adding their permittivities. But if the total permittivity is $\varepsilon_T = \varepsilon_1 + \varepsilon_2$; then the total index, $n = \sqrt{\varepsilon_1 + \varepsilon_2}$. Therefore $b^2 = D^2 + L^2$, where D and L are Debye and Lorentz functions respectively and $b = \sqrt{D^2 + L^2}$. This is not what the paper shows. In the paper $b = \sqrt{D} + \sqrt{L}$ and therefore this does not make sense.

6.3 Physical Inconsistencies

There are many assumptions and over simplifications in the Shubitidze and Osterberg paper that are at best risky. In addition, parameters are mixed up such that the electronic excitation frequency and vibration frequency are considered the same. The mass of the

molecule is substituted for the mass of the electron and their assumption on a varying radius of adjacent oxygen atoms and of a Fermi-Dirac distribution and degrees of freedom are not grounded in physical reality. Some of these are illustrated below.

6.3.1 Thermodynamic Problems

Shubitidze and Osterberg only consider the adjacent oxygen-oxygen interaction for the potential energy term in their Fermi-Dirac expression. Dr. James Adams states this is a very poor representation of water as the O-H bond and H-H interactions are still significant and comparable to the O-O interactions.

$$E_p = \frac{k1q \cdot 2q}{r}$$

Since r, the distance between oxygen atoms is greater due to repulsive forces between adjacent oxygen atoms; we would expect this O-O interaction to be much weaker. In addition the degrees of freedom for the kinetic energy term in the Fermi-Dirac Distribution Function has only three degrees of freedom 3/2kT; which would be true for a monatomic gas, for a diatomic gas this would be 5/2kT because of two addition rotational components. However water is tri-atomic and even more complex as it is not a linear molecule.

6.3.2 Frequency Discrepancy

The frequency associated with electronic excitations in $E = \hbar\omega$ is not the same as frequency of the molecular vibrational or rotational frequencies of water where $\frac{1}{2}m\omega^2 r(\omega)$. So solving for ω using the equation below (as done in the paper) assumes these ω frequency terms are the same.

$$\frac{1}{2}m\omega^2 r(\omega) = \hbar\omega$$

In addition as we saw in section 6.3.1, there are many rotational and vibrational modes of water and this equation only addresses the adjacent oxygen rotation relative to each other with a radius of $r(\omega)$and ignores all other modes and interactions. This $r(\omega)$ is used as a function of the frequency in the Lennard Jones potential. The authors use this as fitting parameter as a function of frequency and $r(\omega)$ varies from 0.18 Angstroms to $2 \cdot 10^{-5}$meters with about 3 Angstroms at the optical valley. But the authors claim that this is physically reasonable because it describes natural water network vibrations. There are two problems with this. One is that they claimed the $r(\omega)$ is the distance between adjacent oxygen atoms and the energy was coming from the rotational energy of the water molecule alone. Secondly although the potential energy drops off as 1/r and this could go on indefinitely there would be many other water molecules interfering in between. And finally the minimum $r(\omega)$is much smaller than the minimum distance observed by Bergman et al to be 2.7 – 2.8 Angstroms between adjacent oxygen atoms (U, et al. 2007).

The other problem was that the mass m used in the program to calculate the kinetic energy used in their MATLAB program was the electron mass. It should have been the mass of the molecule.

6.3.3 The Fermi Dirac Function

Shubitidze and Osterberg state "We multiply the refractive index parts by the Fermi-Dirac distribution to compensate for the drastically reduced density of states in the visible window range". But the physical justification for this assumption is not given.

When we plot the normalized Fermi-Dirac function using the author's MATLAB program in Figure 6-8 we are not sure what the significance is of the function beginning at 0.5, then reducing to zero in the optical valley and going back up to 1, a higher energy state at the frequencies above the optical valley frequencies. Why would the electrons jump to a higher energy state after having no states? Furthermore for photons the Bose Einstein equation is used not the Fermi Dirac. In their program they say Bose Einstein equation but they actually use the Fermi Dirac expression as they do in the paper. Dr. Ponce agreed he has not seen any known material to behave this way.

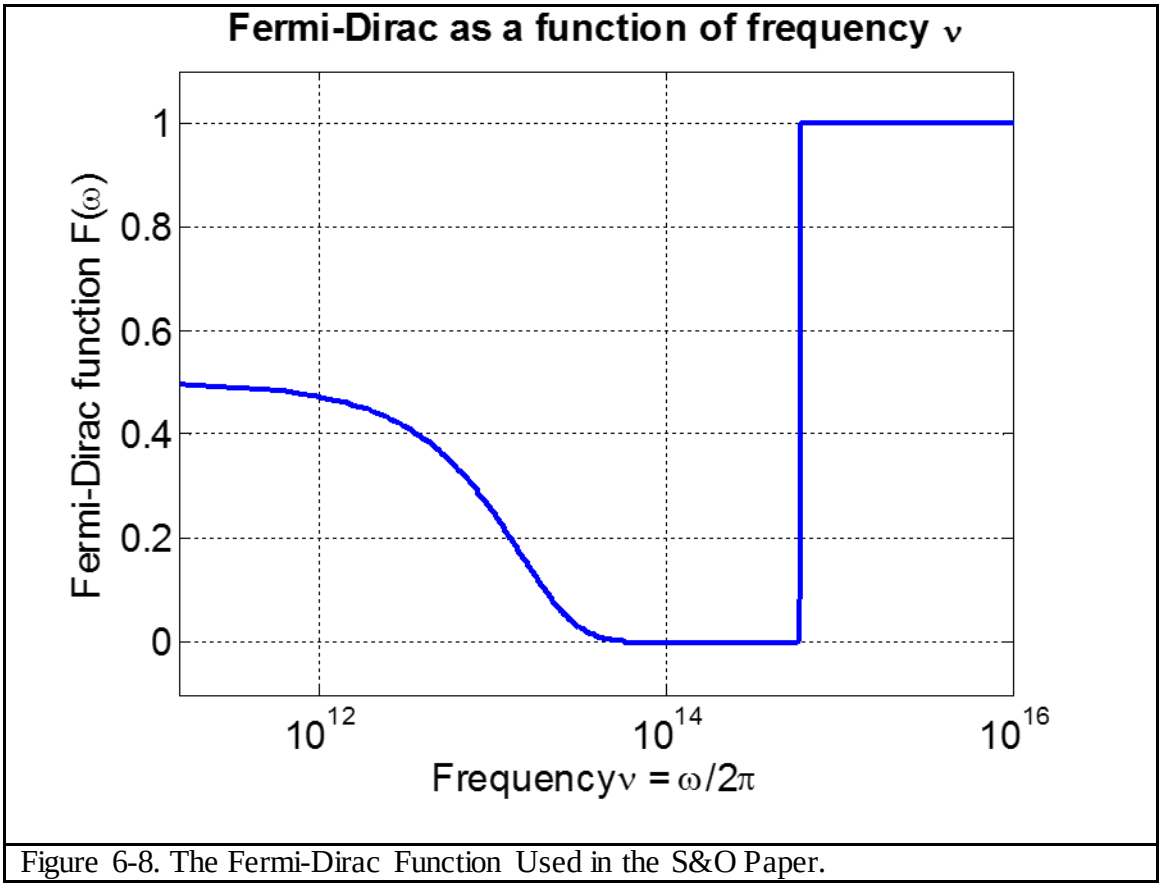

Figure 6-8. The Fermi-Dirac Function Used in the S&O Paper.

6.4 Is the S&O Permittivity Function Causal?

Given that so many of the definitions in the Shubitidze and Osterberg paper are either illegal (in the sense of following no known physical law) or unjustified, physically or mathematically, it is imperative to ensure that their model is causal otherwise it is strictly a model that tried to fit water but cannot be applied to any other material which is ultimately the objective of this dissertation.

In order to be able to determine causality we apply the Hilbert transform to the functions provided in the paper. However due to the inconsistencies with the paper and the program mostly related to typos and the complexity of the equations coupled with an enormous quantity of fit parameters, this proved to be too difficult to transform in a closed form. So we first verified that the program generated the same function as plotted in the paper and assumed that their MATLAB program exhibited the correct equations. We then proceeded to manipulate the program to generate terms using the first term of function a, which we will call M=1 and then all 15 terms of a, which we called M=15. Numerical tables of these values were directly exported from the author's program and then converted from refractive index to permittivity. The data was logarithmically spaced and then was linearly interpolated to perform a Hilbert transform on the imaginary part to generate the real part (within a constant) of the original function. This was performed on both M=1 and M=15 terms.

In order to ensure that our procedure was correct and that it was valid in the range of the water model, a Debye mimicking the properties of water at the low frequencies and a Lorentz mimicking the water resonances at higher frequencies was demonstrated using the same MATLAB program written to generate the Hilbert transform of a given function. The program written can be found in Appendix A. Below in Figure 6-9, a Debye function is chosen with the same low frequency slope and resonance of water.

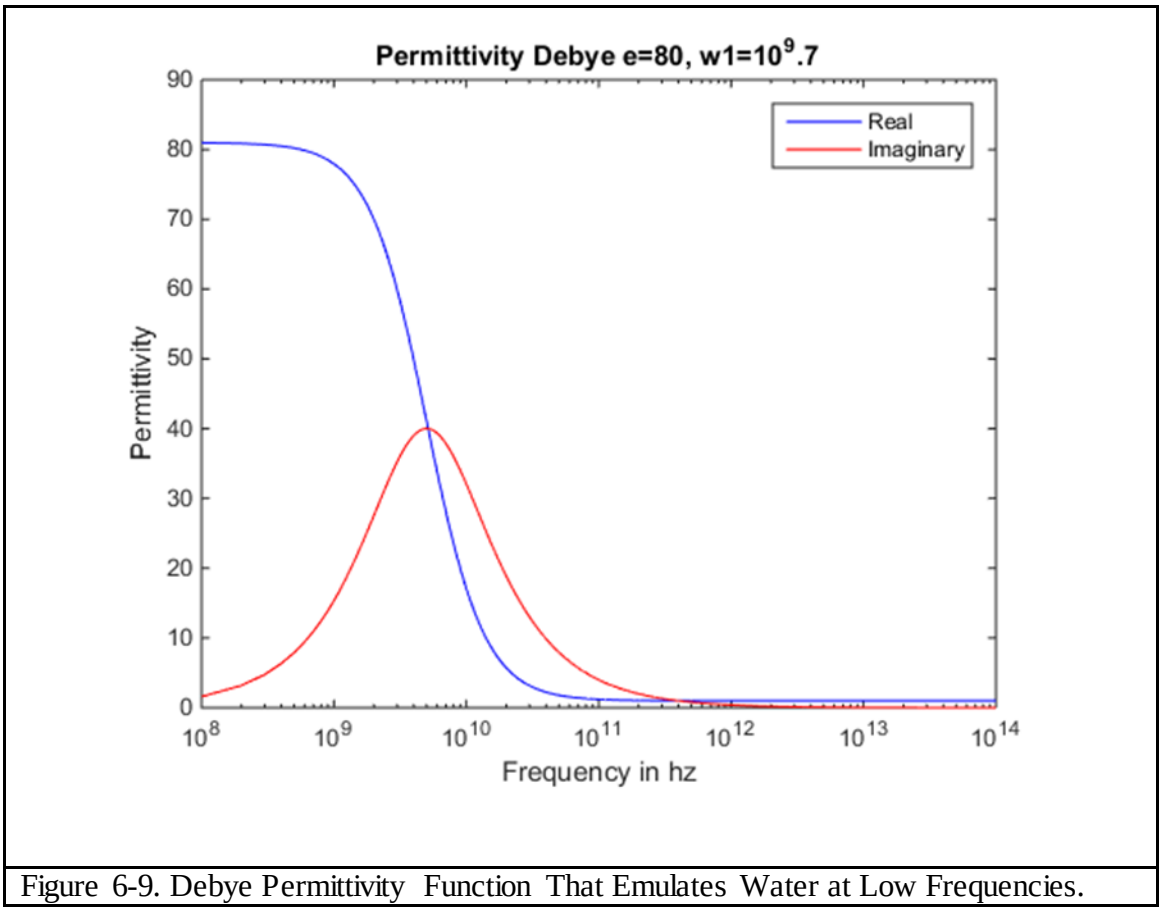

Figure 6-9. Debye Permittivity Function That Emulates Water at Low Frequencies.

Also below in Figure 6-10 a higher resonant frequency Lorentz function is chosen to mimic the resonances of water.

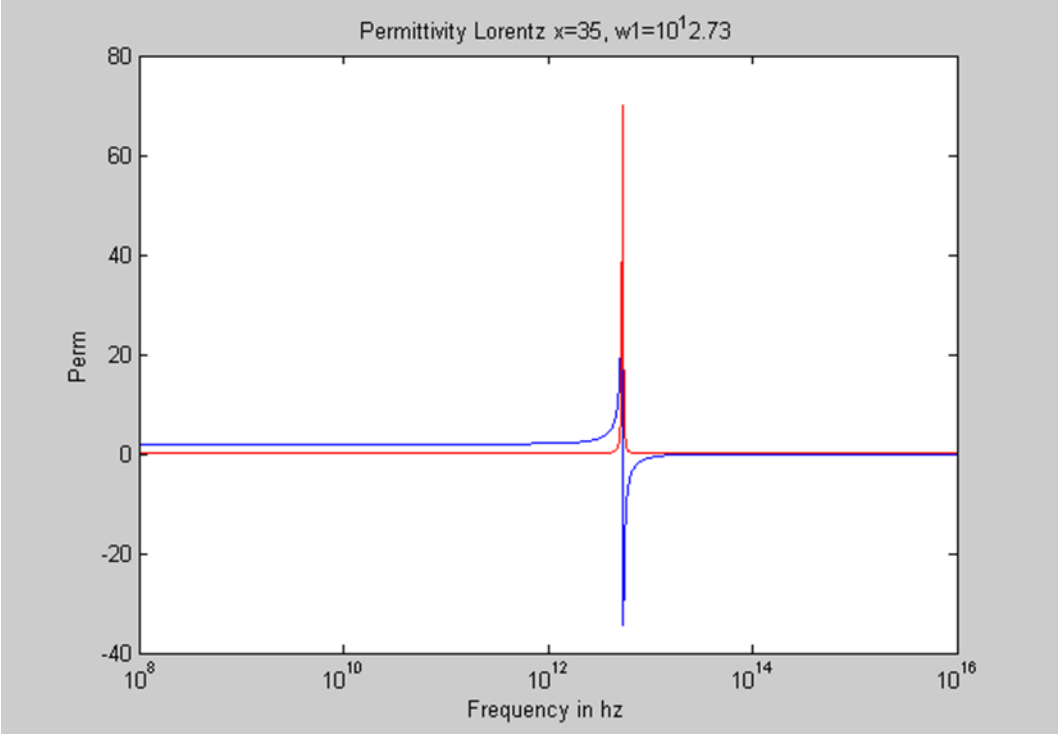

Figure 6-10. A Lorentz Function That Mimics the Resonances of Water.

In both instances using the program we wrote, applying the Hilbert transform on the imaginary part of the function we were able to recover the real part of the function exactly. Because the Hilbert transform gives the susceptibility, for the surrounding background 1 was added to the transform. Plots below show the original and recovered real permittivities from the imaginary Debye and Lorentz permittivities respectively.

As shown in Figure 6-10 a higher resonant frequency Lorentz function is chosen to mimic the resonances of water.

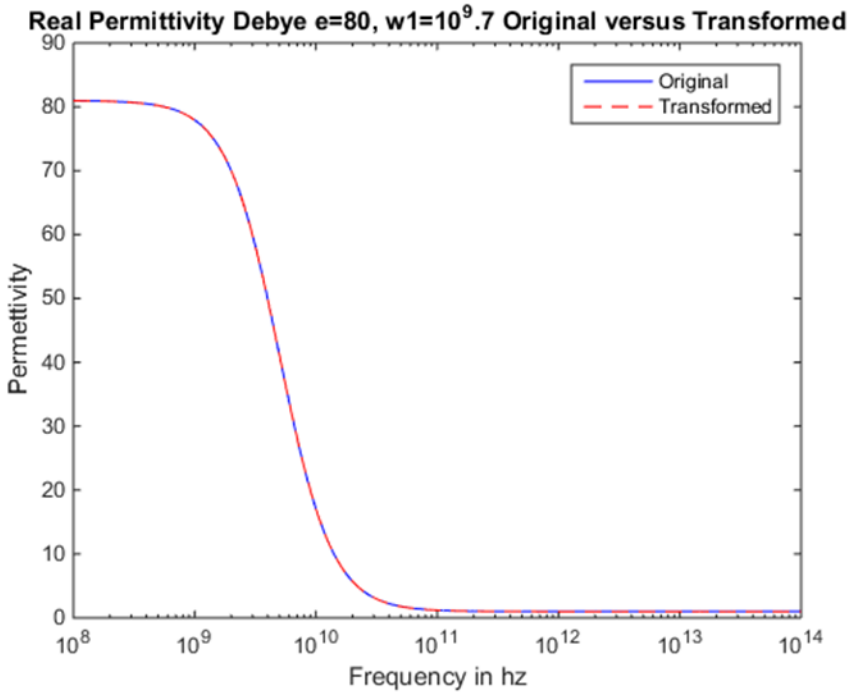

Figure 6-11. Real Part of Debye Function Recovered from Hilbert Transform of Imaginary Part Using a Semi-Log Plot.

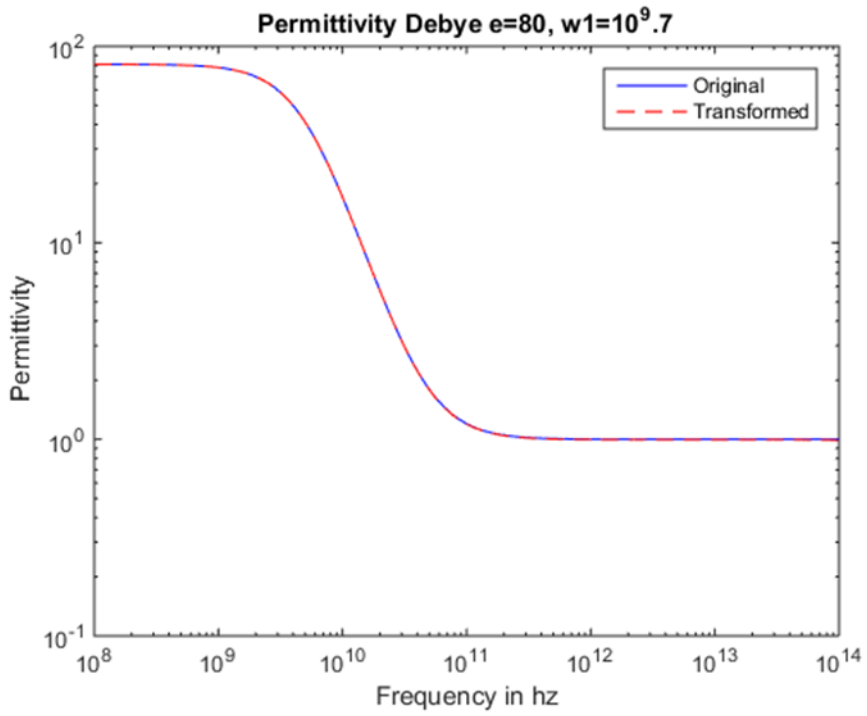

Figure 6-12. Real Part of Debye Function Recovered from Hilbert Transform of Imaginary Part Using a Log-Log Plot.

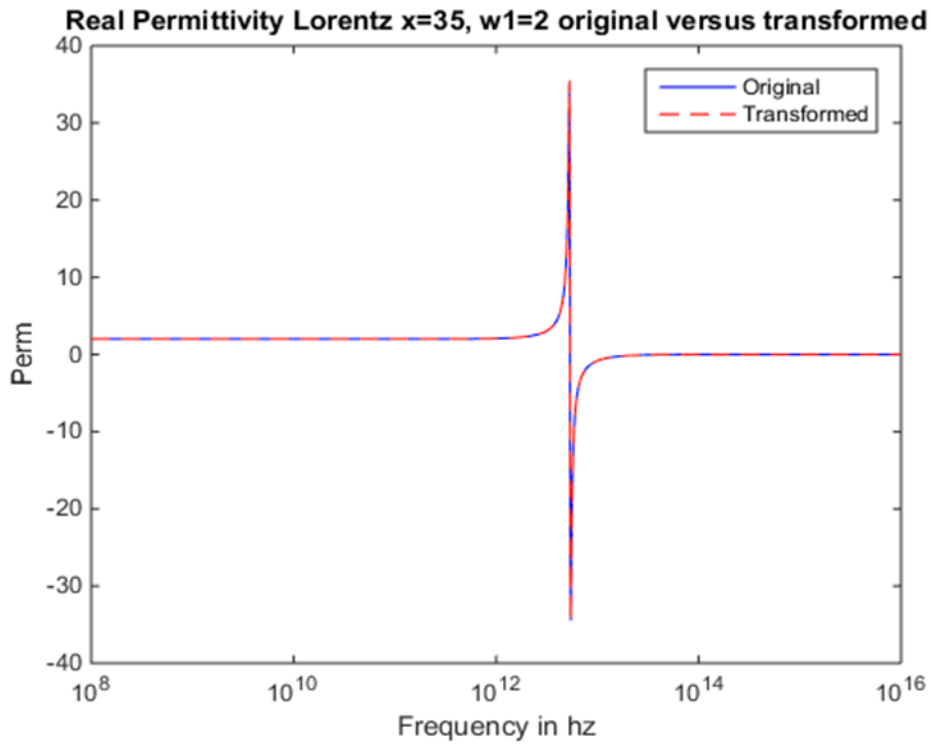

Figure 6-13. Real Part of Lorentz Function Recovered from Hilbert Transform of Imaginary Part Using a Semi-Log Plot.

Given now that we trust our Hilbert transform procedure illustrated on known Debye and Lorentz causal models, we then proceeded to the first order fit using the rational function *a* where M=1. The real and imaginary permittivity of M=1 numerically extracted from the author's program are shown below. The imaginary part is linearly interpolated and reconstructed below showing that it generates the same function. However after performing the Hilbert transform we were not able to recover the real part of the M=1 function. We also verified that the Debye function we proved is causal, overlays on the M=1 function so we have demonstrated that our procedure works in the frequency range of interest.

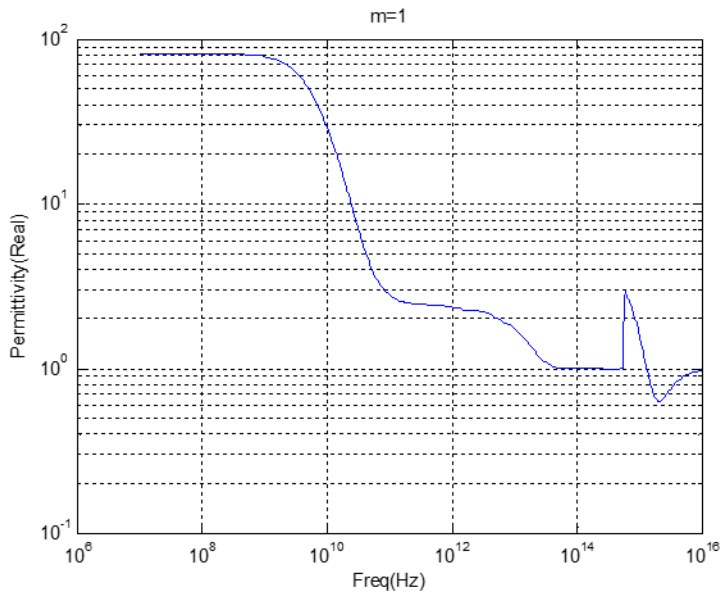

Figure 6-14. Real Part of Water Permittivity M=1 Function from S&O.

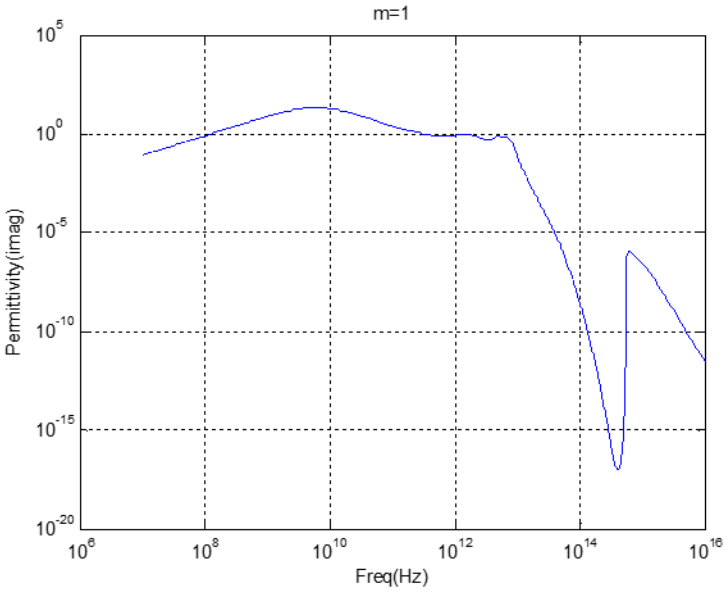

Figure 6-15. Imaginary Part of Water Permittivity M=1 Function from S&O.

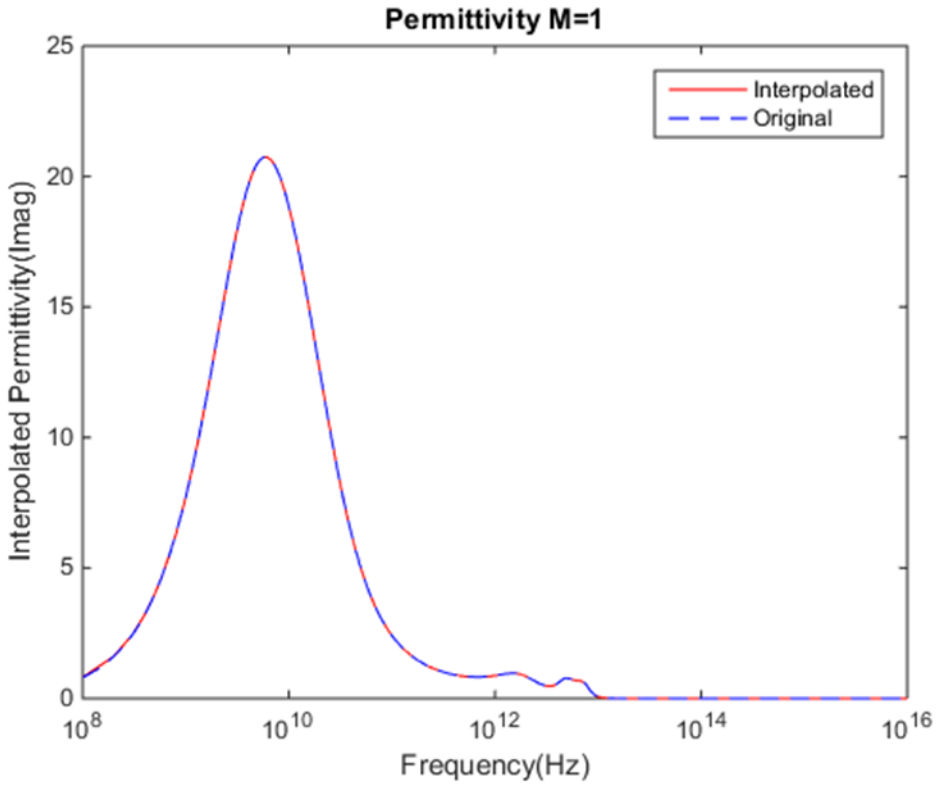

Figure 6-16. Imaginary Interpolated Part of Water Permittivity M=1 Function from S&O.

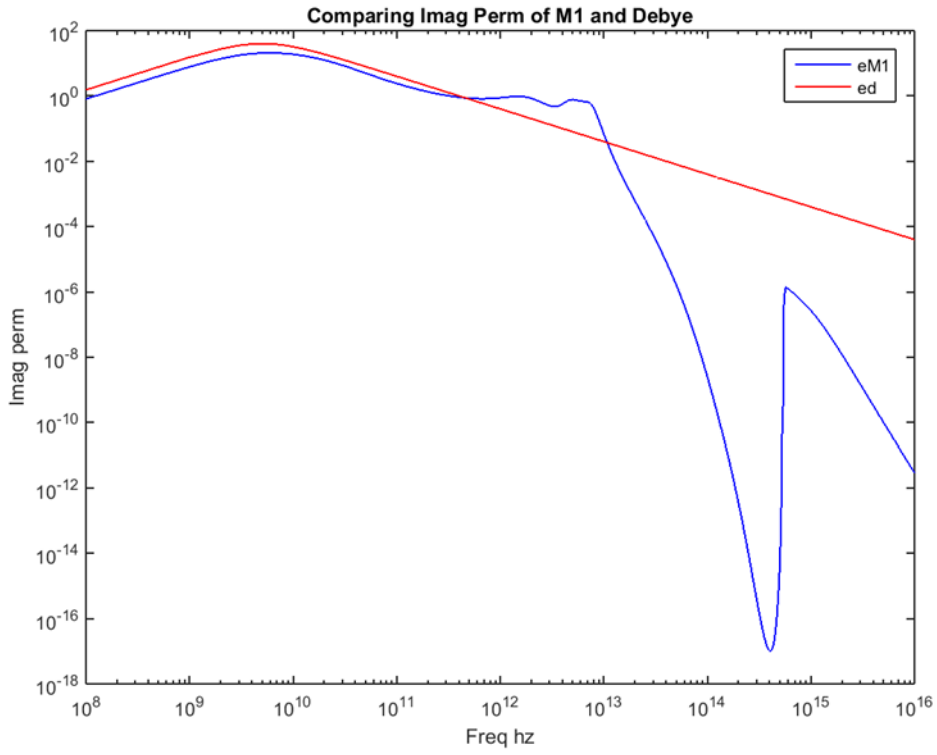

Figure 6-17. Imaginary Part of Water Permittivity M=1 Function from S&O Compares Well with the Debye Function We Chose to Overlay at the Lower Frequencies.

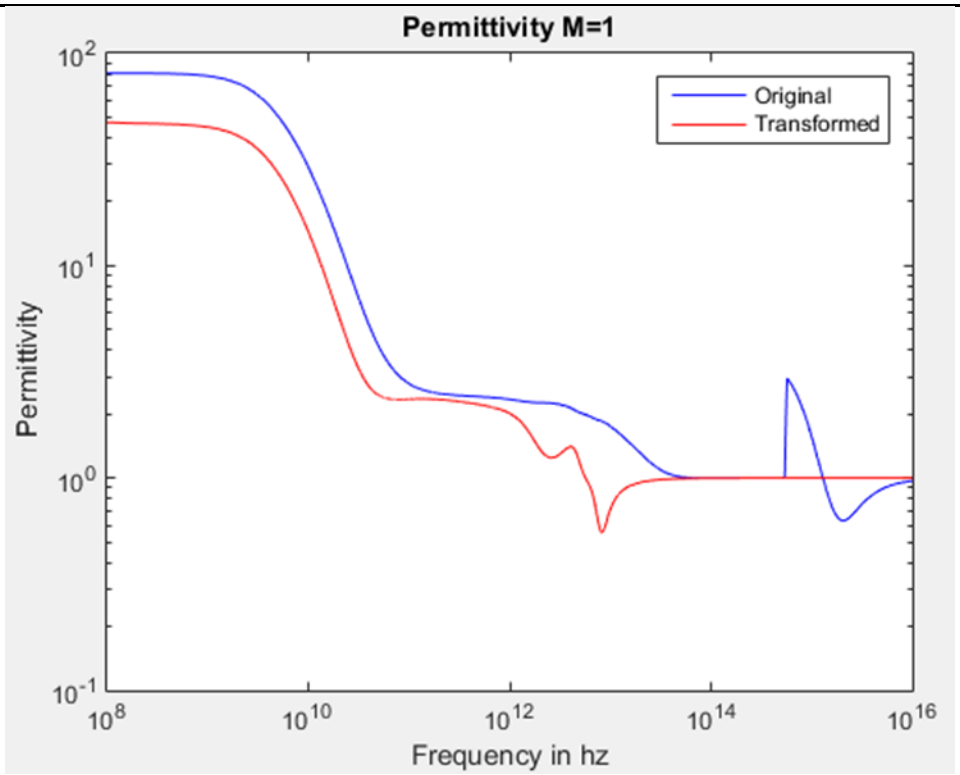

Figure 6-18. Hilbert Transformed Imaginary Part of M=1 Function from S&O Does Not Match the Original Real Part of the Function Log-Log Plot.

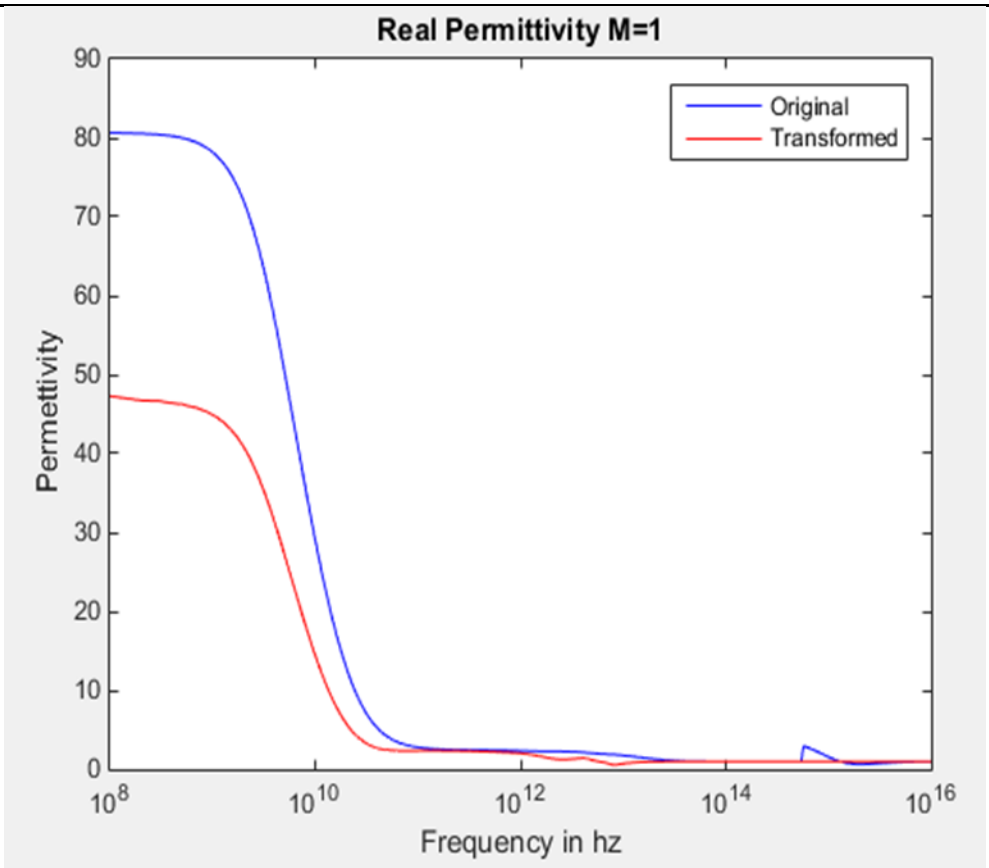

Figure 6-19. Hilbert Transformed Imaginary Part of M=1 Function from S&O Does Not Match the Original Real Part of the Function Semi-Log Plot.

Plotting the results both in log-log and semi-log show that M=1 is not a causal function. So our method is repeated on M=15 with all the terms used to generate Shubitidze and Osterberg's model of water. However in this case the results are the same: we are not able to recover the real part of their function by a Hilbert transform on the imaginary part of their function.

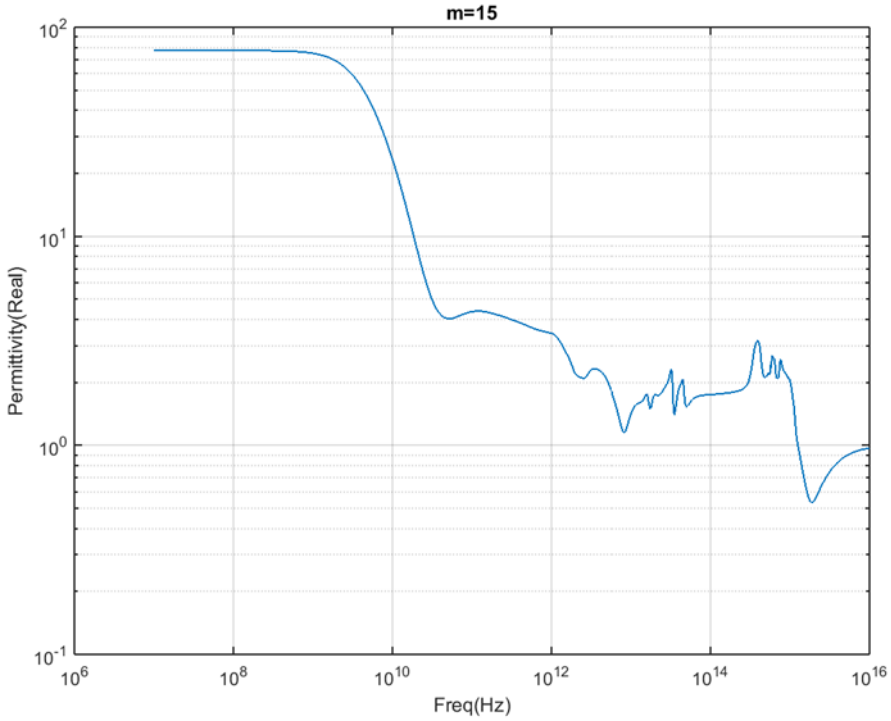

Figure 6-20. Real Part of Water Permittivity M=15 Function from S&O.

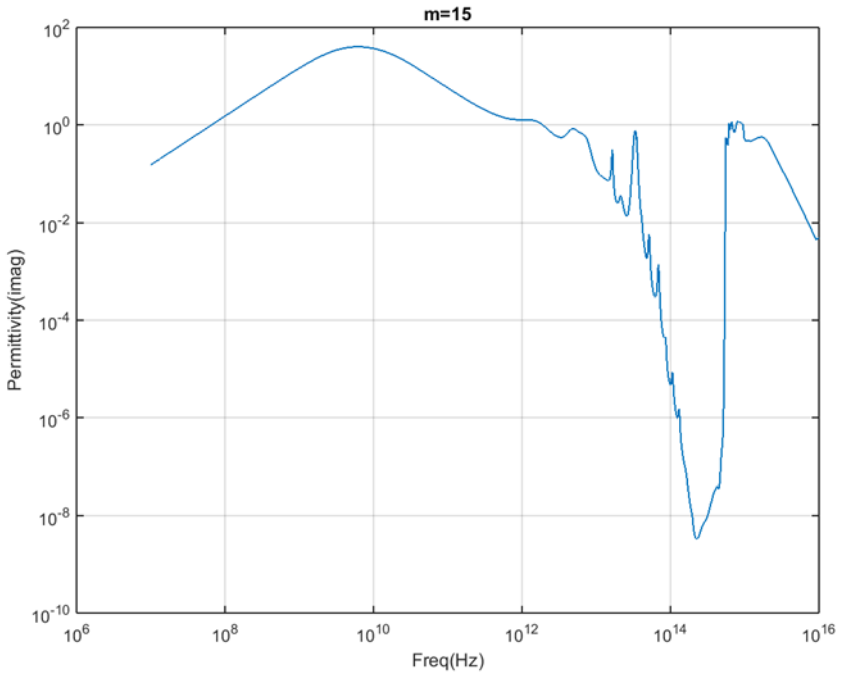

Figure 6-21. Imaginary Part of Water Permittivity M=1 Function from S&O.

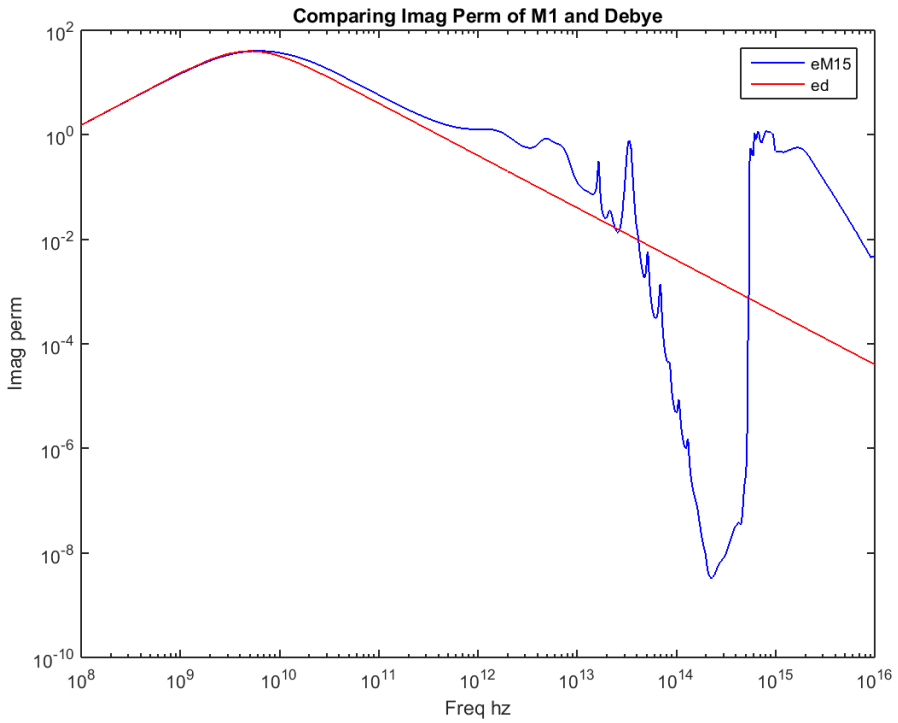

Figure 6-22. Imaginary Part of Water Permittivity M=15 Function from S&O Compares Well with the Debye Function We Chose to Overlay at the Lower Frequencies.

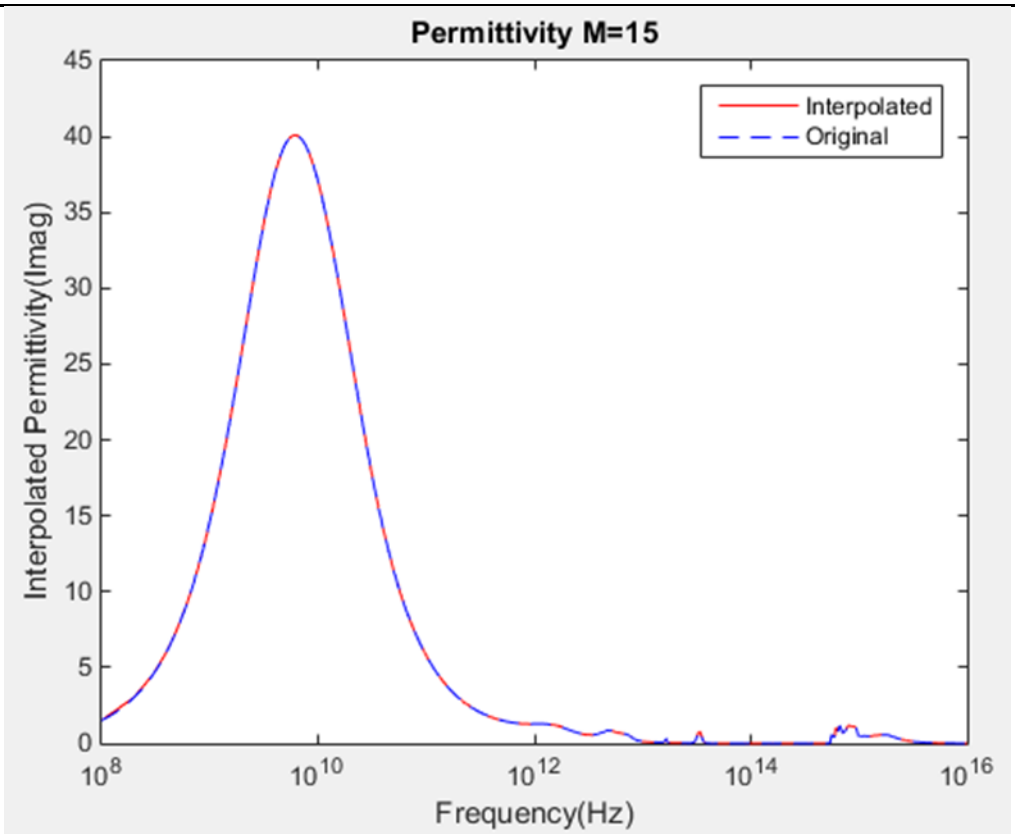

Figure 6-23. Imaginary Interpolated Part of Water Permittivity M=15 Function from S&O.

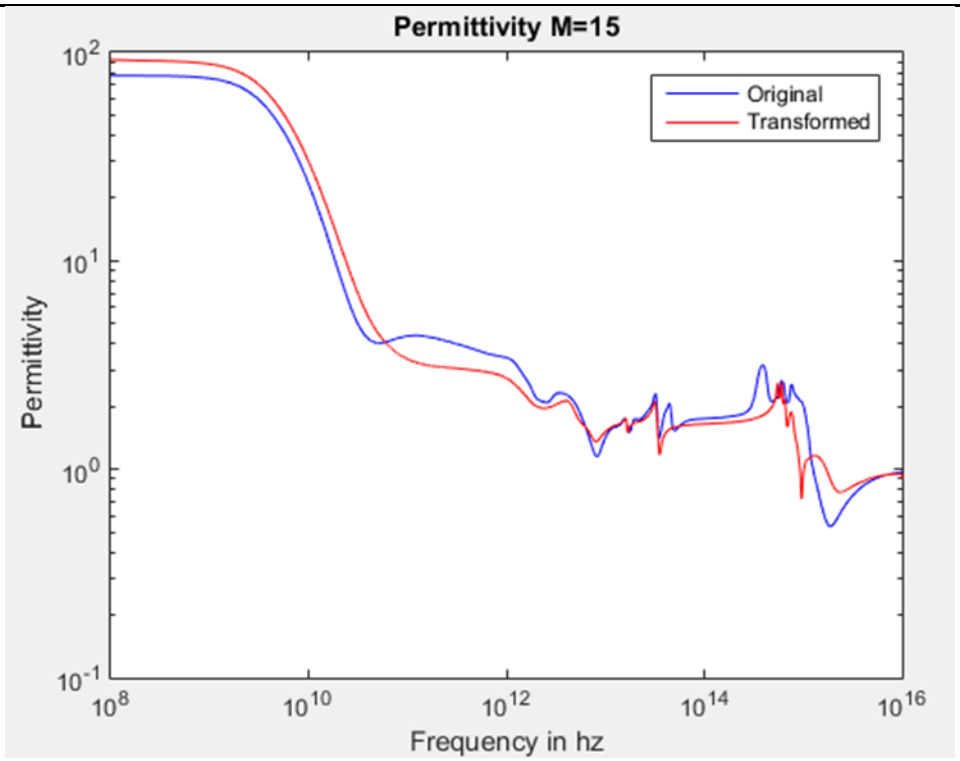

Figure 6-24. Hilbert Transformed Imaginary Part of M=1 Function from S&O Does Not Match the Original Real Part of the Function Log-Log Plot.

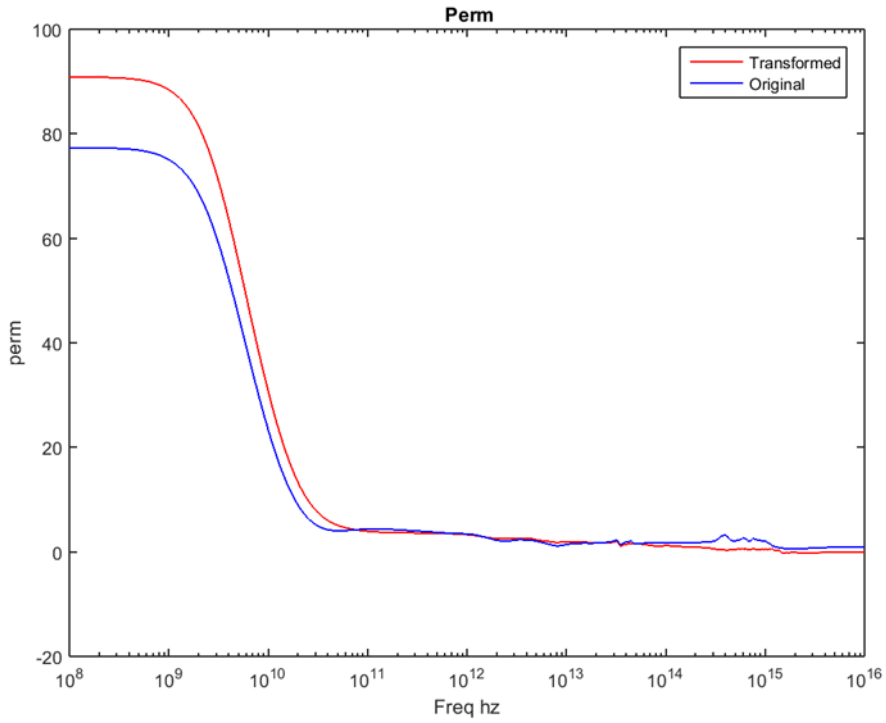

Figure 6-25. Hilbert Transformed Imaginary Part of M=15 Function from S&O Does Not Match the Original Real Part of the Function Semi-Log Plot.

We also applied sum rules (Shiles 1980) to check our work at the low frequencies for M=1, M=15 and our Debye that we used before to further verify that the Hilbert transform was correct. We were able to generate the same value at low frequency in each case.

$$\int_0^\infty \frac{2}{\pi}\frac{\varepsilon(\omega)}{\omega}d\omega = \varepsilon(0)$$

Function	FFT Method Using Hilbert ε(0)	Sum Rules ε(0)
Debye	80	79.697
M=1	46	45.375
M=15	90	89.56

Table 6-1. Sum Rules Summary

So we can conclude that our method is correct and that the model offered by Shubitidze and Osterberg is not causal. Both the individual terms as well as the complete terms together are not causal. So why did the water data appear to match their model in their paper? Further examination of their results and plotting their prediction against Segelstein's data on semi-log plot illustrate a match that is not as good as it seems in a log-log plot shown in Figure 6-24 and Figure 6-25 especially in the imaginary part in the optical valley.

But the key point here is that even though their fits to the real and imaginary parts of water appear to get close to the measured data, their process is yielding real and imaginary parts that violate the Kramers-Krönig relations.

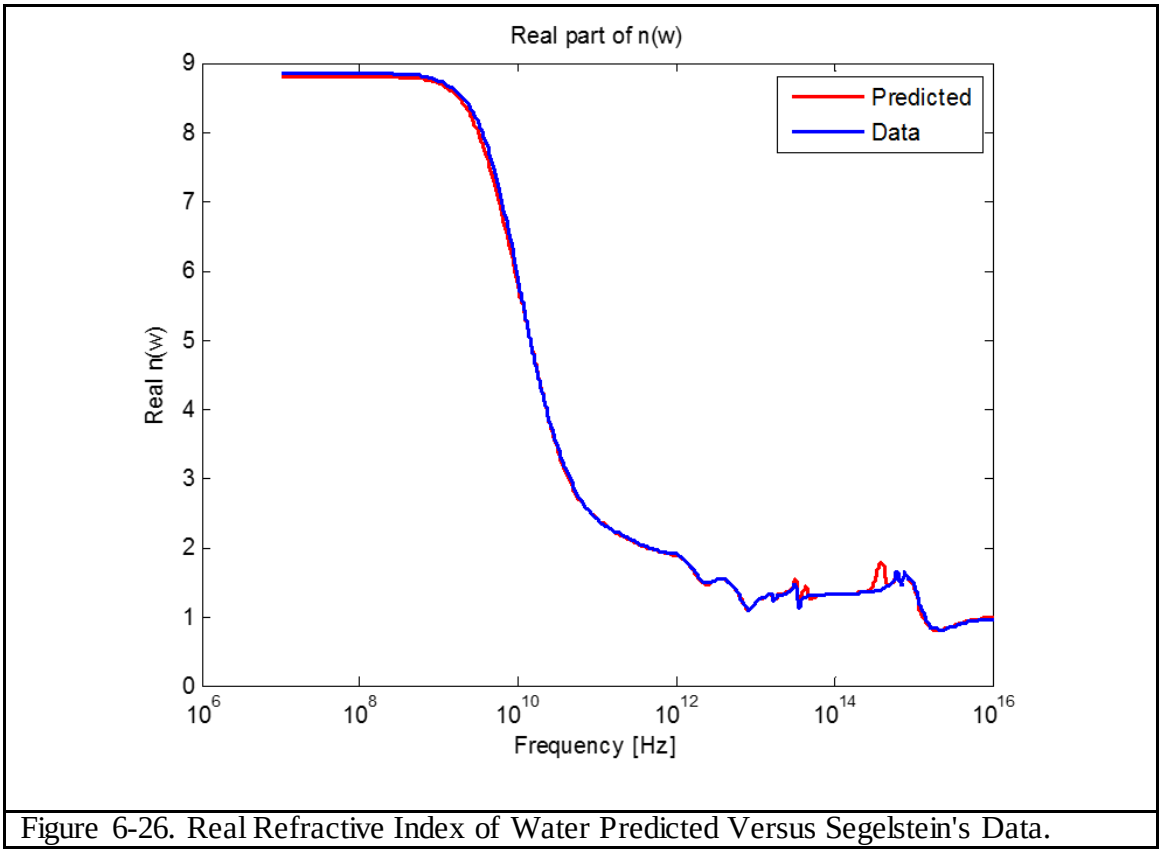

Figure 6-26. Real Refractive Index of Water Predicted Versus Segelstein's Data.

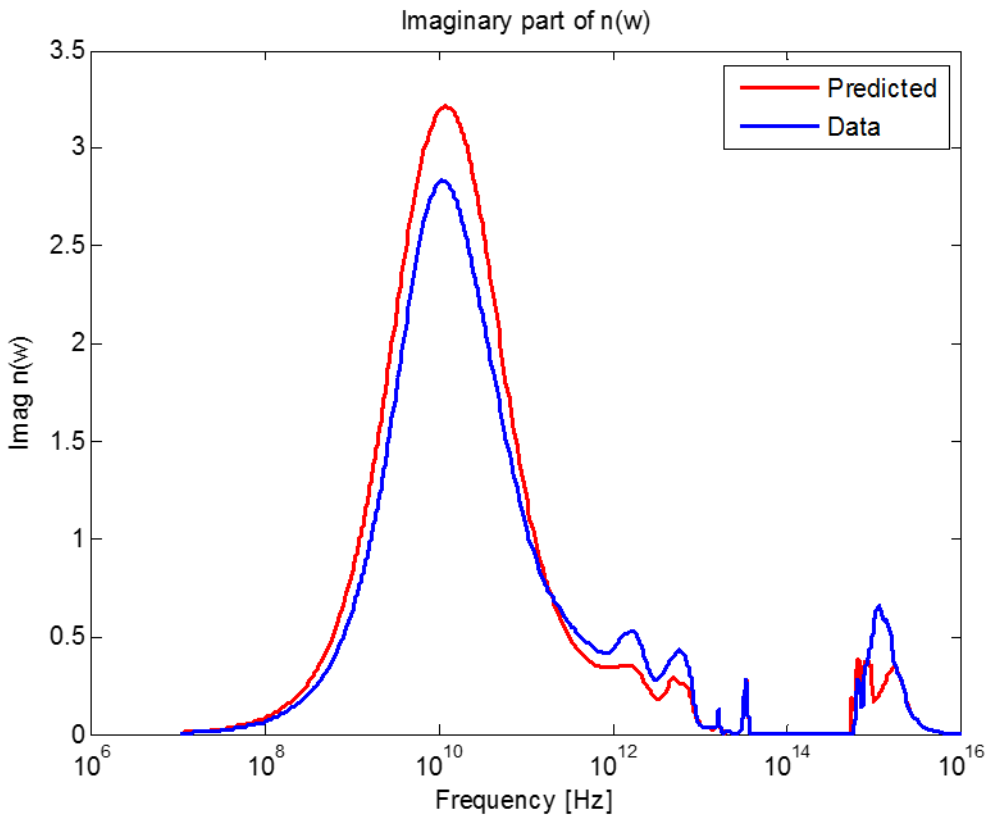

Figure 6-27. Imaginary Refractive Index of Water Predicted Versus Segelstein's Data.

Therefore we are only left with one model of water that is causal – the Diaz model.

CHAPTER 7

CONSTRUCTING THE CIRCUIT MODEL FOR A DEBYE OR LORENTZ MATERIAL

So we have shown that the Diaz-Alexopoulos model of water is the only model of water that is causal and produces the window (optical valley of water). And as we discussed before, Brillion has demonstrated circuit models are equivalent to the molecular material models. Therefore we can design a material (Debye or Lorentz) using circuits and then add the zero circuit to create a window.

We do not know of any Lorentz solid that resonates at the RF frequency of interest where we can measure (2.5 - 5 GHz). So we must design and artificially create both our Debye and Lorentz materials.

In order to design our Debye or Lorentz material using circuits we must have a method to design an effective medium. We can use HFSS (High Frequency Structural Solver) to physically model a material. But first we need to create an effective medium model of our Debye and Lorentz knowing its individual sheet capacitance and desired effective bulk permittivity.

If we have a three dimensional solid that can be explained by a single tube of elements we have to figure out the effective dielectric of this tube of elements.

If we have a cascade of elements and we want to calculate the effective permittivity of this medium; there are two ways to accomplish this.

Seymour Cohn says we need to calculate the shunt susceptance of an obstacle, (a single shunt element), calculate the individual shunt susceptance then cascade them to obtain a medium and determine the effective permittivity in a transmission line (Cohn 1948). So if we know the single obstacle susceptance we can connect it with a length of transmission line.

The low frequency unit cell approximation (Laplace Method) looks at each shunt element contained in an individual box. And based on the properties of the single box, if we have a uniform density of those boxes, we know they will behave the same and we obtain the properties of the material.

Both methods are expounded below.

Excess Capacitance

If we solve for an empty space unit cell we get the empty capacitor capacitance C_0. If we now put one metal square in the unit cell there is excess capacitance. The capacitance increases due to the polarization of the square, we obtain C_1.

The relative effective permittivity is $\varepsilon_r = \frac{C_1}{C_0}$ because the capacitance of the empty cell has increased by the change in this capacitance which is the excess capacitance $\Delta C = C_1 - C_0$.

This delta capacitance is frequency independent for a metal.

Cohn Method

For the Cohn method we can determine the individual shunt susceptance or capacitance of a single obstacle given by the equations below.

For the diagram shown in Figure 7-1 the reflection coefficient is

$$S11 = \frac{Y_0 - (Y_0 + Y_{shunt})}{Y_0 + (Y_0 + Y_{shunt})} \rightarrow Y_{shunt}(\omega) = Y_0 \left(\frac{-2 \cdot S11}{1 + S11}\right) \text{ and}$$

$$Y_0 = \frac{1}{377} \cdot \frac{b}{a} \text{ and } j\omega C_{shunt} = Y_{shunt}.$$

The capacitance of the unit cell is given by

$$C_{empty} = \varepsilon_0 \frac{s \cdot b}{a} \text{ if}$$

We assume the empty cell is filled with air, and the squares are floating in air.

Laplace (Unit Cell) Method

Then the effective relative permittivity in the low frequency limit per the Laplace equation is given by the following equation.

$$\varepsilon_r(\omega) = \frac{C_{empty}+C_{shunt}}{C_{empty}}$$

This assumes no wave interaction between the layers per the Laplace equation.

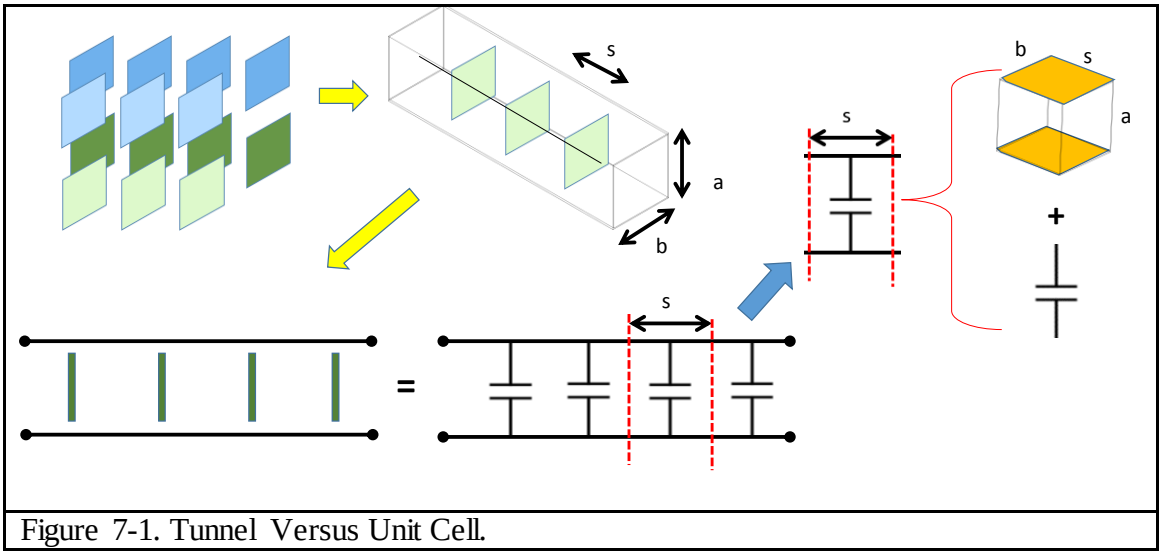

Figure 7-1. Tunnel Versus Unit Cell.

This unit cell is not a continuum like a tunnel. A stack of these cubes based on the Laplace equation would constitute the transmission line. The difference between the properties in the cube (Laplace method) and the shunt susceptance properties in the transmission line (Cohn Method) to determine the relative permittivity of an artificial medium is that the Cohn Method takes into account the periodicity of the obstacles and the cascade interacts with the transmission line which is not taken into account in the low frequency limit Laplace model.

We use the Cohn equations for a metal strip media (described below) to determine the required geometry of a Cohn Square to make our desired Debye material using multiple layers of these Cohn squares and to show that it is equivalent to a representative circuit model.

We also employ the Laplace Low Frequency Limit model to double check our Cohn model and validate our HFSS modelling results.

7.1 Using the Cohn Model of Strip Media to Make a Debye Material in HFSS

The goal was to model an infinite array of Cohn squares using HFSS in order to represent a Debye material. This can be done by simply modelling a single element in a periodic unit cell where all other elements are copies of it. The laboratory setup consists of a Cohn square placed in a tunnel where the top and bottom walls are perfect electric conductors (PEC) and the side walls are perfect magnetic conductors (PMC). The Cohn Square in the unit cell is infinitely copied in the x and y directions resulting in a periodic boundary condition. When an electromagnetic wave is sent through this tunnel at normal incidence the Cohn square will interact with it. This setup will behave as a transmission line with a shunt capacitive obstacle. When the wave gets to this point the electric field wants to align perpendicular to these PEC walls and tangential to the PMC boundaries. The Cohn square shorts out the electric field. Because the current is going to flow through the metal squares,

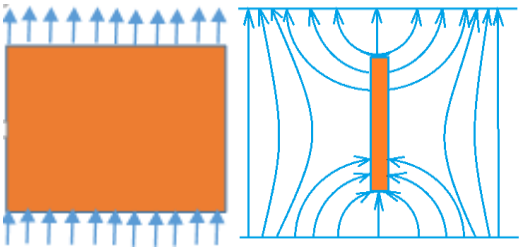

Figure 7-2. Flux Lines Around Metal Object.

the tangential electric fields have to go to zero at the metal object surface and the flux lines have to be perpendicular to the edge of the object. As a result the object is storing charge by charge separation at the two ends of the obstacle. As it passes the square the electric field becomes deformed because the electric field must terminate perpendicular to the metal.

Originally the transmission line was neutral. The charges were separated by the height of the unit cell between the PEC layers. When we placed the metal square, negative and positive charges arose at the two ends of the metal square. Before there was a capacitor with charge separation equal to the height of the unit cell height; now there is capacitor with much shorter separation, shorted and then another capacitor separated with much shorter separation.

Prior to placing the metal obstacle, we had the capacitance of the unperturbed transmission line. After placing the metal square in shunt; there is still the capacitance of the transmission line but in the neighborhood of the obstacle we have created excess capacitance by adding the metal Cohn square. This excess capacitance is the same regardless where this

metal obstacle is placed in the unit cell because it shorts out the same amount of flux lines. In his paper Analysis of a Metal-Strip Delay Structure for Microwave lenses (Aug 3rd, 1948) Cohn provides formulas for the susceptance (the imaginary part of the admittance) per square for an obstacle at normal incidence where the thin metal obstacle can be of any shape; arranged uniformly in multiple parallel planes.

Given that

$Y = G + jB$ where

Y is the admittance,

G is the conductance and

B is the susceptance

we can determine the sheet capacitance.

A capacitance can also be considered a susceptance because a capacitance is related to admittance in the following manner

$Y = j\omega C,$

$B = \omega C.$

We can test this closed form susceptance equation by Cohn using HFSS. If we send one volt in the transmission tunnel consisting of free space, the discontinuity at the obstacle will cause a reflection (S11 = reflection coefficient) and there will also may be some transmission (S12 = transmission coefficient); where

$S_{11} = \Gamma_{obs} = \frac{Y_0 - Y_L}{Y_0 + Y_L}$ where

$Y_L = load\ admittance\ and\ Y_0 = admittance\ of\ free\ space$

according to transmission line theory. Since measurements in the HFSS laboratory are made in port 1; we must move our observation to the obstacle location. We account for the phase delay by using the following equation

$$\Gamma_{11} = \Gamma_{obs} e^{-jk_0 2L},$$

where L is the length of the transmission line. Once we know the Γ_{obs}, we can solve for the admittance of the load.

Cohn provides a closed form equation in his paper for the normalized shunt susceptance of an obstacle with the geometry described below in Figure 7-3 and Figure 7-4;

$$B_{ii} = \frac{4b}{\lambda_{ii}} \ln(\csc(\frac{\pi c}{2b}))$$

where b is the obstacle height and c is the unit cell dimension minus the obstacle height. Given a specific geometry, this equation provides the normalized susceptance per square. Using a metal square we validate our HFSS set-up for a given geometry and periodicity and compare it to the susceptance calculated using Cohn's article. The following geometry was selected in a 6 mm by 6 mm unit cell.

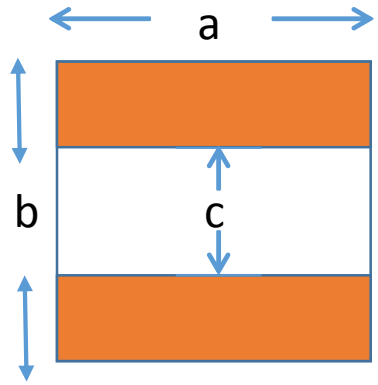

Figure 7-3. HFSS Model of the Cohn Strips.

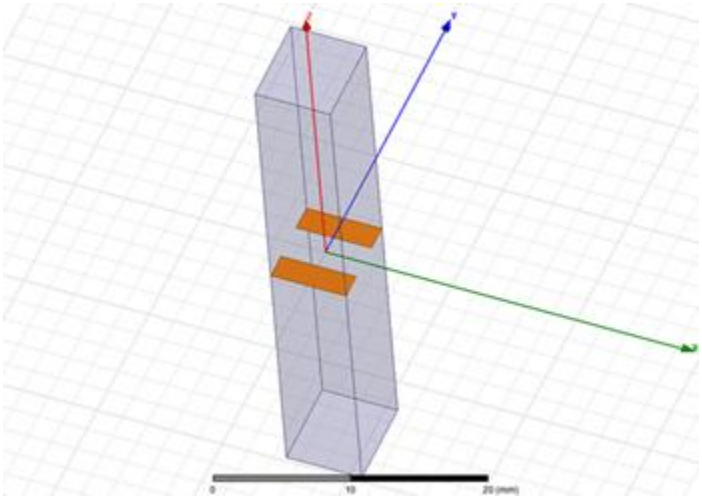

Figure 7-4. HFSS Unit Cell with Cu Strips.

A copper thin obstacle consisting of two infinite strips as described in the Cohn paper, with a unit cell geometry shown in Figure 7-4, was inputted into HFSS. The reflection coefficient of the obstacle was measured and the load admittance was determined. The normalized susceptance was determined from the imaginary coefficient of the load admittance using the equations described below.

$$Sobs_{ii} = \frac{S11Comp_{ii}}{exp[-(ik_{ii}2L)]}$$

$$Yload_{ii} = -2\frac{SFobs_{ii}Y0_{ii}}{SFobs_{ii}+1}$$

$$Bhfss_{ii} = \text{Im}(Yload_{ii})$$

Comparing the normalized susceptance determined using HFSS with the Cohn equation we obtain validation of our HFSS methodology as shown in Figure 7-5, where the Cohn calculations are in red and the HFSS determination is the dotted blue line.

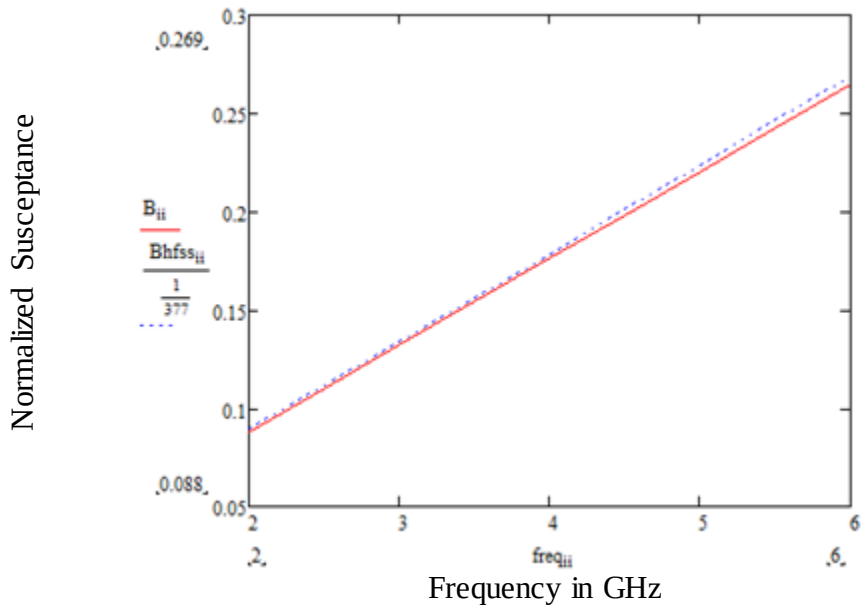

Figure 7-5. Cohn Susceptance Compared to HFSS Susceptance.

Clearly as shown in Figure 7-5, the Cohn susceptance per square matches the susceptance determined by HFSS for the identical geometry and periodicity. We know that the excess capacitance is the same if we place the two strips anywhere in the unit including the center of the unit cell.

If we can model the susceptance, we know the capacitance of a single layer of a metallic Cohn square. If we know the shunt susceptance of one plane, Cohn also shows how to create an effective medium by cascading these planes. Cohn provides the following equation where the refractive index and admittance are the same at the low frequency but diverges considerably at higher frequencies for $l \geq b$, where l is the distance between the Cohn square planes and b is the height of the unit cell. The equations for the image admittance and the index of refraction function of a thin strip are the following; where a=b=0.008 meters are the unit cell dimensions that we selected, b' is the gap = 0.0128 meters and l is the distance between planes, and n is the number of planes.

$$\delta = \frac{b'}{b}$$

$$Boc_{jj} = tan\left(\pi \frac{l}{\lambda_{jj}}\right) + 2\frac{b}{\lambda_{jj}} ln\left(csc\left(\pi \frac{\delta}{2}\right)\right) + 2\frac{b}{\lambda_{jj}} \sum_{n=1}^{50} \left[\frac{tanh\left[n\pi \frac{l}{b}\left[1 - \left[\frac{b}{n\lambda_{jj}}\right]^2\right]^{0.5}\right]}{\left[1 - \left[\frac{b}{n\lambda_{jj}}\right]^2\right]^{0.5}} - 1 \right] \frac{\left(\sin(\pi n\delta)\right)^2}{n(\pi n\delta)^2}$$

$$Bsc_{jj} = cot\left(\pi\frac{l}{\lambda_{jj}}\right) + 2\frac{b}{\lambda_{jj}} ln\left(csc\left(\pi\frac{\delta}{2}\right)\right)$$

$$+ 2\frac{b}{\lambda_{jj}}\sum_{n=1}^{50}\left[\frac{coth\left[n\pi\frac{l}{b}\left[1-\left[\frac{b}{n\lambda_{jj}}\right]^2\right]^{0.5}\right]}{\left[1-\left[\frac{b}{n\lambda_{jj}}\right]^2\right]^{0.5}} - 1\right]\frac{\left(\sin(\pi n\delta)\right)^2}{n(\pi n\delta)^2}$$

$YI_{jj} = \left(-Boc_{jj}Bsc_{jj}\right)^{0.5}$ The image admittance

$r_{jj} = \left(\frac{\lambda_{jj}}{\pi l}\right) atan\left(\frac{Boc_{jj}}{Bsc_{jj}}\right)^{0.5}$ The refractive index

We find that for $l \geq b$ at low frequencies the admittance and refractive index are the same but diverge at higher frequencies as shown in Figure 7-6 as the wavelength becomes comparable to the unit cell (no longer an effective medium).

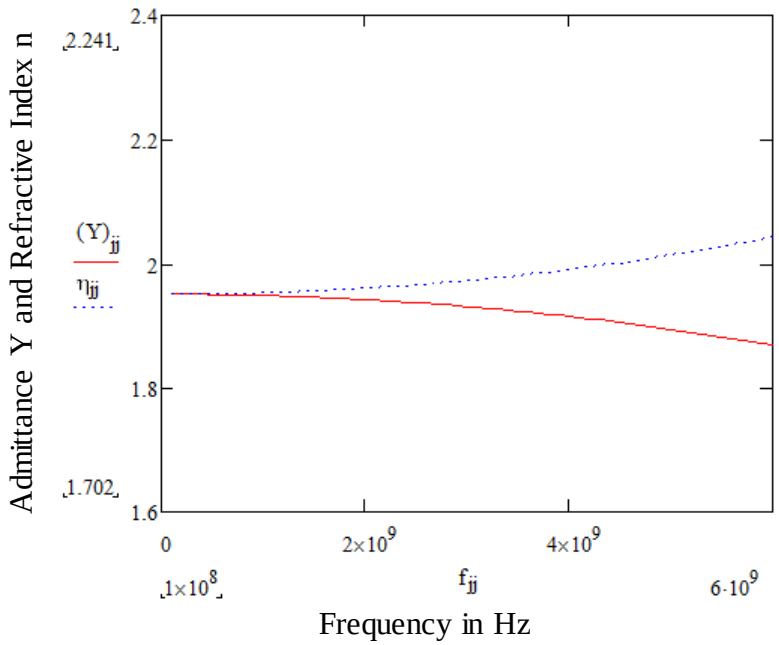

Figure 7-6. Admittance and Refractive Index Diverge at Higher Frequencies.

For the geometry described above, we find that for 17 layers of Cohn square planes both the admittance and the refractive index at low frequencies are 1.95. Taking the square of the refractive index we obtain the permittivity of our medium. In this case the refractive index was 1.95 and the relative permittivity was 3.8. Because the level of interaction Cohn assumes here is only interaction between adjacent strips; changing the layers from 7 to 17 makes no difference in the calculated admittance or refractive index of the effective medium.

But we were also interested in a bulk permittivity of 1.95. In order to make sure that a bulk medium of relative permittivity of 1.95 would exhibit the same properties as the Cohn strip media we constructed, using 17 layers of Cohn squares, with similar geometry of the unit cell described above; we modeled a medium in HFSS described by the equations above.

The unit cell extended ½ cell past both ends of each Cohn square plane to simulate a bulk material. We also ran a bulk material of the same size with an assigned value of 1.95 relative permittivity. Figure 7-7 shows the configuration of the bulk material and Figure 7-8 shows the construction of the Cohn medium inputted into HFSS.

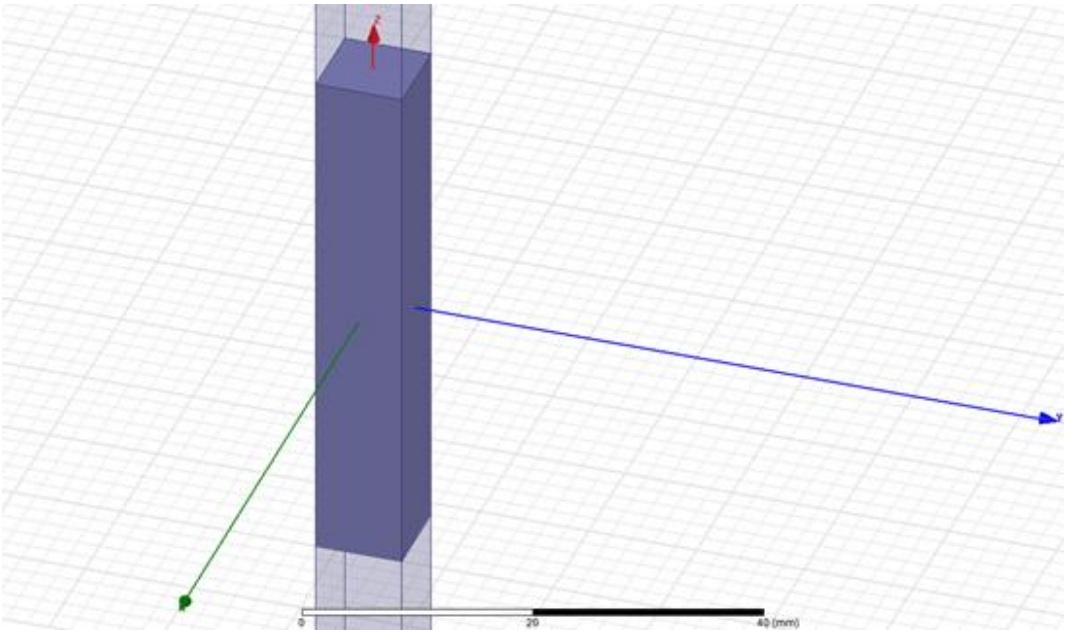

Figure 7-7. Bulk Material with 1.95 Permittivity.

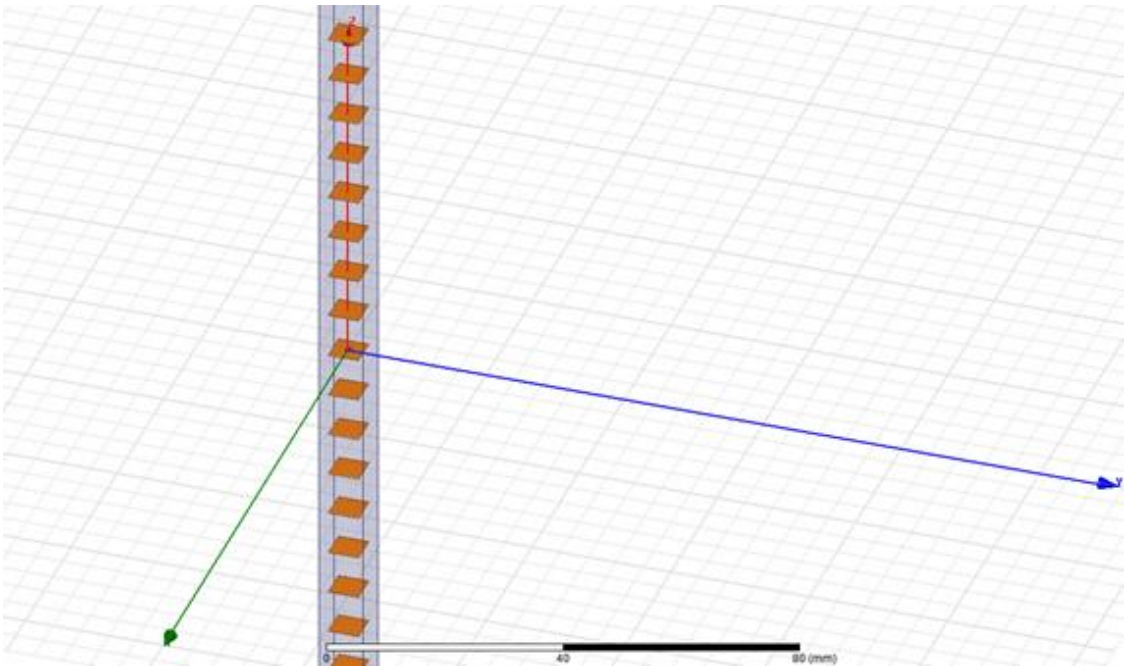

Figure 7-8. Cohn Media.

The unit cell geometry is l=a=b=8 mm and b' = 1.2 mm. The resulting transmission coefficient S21 measured from HFSS are compared for both the bulk and Cohn media and they are found to be identical as shown in Figure 7-9. The red is real part and the blue is imaginary part of the transmission coefficients. The dashed line is for the Cohn cascade and the solid lines represent the bulk material.

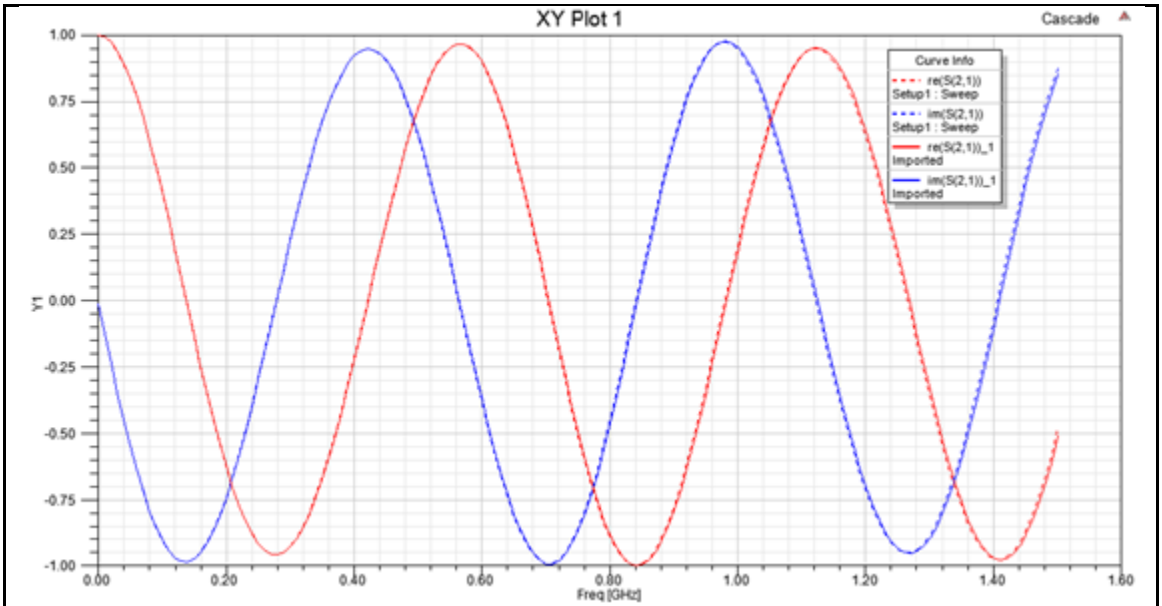

Figure 7-9. Cohn Strip Media Versus Bulk Real and Imaginary Transmission Coefficients.

We also showed that that the Cohn strips are equivalent to a Cohn square in the unit cell. In Figure 7-10 the square geometry dimensions were iterated to obtain the same value as the reflection coefficient of the strip we just analyzed.

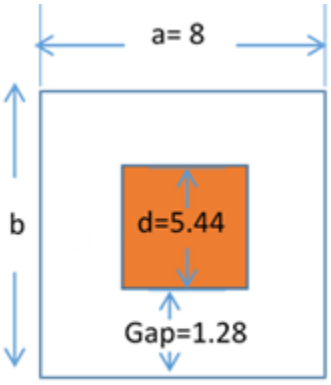

Figure 7-10. Cohn Square.

The S21 transmission coefficient compares well with the bulk values shown in Figure 7-11.

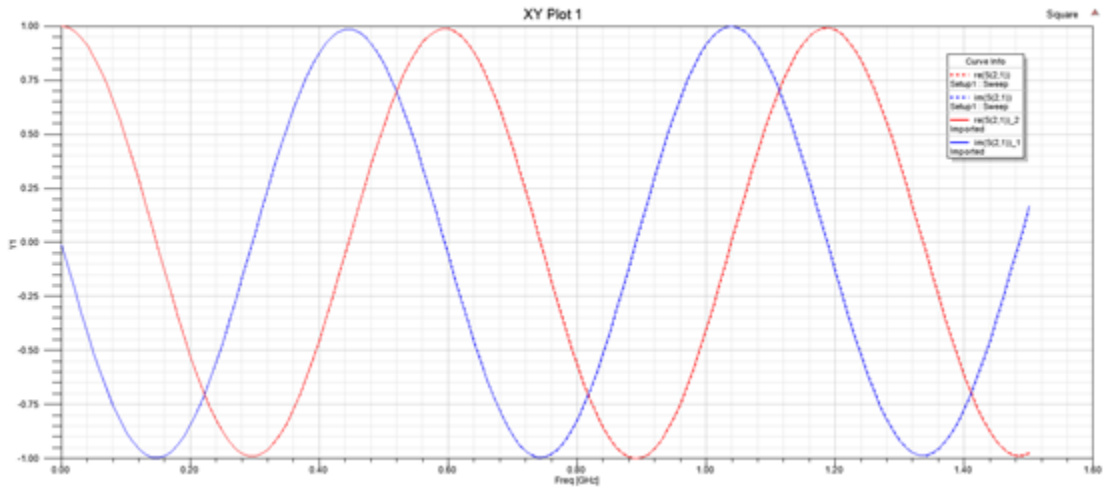

Figure 7-11. Cohn Square Media Versus Bulk Real and Imaginary Transmission Coefficients.

In order to verify the Cohn method on a material with relative permittivity of 1.95 using a cascade of 17 layers where each sheet has the above geometry, the permittivity was extracted from S21. Results are shown in Figure 7-12 and Figure 7-13 below. Both the bulk and effective medium (cascade of 17 layers) relative permittivity values matched the HFSS inputs and the Cohn predictions.

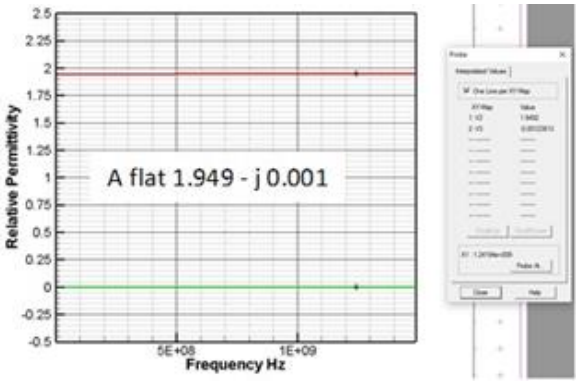

Figure 7-12. A Bulk Material of Relative Permittivity of 1.94.

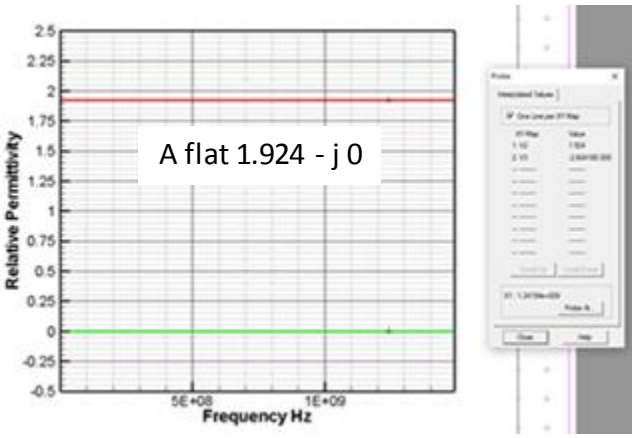

Figure 7-13. An Effective Medium Material of Relative Permittivity of 1.924.

The DC permittivity value for the capacitance of these metal squares is the same for the bulk and the cascade of 1.924.

7.2 Excess Capacitance due to a Metal Square in a Unit Cell

Cohn states that if the shunt susceptance is known and the adjacent layers are close enough to be quasi-static, but not so close that they interfere with each other (i.e. disturb the field at the gap); and the distance between them are small compared to the wavelength; the effective permittivity of the media made of such cascading layers are embodied in the following equations for $l \geq b$:

$$nF_{ii} = \frac{1}{\varphi_{ii}} acos\left[\cos(\varphi_{ii}) - \left[\left(\frac{BFobs_{ii}}{2}\right)\right]\sin(\varphi_{ii})\right] \text{ where}$$

$$\varphi_{ii} = \frac{\omega_{ii} l}{c}$$

$$\varepsilon F_{ii} = (nF_{ii})^2$$

$$BFobs_{ii} = \frac{Yload_{ii} 377}{i}$$

An HFFS experiment was run using a single Cohn square made of copper where the unit cell dimensions were *a=b=l=10 mm.* The metal square was 5 mm x 5 mm. The S11 measurements were used to calculate the load admittance and the susceptance and capacitance was determined from this data. This data is used to calculate permittivity using both the Cohn method and the Laplace method described above for the sake of comparison, and to determine the low frequency limit dielectric constant. The HFSS model is shown in Figure 7-14.

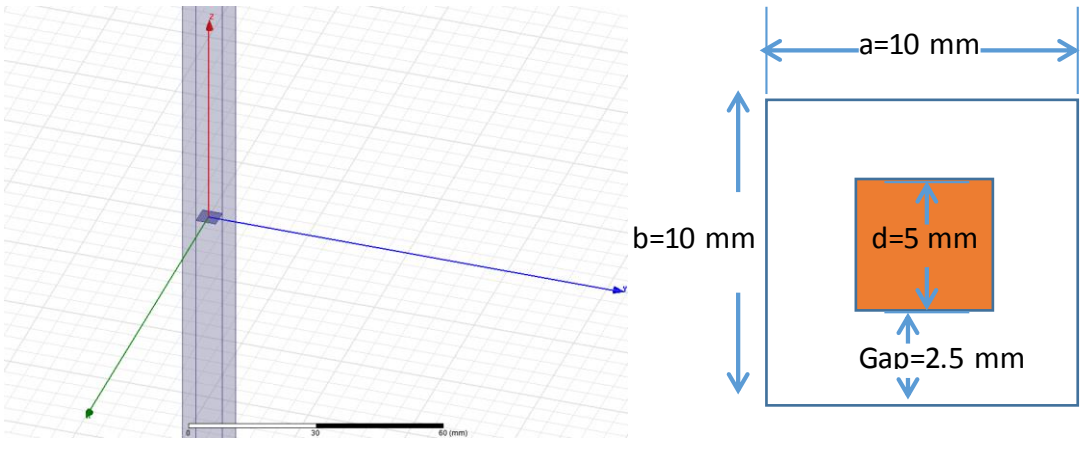

Figure 7-14. A 5 mm x 5 mm Copper Cohn Square.

The low frequency limit dielectric constant of a medium made with these obstacles are shown using the Cohn Method and Laplace Method in Figure 7-15 and Figure 7-16 respectively.

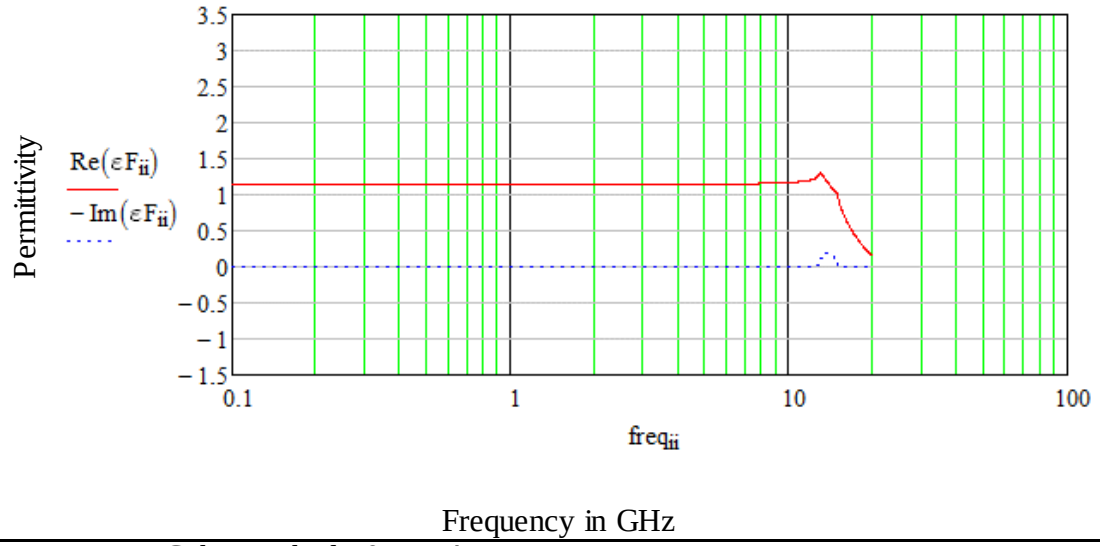

Figure 7-15. Cohn Method 10 mm Apart.

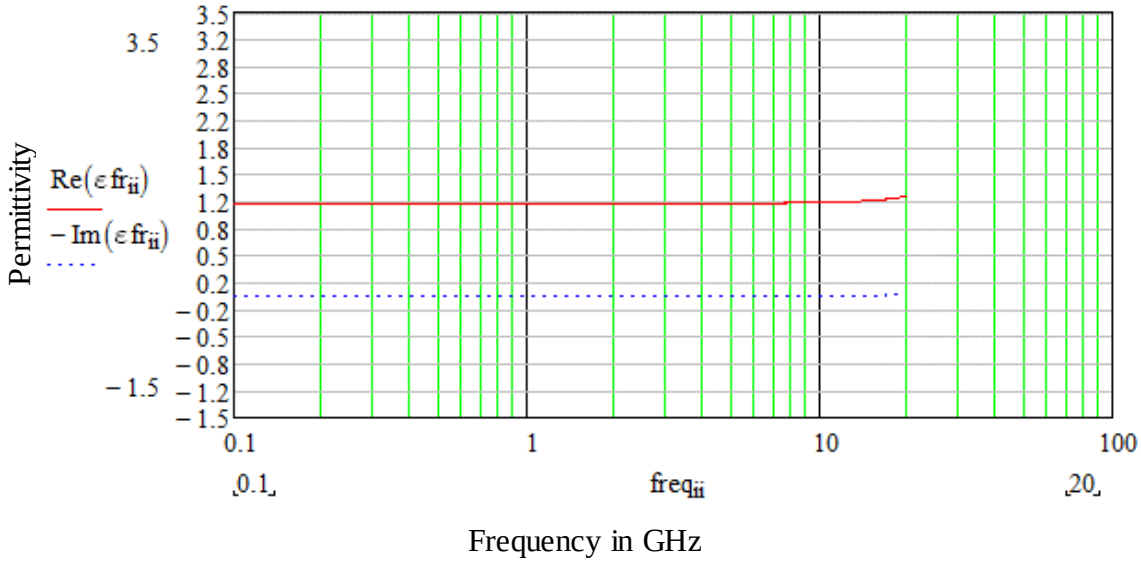

Figure 7-16. Laplace Method 10 mm Apart.

The dielectric constant was found to be 1.22 for both the Cohn and the Laplace method. Using a Cohn square of 9 mm sides centered in the same 10 mm square unit cell we obtained the DC permittivity to be 2.2 as shown in Figure 7-17 and Figure 7-18 for the Cohn Method and the Laplace Method.

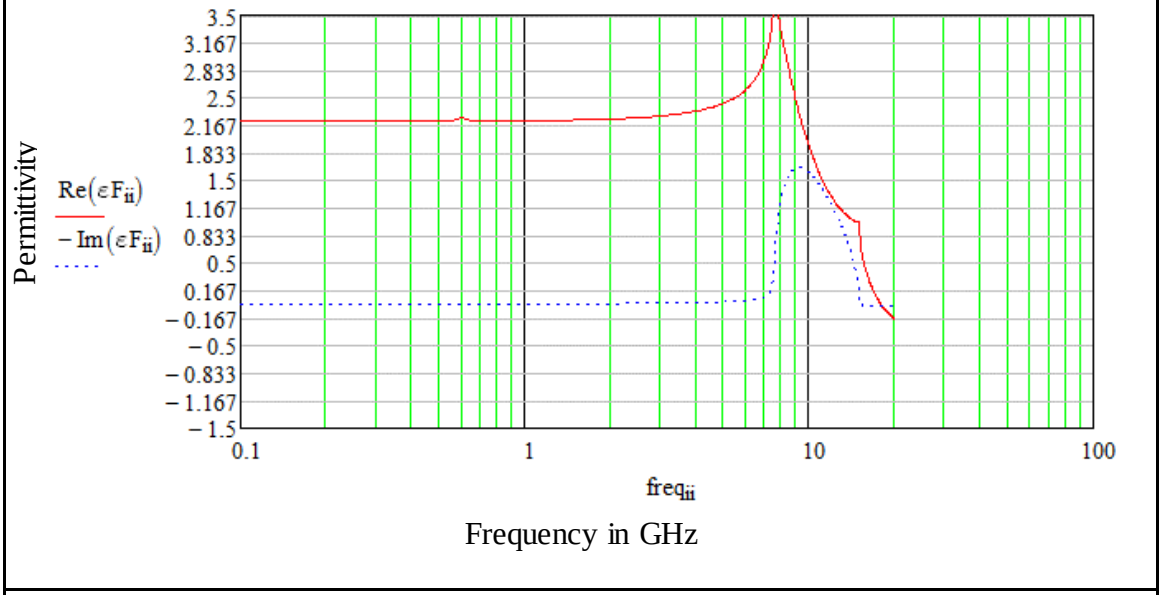

Figure 7-17. Cohn Method 10 mm Apart.

We see that the DC limit of the relative permittivity is 2.2 using both methods. The Cohn method as expected diverges at the high frequencies (because it includes wave effects between the layers) unlike the Laplace method as noted in his article due to the periodicity built into his equations. We now bring the layers closer together and see if it changes the low frequency limit. Cohn states for the single shunt susceptance per unit cell model to hold, we cannot bring the layers any closer than the unit cell dimensions. (If they were to be closer the model would require additional series terms to model the coupling between

the layers.) Since we are at a 10 mm distance between layers we will bring them to 6 mm and 4 mm progressively.

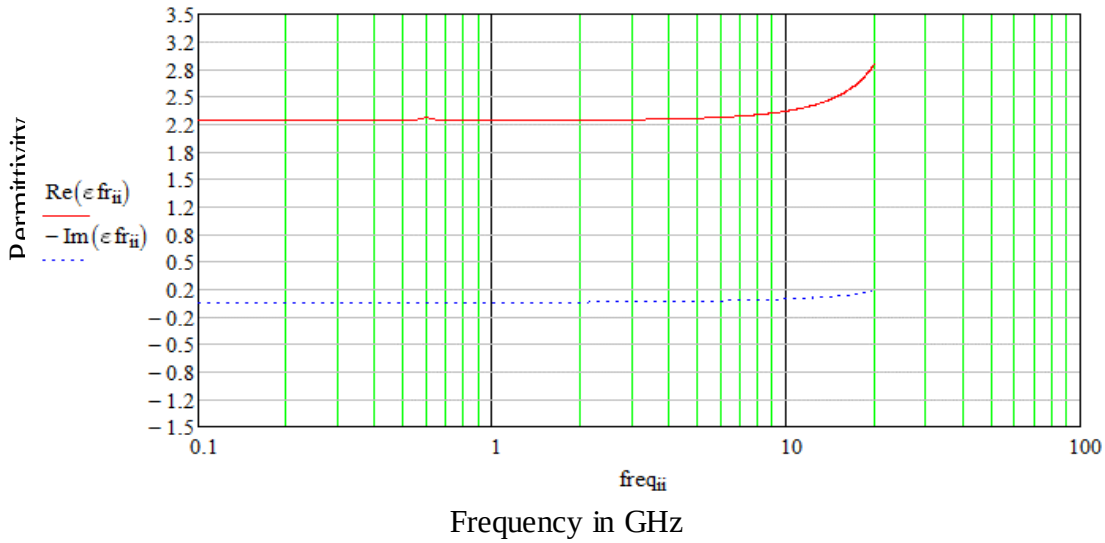

Figure 7-18. Laplace Method 10 mm Apart.

As expected as we bring the layers closer together the DC relative permittivity rises to 3 as shown in Figure 7-19 and Figure 7-20. The divergence of the Cohn square shifts to the right as we bring the layers closer together.

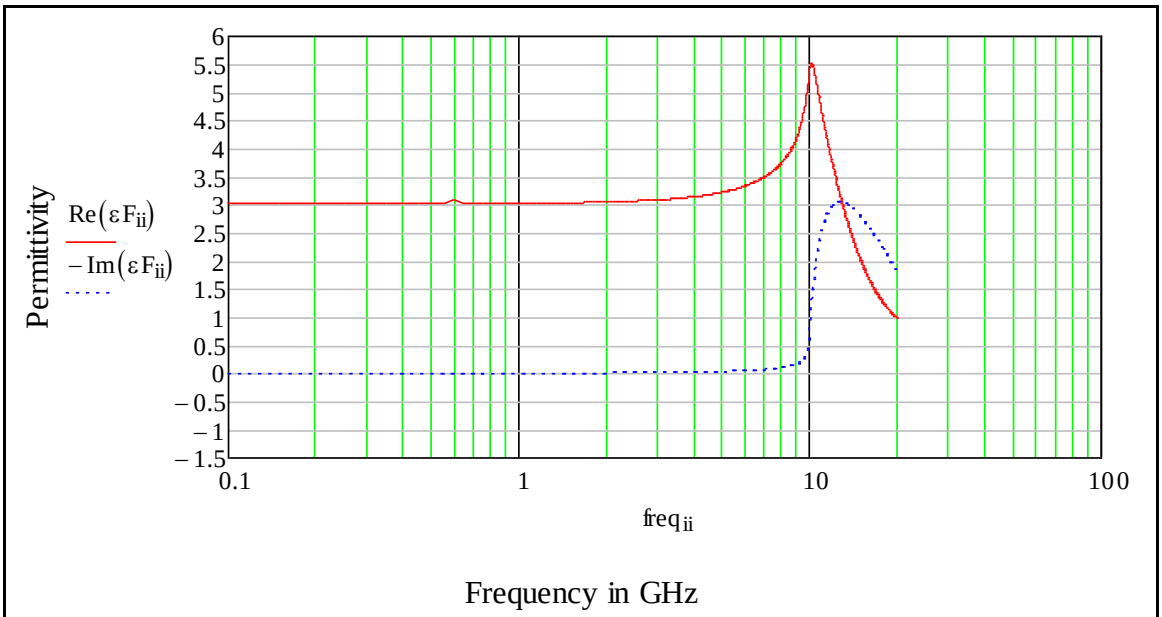

Figure 7-19. Cohn Method 6 mm Apart.

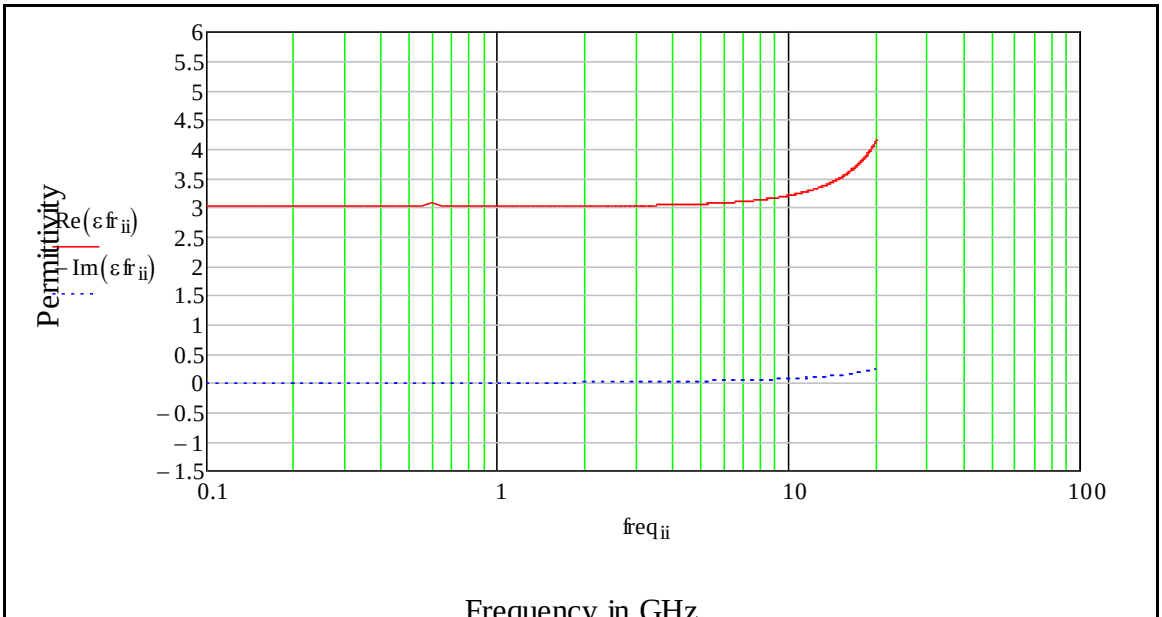

Figure 7-20. Laplace Method 6 mm Apart.

If we bring the layers even closer together to 4 mm apart, we obtain even a higher DC relative permittivity of 3. Furthermore the Cohn divergence shifts further to the right. So

bringing the layers closer we expand our valid frequency range for the low frequency equations. The Cohn method and Laplace or unit cell method are shown in Figure 7-21 and Figure 7-22 respectively.

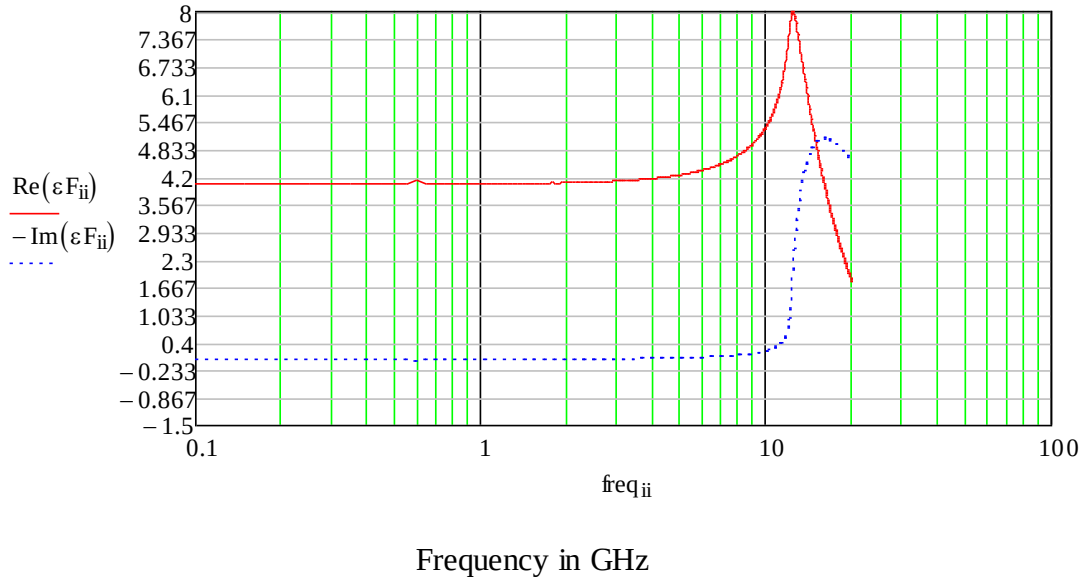

Figure 7-21. Cohn Method 4 mm Apart.

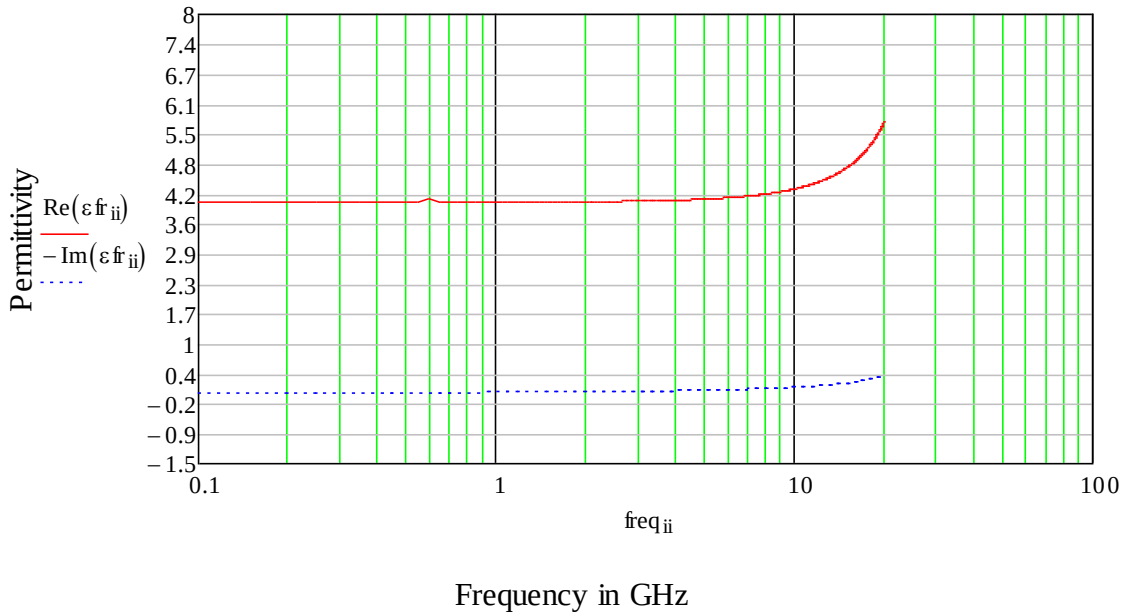

Figure 7-22. Laplace Method 4 mm Apart.

So we conclude that once we know the sheet shunt susceptance or capacitance we can obtain a very good model of the effective medium property of a cascade of Cohn squares.

7.3 Excess Capacitance in a Resistive Square

Now we make these metal Cohn squares resistive. Given a single, square, resistive obstacle we saw before in a unit cell wide, infinite transmission line, we now expect the charges that accumulated at both ends of the obstacle for a metal to flow as current through the square and thus see the resistance of the square. The obvious circuit model is a series RC and therefore must be Debye like. To the zeroth order we would expect the resistance of the R in the circuit to be the ohms per square assigned to the square but the fact that all the flux lines do not enter through the edge, as seen in Figure 7.1; will change the *circuit model* resistance to an effective value.

In order to understand this relationship between the HFSS assigned square resistance of the material and the Debye circuit model (a circuit model representing this geometry) resistance we ran HFSS for a 9 mm x 9 mm square with 800 ohm/square resistance. The shunt capacitance of this obstacle was determined and a Debye circuit model was created to fit the data. The R value of the circuit model was compared to the R assigned value of the square in the HFSS model to determine the proportionality factor between the HFSS material resistance and the effective circuit resistance. This is because there are alternative current paths other than the edge of the square for the flux to go through this resistive material. The same equations described above are used to determine the capacitance of the

shunt obstacle from HFSS reflection measurements to determine the obstacle load. The Debye circuit model is given by the following equation where L= 0 for a Debye and non-zero for a Lorentz. We start with the following equations of a capacitor in series with a resistor.

$$Z_{ii} = R + i\omega_{ii}L + \frac{1}{i\omega_{ii}C}$$

$$Y_{ii} = \frac{1}{Z_{ii}}$$

$$YT_{ii} = Y_{ii}$$

$$CT_{ii} = \frac{YT_{ii}}{i\omega_{ii}}$$

By assuming R to be 800 ohm per square for our first guess and since we know that $\omega = 1/RC$, we can make a good estimate of the capacitance knowing the relaxation frequency. We iterated the values of R and C till they fit the complex capacitance of the sheet determined by HFSS. For $C = 1.13x10^{-13} Farads$ and $R = 1120\ Ohms/square$ we are able to achieve the Debye Circuit model for the sheet capacitance to fit the HFSS sheet capacitance as shown in Figure 7-23. The real and imaginary capacitance of the sheet observed in HFSS for the zeroth order are the red and blue curves and the Debye circuit model curves are in purple and green in Figure 7-24.

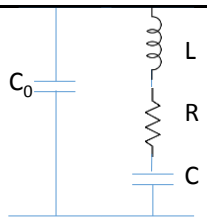

Figure 7-23. Debye Circuit Model. The Debye Term Is the Series RC.

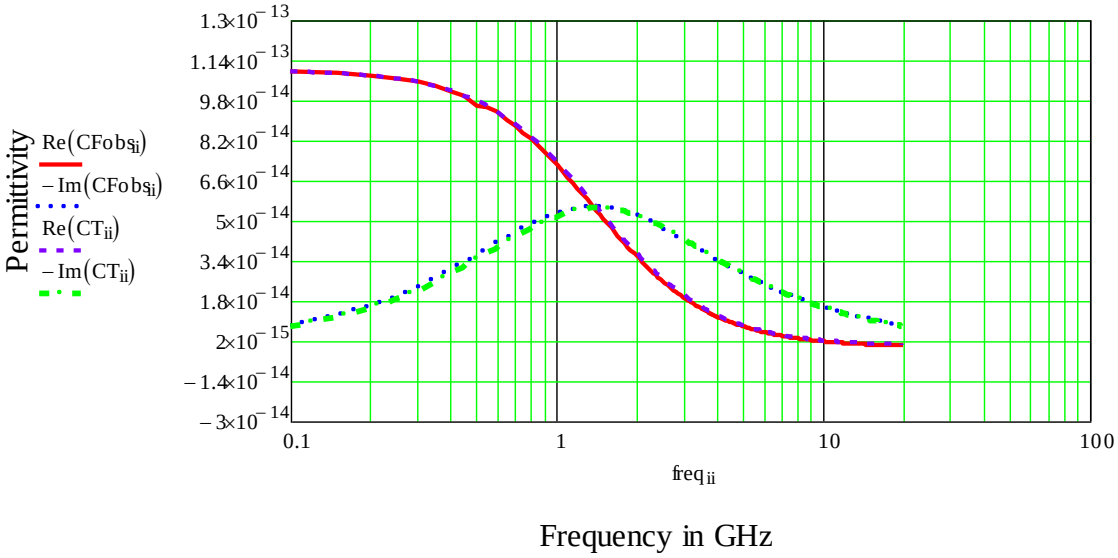

Figure 7-24. Capacitance of a 9 mm² 800 Resistive Square HFSS Versus Circuit Model.

Taking the ratio of the Debye circuit R versus the HFSS R we obtain 1.28; which is the order of proportionality factor we expect to obtain for future HFSS runs modelled by our circuit for the same Cohn square size in the same unit cell dimensions and geometry.

To ascertain we have the same proportionality factor we ran another 9 mm x 9 mm resistive square at 400 ohms/square in HFSS. Figure 7-25 below shows the Debye Circuit for this model fit with HFSS data. As expected as we reduce the R, the relaxation

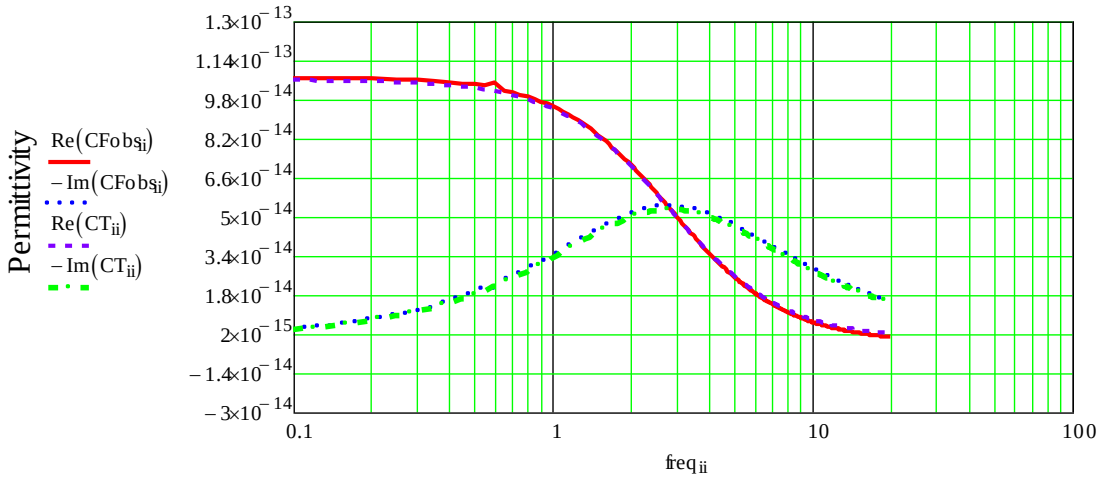

Frequency in GHz

Figure 7-25. Capacitance of a 9 mm² 400 Resistive Square HFSS Versus Circuit Model.

frequency increases and the capacitance shifts to the right. Taking the ratio of the Debye circuit R versus the HFSS R again, we get 1.32; which is the same order of the proportionality factor we obtained before for the Rcircuit/RHFSS. This proportionality constant will not be valid in extremely resistive cases where the flux lines are not perpendicular to the sheet and the current through the sheet is not uniform; the flux enters and exits also from the sides of the resistive sheet.

Comparing the 9 mm x 9 mm metal squares to the resistive squares we find the DC capacitance to be 1.1 x 10^{-13} Farads the same as before as shown in Figure 7-26.

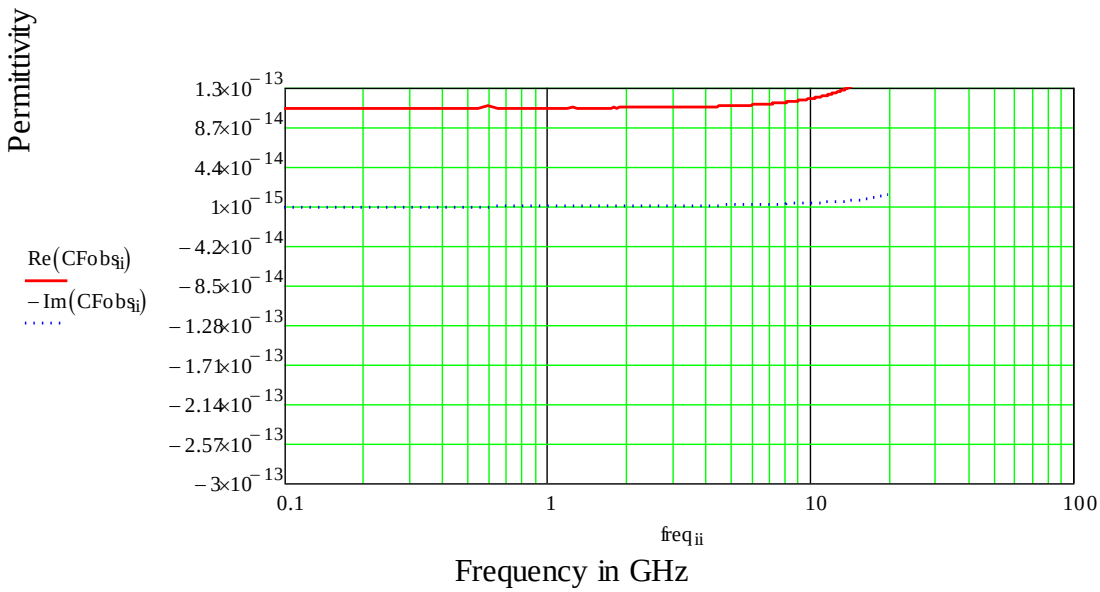

Figure 7-26. Capacitance of 9 mm x 9 mm Cu Metal Square Using the Cohn Method.

Therefore we can tune our Debye sheet because once we choose the excess capacitance, we can change R to choose our relaxation frequency. Since the relaxation frequency, $\omega = \frac{1}{RC}$, once we know the capacitance of the obstacle we can select the relaxation frequency that will give us the resistive sheet properties we need. And because we have shown we know the proportionally factor due to the alternative flux path effect we can from the circuit know what RHFSS should be for our HFSS model.

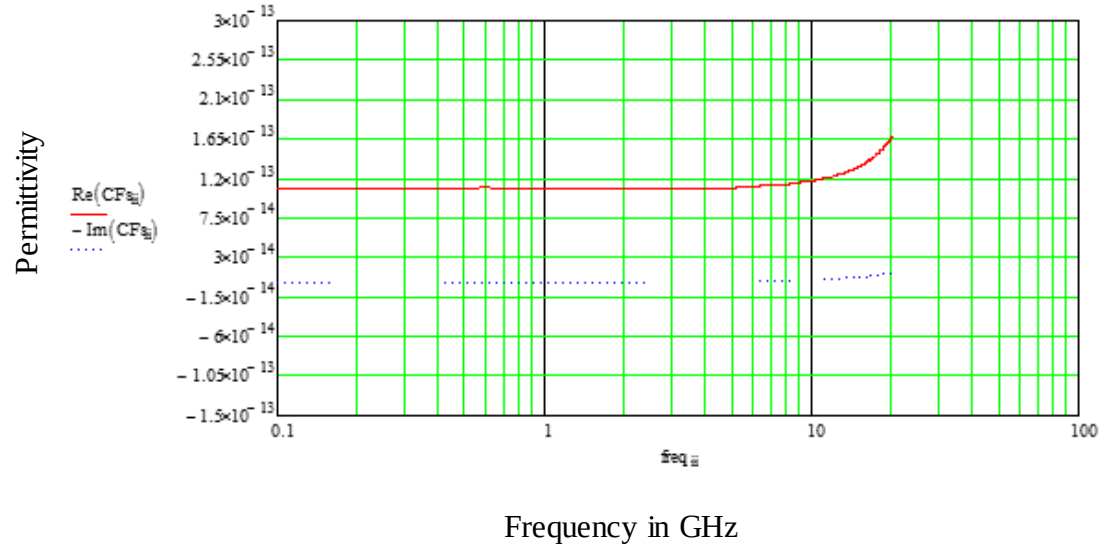

Figure 7-27. Capacitance of 9 mm x 9 mm Cu Metal Square Using the Laplace Method.

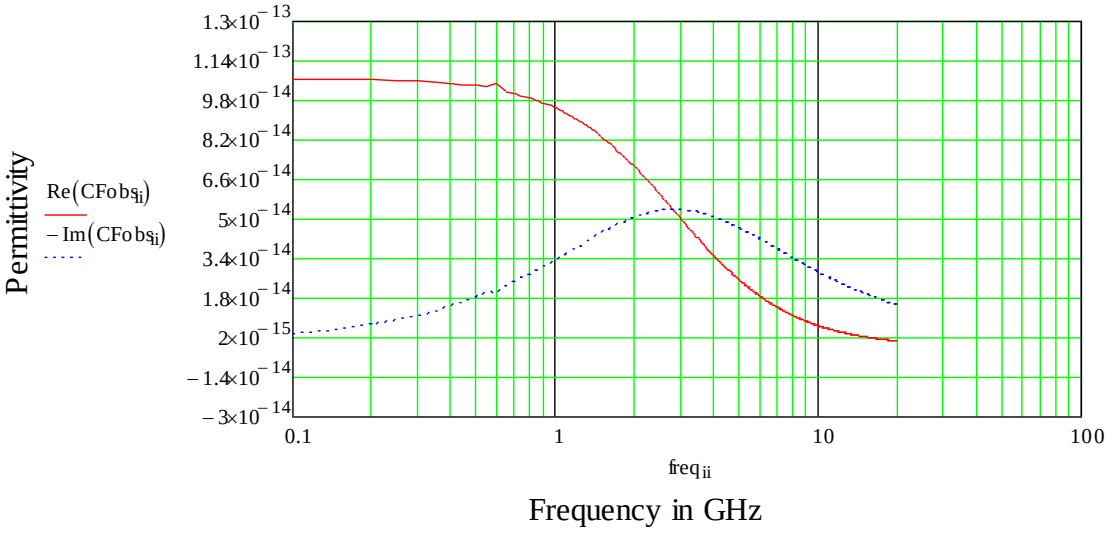

Figure 7-28. Capacitance of 9 mm x 9 mm Cu 400 Ohm/ Square Using the Cohn Method.

Since we can model these Cohn Squares in terms of the circuit models just used, we are able to add the zero circuit to this model. The question is what would be the best approach to implement this circuit model physically.

7.4 Designing the Debye Circuit Model

We first explore the Debye circuit model that represents the Cohn squares before we model the Debye circuit with the zero circuit. From the perspective of the Debye model, we have already explored that a Cohn square in HFSS can be represented as circuit model in terms of a series RC circuit for a given geometry.

We design an RC circuit knowing we want a Debye material that has a similar or higher capacitance value than our previous designs; where we achieved a DC capacitance of 1.13 x 10^{-13} farads. If we assumed that the separation between capacitive sheets were to be the same as the unit cell dimension, we would obtain a DC permittivity in the order of 1.4. Because we selected a larger unit cell in the order of 48 mm x 48 mm x 48 mm and the Cohn square of dimensions of 35.75 mm x 35.75 mm, and our geometry is considerably different, i.e. the Cohn square occupies less percentage of the area of the unit cell, we double the desired capacitance to remain in the same ball park. If we want the relaxation frequency to be 0.6 GHz, assuming a capacitance of 2.5 x 10^{-13} farads, we need a resistance in the order of 1040 ohms/square. A circuit model resistance of 1040 ohms will indicate a

lower HFSS resistance in the order of 800 ohms per square, given that we found that the

proportionality factor was 1.3 between R circuit and R HFSS; as we found out that the flux does not flow only through the top and bottom of the square; but also from the sides. We select the Cohn square to be 800 ohms per square. We run this Cohn square as before in HFSS and compare the sheet capacitance with our Debye model. We find we are very close to our circuit model with some minor tweaks. R = 1590 for the circuit model with a proportionality factor of 2.0 as the cell geometry is considerably different from before, and C is 2.55 x 10^{-13} farads.

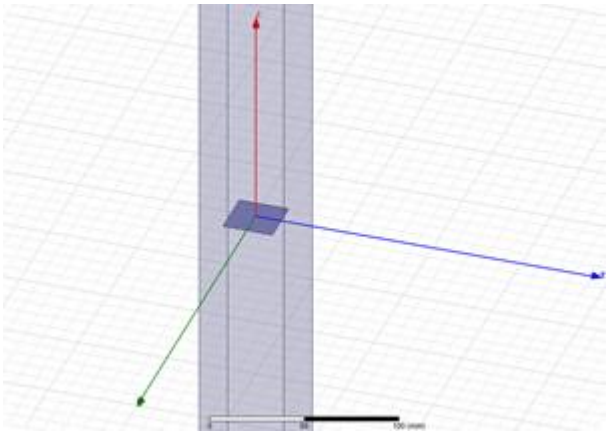

Figure 7-29. 35.75 mm x 35.75 mm Cohn Square of 800 Ohms.

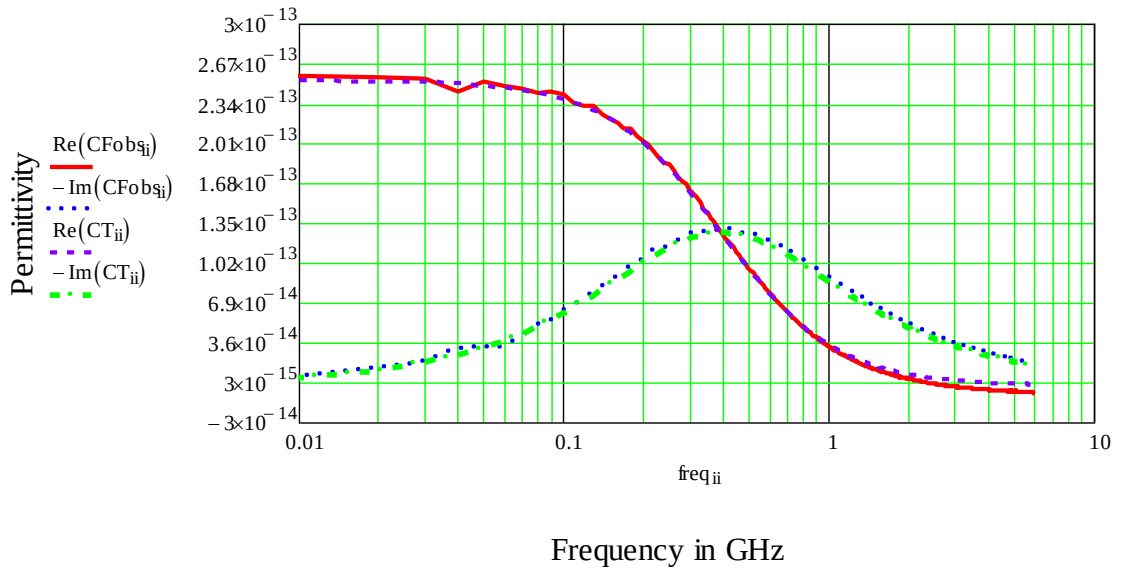

Figure 7-30. Debye Circuit Model Predicts HFSS Cohn Square.

7.5 Designing the Zero Circuit Model

Now that we have our Debye circuit model we need to add the zero circuit to our Debye model as was done in the Diaz dissertation for water.

For the purpose of ease of measurement of the demonstration article that we will fabricate; we choose a relaxation frequency of 3 GHz. A one cm unit cell has dimensions that are one tenth of the wavelength length at that frequency. For such a geometry where the Cohn square is 9 mm square we calculate the Cohn capacitance to be 9.411×10^{-14} and we determine R of the circuit. We divide the R of the circuit by a factor of approximately 1.4, using a proportionality factor in the order of what we observed before. And we find the sheet Debye capacitance as outlined in Figure 7-31.

$$CDeb(f) = \frac{Ccohn}{1 + i\frac{f}{f_0}}$$

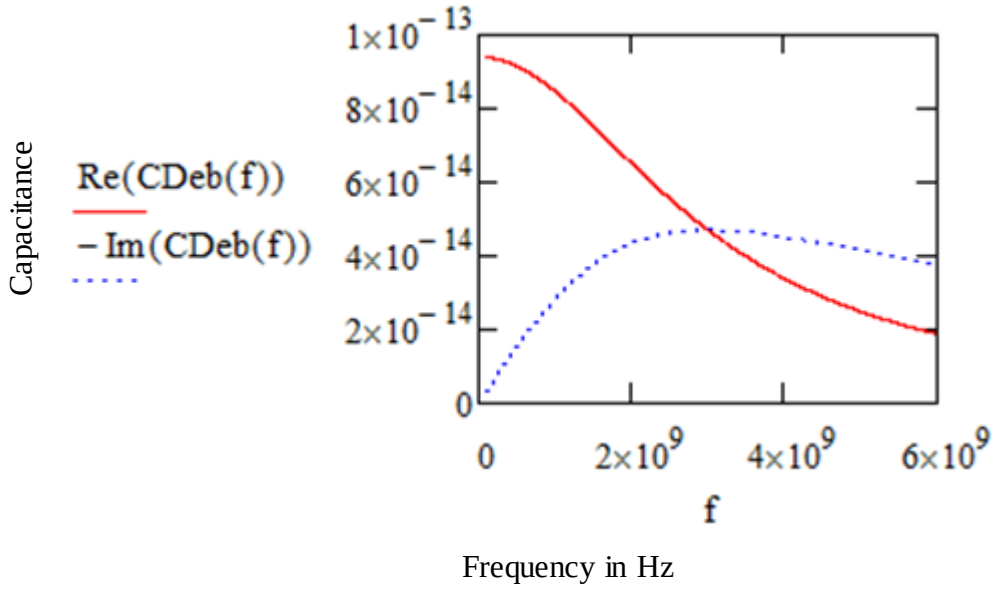

Figure 7-31. Debye Capacitance of a 1 cm Unit Cell with 0.9 mm Cohn Square.

We know that the zero circuit is an LRC circuit in shunt with the resistor. For this Lorentz branch we pick a resonant frequency of $f_z = 4 * 10^9$.

Now we explore what size capacitor we need for the LRC circuit relative to the Cohn capacitance we determined in the Debye branch. If we assign values of the zero circuit capacitance as a function of the Cohn capacitance the inductance is then constrained.

$$Lz(Cz) = \frac{1}{\omega z^2 Cz}$$

Since $\omega = \frac{1}{\sqrt{LC}}$

Assuming the zero circuit R_z is much smaller than the Debye, R we get the following equation for the series impedance for the zero circuit.

$$Zz(f, Cz, Rz) = Rz + i\omega(f)Lz(Cz) + \frac{1}{i\omega(f)Cz}$$

Adding the Debye resistor in shunt we obtain

$$Ypar(f, Cz, Rz) = \frac{1}{Zz(f, Cz, Rz)} + \frac{1}{R}$$

Adding this in series with the Cohn capacitance we get the new sheet impedance and admittance respectively.

$$Znew(f, Cz, Rz) = \frac{1}{i\omega(f)Ccohn} + \frac{1}{Ypar(f, Cz, Rz)}$$

$$Ynew(f, Cz, Rz) = \frac{1}{Znew(f, Cz, Rz)}$$

If R_z of the zero circuit is made very large than the zero circuit is open and nothing changes regardless of the value of C_z as shown in Figure 7.32.

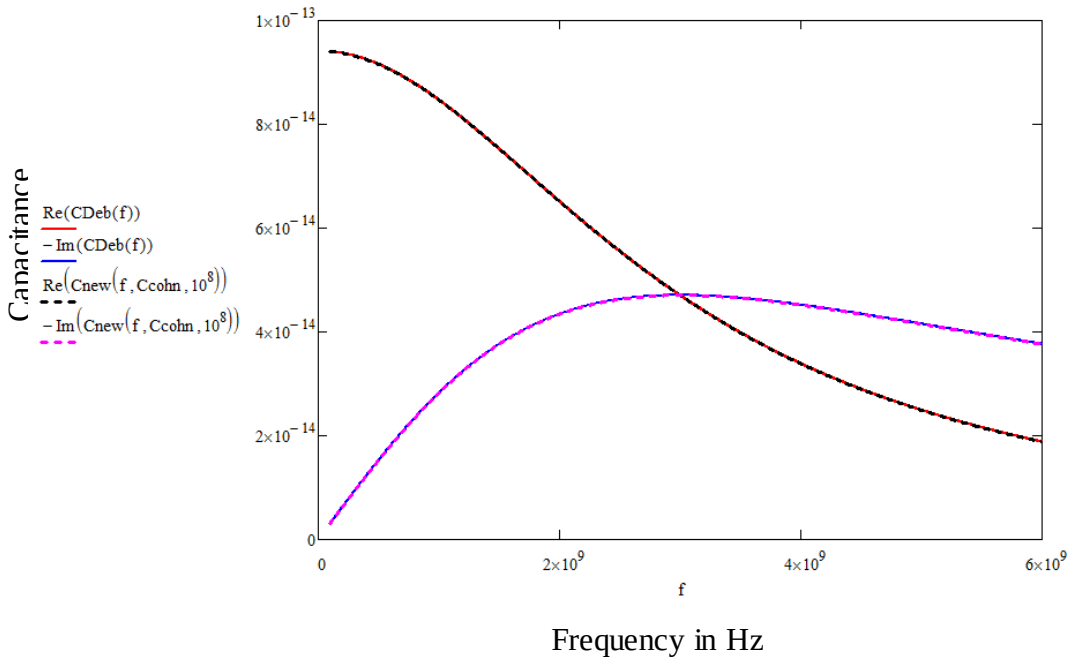

Figure 7-32. Capacitance of a 1 cm Unit Cell with 0.9 mm Cohn Square with and without a Zero Circuit with Very Large Rz.

Now assigning R_z to be 1/10th the value of the Debye R, and assigning Cz to be1/10 of the Cohn capacitance and 10 times the Cohn Capacitance we obtain the following results shown in Figure 7-33.

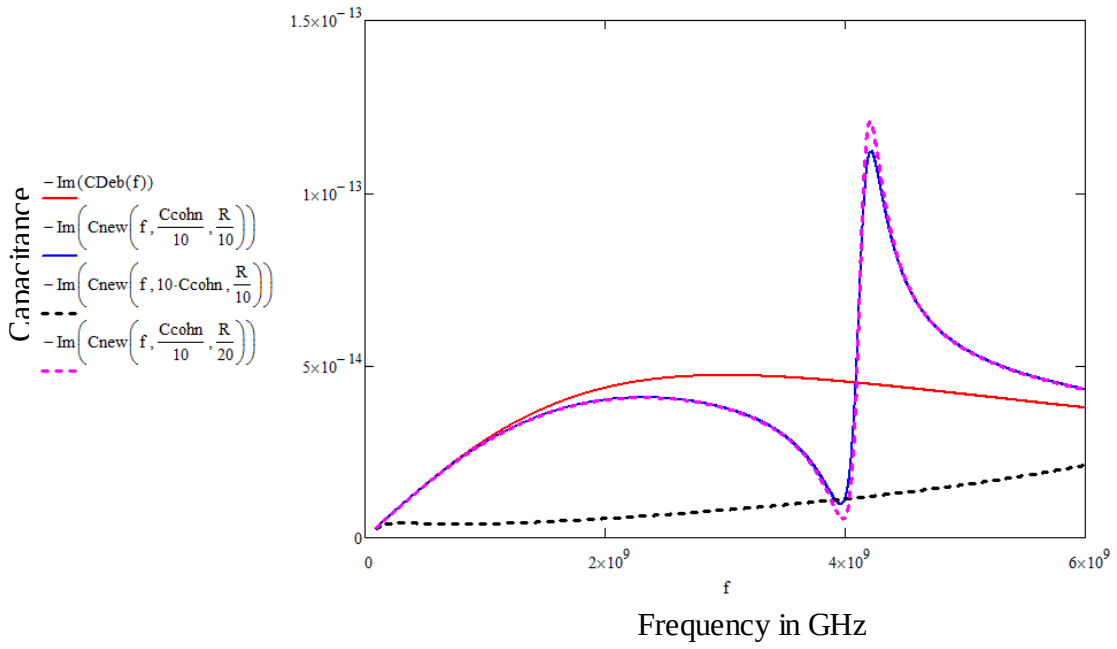

Figure 7-33. Imaginary Part of the Complex Sheet Capacitance of the Circuit for Varying Cohn Capacitance and Rz with Reference to No Zero Circuit.

It is clear from Figure 7-33, if we want to stay on the blue curve to obtain a window. This means that the capacitance of the zero circuit must be much less than the Debye circuit; which mean we need high inductance. If R_z is one tenth of the Debye R than the window drops an order of 5 whereas for a 1/20th R the window drops an order of 9.

Now if we assemble several of these capacitive sheets 10 mm apart we can make an effective medium consisting of these sheets. Assuming no interaction between adjacent sheets using the following equations we obtain the real and imaginary permittivity shown in Figure 7-34.

$$Cunit = \varepsilon_0 \frac{0.01*0.01}{0.01}$$

$$Cexcess(f) = CDeb(f)$$

$$Cexcess2(f) = Cnew\left(f, \frac{Ccohn}{10}, \frac{R}{20}\right)$$

$$\varepsilon Deb(f) = \frac{Cunit + Cexcess1(f)}{Cunit}$$

$$\varepsilon Win(f) = \frac{Cunit + Cexcess2(f)}{Cunit}$$

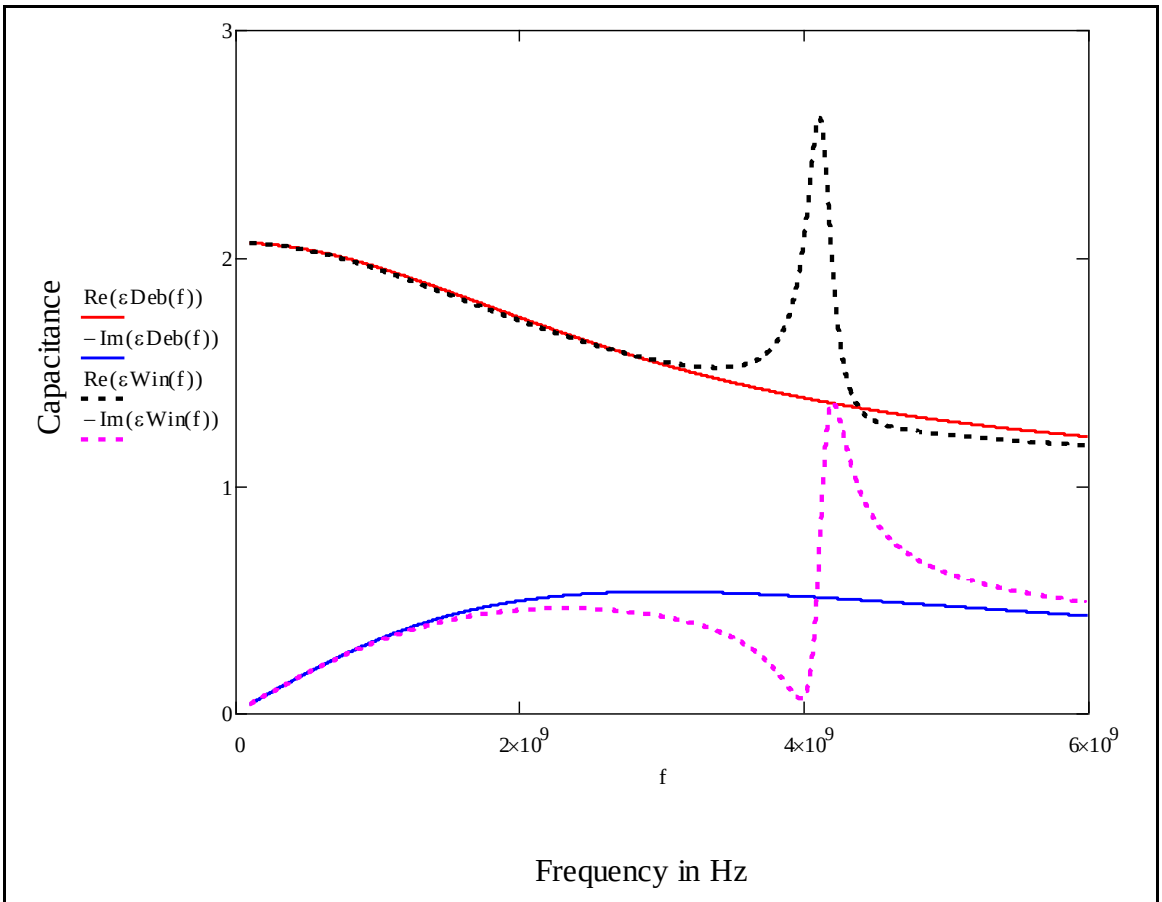

Figure 7-34. Cohn Permittivity and Permittivity with Zero Circuit.

As predicted the window occurs at 4 GHz and returns to its original DC permittivity of 2 like the metallic Cohn squares. As we would expect from the Hilbert Transform, creating a window like this must also create a kink on the real part. Focusing on the window region in Figure 7-35 this kink is clear with the dotted black and magenta curves.

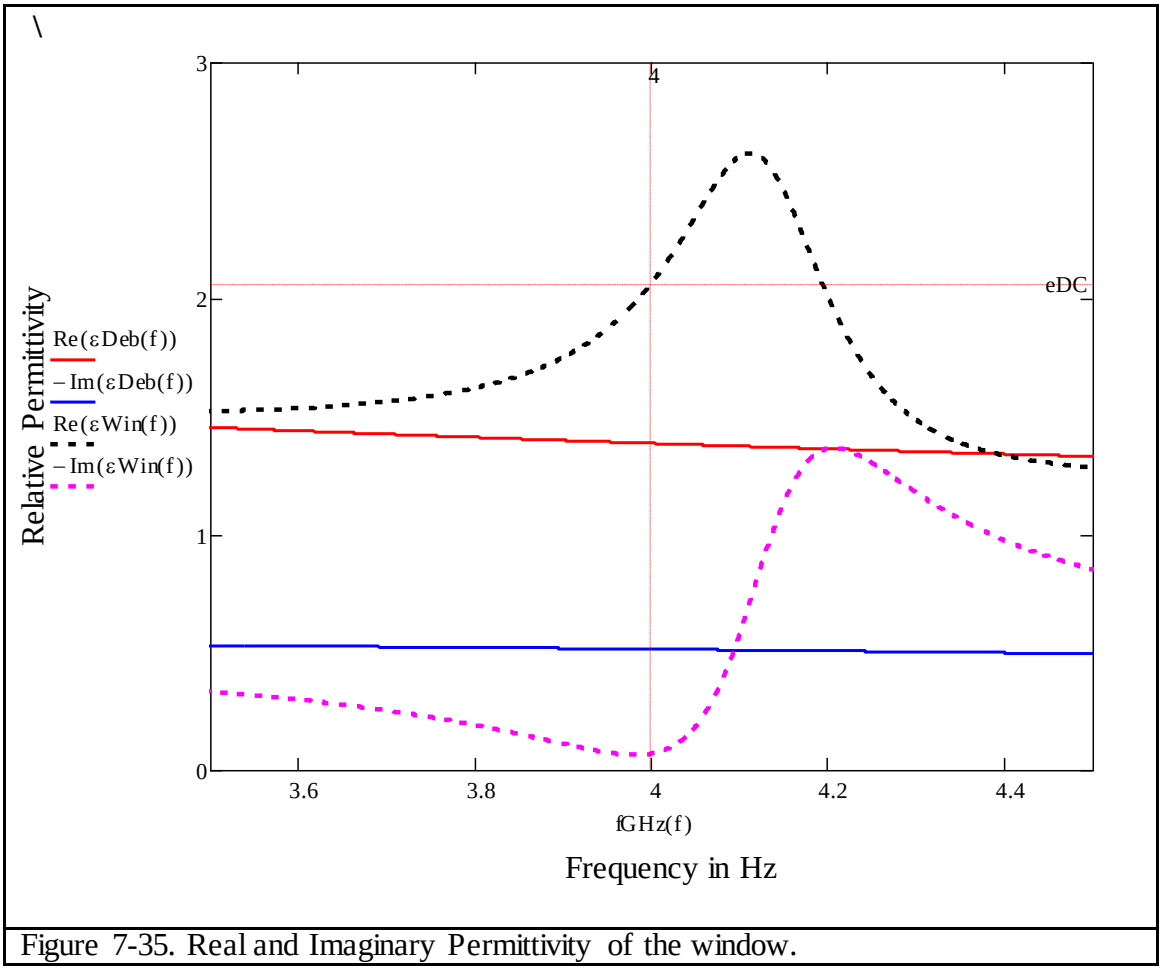

Figure 7-35. Real and Imaginary Permittivity of the window.

So we conclude when we modify the Debye circuit model to add the zero circuit we must be sure that the capacitance of the zero circuit be much less than the Debye circuit, the inductance must be very high and Rz must be smaller than R of the Debye so that the zero circuit is the path of least resistance.

These guidelines lead us to developing an HFSS to model of a physically realizable material consisting of Cohn squares with a zero circuit. We know if we can model this in HFSS we can actually manufacture such a material.

CHAPTER 8

MODELLING OF A WINDOW IN HFSS

The question is how to best implement a zero circuit physically in a material that can be fabricated and ensure the window that can be physically measured with the tools at our disposal.

In Diaz and Alexopoulos (Diaz, The Analytic Continuation Method for the analysis and Design of dispersive Materials 1992) and Kyriazidou et al, the zero circuit on an otherwise absorbing material was theoretically implemented by surrounding the lossy particle or molecule (Debye material) with a Lorentz shell (Chryssoula A. Kyriazidou January 2000). This could be done in principle by surrounding the Cohn square with a Lorentz frame.

8.1 First Try: HFSS Design of the Cohn Square Debye Sheet Using Picture Frames as the Lorentz

We start with Cohn square in HFSS already discussed in section 7.4 with dimensions of 37.5 mm x 37.5 mm in a 48 mm x 48 mm unit cell where the assigned resistance is 800 ohms per square. We use a large unit cell because we want to cover the Debye with small Lorentz resonant frames; so we require a larger area to work with.

We already know from section 7.4 what the Debye capacitance baseline looks like. The objective of the next set of HFSS runs were to find if a double frame of Lorentz (C and H

loop combined in parallel) on both sides of a single resistive sheet would erase loss as shown in Figure 8-1.

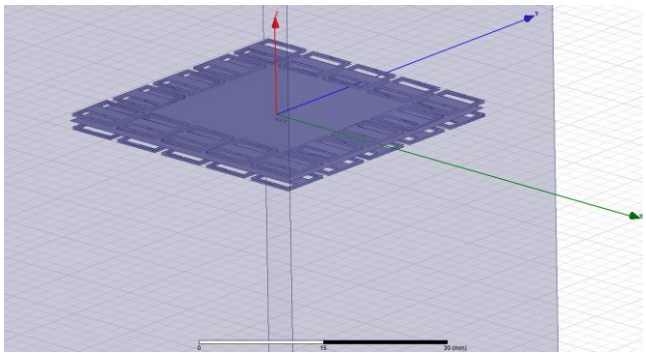

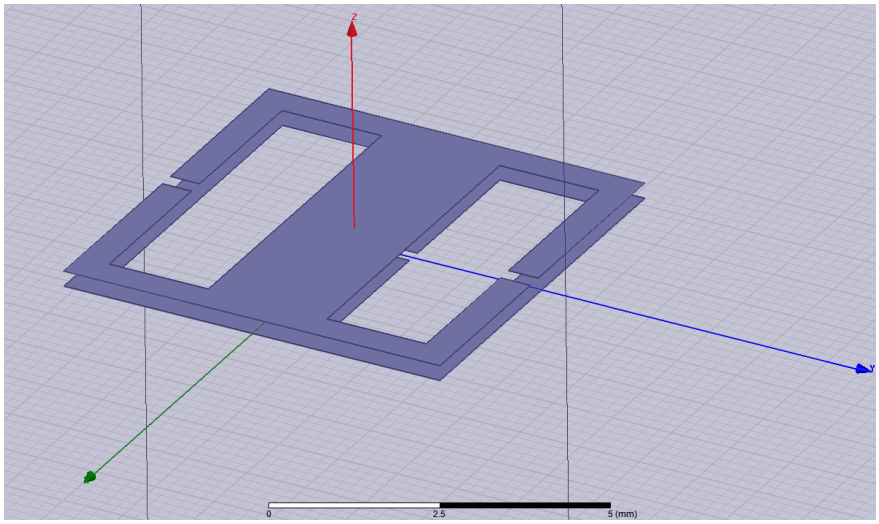

Figure 8-1. (a) Double Lorentz frame on both sides of 800 ohm resistive sheet 1 mm with gap. vacuum box 48 x 48 x 480 mm^3: resistive sheet at 0 mm and outer Lorentz frames at +/-1 mm; (b) A single Lorentz frame pair: A double C-loop on top of another double C-loop.

Using the Cohn's low frequency estimate for non-coupled sheets where the distance between sheets are greater than or equal to the square unit cell dimensions, we obtained the following permittivity from the S11 reflection parameters run in HFSS. Figure 8-2 show the permittivity calculations using the Cohn method.

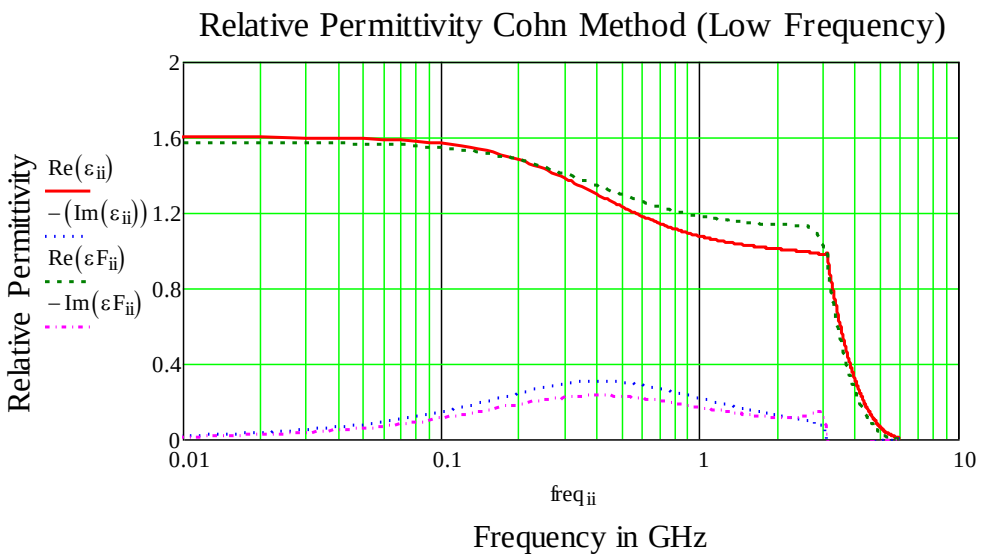

Figure 8-2. Permittivity of 800 Ohm Cohn Square with Lorentz Frames on Both Sides with a Unit Cell 48 mm Cubed Using the Cohn Method.

The red and blue curves are the real and imaginary permittivity of a single resistive sheet. The green and magenta are the real and imaginary permittivity of the same resistive sheet with a Lorentz frame on both sides. The Cohn square behaves strangely above the 2 GHz. But overall we have a material that exhibits slightly less loss than we had with the Debye Cohn square alone.

Because the Debye relaxation is happening at 0.6 GHz and our Lorentz resonance is between 4 and 5 GHz we wanted to shift the Debye relaxation to right by reducing R to 100 ohms per square. We also noticed in our many iterations that the Debye sheet was absorbing energy from the Lorentz. So we changed two parameters; we made the Debye sheet smaller than the Lorentz frame to 28 mm x 28 mm and removed one set of the frames from one side of the Debye sheet as shown in the Figure 8-3 in case the frames were interacting.

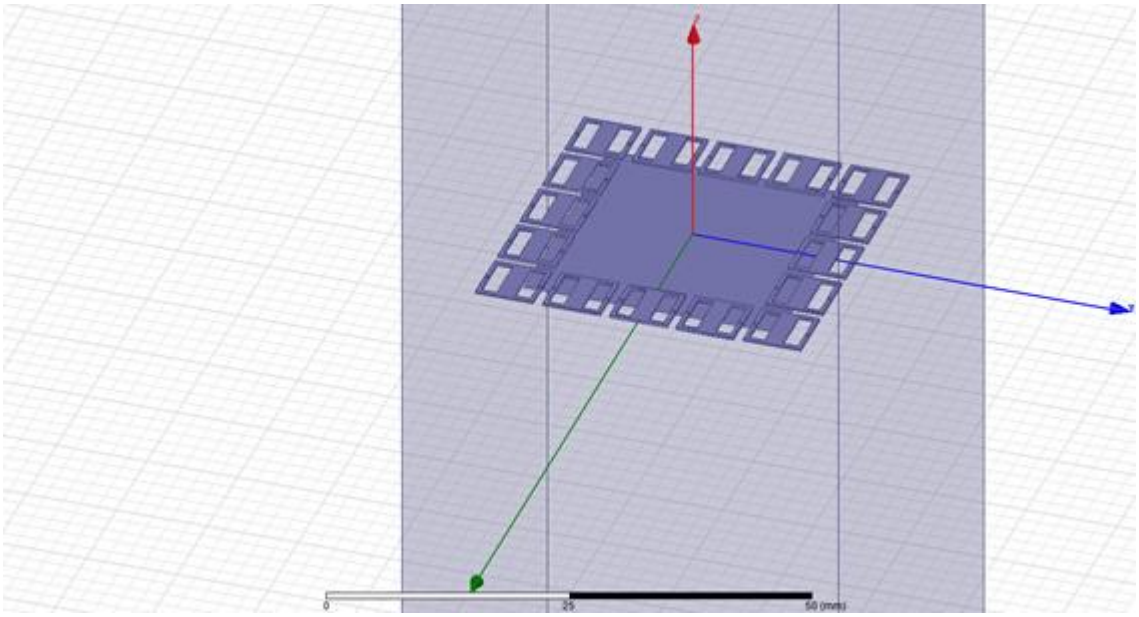

Figure 8-3. Single Lorentz Frame over 100 Ohm Resistive Sheet.

The frame extends beyond the edge of the Cohn square with a dimension of 35.75 mm square.

For the 28 mm x 28 mm Cohn square with 100 ohms per square resistance we needed to redesign the Debye circuit model as we did in section 7.4; since both dimensions of the Cohn square and the resistance were changed. But when we tried to fit the HFSS data to our circuit model we found that we needed to use a Lorentz circuit model where this time L was not zero. Since the Cohn square sheet is less resistant there is also greater inductance due to the sheet. We obtained the same DC sheet capacitance of C= 1.106 x 10^{-13}, a resistance R = 365 ohms per square and an inductance of L= 110x10^{-10} Henrys for our circuit model to fit the data shown in Figure 8-4 below. The ratio of Rcircuit to RHFSS changed to 3.65 because the size of the Cohn square changed drastically.

At DC there is no current flow so only the capacitor shows up. We saw in section 7.4 what the Debye capacitance looked like for an 800 ohm/square Cohn square. We keep the same DC capacitance but we see that the individual sheet consisting of Cohn squares of 100 ohm per square does not look Debye like anymore. Unlike modelling a material when we model a sheet there is no free space capacitor in parallel; it is only a shunt obstacle which is the excess capacitance calculated from the shunt admittance. For a medium we add the free space to the excess capacitance. Without that free space the capacitance should go to zero at infinity. Clearly this sheet capacitance for the 100 ohm/square array does not have the shape of Debye where the imaginary peak is not half of the real part. It could also go negative to recover like a Lorentz if we had gathered data at a higher frequencies.

We also made the unit cell larger compared to the Cohn square. The unit cell appears to be too big because at 4 GHz, the 100 ohm Cohn square is starting to resonate like an antenna and that is why we see the inductance. There is always inductance but in this case it is significant. If L dominates, the admittance equation the sheet is a Lorentz; if the R dominates it is a Debye.

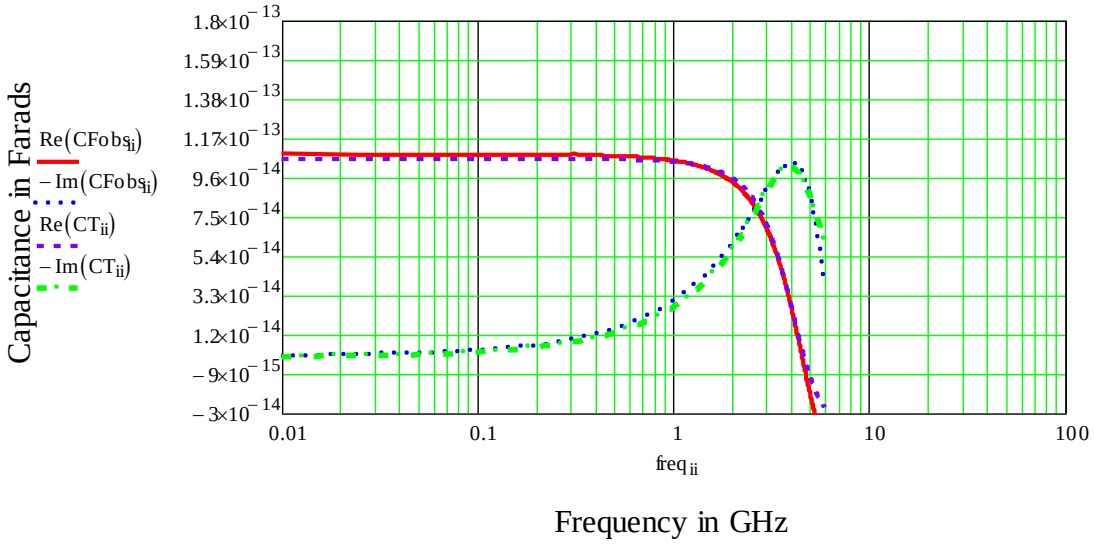

Figure 8-4. Inductance Is Required to Fit the Circuit Model as the Cohn Square Becomes More Metallic.

Thus using a smaller and a less resistive Cohn square we were able to shift the Debye relaxation to the right and using the Laplace method we were able to see a very shallow window in the regime of the Lorentz resonance in Figure 8-5. We also see a blip in the real part at the same frequency as one would expect with the Hilbert rules of causality.

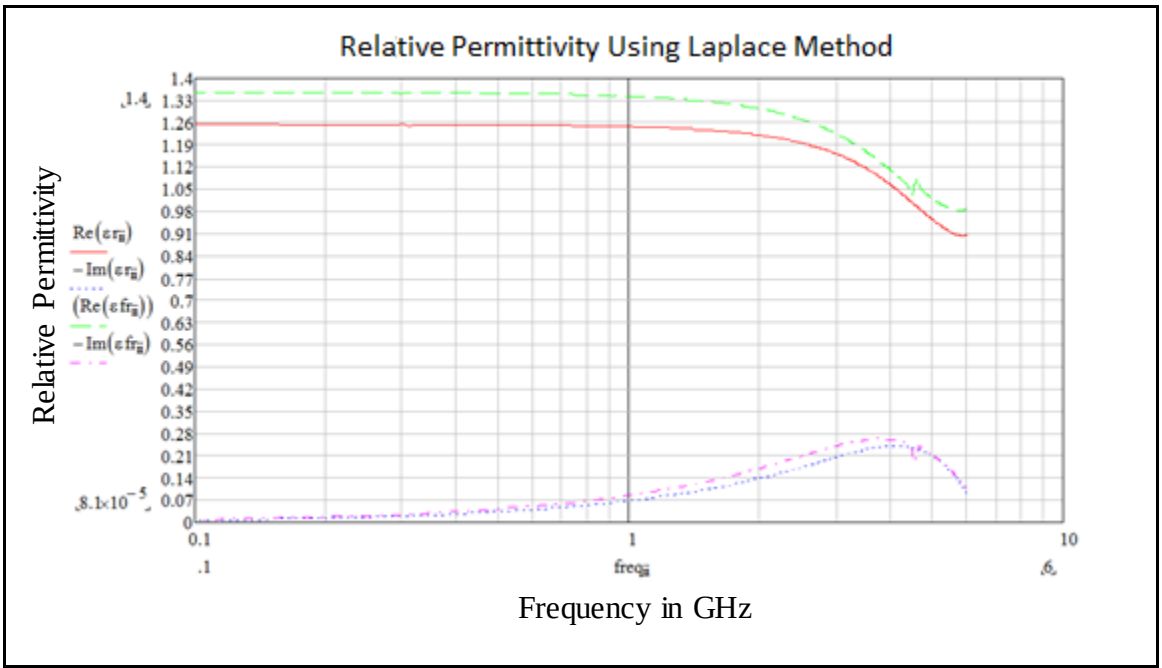

Figure 8-5. Permittivity of 100 Ohm Cohn Square with Lorentz Frames on One Side with Cohn Square 28 mm X 28 mm Using the Laplace Method.

Zooming on the imaginary part of the permittivity we see a shallow window in Figure 8-6.

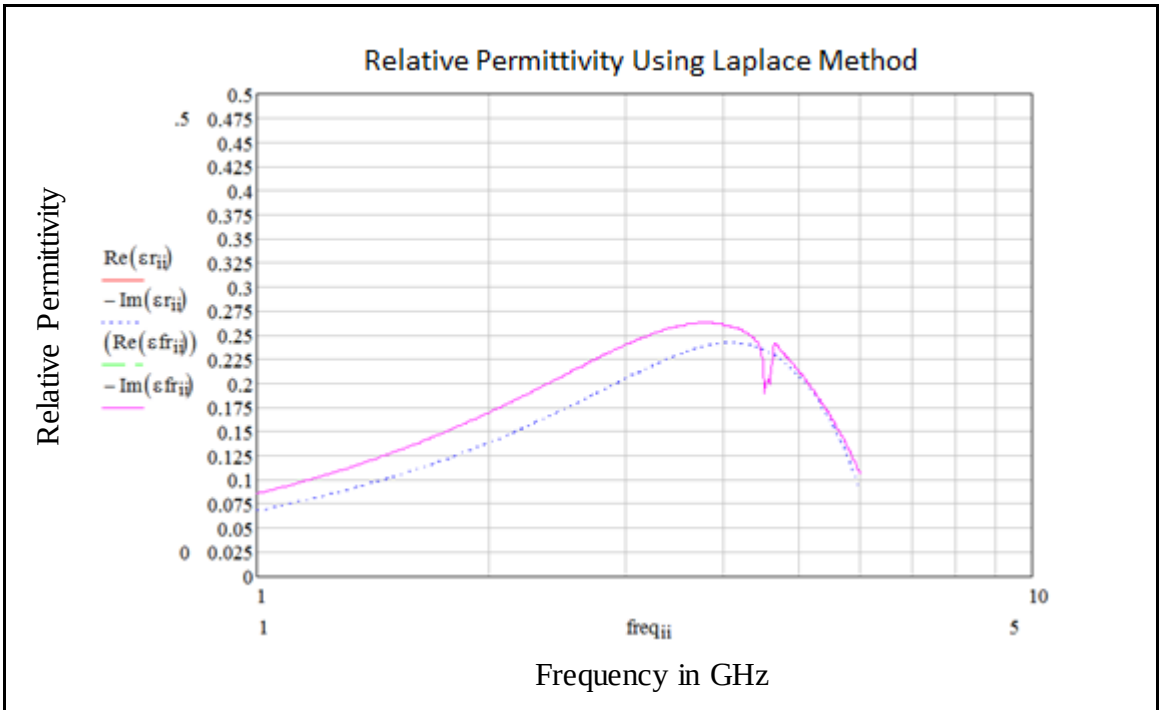

Figure 8-6. Permittivity of 100 Ohm with Lorentz Frames on One Side with Cohn Square 28 mm X 28 mm Using the Laplace Method: Zooming In.

In order to further explore whether the Debye was absorbing the Lorentz resonance we moved the Double Frame layer 1 mm further away from the Debye sheet. Using the Laplace method, focusing on the imaginary permittivity only, we achieved a very slight improvement as shown in Figure 8-7. So our hypothesis that the Cohn was absorbing energy from the frame is valid.

However in order to make a manufacturable material that can be tested in the laboratory in the range of 2 GHz to 10 GHz, the resonant elements of the Lorentz frame must resonate strongly at this frequency range. But the unit cell (the Cohn square) is electrically small to begin with, so the frame elements have to be very very small and still resonate sharply. This can be done in principle with these split ring resonators with very small gaps on a very thin PCB substrate.

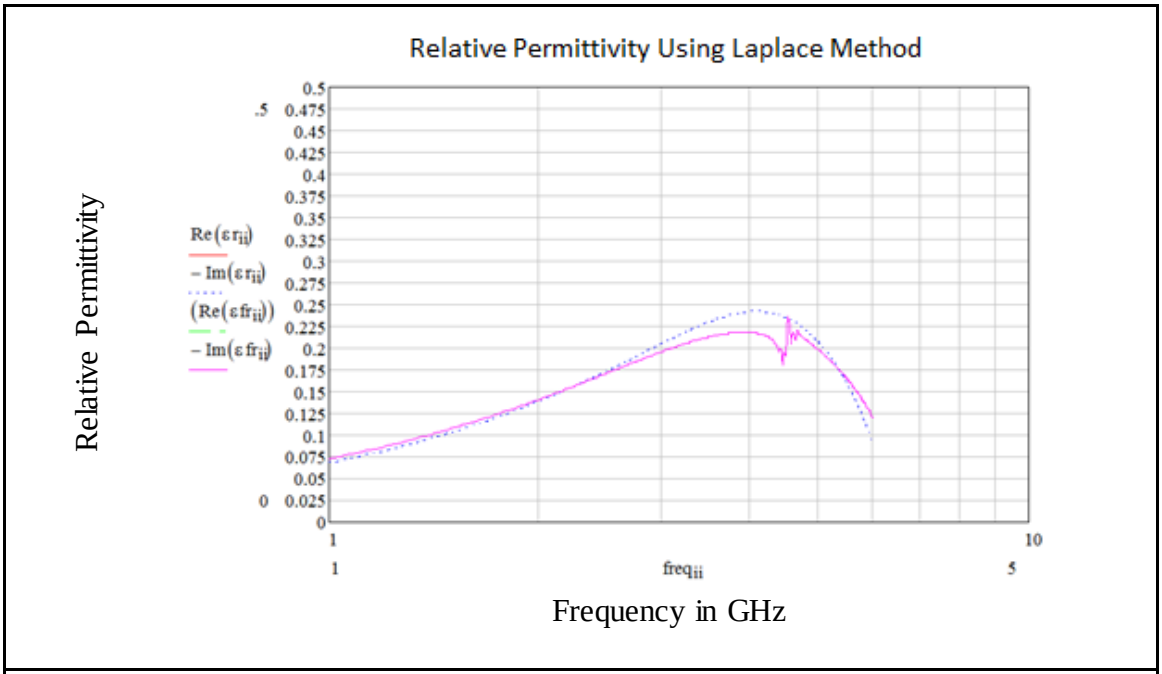

Figure 8-7. Permittivity of 100 Ohm Cohn Square with Lorentz Frames on One Side 2 mm Away with Cohn Square 28 mm x 28 mm Using the Laplace Method: Zooming In.

8.1.1 Lessons Learned

However we find that here is a much bigger problem here. In the coated sphere model the Lorentz material is a continuum (homogeneous - no atomic constitution) with intrinsic Lorentz properties that are not affected by the proximity (contact with) to the lossy particle. In other words when we bring the Lorentz material close to a lossy Debye material it does not change the properties of the Lorentz medium. In other words it retains its properties as was designed. If its atoms are placed close together in close proximity of a carbon atom it is not relevant. In an effective medium this is not the case especially if we have only a few atoms in a big medium called a Cohn circuit, it may no longer have the constitutive properties of a Lorentz medium. For a Lorentz effective medium made of macroscopic artificial molecules this is the challenge. The nearby Cohn square as we saw is always "loading down" the Lorentz frame element and it becomes very difficult to decouple them to control the Lorentz independently. If we could make nanometer resonators that were 10 deep layers and 10 wide so that they could maintain their properties there would be no problem. But we only had one double layer of frames. It is in principle possible with very small elements and details but is not practical to model or easily manufacture.

Also for a split ring resonator the current path is the inductor and the gap in between is the capacitance. That is our LC circuit. If we bring them really close the capacitance is very high. Or if we fill the gap with a high dielectric constant the capacitance is very high. Assuming this object is ½ wave resonant at 30 GHz; but we want the frame to resonate below 6 GHz, the resonant frequency needs to be lowered. If the ends are brought closer together and a high dielectric material is in the gap the capacitance can be made very large

to lower the resonant frequency. The problem is that these designs accomplish the Lorentz resonance of the frame with an enormous C (capacitance) violating the rule for a deep window. As discussed before in chapter 7, we want high inductance and low capacitance to accomplish our window. For a small object to resonate at low frequency the only choices are high L or high C. In order to move the resonance to be lower in frequency we added too much capacitance which is not a feasible proposition for a window. For the many iterations we performed with the Cohn square array covered with a Lorentz split ring resonator frames of various geometries, the capacitance was always enormous and the inductance very low.

8.2 Second Try: HFSS Design of the Cohn Square using a Bowtie Antenna with Chip Components

In this new approach the element in the unit cell was made to mimic the circuit as closely as possible. The LRC circuit zero circuit path was only placed around the resistor in the antenna. The antenna Cohn square element unit cell was now made as large as the effective medium model would allow given the intended frequency of the test (targeting 3 GHz) in the order of one eighth the wave length in order to make it as easy as possible to manufacture. We acknowledge that it will be too large at higher frequencies when it is close to half a wavelength in size invalidating the effective medium design in that case.

We didn't succeed with frame design because the frame was very small, so this time we make the Cohn square as big as possible so we have room to work. This way we can make the elements larger so they have greater resonance.

There were many other lessons learned from our first approach using the Cohn square and double frames. One was that the resonator element must be large enough to create a large resonance to create a deep window; but also the Cohn square cannot be so small relative to the unit cell size such that the resistive square themselves resonates.

So this time we start with a Bowtie Antenna design that occupies most of the unit cell as shown in Figure 8-8.

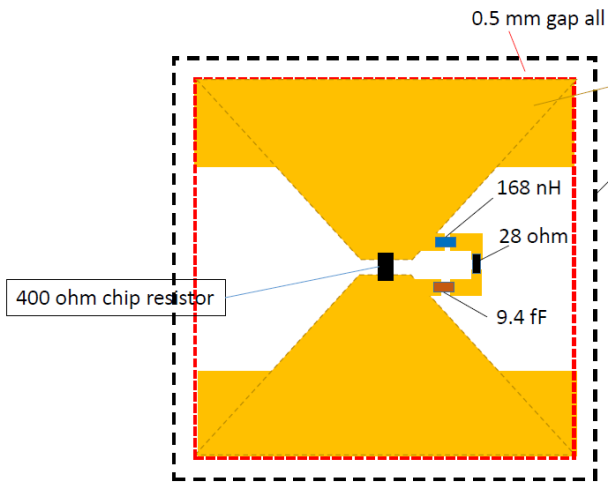

Figure 8-8. A 9.5 mm Bowtie Antenna in a 10 mm Square Unit Cell.

The shorted bowtie antenna (without the 400 ohm resistor) was run on HFSS to determine the resonant frequency of this antenna which was found to be 8.2 Ghz as shown in Figure 8-9.

The bowtie equiped with a 400 ohm physical chip resistor to emulate the resistive path was also run on HFSS in lieu of a Cohn square to create a Debye material. Figure 8-10 shows this HFSS configuration.

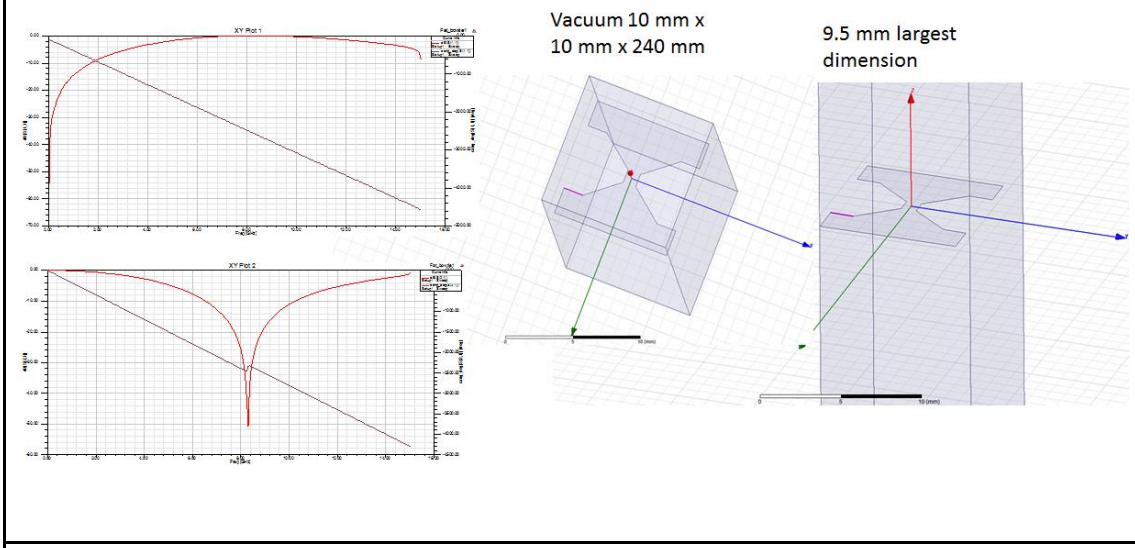

Figure 8-9. Bowtie Antenna Resonant Frequency.

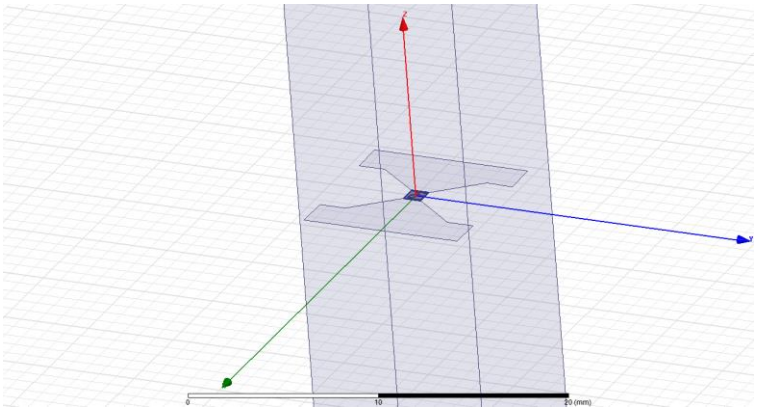

Figure 8-10. Bowtie Antenna with 400 Ohm Resistor.

Many iterations of a 9 mm by 9 mm Cohn square were run along with the 9 mm by 9 mm Bowtie. We found HFSS does not have the dynamic range to optimize at 0.001 GHz to 15 GHz. HFSS runs that were optimized to 15 GHz did not give accurate values at 0.001 GHz. So we stepped down the optimization frequency to 6 GHz, 5 GHz and then 1 GHz. The Bowtie and the Cohn square started to converge at 1 GHz; however around 0.001Ghz and below the data was clearly unstable. HFSS does not have a dynamic range of 5 orders of magnitude below the optimized frequency. The best option was to optimize at 1 GHz and only focus up to 1 GHz using log steps, then truncating points at the frequency where the data fluctuates where the Cohn square was no longer a straight line. Following the same method for the Bowtie reasonable results were obtained. It was also clear from these runs that frequency of optimization was more important than the value of the S parameter in HFSS.

Three configurations a 1) Bowtie antenna shorted, a 2) Cu Cohn square of the same dimensions and the same 3) Cu Bowtie antenna with a 400 Ohm resistor are summarized below.

These experiments were performed in HFSS to make sure HFSS was behaving as expected; the DC capacitance was the same in all cases using both the Cohn and Diaz methods. The results are summarized below in Table 8-1. A 1) Cu Cohn square and the same 3) Cu Bow-tie Antenna with a 400 Ohm Resistor; and 3) Bowtie antenna shorted.

Design	DC Capacitance	DC Permittivity	Variation
9 mm x 9 mm Cohn	4.45x10^-11	2.33	1 = Cohn
9 mm x 9 mm Cohn Bowtie + 400 Ohm resistor	4.1x10^-11	2.2	0.92Cohn = Bowtie +400 ohm
9 mm x 9 mm Cohn Bowtie	4.175x10^-11	2.293	0.94 Cohn = Bowtie

Table 8-1. A 1) Cu Cohn square and the same 3) Cu Bowtie Antenna with a 400 Ohm Resistor; and 3) Bowtie antenna shorted

Figure 8-11 and Figure 8-11 show the capacitance of the sheet and the expected permittivity of an effective medium design with 10 mm separation length between capacitative sheets; prior to adding the zero circuit. This is a typical Debye material.

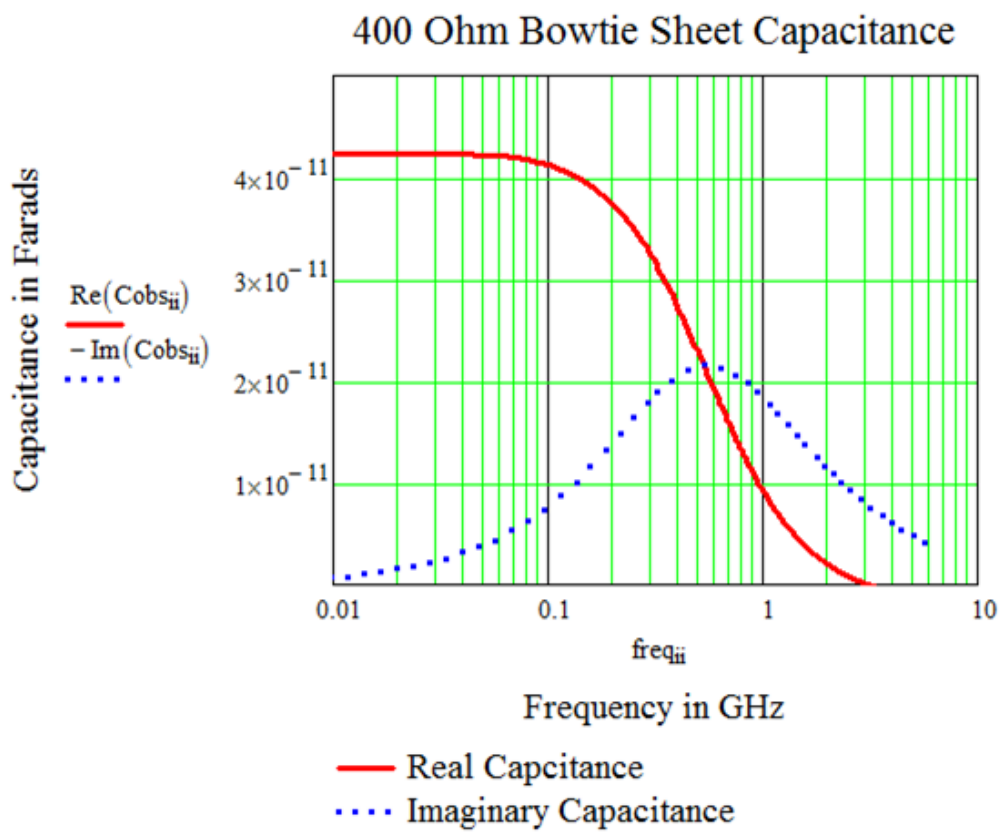

Figure 8-11. Capacitance in Farads Using the Unit Cell Method of a 9 mm x 9 mm Bow-tie Antenna with a 400 Ohm Resistor.

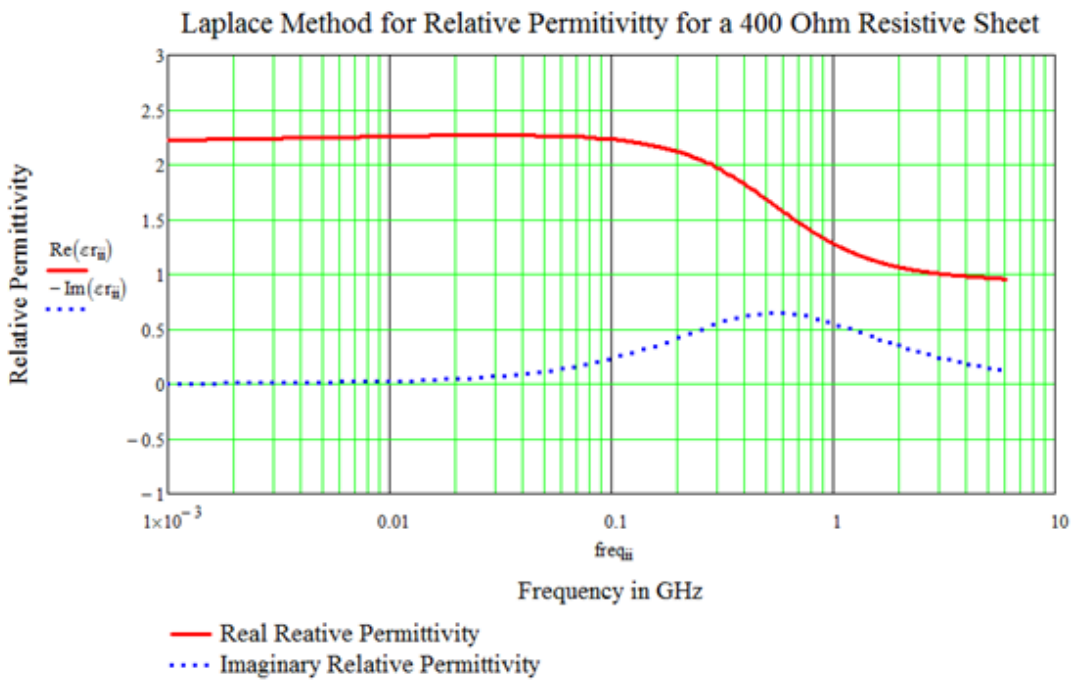

Figure 8-12. Capacitance in Farads and Relative Permittivity Using the Laplace Method of a 9 mm X 9 mm Bowtie Antenna with a 400 Ohm Resistor.

Determining the sheet Capacitance and DC Permittivity we found that they were in the same range but not exactly the same ratio of 0.94/0.96 = 0.98 for the bowtie to the Cohn square but similar in range using the Markowitz approach as shown in Figure 8-13.

Finally the bowtie resistor is in the same range but the lowers value as we would expect, to 0.92 Cohn square.

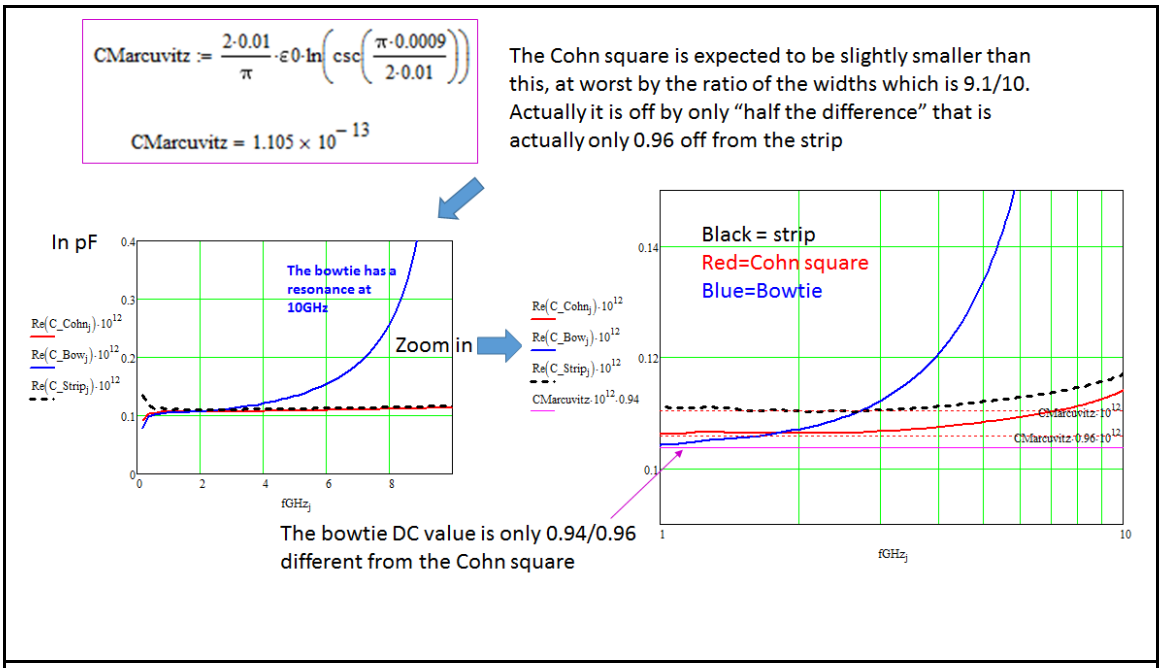

Figure 8-13. The Cohn Square and Bowtie DC Capacitance Should Be Very Close.

Once we validated our HFSS process and determined our base permittivity without the zero circuit, we chose to insert chip inductors, resistors and capacitors in shunt with the 400 ohm resistor at the center of the Bowtie antenna as shown in Figure 8-8. COTS (Components of the Shelf) were surveyed to determine the size and footprint for lumped circuit elements for our window design. Digi-Key and Mouser Electronics were what most of the PCB manufacturers are using.

8.2.1. Resistors

The 28 and 400 ohm resistors are pretty straight forward to obtain the correct value and were available in the sizes we needed.

28 Ohm Resistor http://www.digikey.com/products/en/resistors/chip-resistor-surface-mount/52?k=&pkeyword=&pv7=2&FV=ffe00034%2C4040d&mnonly=0&newproducts=0&ColumnSort=0&page=1&stock=1&quantity=0&ptm=0&fid=0&pageSize=250

400 Ohm Resistor http://www.digikey.com/products/en/resistors/chip-resistor-surface-mount/52?k=resistor&k=&pkeyword=resistor&pv7=1&FV=fff40001%2Cfff800e9%2Cffe00034%2C401f8&mnonly=0&newproducts=0&ColumnSort=0&page=1&stock=1&quantity=0&ptm=0&fid=0&pageSize=100

However these resistors were double the size of the gap that was in the middle of the Bowtie antenna.

8.2.2 Inductors

The inductors could only be found in 165 or 169 nH. We selected the 169 nH, inductor. It was very difficult to find an inductor where the self-resonance was greater than the desired window frequency of 2 to 6 GHz. When we found one that had a self-resonance below 0.88 GHz, that we could use if we could bring the Lorentz resonance to be less than 1 GHz; but the problem became that the inductors were rather large compared to our unit cell; almost half the cell size. The problem was further complicated by the fact that inductors have a capacitor in shunt and we would have to determine the effective inductance.

169 nH Inductor http://www.digikey.com/products/en/inductors-coils-chokes/fixed-inductors/71?k=inductor&k=&pkeyword=inductor&pv19=2856&pv19=411&FV=fff40003%2Cfff80013&mnonly=0&newproducts=0&ColumnSort=0&page=1&quantity=0&ptm=0&fid=0&pageSize=100

8.2.3. Capacitors

The smallest capacitor we found was 0.05 pico-Farads. We would have to put 5 in series to obtain an effective capacitance of 10 femto-Farads which may prove to be cumbersome.

Five 0.05 pF in series http://www.digikey.com/product-detail/en/avx-corporation/04021JR05ZBSTR/478-9743-2-ND/5764927

The survey selections are summarized below in Table 8-2. Chip COTS of the Shelf for Bowtie and Zero Circuit.

Circuit Element	Configure		Value	L in mm	W in mm	H in mm	Tolerance	Manufacturer
PAT400ATR-ND			400 Ohm	1.63	0.81	0.46	0.10%	Vishay
311-28.0LRCT-ND			28 Ohm	1	0.5	0.4	-1%	Yageo
535-12008-2-ND			169 nH	9	4.4	5	5%	Abracon LLC
478-9743-2-ND	5 Cap in series	10 fF	0.05 pF	1	0.55	0.5	0.01	AVX Corp
		not 9.4						

Table 8-2. Chip COTS of the Shelf for Bowtie and Zero Circuit

8.2.4 Conclusion

The smallest elements were 1/10 of the unit cell. And the largest components the inductors were about half of the unit cell. This would impede manufacture of the bow tie antenna unless it could somehow be designed out of the plane of the antenna in the Z direction. Using the best case a Bowtie antenna with some minor modification from the above design was run on HFSS with and without a zero circuit. The following results in Figure 8-14 were obtained. Even though we were able to bring the Lorentz resonance below the self-resonance of the inductor we did not get a window.

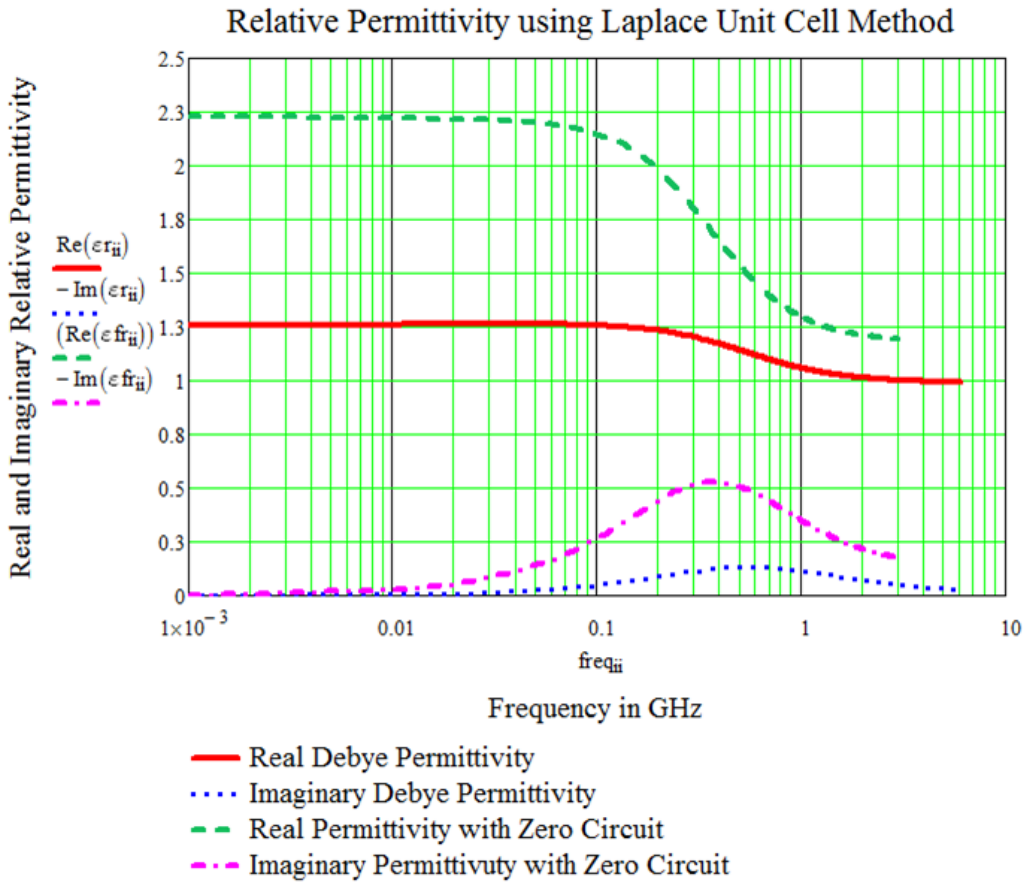

Figure 8-14. Real and Imaginary Permittivity of a Bowtie Antenna with and without the Zero Circuit

After carefully observing the Bowtie antenna at a wider range of frequency we find that there are several competing flux paths across the antenna as seen in Figure 8-15.

All the current does not flow through the resistor via the center path. There are many alternative current path from the hat section of the antenna to the other hat and the flux bypasses the zero circuit. Therefore we do not find a window using the Bowtie design.

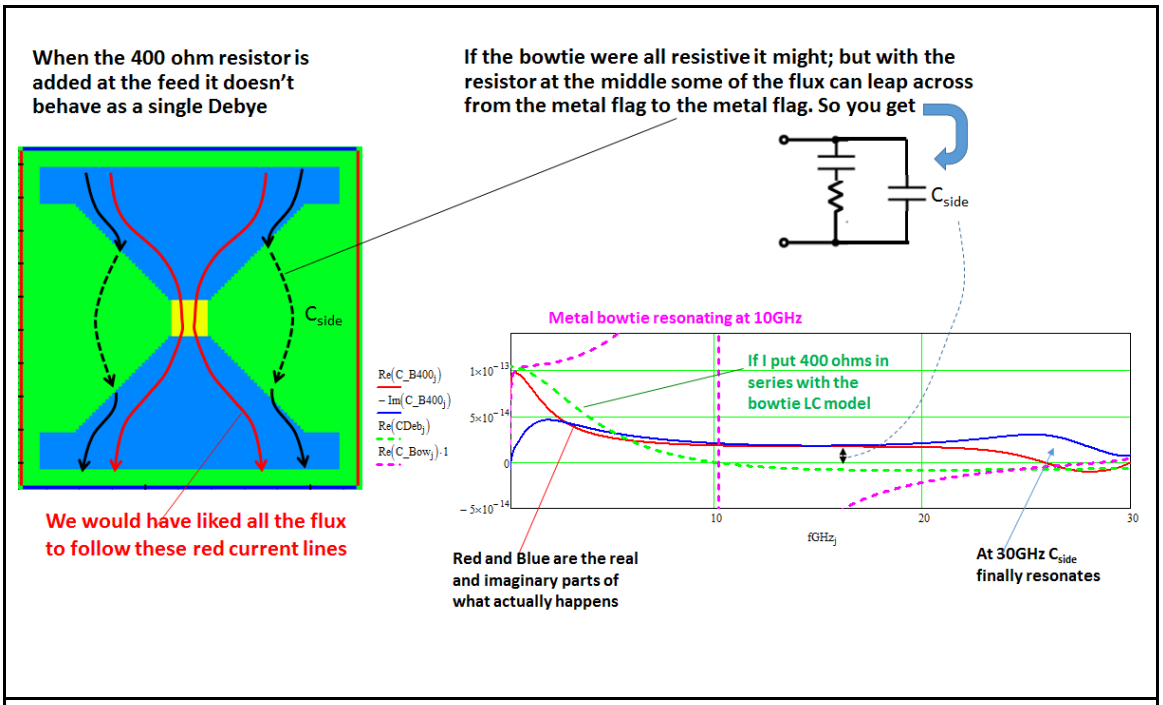

Figure 8-15. The Bowtie with 400 Ohm Resistor Does Not Behave like a Single Debye.

So we go to the Munk's standard dipole which is an I-beam design to avoid these alternative flux paths. Also these chip LRC components surveyed could be potentially used for any other design including the Munk I-beam which is our next try.

8.3 Third Try: HFSS Design of the Cohn Square Debye Sheet with Munk Dipole I-beam

In our third try we use the same approach as the second try explained above but this time with the Munk dipole I-beam so the flux paths do not bypass the zero circuit as shown in Figure 8-16.

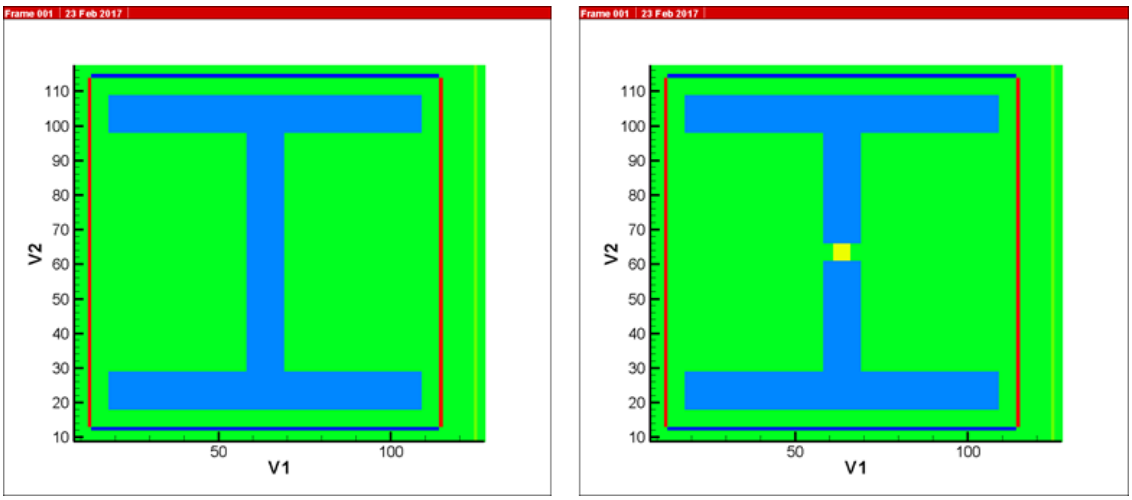

Figure 8-16. Munk Dipole I-Beam Antenna with and without Chip Resistor.

Because of the difficulties with chip inductors and in order to obtain the large self-inductance required for the zero circuit to function properly this time we made two Cu turn loops, as large as would fit the unit cell, and then we enforced symmetry. The series capacitance as required by the window circuit needs to be small and so in lieu of putting five capacitors in series to achieve the desired capacitance we purposefully created capacitance with overlapping Cu strips on two sides of the substrate. Applying these constraints from our lessons learned we dramatically reduced the cost of the part by eliminating the chip inductors and capacitors and we created the following design with the Munk I-beam with the zero circuit

shown in Figure 8-17. The red square is a chip resistor. The zero circuit consists of the highly inductive loops on both sides of the I-beam and the capacitive overlaps across the substrate. We selected Duroid 5880, 10 mils thick, as the substrate where the copper etched I-beam and zero circuit traces are made with ½ oz. copper.

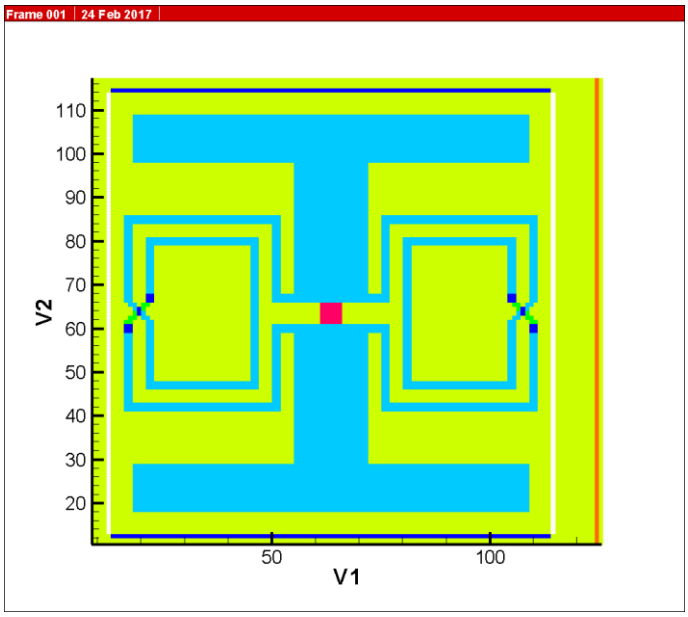

Figure 8-17. Munk I-Beam Dipole Antenna with Zero Circuit Consisting of Chip Resistor and Inductive Loops and Capacitive Overlaps

We designed a single sheet and modeled it in HFSS with and without the inductive loops and the two symmetric capacitive overlaps that emulates the zero circuit. The unit cell is 10 mm x 10 mm and the transmission line is 240 mm long. The I beam was designed to be a 9 mm x 9 mm dipole on a 10 mil Duroid substrate with a 100 ohm resistor as seen in Figure 8-18. Using the methodology established before we determine the sheet capacity from the HFSS obstacle admittance shown in the plots of Figure 8-19.

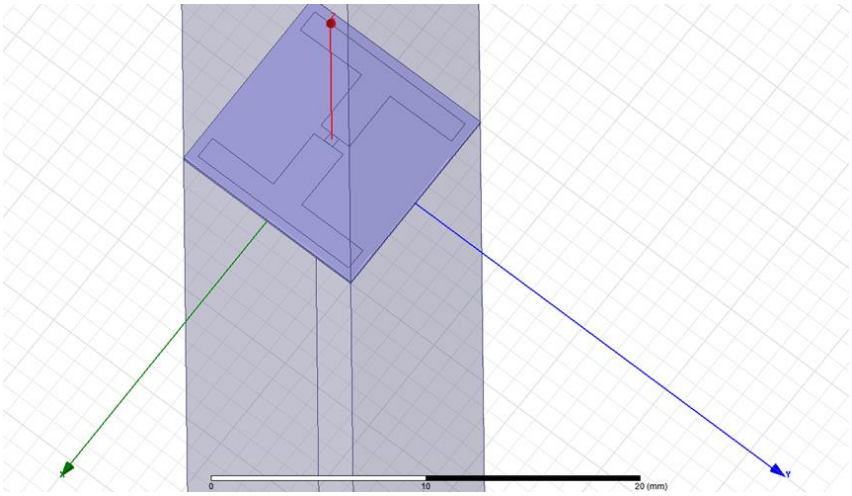

Figure 8-18. I-Beam Design on 5880 Duroid with Before Adding the Zero Circuit.

As expected the capacitance, looks similar to the Debye Cohn squares we saw before. If we assume an effective medium consisting of these sheets 10 mm apart we see that the permittivity will behaves like a Debye material.

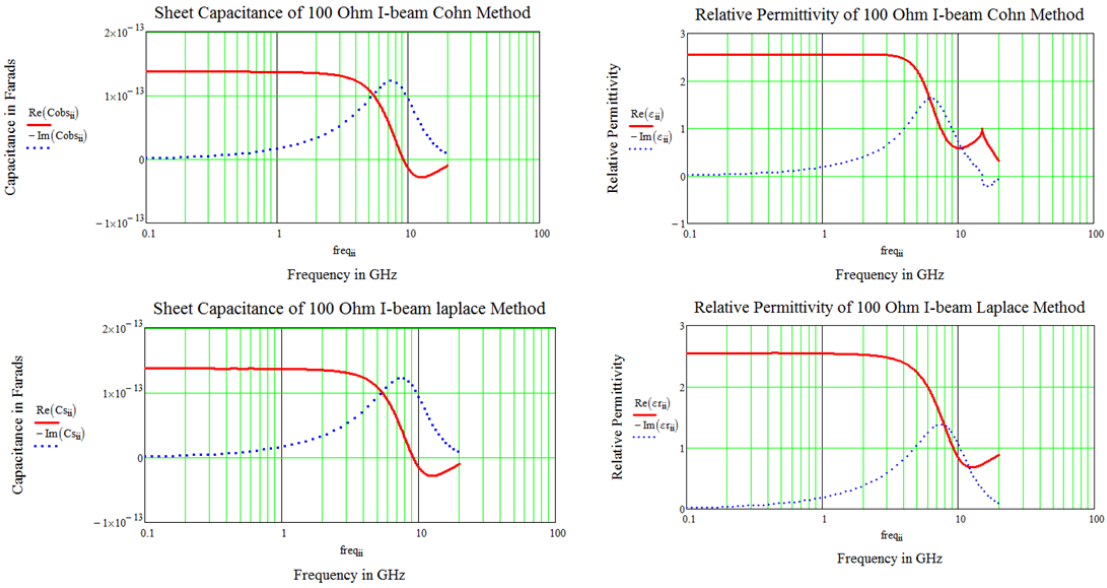

Figure 8-19. Sheet Capacitance and Predicted Permittivity of Layers 10 mm Apart Using the Cohn and Laplace Methods Respectively

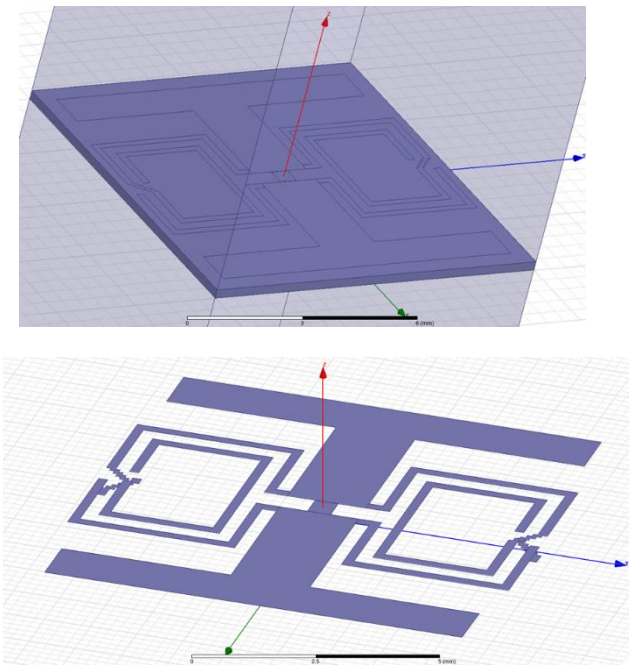

Figure 8-20. Munk Dipole I-Beam Design with Zero Circuit.

We also ran HFSS with the window circuit as shown in Figure 8-20. And as before we determined the sheet capacitance and we find there is a window at 3.2 GHz as shown in Figure 8-21. We see that the real part also has a kink corresponding to the window frequency as we expect due to the Hilbert relationship between the real and imaginary parts. We see the resonance of the I-beam at 10 GHz. If we compare the capacitance before and after the zero circuit was added in HFSS, we find unlike our other designs the window is deep. In Figure 8-22 and Figure 8-23 we plot capacitance where the frequency is not logarithmic for a closer view.

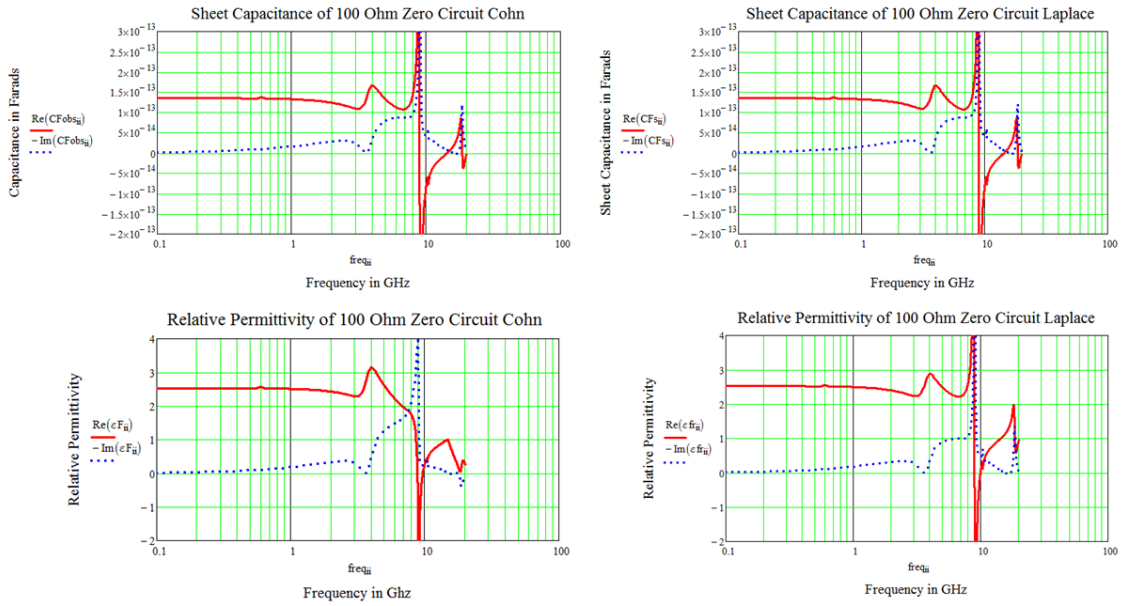

Figure 8-21. Sheet Capacitance of the I-Beam with the Zero Circuit and Predicted Permittivity if Layers Were 10 mm Apart Using the Cohn and Laplace Methods.

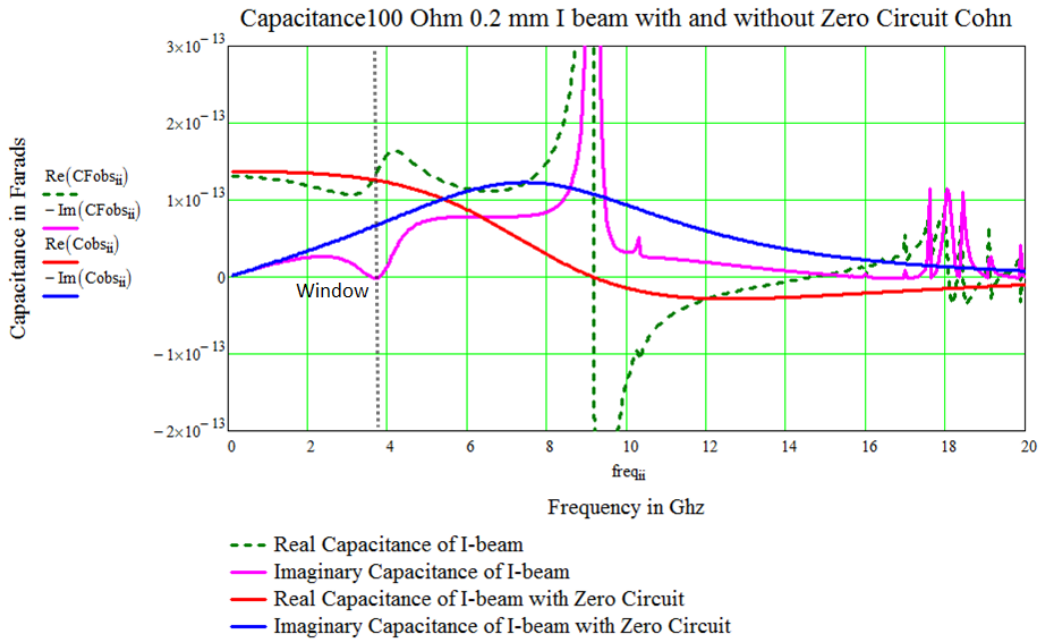

Figure 8-22. Sheet capacitance of the I-beam with the Zero Circuit 2 mm lines 100 ohm I-beam, window is formed at 3.9 GHz.

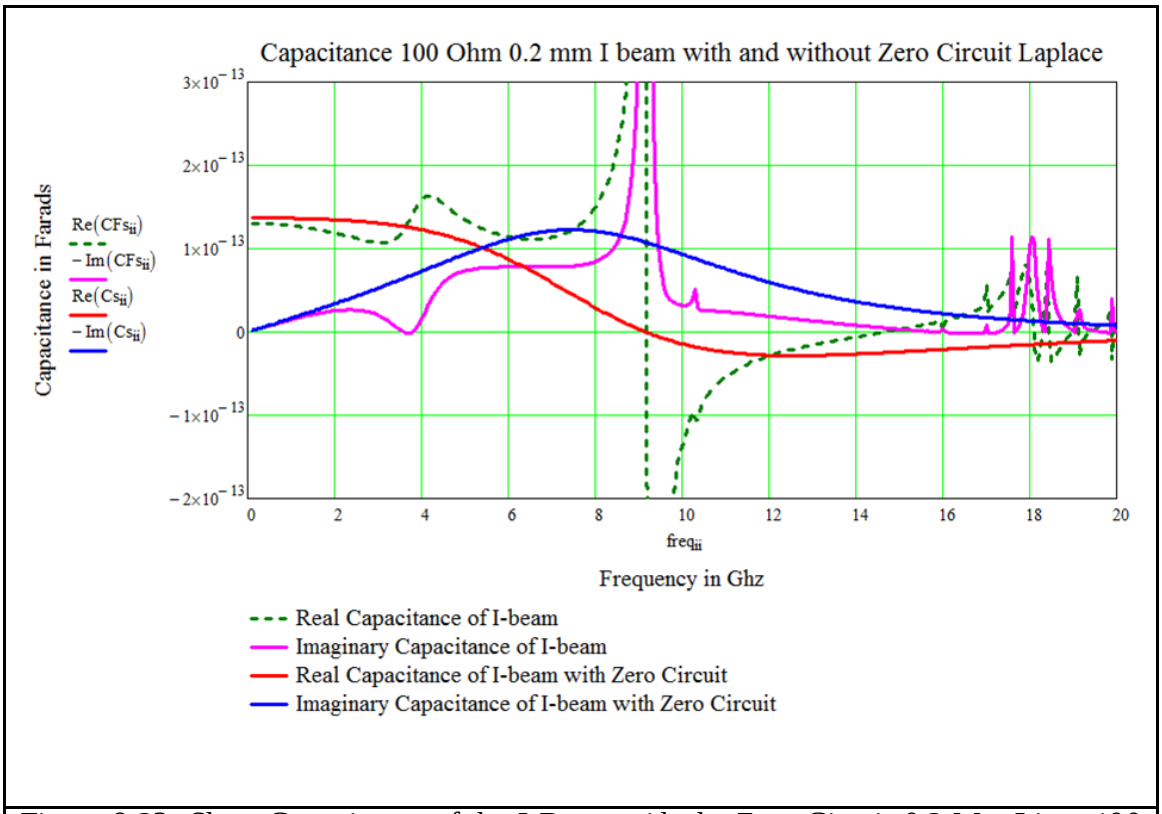

Figure 8-23. Sheet Capacitance of the I-Beam with the Zero Circuit 0.2 Mm Lines 100 Ohm I-Beam.

The thinnest lines in the inductive loops were originally designed to be 0.2 mm thick considering the limits of etching thin lines. Advanced Circuits claimed that they can do a Cu line 0.00275 inches which is 0.07 mms. Because we wanted to have as high an inductance as possible to obtain the best window, we made the inductive loops as thin as possible redesigning them to half the original width to be 0.1 mm thick. This way it was still manufacturable using PCB copper etch processes. With this new iteration the window in the capacitive sheet appears to be slightly narrower in other words sharper. Please see Figure 8-24 and Figure 8-25.

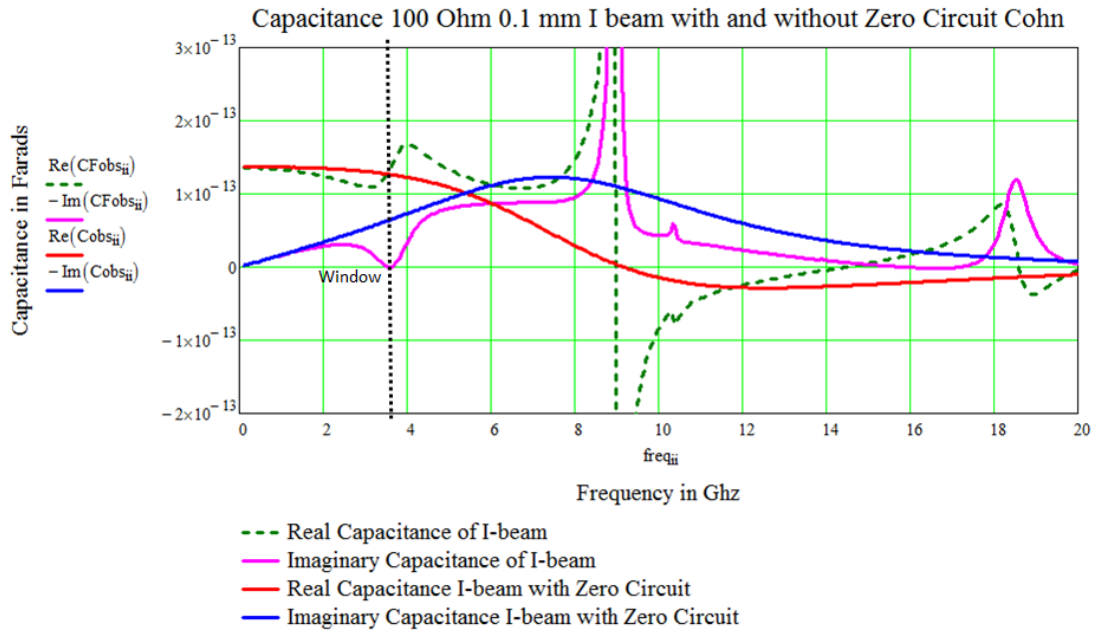

Figure 8-24. Sheet Capacitance of the I-Beam with the Zero Circuit 0.1 mm Lines 100 Ohm I-Beam.

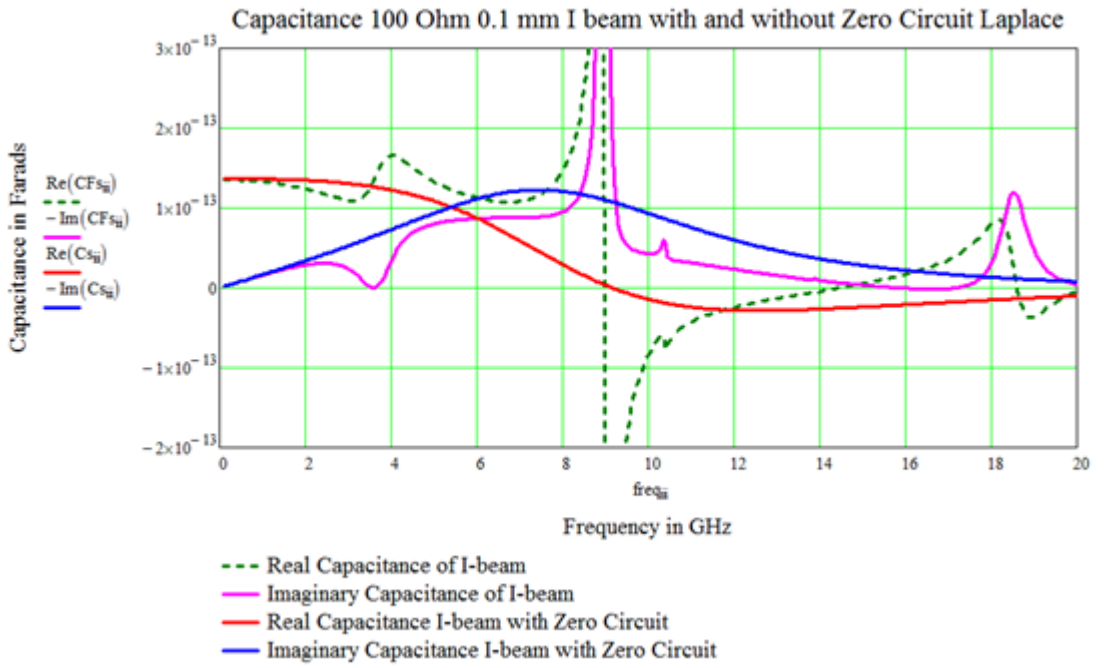

Figure 8-25. Sheet Capacitance of the I-Beam with the Zero Circuit 0.1 mm Lines 100 Ohm I-Beam.

Since we may need to tune our Debye as we did in the previous sections we also determined the sheet capacitance of the I-beam using a 50 ohm resistor. The results are very similar. This design gave us our best window as seen in Figure 8-26 and Figure 8-27.

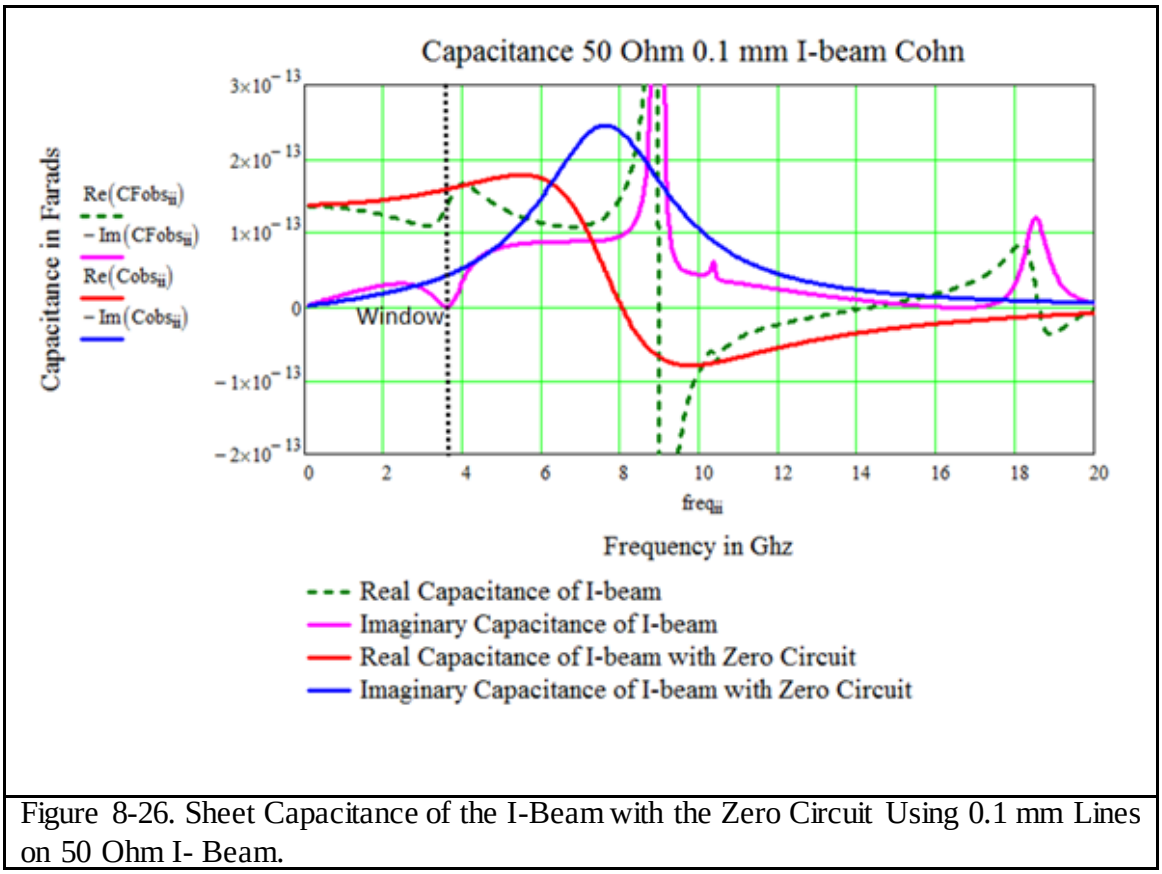

Figure 8-26. Sheet Capacitance of the I-Beam with the Zero Circuit Using 0.1 mm Lines on 50 Ohm I- Beam.

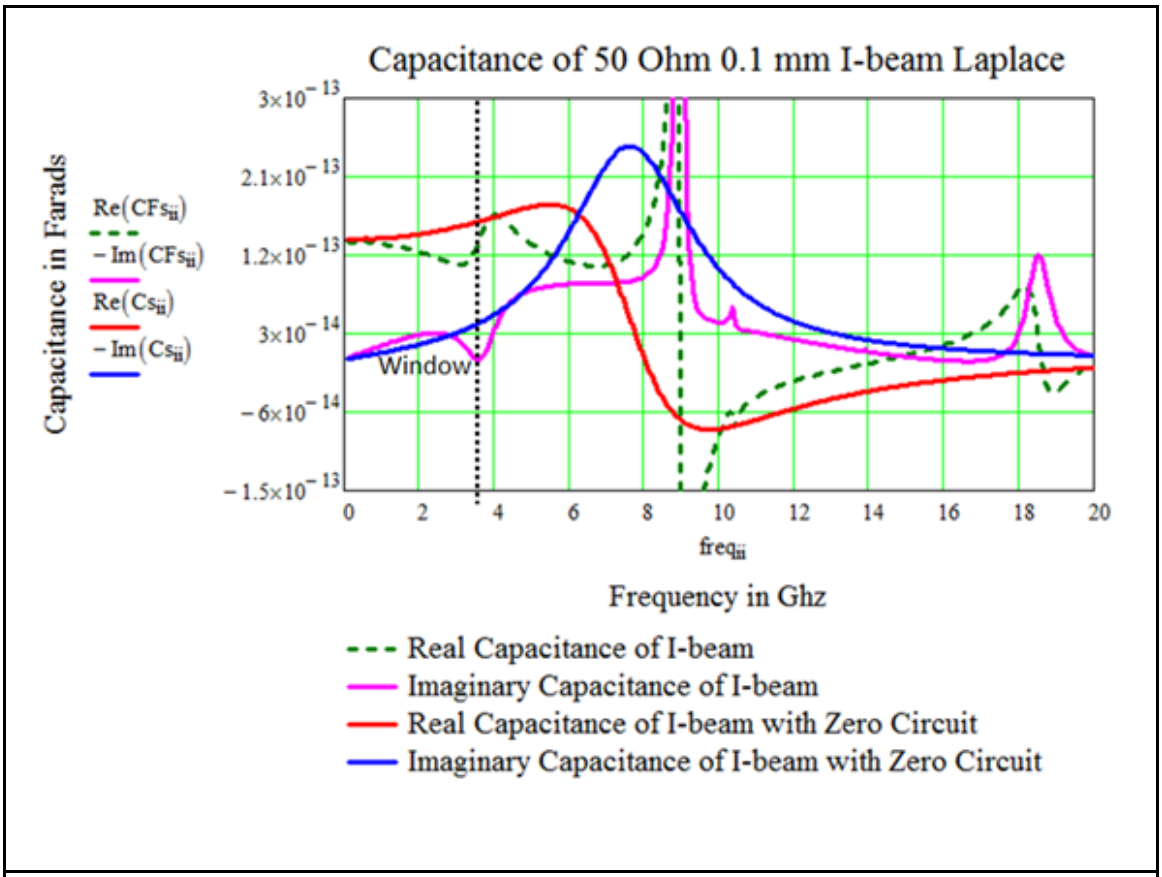

Figure 8-27. Sheet Capacitance of the I-Beam with the Zero Circuit 0.1 mm Lines on 50 Ohm I- Beam

8.3.1 Does the Munk I-beam Data without the Zero Circuit fit the Debye Circuit Model?

We have demonstrated before that in chapter 7 that we can fit the admittance data of an RC material (Debye Material) with a Debye circuit model. If the material has inductance, as we would expect the I-beam to have; we need to fit it to the more generic Lorentz circuit model. So for our best window shown in Figure 8-20 we use the calculated sheet admittance and capacitance and try to fit it to a Lorentz circuit model described in section 7.5. Given that the S11 reflection coefficient from our HFSS simulation, we obtained the shunt admittance of the obstacle and fit a circuit model to the data as shown in Figure 8-28 below; where the model is represented by the black and magenta curves for the real and imaginary

capacitance respectively. And the red and blue curves are the real and imaginary values of the sheet capacitance derived from HFSS.

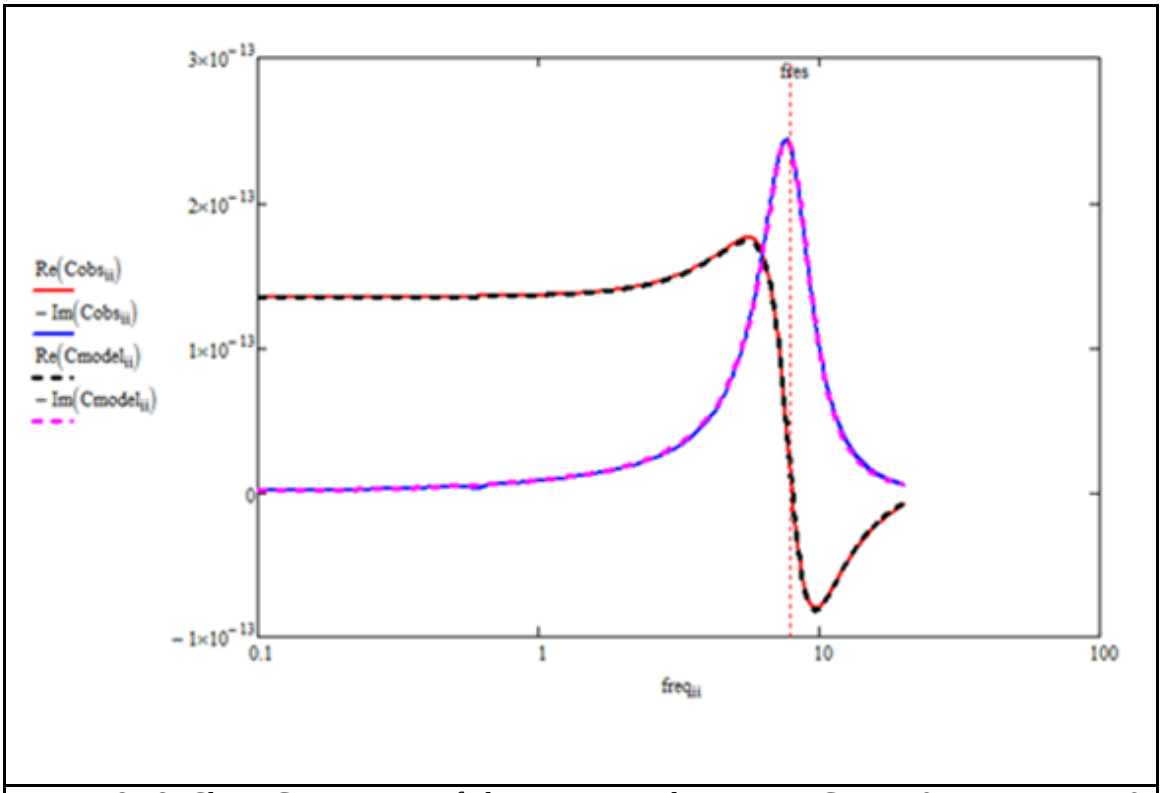

Figure 8-28. Sheet Capacitance of the I-Beam with No Zero Circuit 0.1 mm Lines 50 Ohm.

The circuit model is guided by the expectations that we will have an LRC series circuit as seen in section 7.4 because we expect the I-beam to be a Lorentz given that it is an antenna. We then vary the parameters in the circuit equation to get the best fit.

From the data we observe the DC value of the capacitance, CDC0 = Re ($Cobs_1$) which tells us the sum total of all capacitances in the infinite sum of LRC circuit model. This value in this instance is 0.1334 pico-Farads. We expect as a minimum that this might be $C_{infinity}$ plus the C of the LRC series branch.

Determining the LRC Circuit Parameters

We model an LRC permittivity as a Lorentz capacitance in the following form.

$$C_{Lorentz} = \frac{\Delta C}{1 + j\frac{f}{f_{res}}\frac{1}{Q} - \left(\frac{f}{f_{res}}\right)^2}$$

where ΔC is a fraction of CDC0, f is the frequency, f_{res} is the resonant frequency and Q is the damping factor of the oscillator.

Since the imaginary part of the Lorentz is independent of the $C_{infinity}$, from the strength of the Lorentz we can obtain the DC value and the Q. The Q can be deduced from the half-height width of the peak of the imaginary part or from the ratio of the peak of the imaginary part to the DC real part which in this case is about 2. Assuming the resonance frequency is close to the frequency where the real part goes to zero, or close to the frequency of the peak imaginary part and then it is a matter of varying these slightly to fit the data.

With a moderate amount of iteration we determined $\Delta C = 0.9 CDC0$, $f_{res} = 7.9\ Ghz$ and $Q = 1.975$, and the expression becomes the following:

$$C_{Lorentz} = \frac{0.9\ CDC0}{1 + j\frac{f}{f_{res}}\frac{1}{1.975} - \left(\frac{f}{f_{res}}\right)^2}$$

This leaves $C_{infinity}$ = 0.1CDC0. To find the circuit parameters, we know that inductance, L is related to the capacitance, C by the frequency and that the definition of the Q is the square root of the ratio of the inductive time constant (L/R) to the capacitive time constant (RC).

$$L00 = \frac{1}{(2\pi fres\, 10^9)^2 (C00)}$$

$$L00 = 3.355x10^{-9}$$

The Q is the square root of the ratio of L/R to RC

$$R00 = \sqrt{\frac{L00}{C00}}\frac{1}{Q0}$$

$$R00 = 84.313$$

So the circuit becomes the following in Figure 8-29.

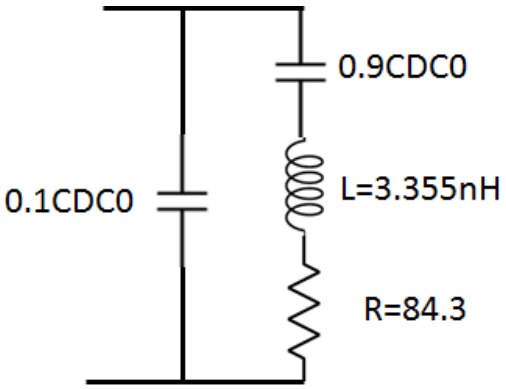

Figure 8-29. Sheet Capacitance of the I-Beam with 50 Ohm Resistor Circuit Model.

So the I-beam with the 50 ohm resistor turns out to be the parallel sum of a capacitor and a Lorentz LRC expressed by the following admittance equation.

$$Y00_{ii} = \left[R00 + i2\pi freq_{ii}10^9 L00 + \frac{1}{i2\pi freq_{ii}10^9 C00}\right]^{-1} + i2\pi freq_{ii}10^9 C0i$$

And therefore the capacitance is given by the following equation which is plotted Figure 8-28.

$$Cmod00_{ii} = \frac{Y00_{ii}}{i2\pi freq_{ii}10^9}$$

The First Circuit Branch

The *first circuit branch* represents the I-beam (L=3.355 nH) in series with the 50 ohm resistor and the adjacent I-beam (on the top or bottom in the adjacent unit cell). The HFSS resistor is not equal to the circuit resistor because there are multiple flux paths from the

PEC to the resistive obstacle. For the circuit there is only one path for the current to flow through the resistor. This makes the resistor in the representative circuit 1.67 times greater to emulate the resistive square interaction in HFSS. The 0.9CDCO capacitance is due to the capacitance between the I-beams elements themselves.

The Second Circuit Branch

The *second branch* which is a single capacitor (C= 0.1CDCO) represents the capacitance between the two hats within a single I-beam itself. Also it makes sense that the fraction of the CDCO capacitance is much less for the intra I-beam capacitance than the inter I-beam capacitance. The distance is 6.15 mm for the former and 1 mm for the latter. So we expect the series capacitance to be greater in the first branch than the parallel capacitor. There is some inductance in the second branch in series with 0.1CDCO due to the hats of the I-beam but are negligible.

Conclusion

So the I-beam data closely fits the circuit model that was designed and behaves as expected. The I-beam by itself is Debye like with slight Lorentz traits because of the self-inductance of the I-beam. But this inductance depends on the value of the resistor used. Also in some cases this Lorentz like behavior as we have seen before in chapter 7 can be due to the proximity coupling to the nearby sheets.

8.3.1.1 Variation of I-beam Inductance on the Material Model

The Debye (or Lorentz) permittivity as expected changes as a function of the resistor value in the Debye (Lorentz) Circuit Model. ***In the case of this I-beam design the assigned value of the resistor significantly changed the permittivity behavior of the material from a Debye to a Lorentz as the resistor value is decreased. This is because when there is less resistance in the current path of the I-beam, it is free to resonate and the inductance shows up in the permittivity behavior of the material; and therefore starts resembling a Lorentz material.***

S11 reflection measurements were performed in HFSS for a single layer of the I-beam in a 10 mm by 10 mm unit cell. Resistor values of 100 ohms, 75 ohms and 50 ohms were constructed and the resulting S11 measurements were used to calculate the permittivity as a function of frequency to determine the baseline properties of the material. Both the Cohn method and the Laplace methods described in chapter 7 were used initially assuming a 10 mm separation distance between layers. Results are shown in Figure 8-30 through Figure 8-35. As the resistor values were reduced from 100 ohms progressively to 50 ohms, the material behavior changed from a Debye to a Lorentz.

For a Constant 10 mm Separation Distance: Changing Resistor Values

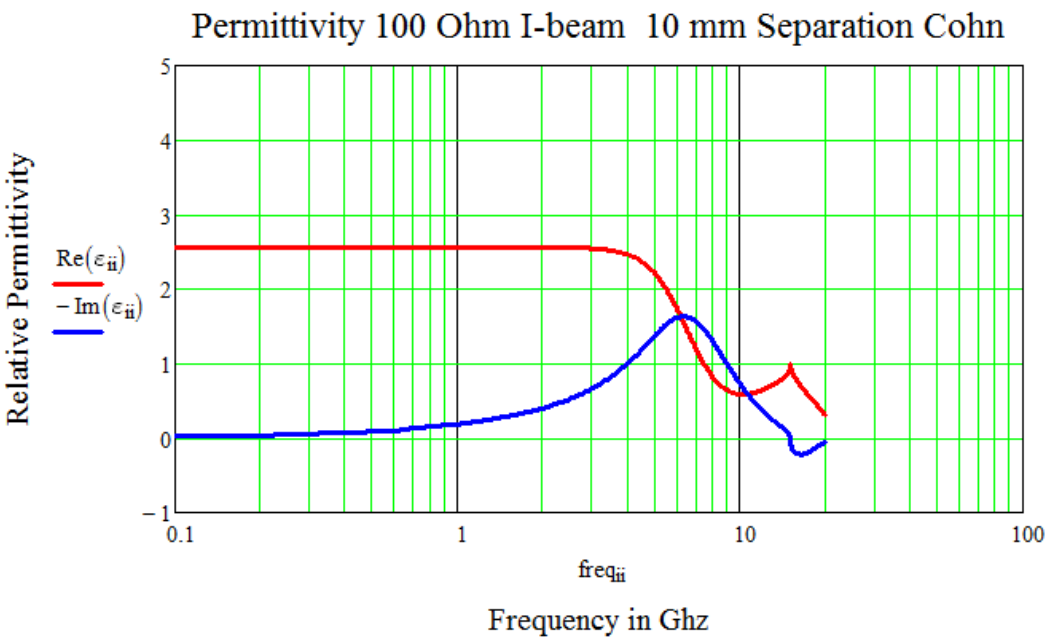

Figure 8-30. Cohn Method Permittivity 100 ohm.

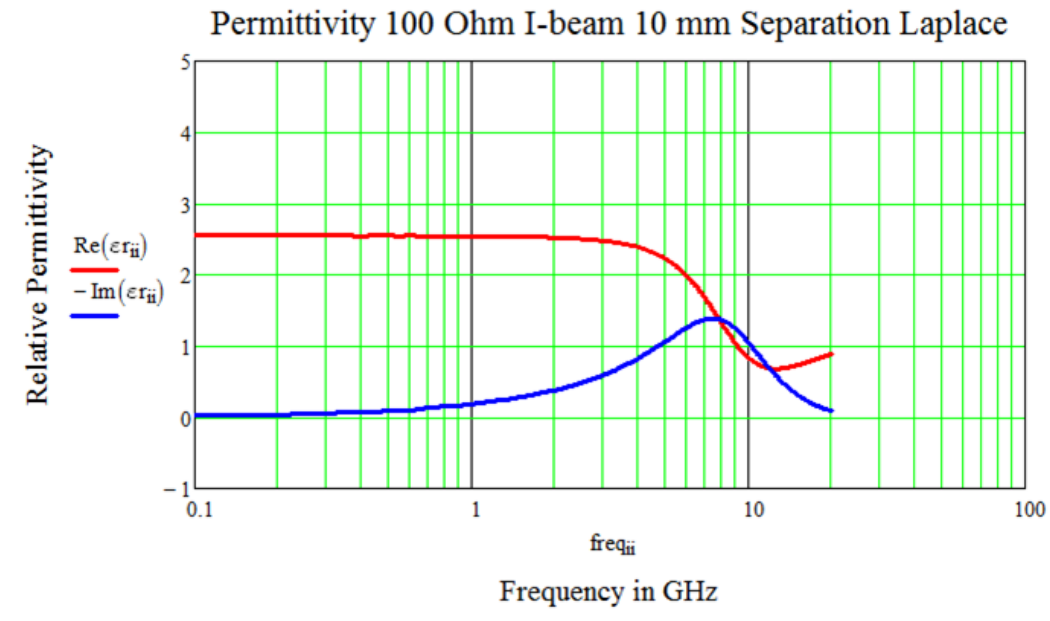

Figure 8-31. Laplace Method Permittivity 100 Ohms.

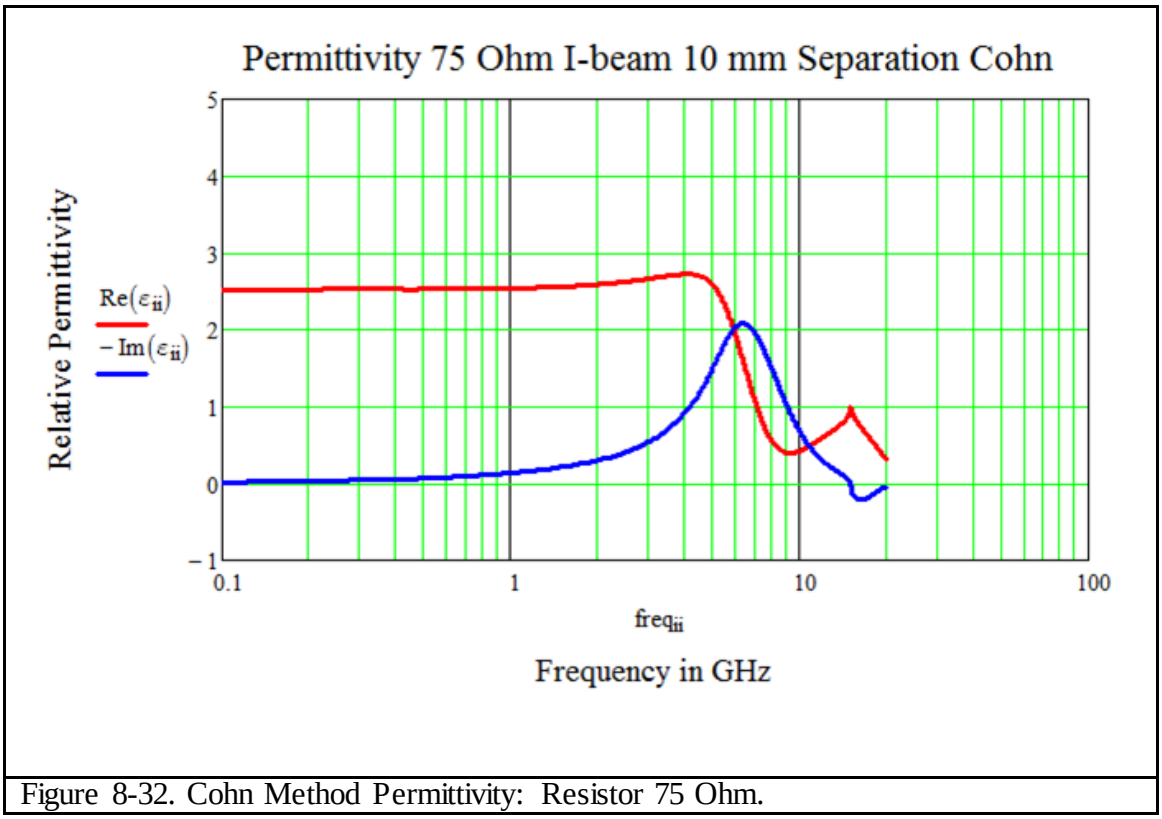

Figure 8-32. Cohn Method Permittivity: Resistor 75 Ohm.

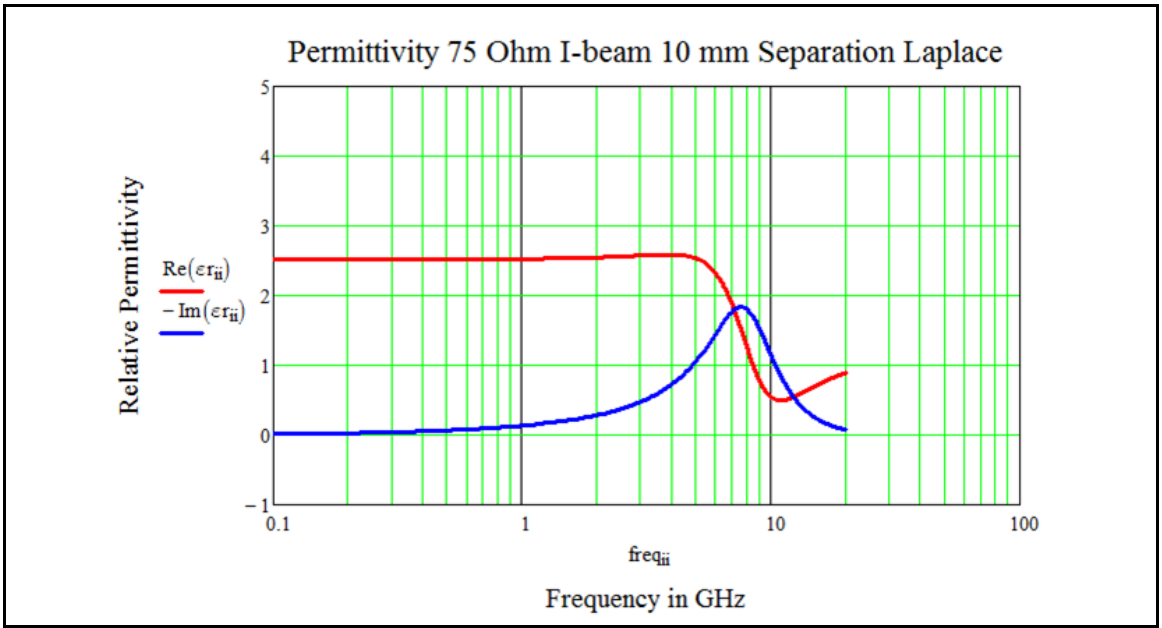

Figure 8-33. Laplace Method Permittivity: Resistor 75 Ohm.

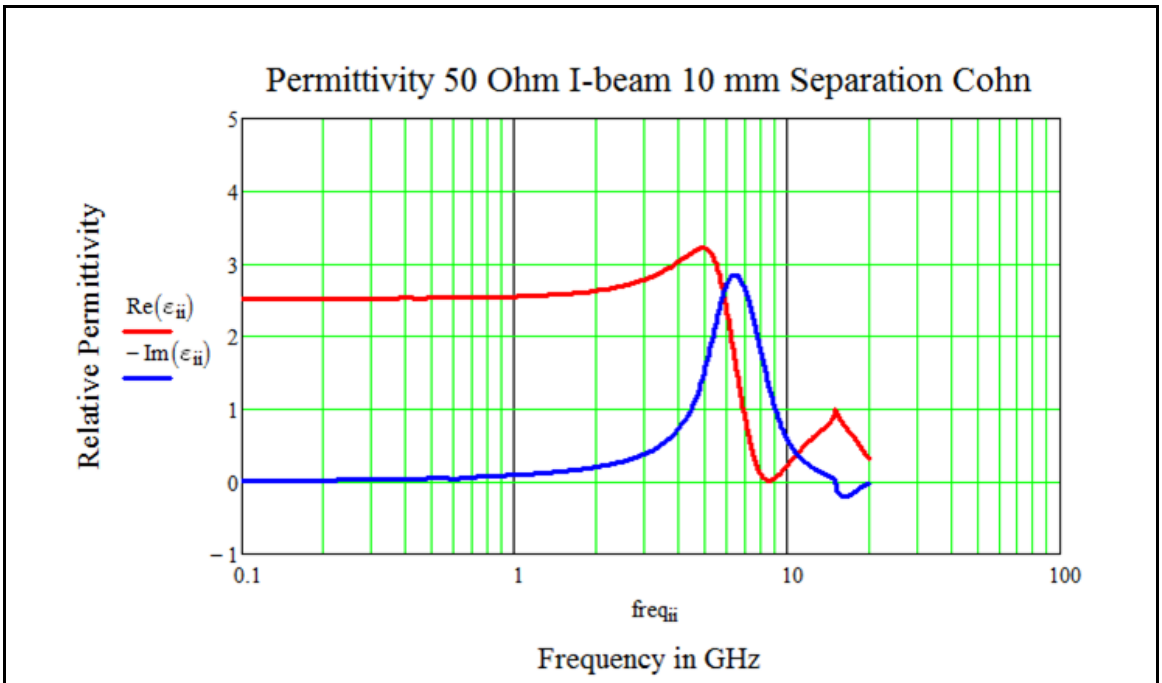

Figure 8-34. Cohn Method Permittivity: Resistor 50 Ohm.

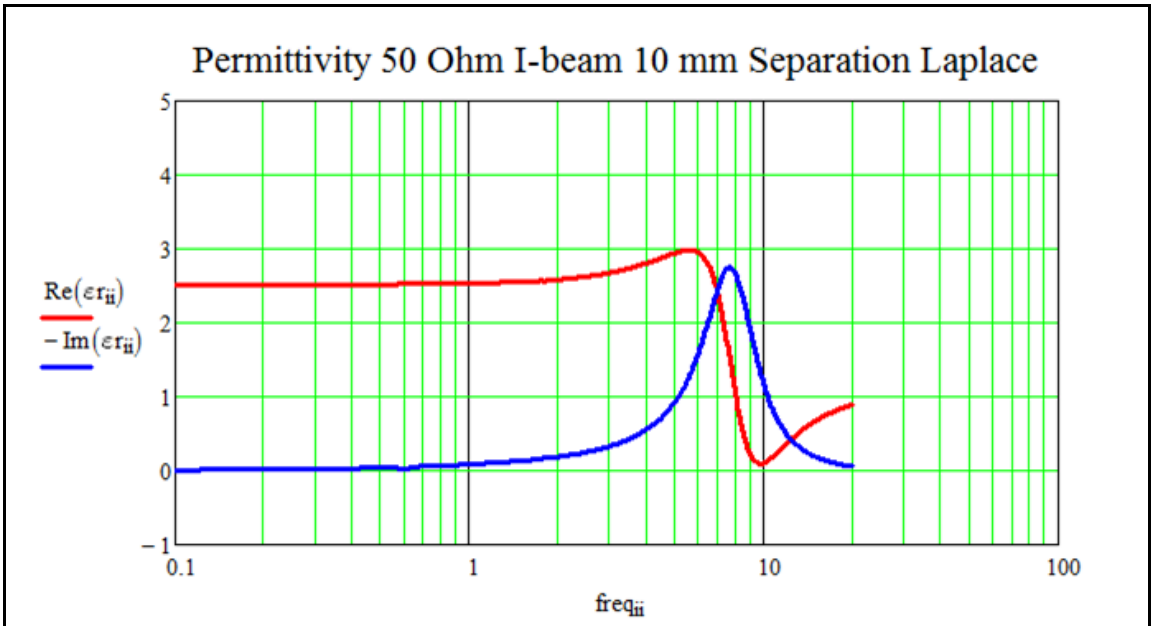

Figure 8-35. Laplace Method Permittivity: Resistor 50 Ohm.

We also investigated secondary effects on the permittivity model by bringing the sheet layers closer together (as was later required in our final design). We went from 10 mm separation to 7.5 mm separation in an attempt to reduce the number of layers in order to mitigate cost. We brought the layer separation even further down to 6.604 mm in order to use inexpensive foam separators that were available and to slightly enhance the window performance. Figure 8-36 through Figure 8-47 show that the ***permittivity using the Cohn method and Laplace method at low frequencies behaves more Lorentz like as we bring the layers closer together due to the interaction between the layers.*** This effect is secondary compared to the effect of changing the value of the resistor itself. Nonetheless changing both the resistor from 100 ohms to 50 ohms and the layer separation distance from 10 mm to 6.604 mms made the I-beam behave like a Lorentz. This was our final design where the base material is a Lorentz; to which we added the zero circuit to create the window.

Constant 100 Ohm Resistor: Separation Distance Varies

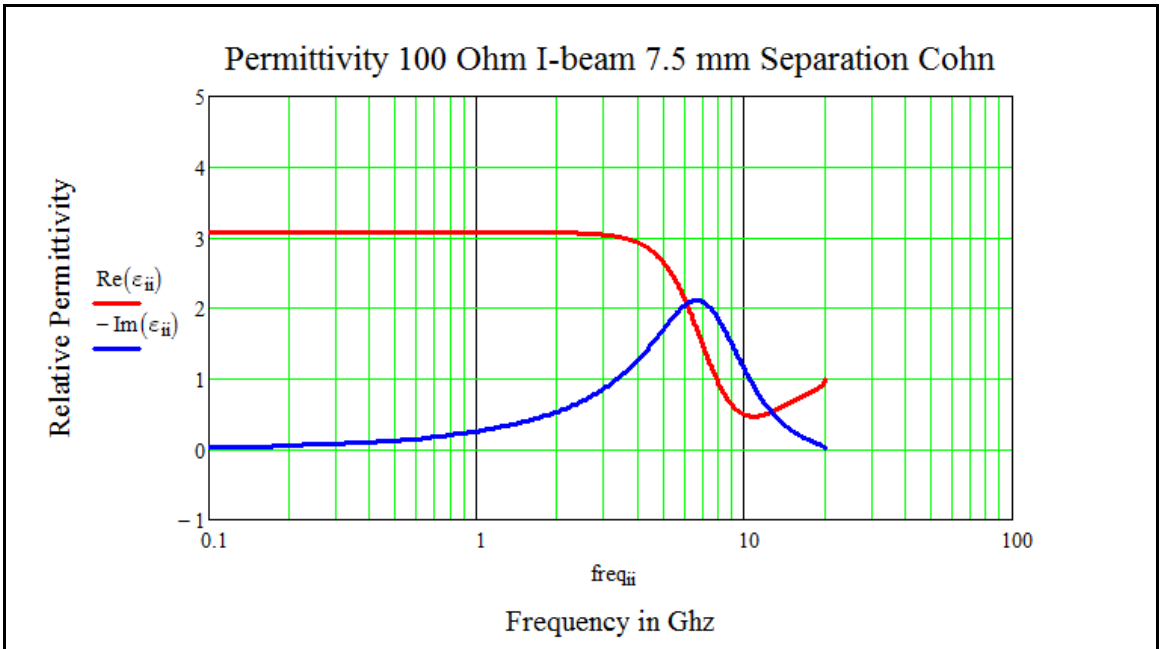

Figure 8-36. Cohn Method Permittivity: 7.5 mm Separation (100 Ohm).

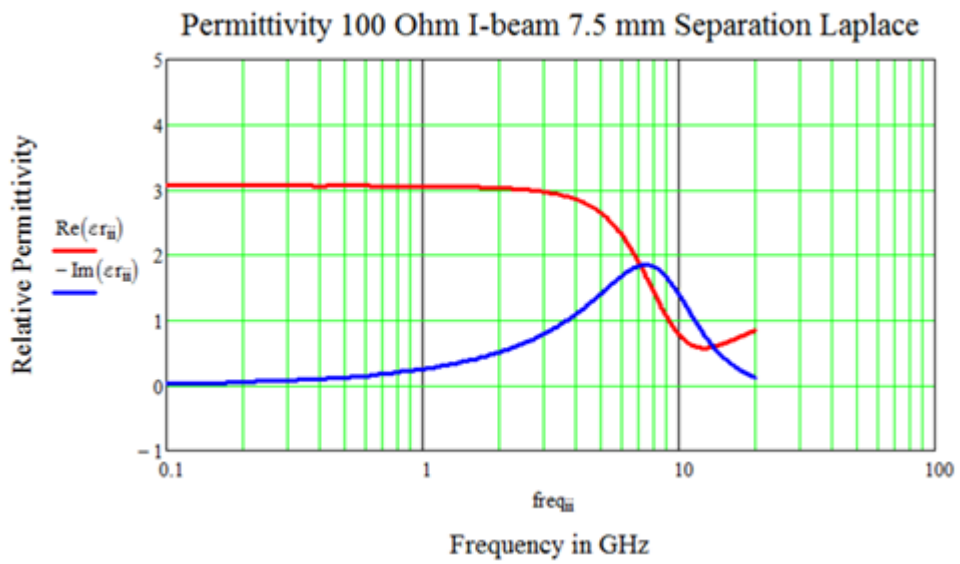

Figure 8-37. Laplace Method Permittivity: 7.5 mm Separation (100 Ohm).

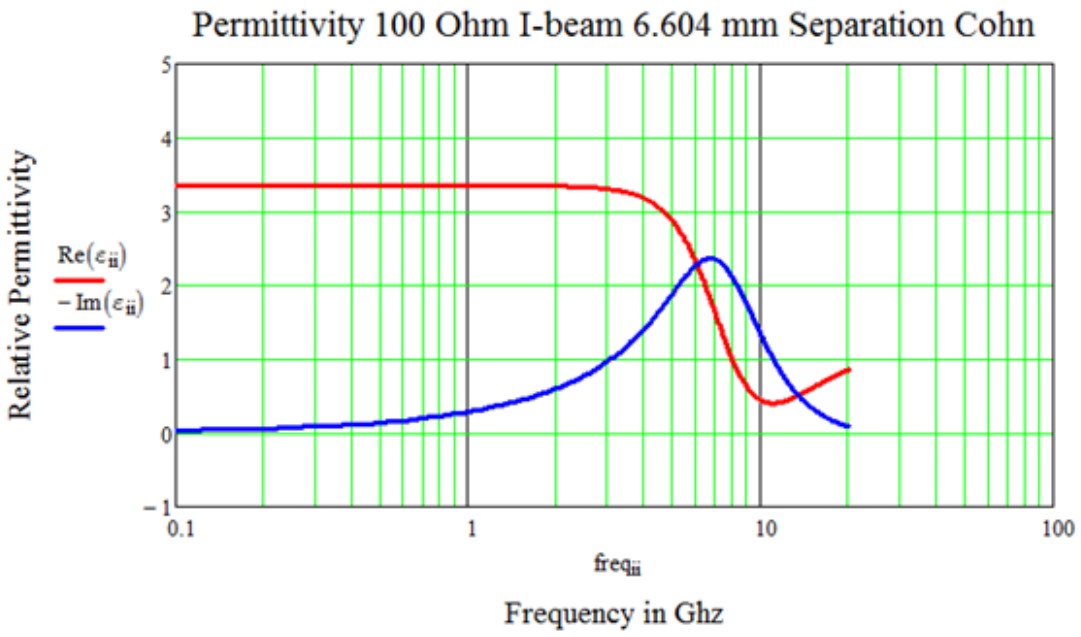

Figure 8-38. Cohn Method Permittivity: 6.604 mm Separation (100 Ohm).

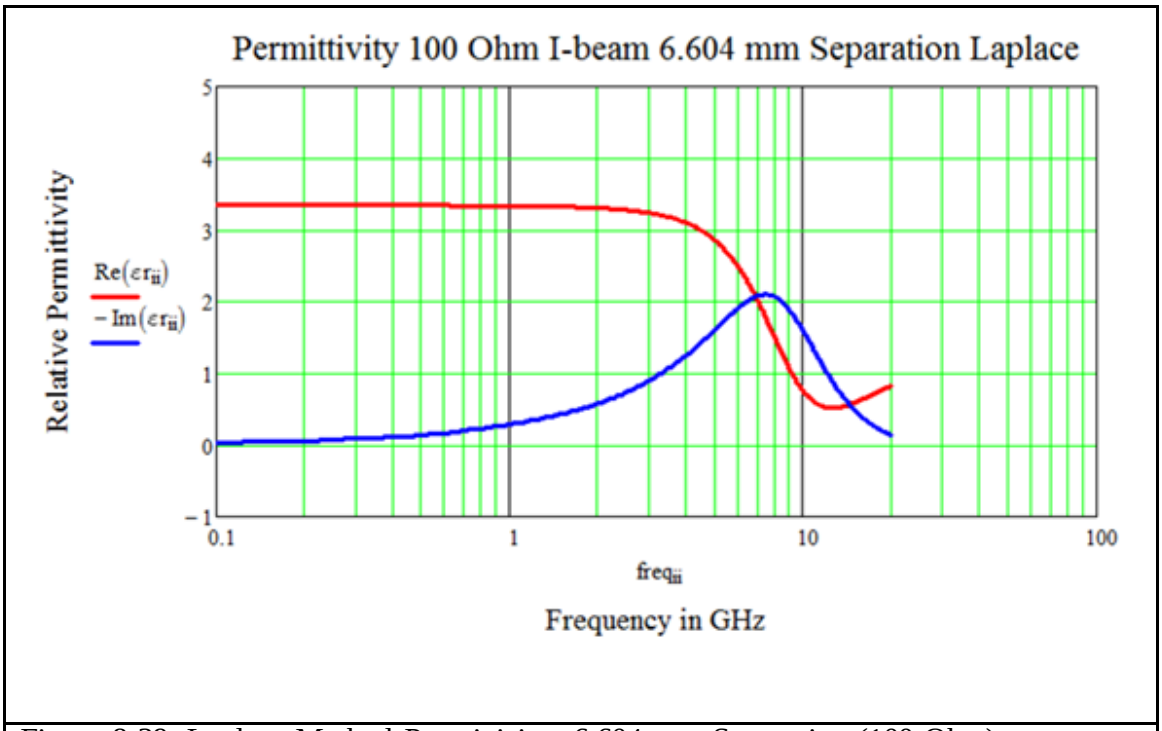

Figure 8-39. Laplace Method Permittivity: 6.604 mm Separation (100 Ohm).

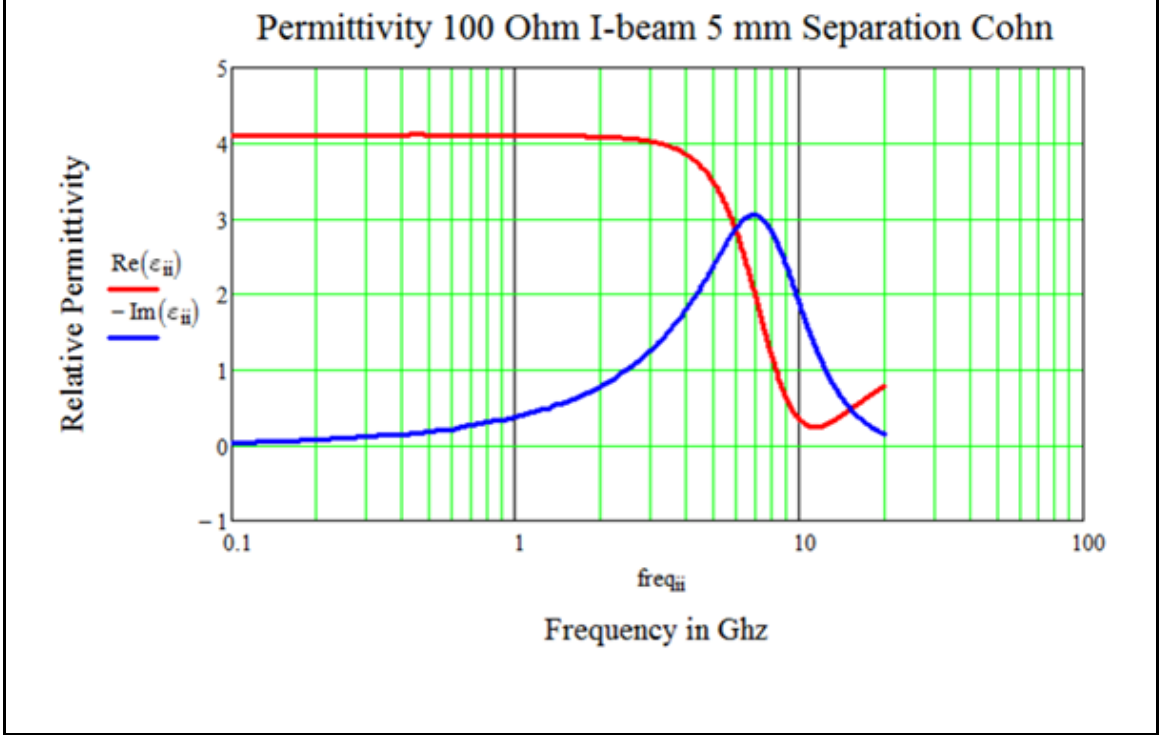

Figure 8-40. Cohn Method Permittivity: 5 mm Separation (100 Ohm).

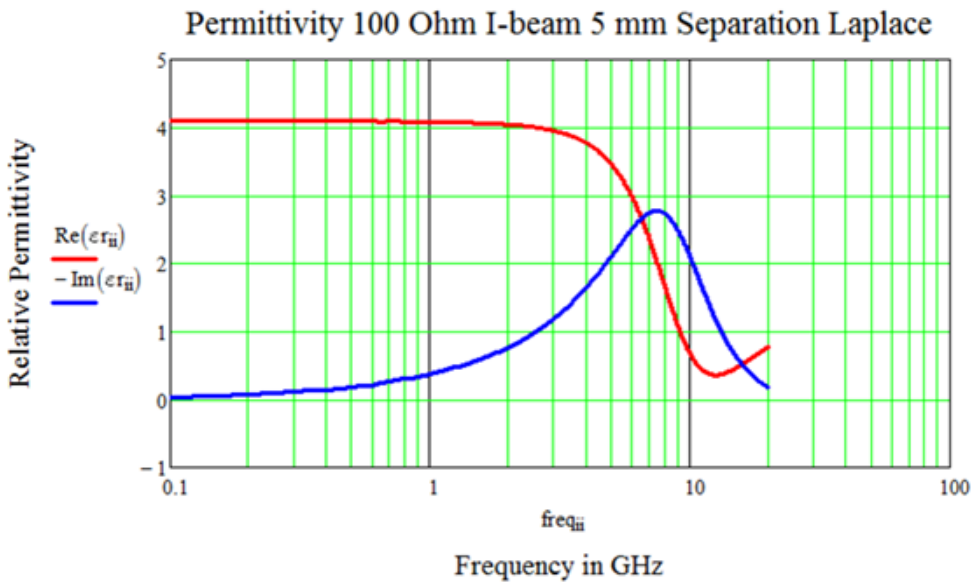

Figure 8-41. Laplace Method Permittivity: 5 mm Separation (100 Ohm).

Constant 50 Ohm Resistor: Layer Separation Varies

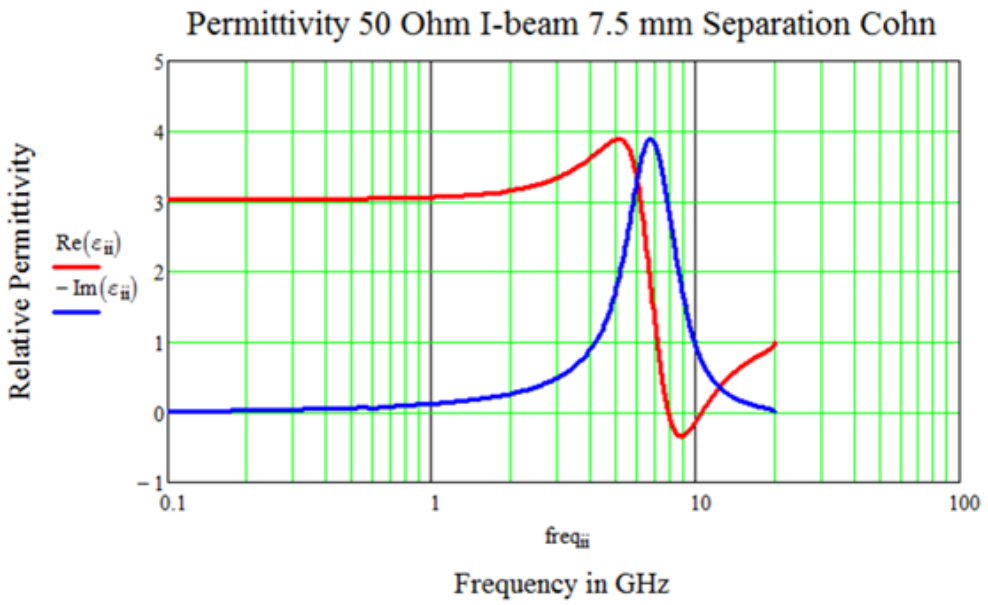

Figure 8-42. Cohn Method Permittivity: 7.5 mm Separation (50 Ohm).

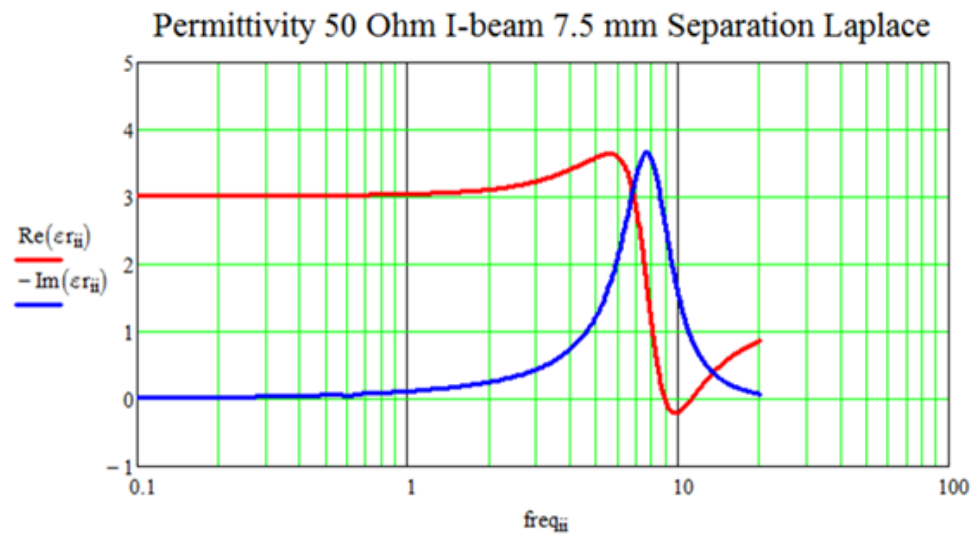

Figure 8-43. Laplace Method Permittivity: 7.5 mm Separation (50 Ohm).

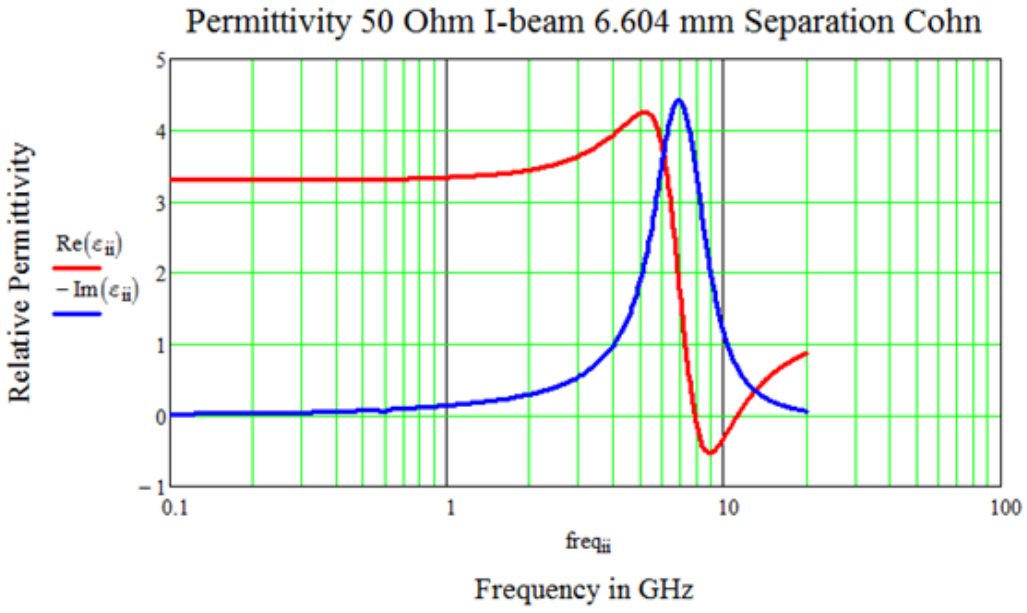

Figure 8-44. Cohn Method Permittivity: 6.604 mm Separation (50 Ohm).

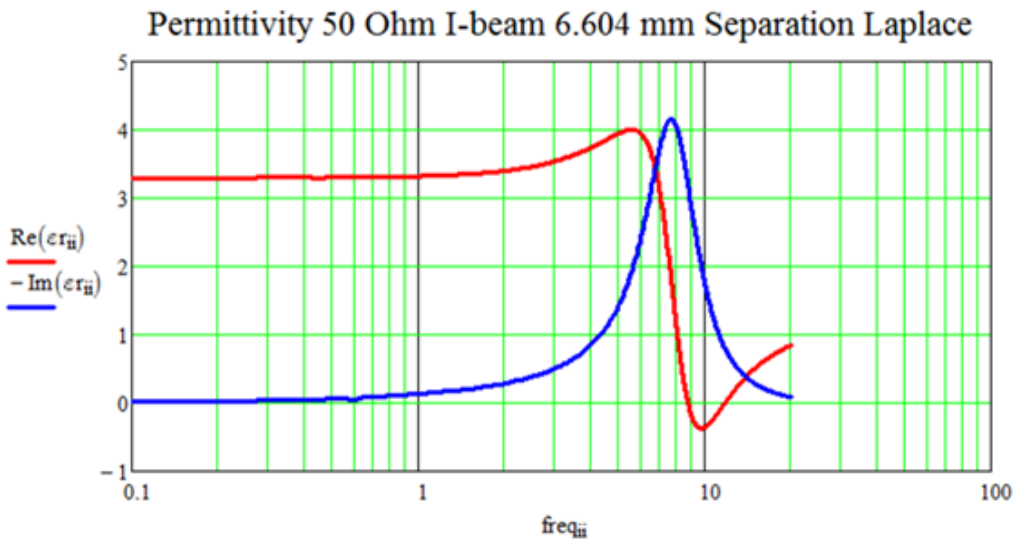

Figure 8-45. Laplace Method Permittivity: 6.604 Mm Separation (50 Ohm).

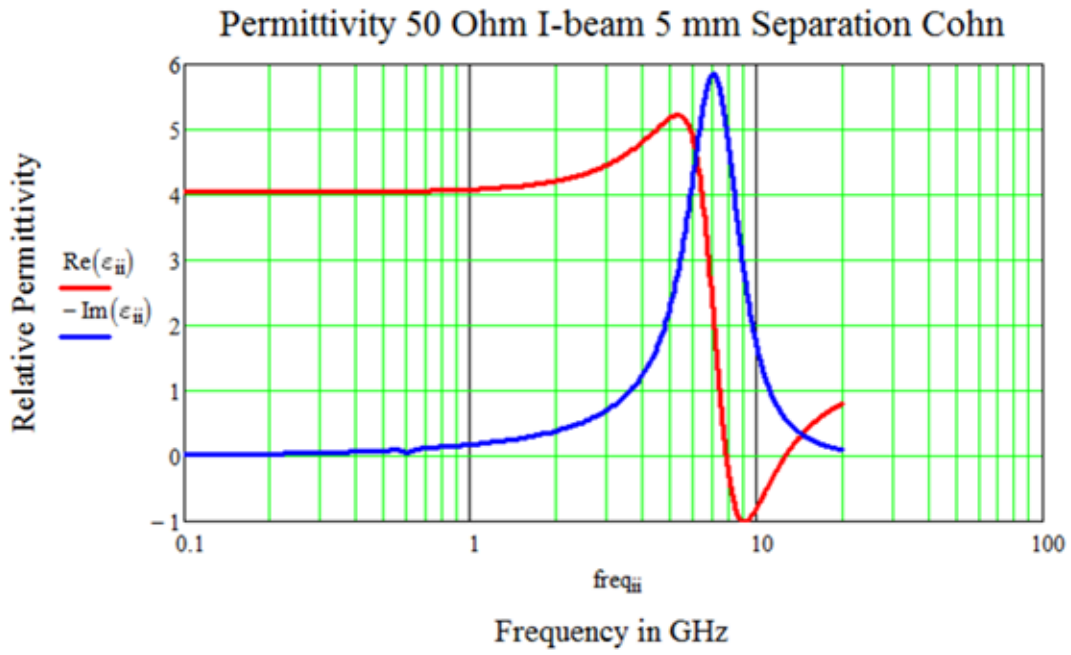

Figure 8-46. Cohn Method Permittivity: 5 mm Separation (50 Ohm).

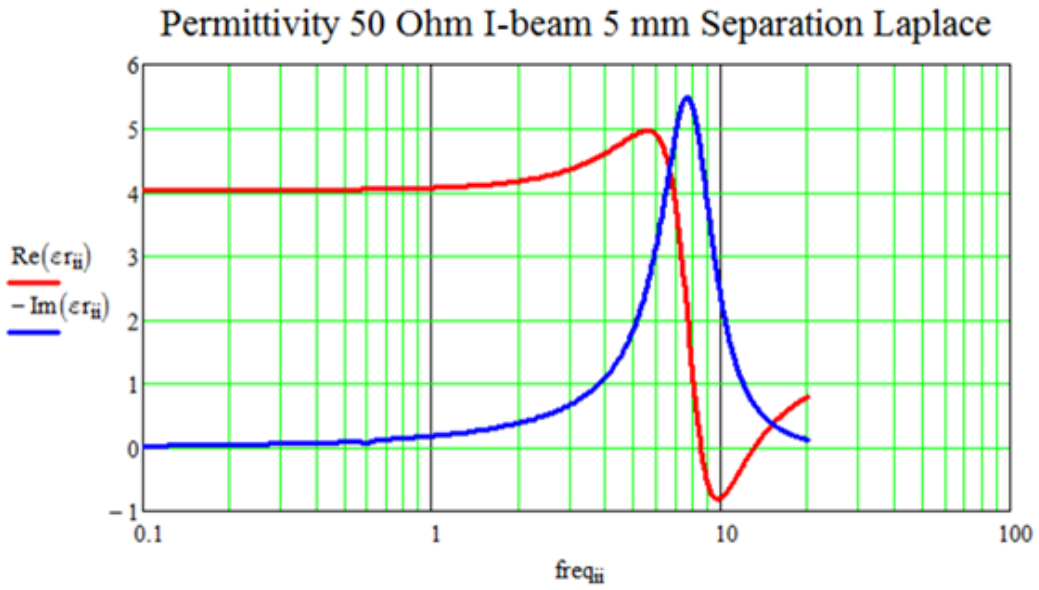

Figure 8-47. Laplace Method Permittivity: 5 mm Separation (50 Ohm).

Figure 8-44 and Figure 8-45 show our final design where the base material is a Lorentz and we will add the zero circuit parallel to it to create the window.

8.3.1.2 Validation of Cohn and Laplace Methods to Determine Permittivity

To support our claim that the complex permittivity behavior of the I-beam goes from a Debye to a Lorentz as we change the resistor from 100 ohms to 50 ohms and if the layers are brought into close proximity, due to the interaction of adjacent layers, that they start reverberating like a Lorentz; we need to check the predictability of the Cohn and Laplace Methods for our application. These permittivity determinations are both only valid for low frequencies. In addition the Cohn method takes the periodicity of the effective medium into account and claims that these equations are only valid when the separation distance is equal to or greater than the unit cell dimension corresponding to the height direction of the

obstacle. In the case where we have chosen a unit cell of 10 mm in the x, y and z directions, we are obeying these restrictions imposed by Cohn's assumptions based on his analysis of the metal strip delay structure for microwave lenses. Cohn further states that a layer separation to unit cell dimension ratio of 0.9 is acceptable for his susceptance calculations as a function of obstacle geometry. Since we are operating beyond this ratio at 0.75 mm separation distance and in the final design this ratio of b/l = 0.604; it is necessary to check the veracity of Cohn's equations in this regime. In order to accomplish this, HFSS S21 transmission measurements were made with seven layers of the I-beam configuration of our baseline design using a 4 GHz solution frequency to obtain robust data at the low frequency regime (prior to adding the zero circuit). This data was then inputted into the Diaz permittivity program that computes the complex permittivity as discussed in chapter 7. An effective medium thickness was assumed to be the distance subtending the first and last layer plus half the separation distance of the unit cell on each side of the cascade.

Figure 8-48 shows the complex permittivity of our base line (final) design using HFSS transmission data and the Diaz program compares well to the Cohn and Laplace method for the low frequency limit shown in Figure 8-44 and Figure 8-45 above. The DC permittivity is 2.5 in all three calculations and the imaginary and real peaks are in the same range of 4.

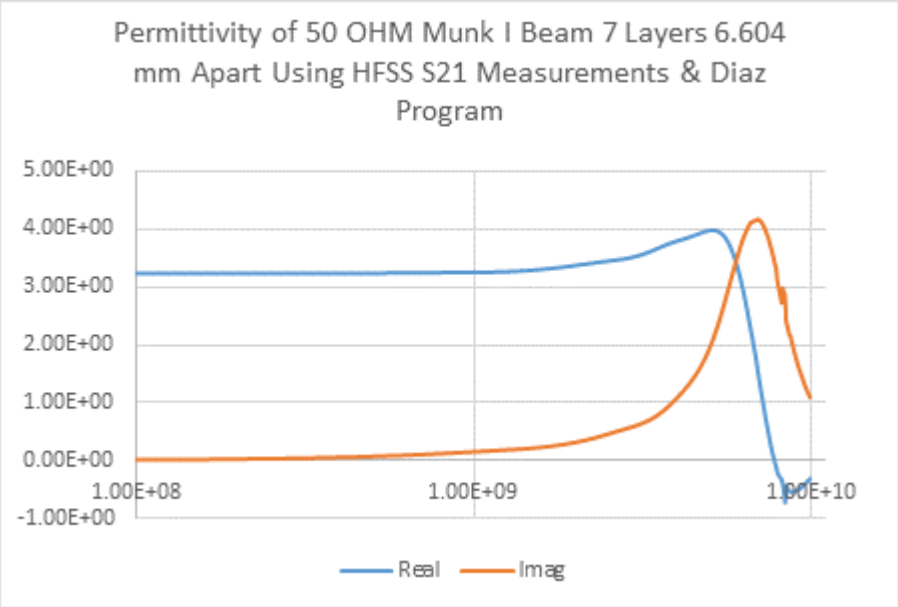

Figure 8-48. Permittivity HFSS/Diaz Extraction 6.604 mm Apart (50 ohm).

Complex permittivity was also computed for the 50 ohm and 100 ohm resistor I-beams at a 10 mm layer separation distance in order to compare with the Laplace and Cohn methods of permittivity calculations that are within the constraints and assumptions of the Cohn analysis of the metal-strip delay structure for microwave lenses.

Figure 8-49 shows the permittivity calculated for 50 ohm I-beam 10 mm apart using HFSS transmission data using the Diaz Program. This clearly matches Figure 8-34 and Figure 8-35 showing the permittivity calculated using the Cohn and Laplace methods respectively.

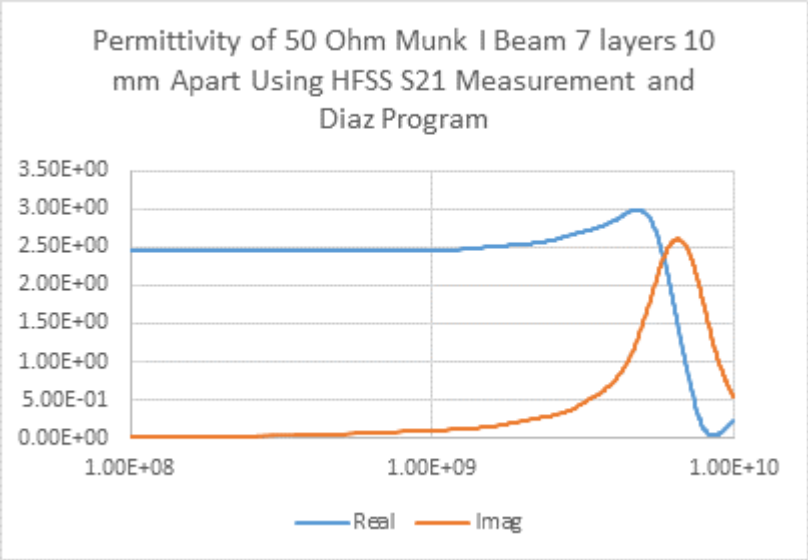

Figure 8-49. Permittivity HFSS/Diaz Extraction 10mm Apart (50 ohm).

Figure 8-50 shows the permittivity calculated for the 100 ohm I-beam 10 mm apart using HFSS transmission data extracted from the Diaz Program. This permittivity also clearly matches Figure 8-30 and Figure 8-31 showing the Cohn and Laplace methods respectively and looks like the Debye we originally started with.

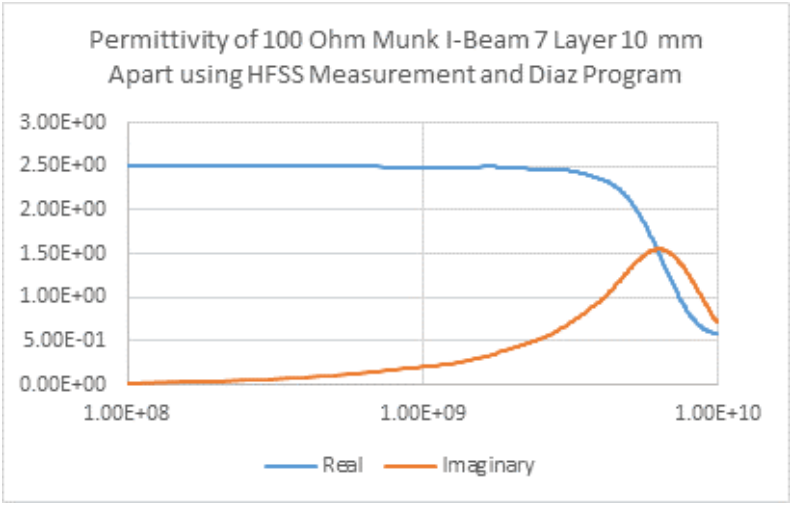

Figure 8-50. Permittivity HFSS/Diaz Extraction 10mm apart (100 ohm).

8.3.1.3 Conclusions

Based on these permittivity calculations using HFSS transmission data and the Diaz Fortran permittivity extraction program we have shown that the Cohn equations for a delay strip media and the Laplace calculations for low frequencies are valid in our application regime.

It is also clear that not only will the choice of resistor impede or facilitate the current flow in the I-beam but the absence or presence of this inductance can drastically change the behavior of this material from a Debye to a Lorentz.

Furthermore close proximity of the layers of the baseline material can cause significant interaction between the layers causing reverberations that make the material behave more like a Lorentz.

8.3.2 Does the I-beam with the Zero Circuit Fit the Zero Circuit Model?

Now we check to see whether the circuit model for the window where we added the zero circuit - a series LRC shunt to the Debye/Lorentz circuit discussed in section 8.3.2 fits the HFSS data. The circuit diagram with the zero circuit is illustrated in Figure 8-51 below. Based on reflection data (S11) obtained from HFSS, we plot the calculated real and

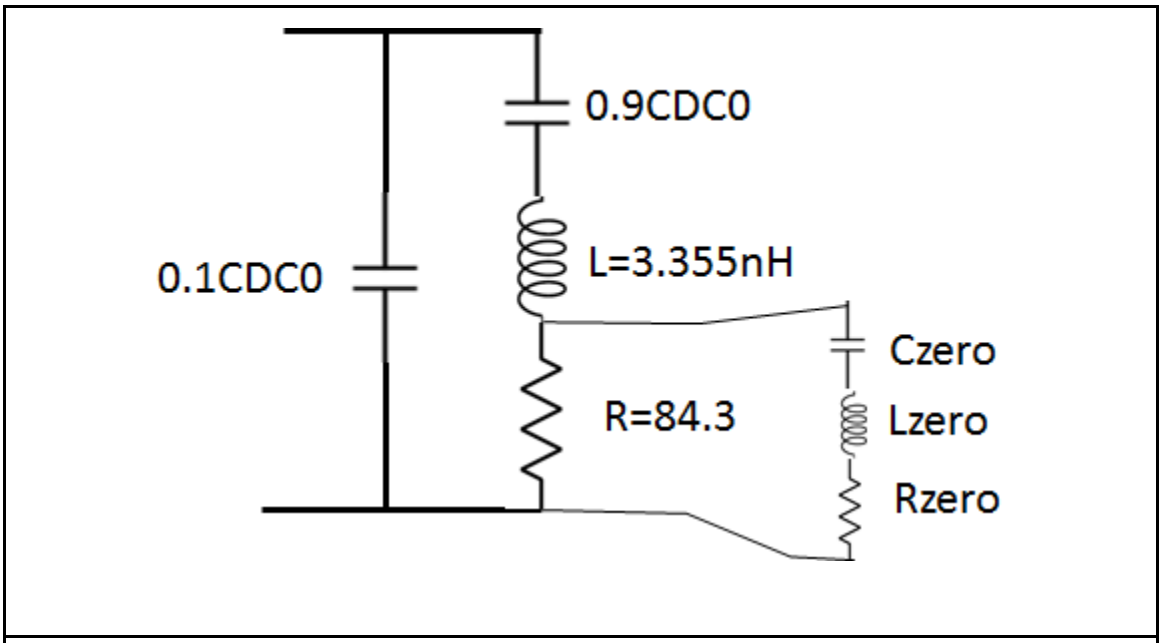

Figure 8-51. Laplace Method Permittivity: 5 mm Separation (50 Ohm).

imaginary capacitance of our I-beam with zero circuit model in Figure 8-52 in solid red and blue lines respectively. Fortunately, the CDC, the total capacitance (within the accuracy of HFSS) is the same as we had found for the I-beam by itself. We note the window, the funny spikes and the Lorentz resonance at 9 GHz. The optimization frequency was run at 4 GHz to obtain good results at the window regime and low frequencies which explains the consistent DC values.

However, when we try to fit this data to the original I-beam circuit model with the zero circuit added, we are unable to do so. The dashed lines as seen in Figure 8-52 illustrate the original circuit model we tried to fit. Therefore the configuration we modeled in HFSS is not represented by the circuit model we designed. Instead we find that the circuit model for the HFSS with the simulated zero circuit is very different.

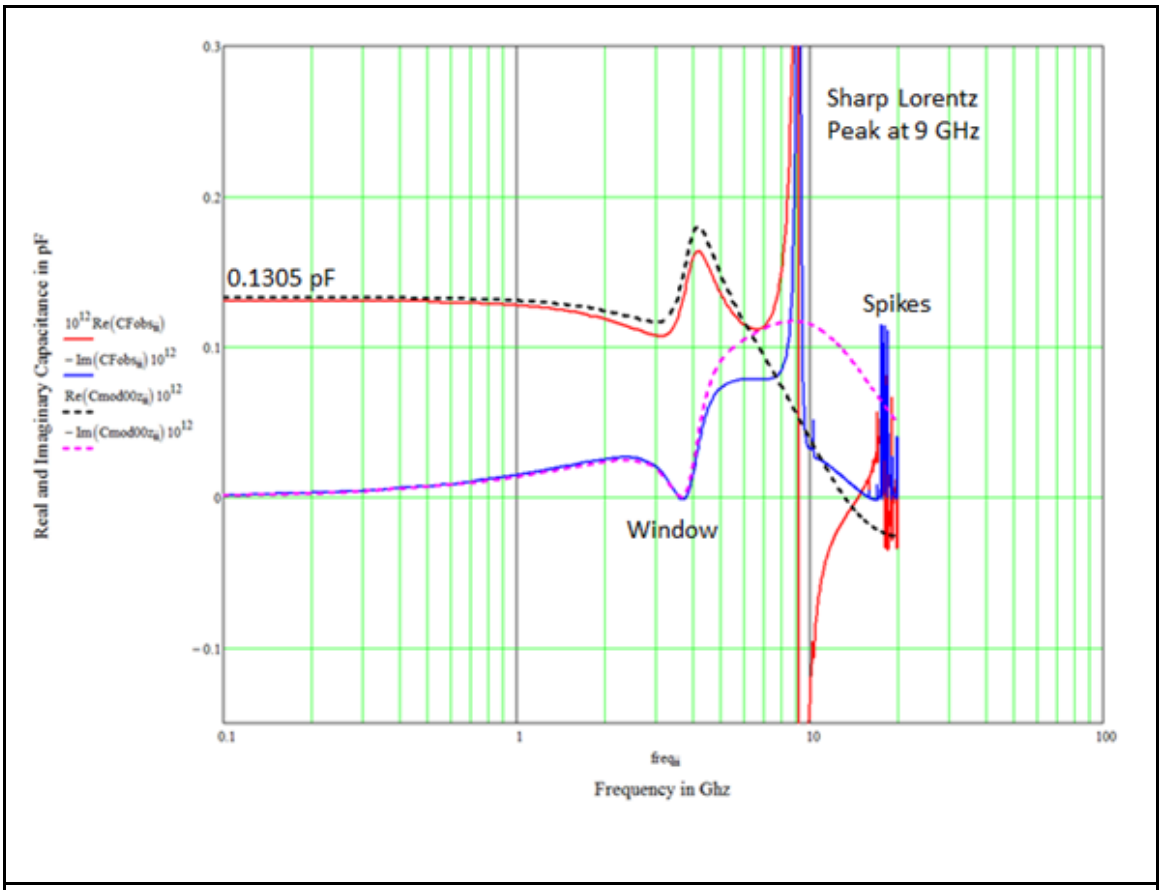

Figure 8-52. Sheet Capacitance of the 50 Ohm I-Beam with the Zero Circuit Does Not Fit Our Original Circuit Model

8.3.2.1 What does the Actual Window Circuit Model Look Like?

At first we tried to model the zero on a Lorentz to replicate the window and after we got close we simply added a sharp Lorentz to explain the new sharp resonance at 9 GHz. We used the circuit elements of the original circuit as parameters and multiplied them by factors to vary their strength. We achieved the following initial circuit model described in the equation below.

$$Y00z_{ii} = \left[\left[\frac{1}{1.99 * R00} + \frac{0.77}{1i2\pi freq_{ii}10^9 * L_z + \frac{1.02}{1i2\pi freq_{ii}10^9 * C_z} + 1R_z}\right]^{-1}\right.$$

$$\left. + \ 1i2\pi freq_{ii}10^9 * L00 * 0.1 + \frac{1.07}{1i2\pi freq_{ii}10^9 * C00 * 1.0}\right]^{-1}$$

$$+ \ 1i2\pi freq_{ii}10^9 * C0_i * 0.001$$

Determination of Circuit Parameters

The $C_{infinity}$, which is $C0_i$ in the admittance equation was verified to be negligible this time. Lz is the inductor in the zero LRC circuit branch in parallel with the resistor. The L00 is the original inductor, L of the I-beam that was found to be small but not negligible. And the C00 is the capacitance which is the same as ΔC we saw in our Debye circuit model before we added the zero circuit. At this point we have the preliminary fit outlined in Figure 8-53.

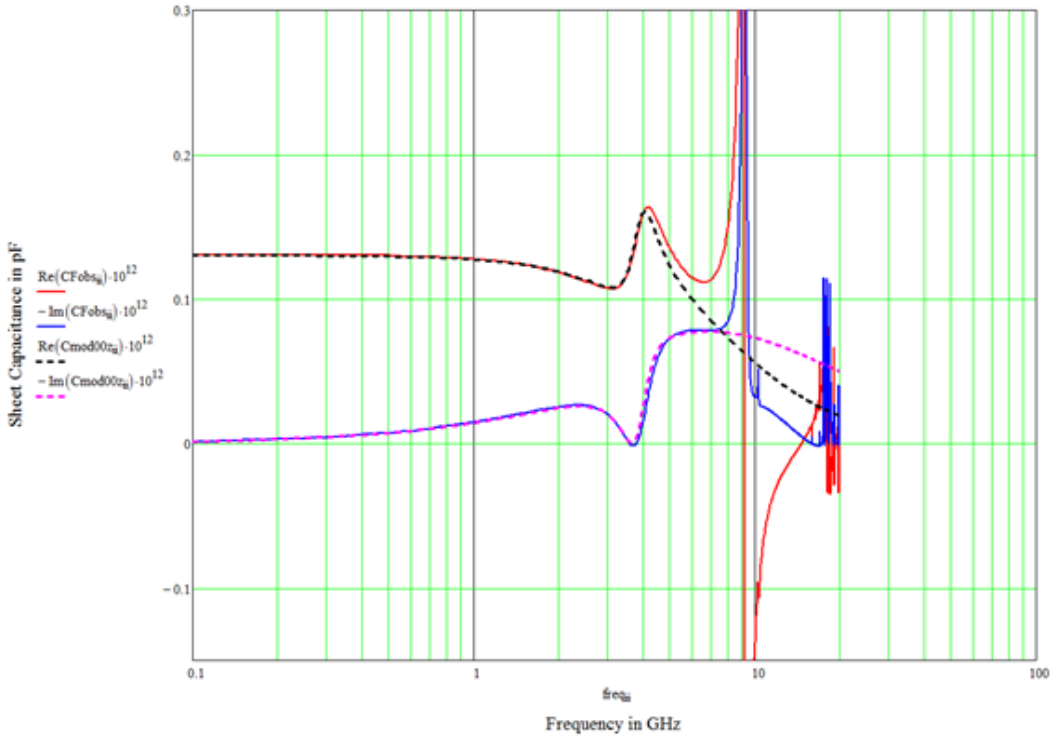

Figure 8-53. Sheet Capacitance of the 50 Ohm I-Beam with the Zero Circuit HFSS Data Versus Preliminary Circuit Model Fit.

As we can see the window is almost dead on before we add the Lorentz resonance at 9 GHz using the equation below.

$$Cq_{ii} = C0_i * 0.1\left[\frac{11}{1 + i\frac{freq_{ii}}{8.7} * \frac{1}{100} - \left(\frac{freq_{ii}}{8.7}\right)^2}\right]$$

Adding the sharp Lorentz will obliterate the deviation by raising the real part and giving the imaginary part a sharp rise. We did several iterations till we were able to match the

HFSS data to the circuit model. The following admittance equation results fit the HFSS data,

where

$$Y00z_{ii}$$

$$= \left[\left[\frac{1}{1.99 * R00}\right.\right.$$

$$\left. + \frac{1}{1i2\pi freq_{ii}10^9 * L_z * 1.287 + \frac{1.0}{1i2\pi freq_{ii}10^9 * C_z * 0.7549} + 0R_z}\right]^{-1}$$

$$+ \ 1i2\pi freq_{ii}10^9 * L00 * 0.1 + \frac{1.0}{1i2\pi freq_{ii}10^9 * C00 * 0.93458}\Bigg]^{-1}$$

$$+ \ 1i2\pi freq_{ii}10^9 * C0_i * 0.00$$

And the circuit model equation becomes

$$Cmod00z_{ii} = \frac{Y00z_{ii}}{1i2\pi freq_{ii}10^9} + Cq_{ii}$$

Figure 8-54 illustrates that the above equation for the sheet capacitance fits the S11 reflection data obtained from HFSS.

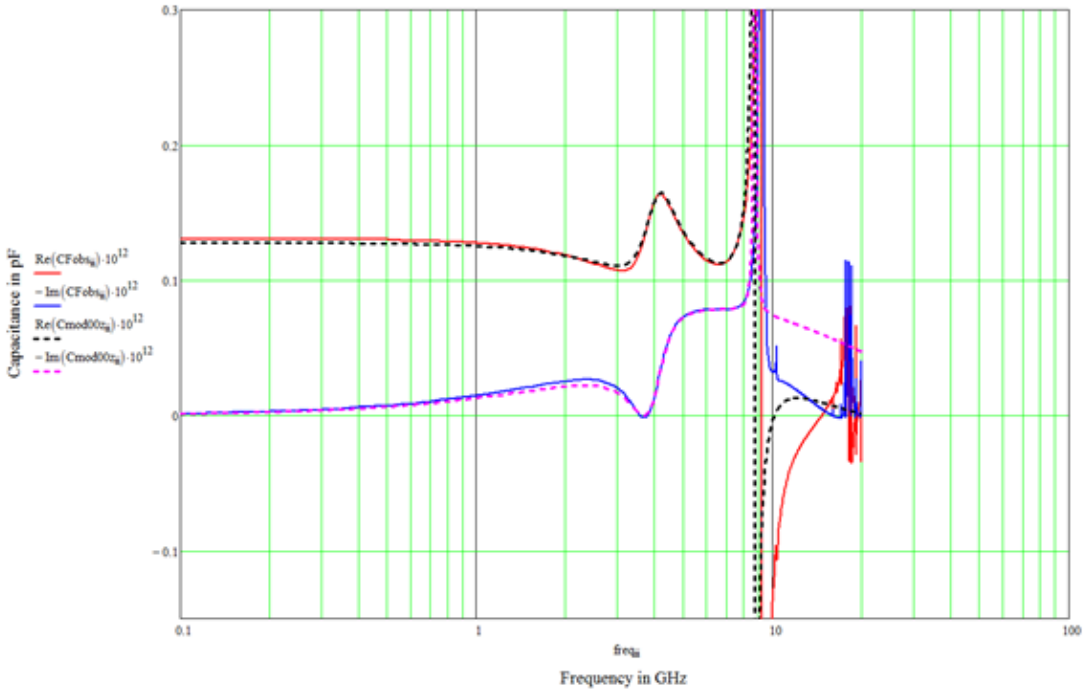

Figure 8-54. The I-Beam Window Data Fit This Circuit Model.

As before in order to determine the Lorentz branch we use the resonant frequency relationship with LC and we obtain the inductance LOL of the LRC branch of the sharp Lorentz.

$$LOL = \frac{11}{(8.7x10^9 x2\pi)^2 (C0ix0.1)} = 2.7386\ \mu Henry$$

And knowing that Q is the square root of the ratio of L/R to RC we obtain the resistor, ROL in the branch causing the sharp Lorentz resonance.

$$ROL = \frac{LOL}{C0ix0.1}\frac{1}{100} = 451.35\ Ohms$$

$$COL = \frac{C01x0.1}{11} = 1.222fFarads$$

All the components of the each branch parameter are summarized below in Table 8-3. Component Values of Each Branch of the Circuit Model.

Sharp Resonant Branch	Munk I beam Branch	Zero Circuit Branch
L=2.7386 μH	L00=0.3355 nH	Lzero=20.23 nH
COL=0.1222 fF	C00=0.1131 pF	Czero=91.31 fF
ROL=451.35 Ohms	R00=167.78 Ohms	Rzero=0 Ohms

Table 8-3. Component Values of Each Branch of the Circuit Model

The other circuit elements L00, R00 and C00 and the zero circuit values can be read off the admittance equations. We obtain the following circuit model shown in Figure 8-55.

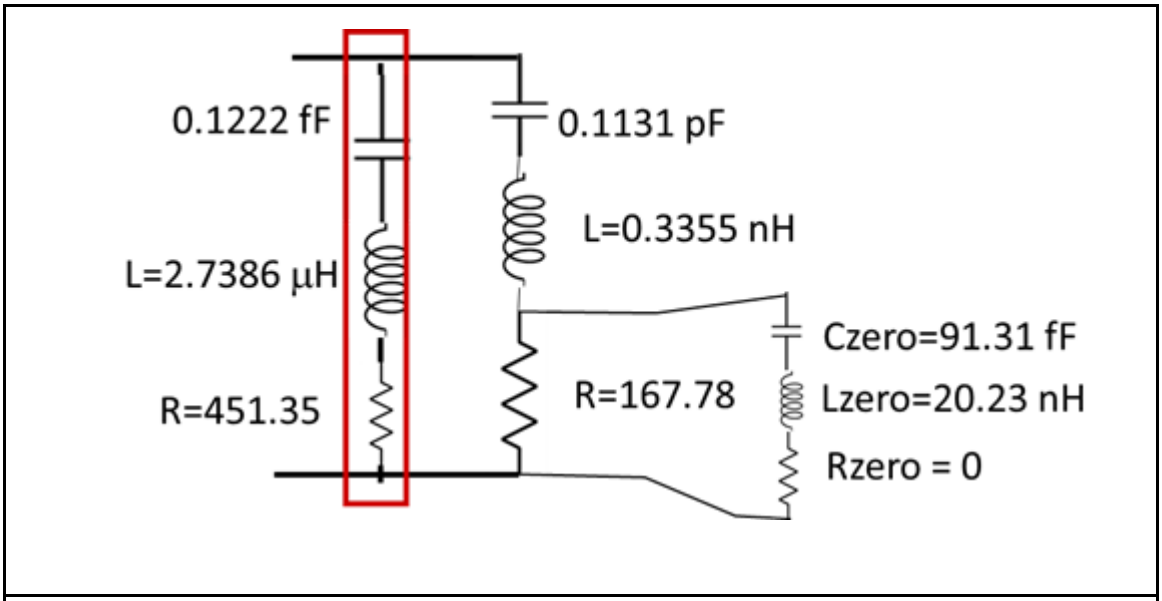

Figure 8-55. The Actual Circuit Model of the Window.

We observe that this fit is not the circuit model we were expecting. The zero circuit instead of appearing as a shunt LRC just across the R of the original circuit it has also shunted the

original LRC I-beam circuit model with another LRC or Lorentz branch where the inductance is high and the capacitance is low. The capacitance has been redistributed and additional inductance added from the loops. The fact that there is another parallel LRC branch in shunt with the original shunt circuit means that the original I-beam is indeed "coated" by a Lorentz. This is because as we saw in the bow tie antenna the flux path could jump across and were not limited to going through the resistor; even in the I-beam there are alternate flux paths especially in the proximity of the loops due to smaller distances between the top of the beam and the loops as shown in Figure 8-56.

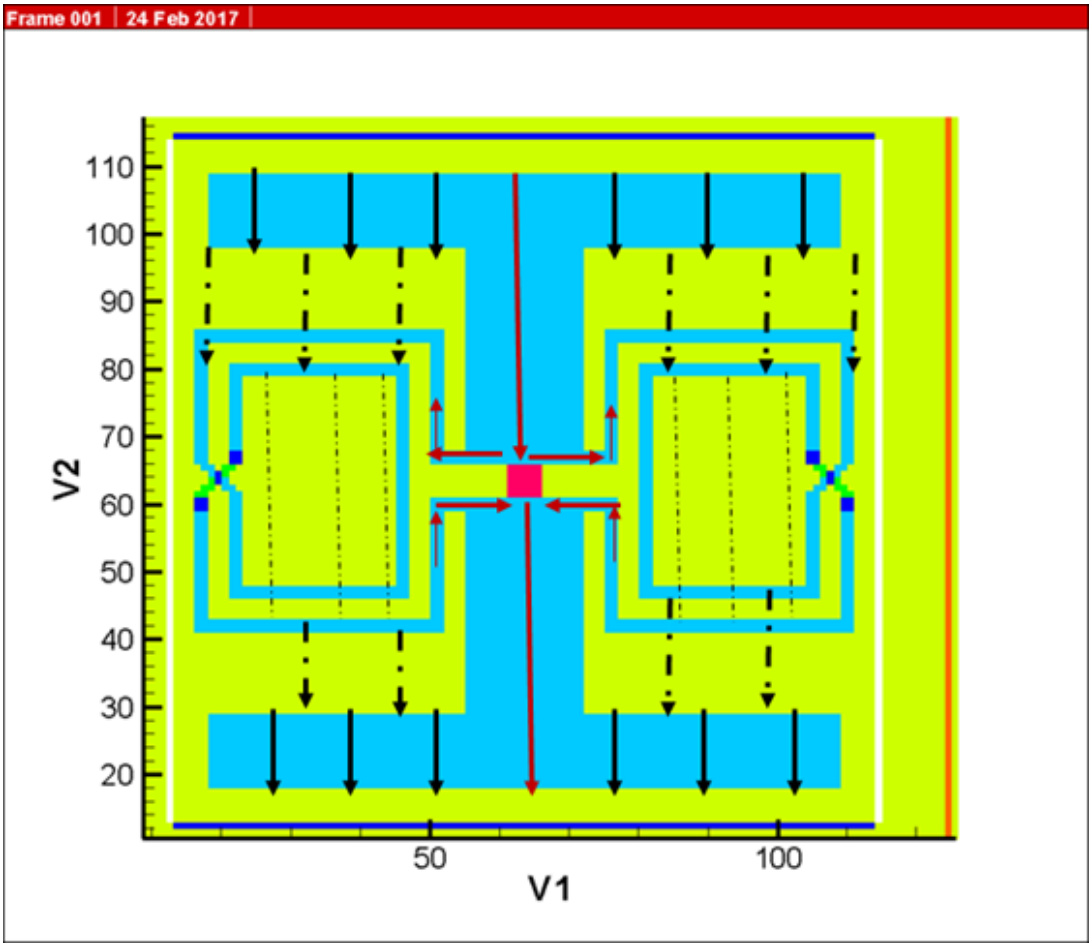

Figure 8-56. The Flux Paths of the I-Beam with Zero Circuit Do Not Only Go Through the Loops.

8.3.3 Fine Tuning the Window Design

So far we have talked about the window observed in an infinitely thin sheet in terms of sheet capacitance using a single sheet layer of the I-beam. We have predicted using the Cohn and Laplace methods what the low frequency permittivity would be for a cascade of such sheets where we could vary the distance between layers. As long as the wavelength is 10 times or more than the sheets separation distance we can create an effective medium with these sheets. And we have some latitude how many sheets we can use to create such an effective medium.

In order to be able to observe this window by testing the window in an arch set up; we evaluate the reflection coefficient placing a metallic ground plane behind this design. At the frequency of the window we should observe 100% reflection from the metal backing plane. Initially we started with 10 of these capacitive sheets, each a unit cell apart with a copper ground plane ½ cell distance away. Later in order to save the cost of fabricating so many layers; we reduced the number of sheets from 10 to 7 and brought them closer together in order to obtain greater permittivity for the effective medium as shown in Figure 8-57 and Figure 8-58.

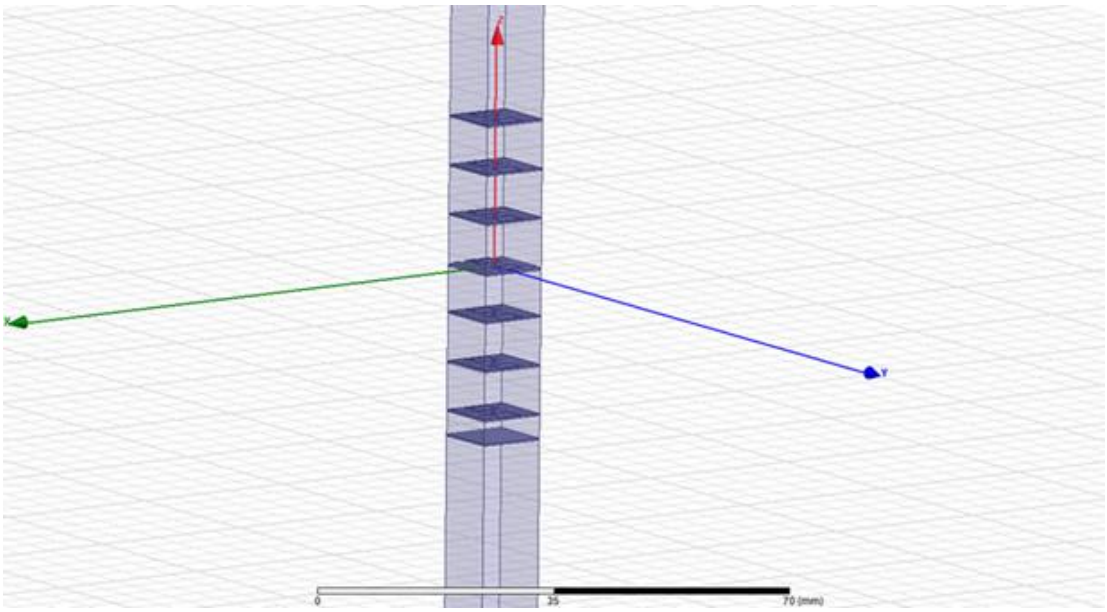

Figure 8-57. 7.5 mm Apart 100 Ohm Resistor with ½ Cell Cu Ground Plane.

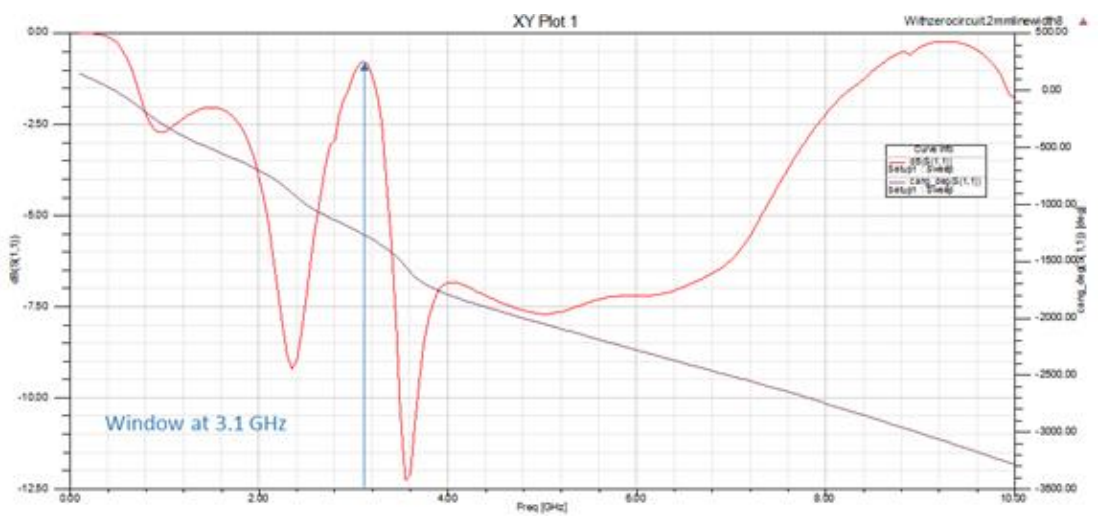

Figure 8-58. S11 Reflection Simulations 7.5 mm Apart 100 Ohm Resistor with ½ Cell Cu Ground Plane

The configuration was modelled in HFSS as shown in Figure 8-57 where the sheets were placed 7.5 mm apart as illustrated for the non-zero circuit. The S11 reflection simulations re shown in Figure 8-58.

To make the window more clear and pronounced we needed to do two things. First we needed to add matched permittivity layers to cancel the front face reflection. We added a layer of Diab foam and then a layer of high density polyethylene (HDPE) to the top sheet in the order to achieve matching layers of 1.4 and 2.3 real relative permittivity respectively.

Second in order to compensate for the higher epsilon matching layer of the HDPE, we tuned the Debye I-beam by changing the dipole resistor from 100 ohms to 50 ohms. The new HFSS S11 reflection simulation results are shown in Figure 8-59 with the matching layers. It clearly doesn't change our window too much.

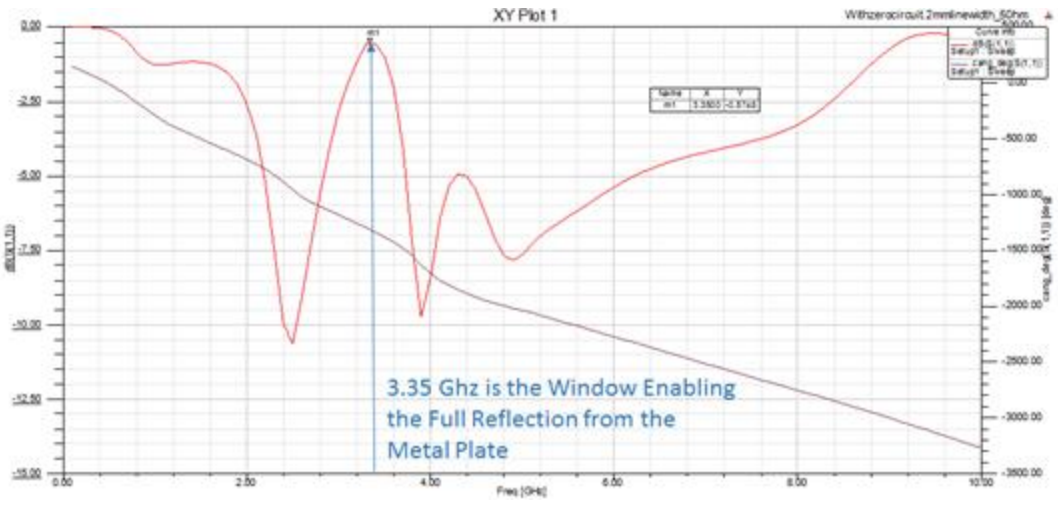

Figure 8-59. S11 Reflection Simulations 7.5 Mm Apart 100 Ohm Resistor with ½ Cell Cu Ground Plane.

We reconfigured the HFSS model with the matching layers of foam and polyethylene and shown in Figure 8-60. Many iterations were performed. We used many types of matching layers including polyethylene, Plexiglas and various foams with low permittivity. We varied the number of layers, the thickness of the layers and the distance from the substrate. Being the closest possible to the substrate without contact yielded the best results. We were constrained by physical materials available for procurement and the inherent permittivity of these materials. The optimal S11 simulation results are shown in Figure 8-61. There is a clear window at 3.35 GHz. The other peak is the Lorentz resonance at 8.7 GHz.

For the final adjustment depending on the availability of spacers and matching layers the thicknesses were tweaked. The final design is shown in Figure 8-62 where only 1/8" Diab H45 foam (1.05 relative permittivity) spacers were available and we went to a thickness of two of these equal to ¼ inch or 6.35 mm (6.604 mm = 6.35 mm spacer + 0.254 mm Duroid). We also changed the high density polyethylene (2.26 relative permittivity) thickness to 0.375 inches (9.525 mm) and the HCP 70 Diab foam (1.39 relative permittivity) to ¼ inch. In the final design we bring the spacing between capacitive sheets from 7.5 mm to 6.604 mm. This does not really change the results allowing us to use matching layer materials and spacers that are more easily available. The complete optimization results are summarized in Figure 8-63 where the red curve is the S11 measurements with the zero circuit and matching layer, the green is the zero circuit with no matching layer and the blue is the I-beam cascade without the zero circuit and the black curve is the I-beam cascade with no zero circuit but with matching layers. Clearly the matching layers help attenuate the front

face reflection for both the I-beam with and without the zero circuit. This is our best window and final design that we will fabricate.

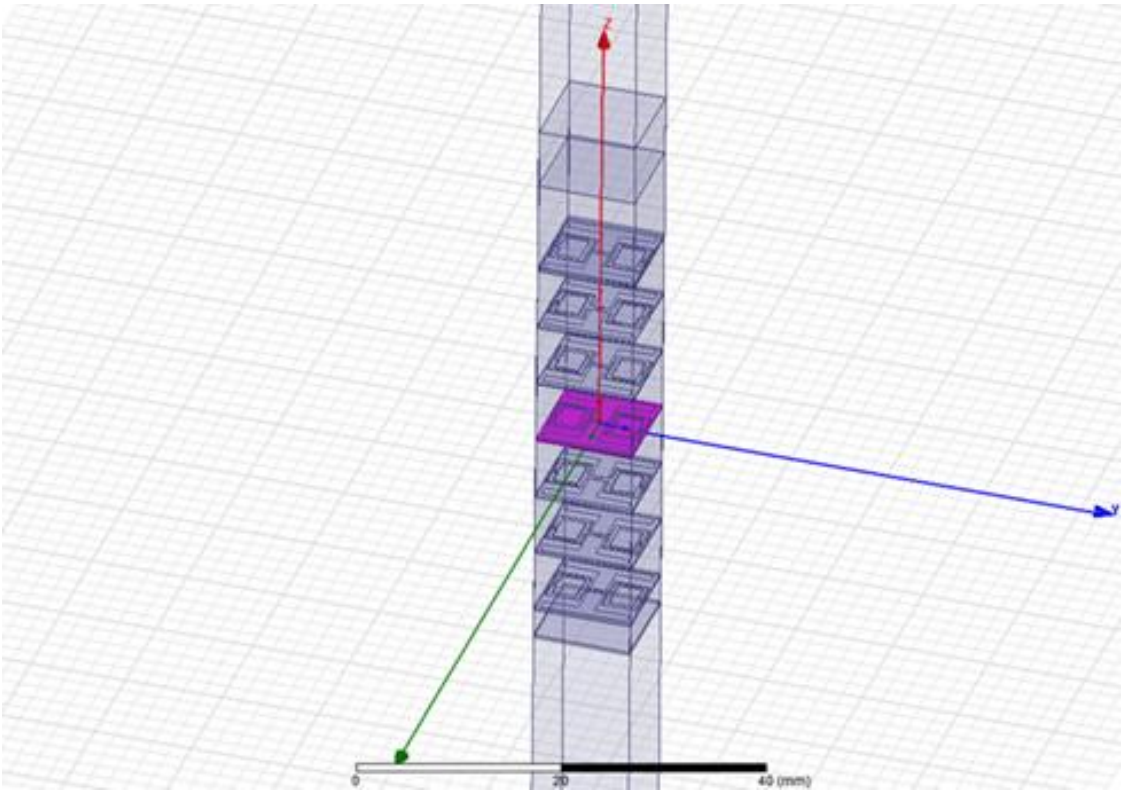

Figure 8-60. S11 HFSS Model of 7 Layers of I-Beam on Duroid 7.5 mm Apart Cascade 50 Ohm Resistor with 0.1 mm Thick Zero Circuit Loops and 6.35 mm Rohacell = 1.4, 9.525 mm HDPE = 2.265, Diab H35 Spacers = 1.05, 0.50 mm Apart (Actual Gap 0.246 mm) Ground Plane Is 2.921 mm Gap, and 3.175 mm 1/ 2 Unit Cell Space Away.

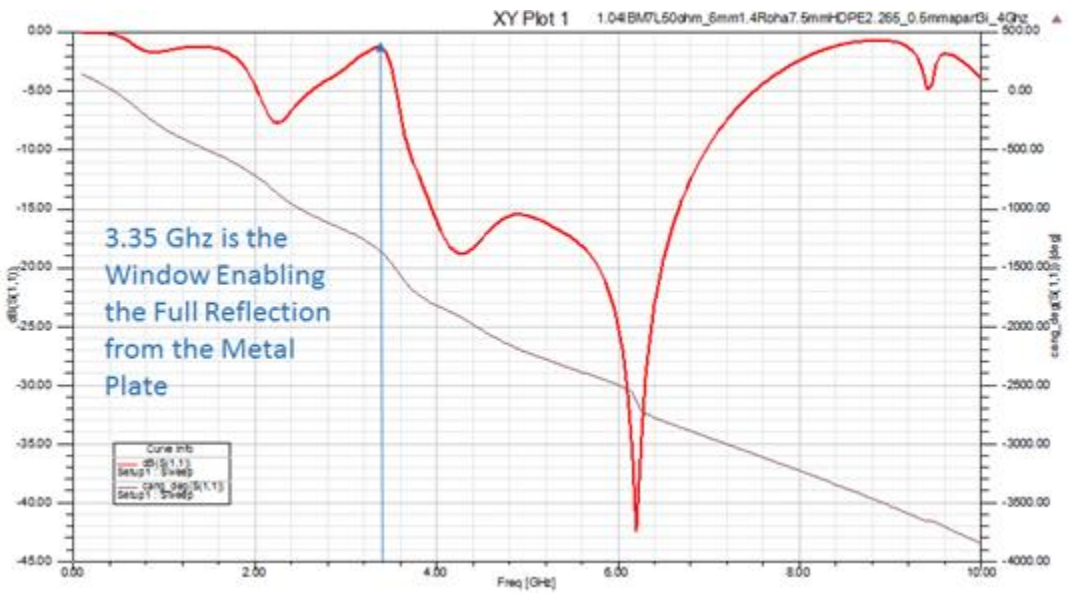

Figure 8-61. S11Simulations in HFSS of 7 Layers of I-Beam on Duroid 7.5 mm Apart Cascade 50 Ohm Resistor with 0.1 mm Thick Zero Circuit and 6.35 mm Rohacell = 1.4, 9.525 mm HDPE = 2.265, Diab H45 Spacers = 1.05, 0.50 mm Apart (Actual Gap 0.246 mm) Ground Plane Is 2.921 mm Gap, and 3.175 mm 1/ 2 Unit Cell Space Away.

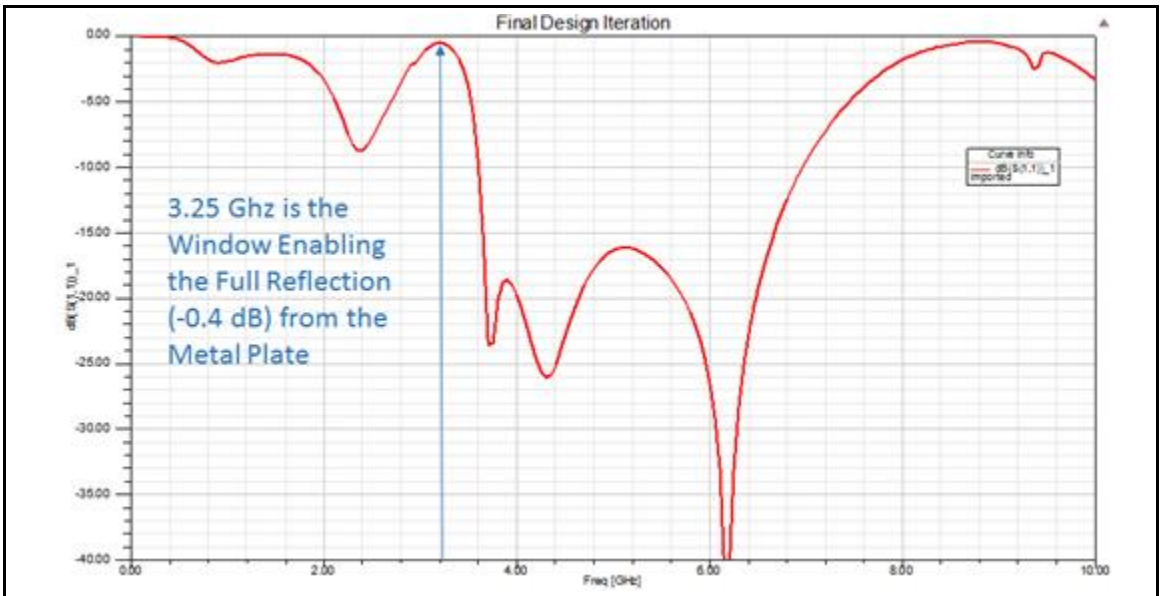

Figure 8-62. S11 Simulated Reflection Measurements in HFSS of 7 Layers of I-Beam on Duroid 6.604 mm Apart Cascade 50 Ohm Resistor with 0.1 mm Thick Zero Circuit and 6.35 mm HCP70 = 1.39, 9.525 mm HDPE = 2.33, Diab H45 Spacers = 1.05 0.50 mm Apart (Actual Gap 0.246 mm) Ground Plane Is 2.921 mm Gap, and 3.175 mm 1/ 2 Unit Cell Space Away.

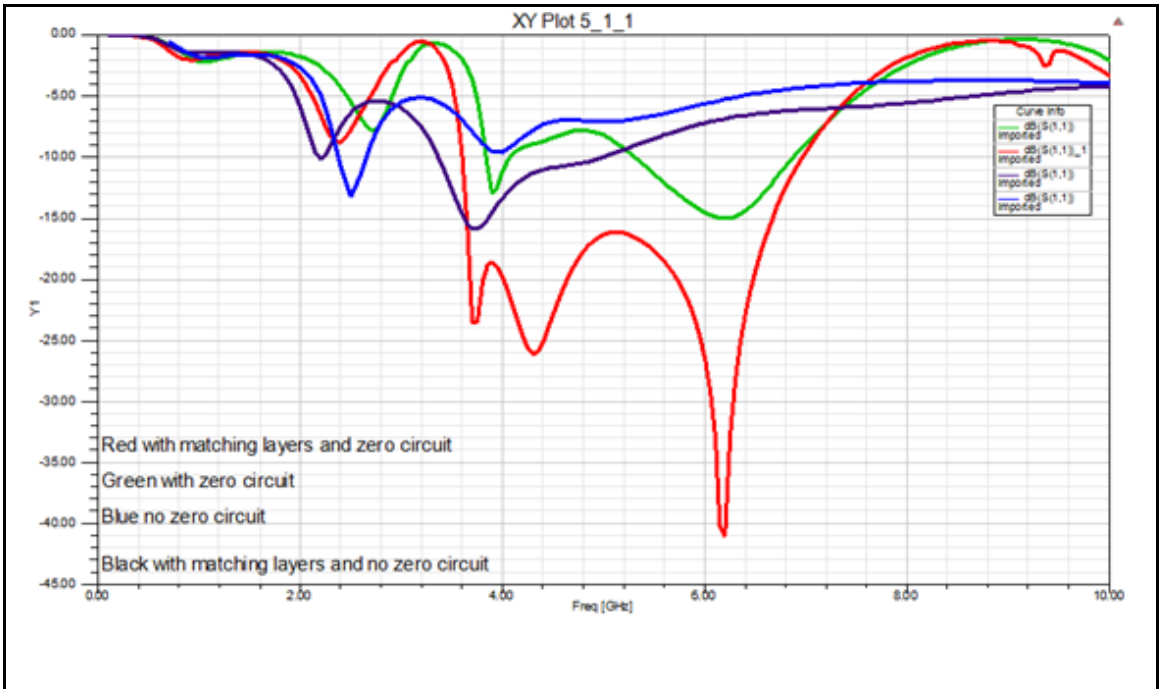

Figure 8-63. S11 Simulated Reflection Measurements of I-Beam with and Without Window Circuit and with and without Matching Layers

8.3.3.1 Validation of the Effective Permittivity Results

Given this final design with an effective medium of a stack of sheets; we wanted to verify if this was indeed equivalent to what was predicted by the Cohn and Diaz models at the low frequency. By using the same method illustrated before, using HFSS shunt admittance data for one sheet we determine the sheet capacitance and then use the Cohn and Diaz methods to calculate relative permittivity of these in effective medium with a layer separation of 6.604mm. The results for the predicted relative permittivity using the Cohn and Diaz method for our best window is shown in Figure 8-64 and Figure 8-65. The red and blue curves as before are the real and imaginary part of the relative permittivity of the I-beam without the zero circuit. The green and magenta curves are the real and imaginary parts of the I-beam with the zero circuit showing the window in the imaginary part.

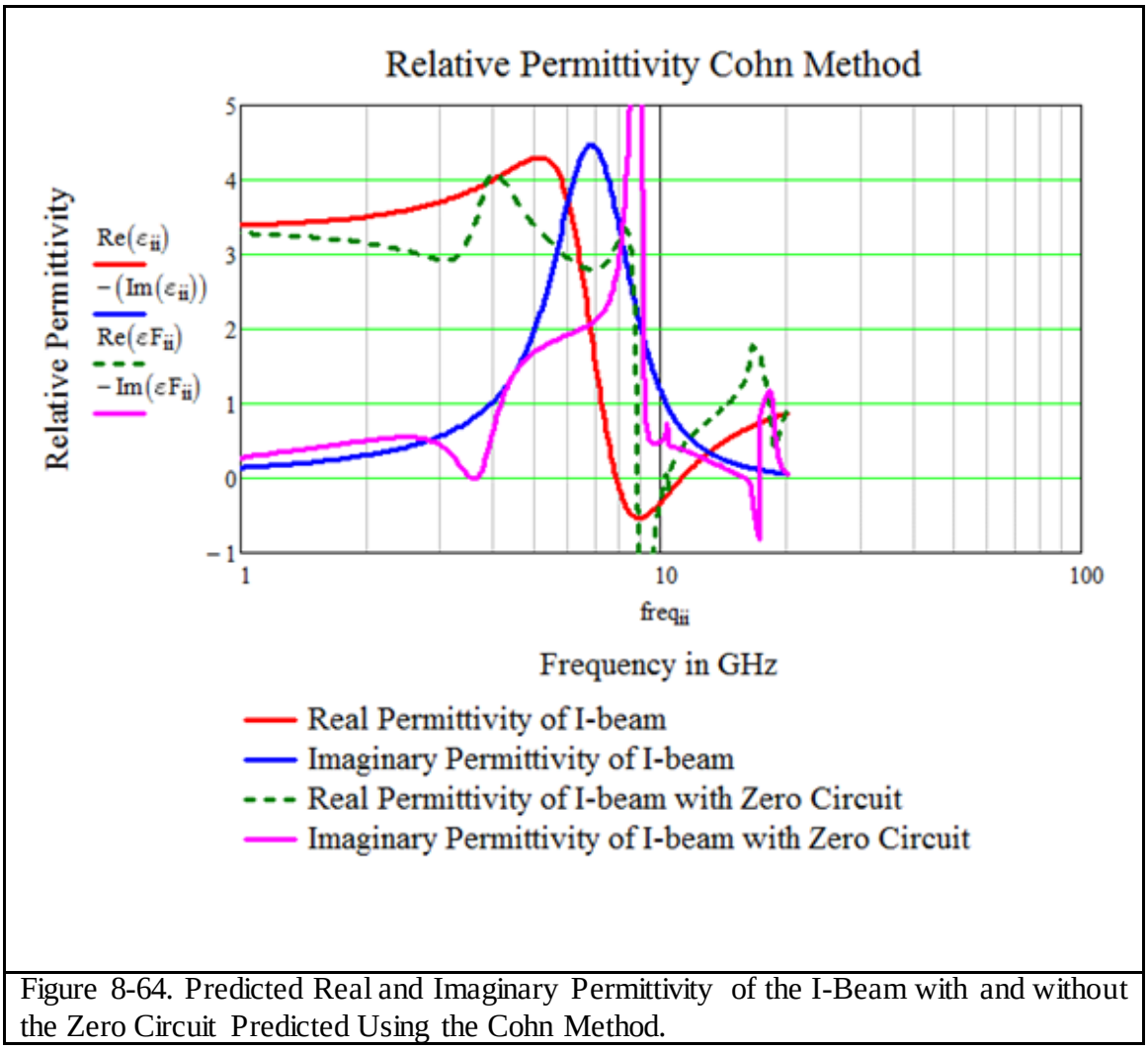

Figure 8-64. Predicted Real and Imaginary Permittivity of the I-Beam with and without the Zero Circuit Predicted Using the Cohn Method.

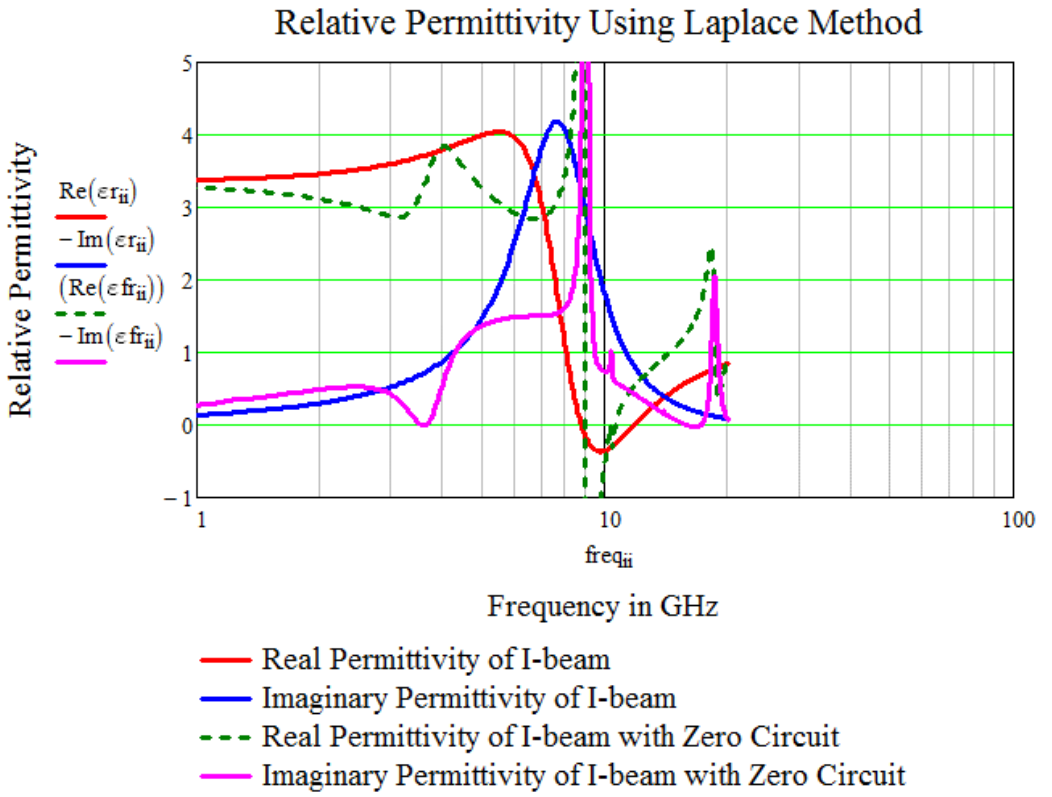

Figure 8-65. Predicted Real and Imaginary Permittivity of the I-Beam with and without the Zero Circuit Predicted Using the Laplace Method.

We then use the S21 transmission data from HFSS simulations for the best window cascade of sheets with and without the zero circuit described above and we extract the relative permittivity from the Diaz Fortran program. In Figure 8-66 we see that we have a clear window in the magenta curve and the results are similar to what was predicted by the Cohn and Laplace methods.

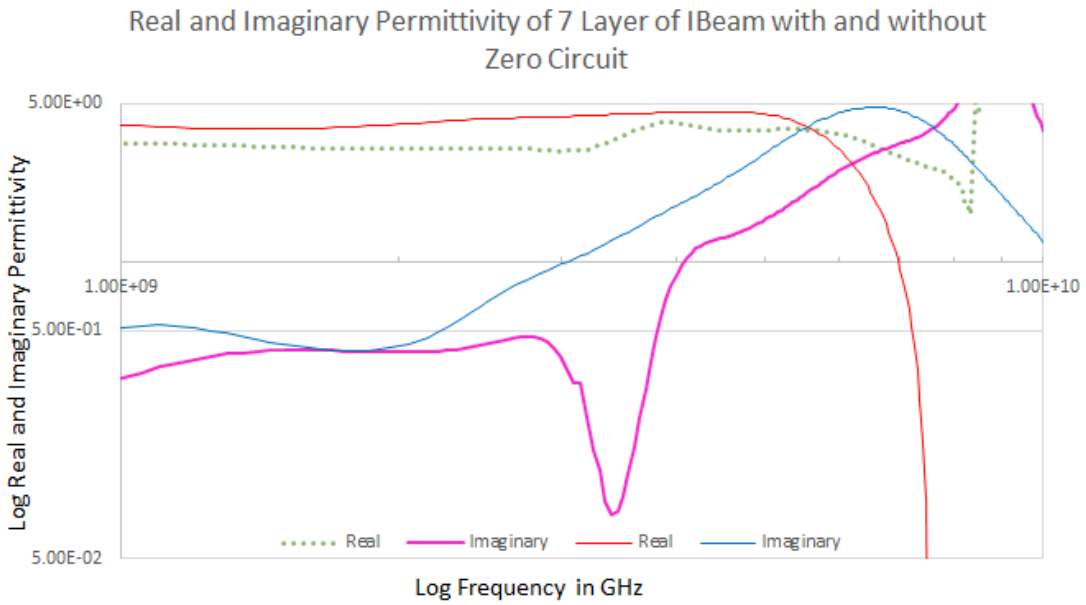

Figure 8-66. Predicted Real and Imaginary Permittivity of the I-Beam with and without the Zero Circuit Using a Cascade of 7 Sheets Extracted Using Diaz Permittivity Program from HFSS Transmission S21 Data.

We also look at the through HFSS S11 measurements for a single sheet of the I-beam design with and without the zero circuit for our final window design in Figure 8-67. The blue curve is the reflection coefficient without the zero circuit and the red curve is with the zero circuit. There is a clear window.

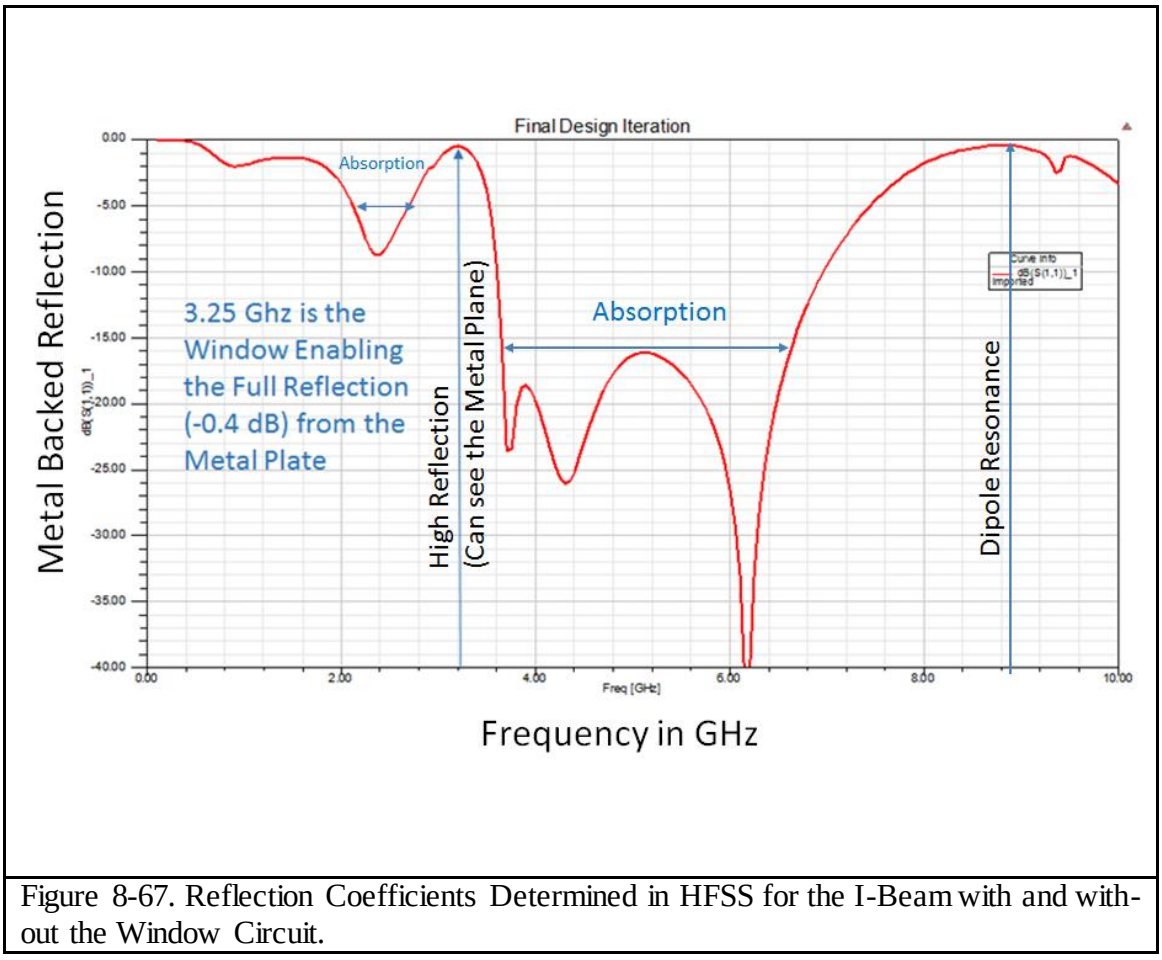

Figure 8-67. Reflection Coefficients Determined in HFSS for the I-Beam with and without the Window Circuit.

Our goal was to make a material that was absorbing over the widest measureable band. We are limited by our ability to manufacture fine features on one hand for LRC components and on the other hand our ability to measure the window article as an effective medium. In order to create an effective medium the unit cell had to be of the order of one tenth of a wavelength or less. Therefore to create an effective medium and observe a window between 2 GHz to 5 GHz our unit cell dimensions had to be between 1.5 cm to 0.6 cm. We chose 1 cm which yielded a window in the 3 GHz range. We were also constrained by the fact that the sheets separation had to be in the order of the unit cell as discussed before to neglect interaction between the sheets. So 10 mm was the largest unit cell we could model

without running into manufacturing constraints and fabricating a reasonable number of layers that were not too cost prohibitive and easy to measure.

CHAPTER 9

MANUFACTURING THE HFSS MODEL

Once we completed our design; our next step was to manufacture the I-beam zero circuit board. Our approach was to etch a double clad Duroid 5880 and then assemble the resistors on the board to physically realize our design.

Our first step was to convert the single sheet design to .dxf files of the resistor, the etched board on both sides and the solder mask as shown in Figure 9-1. The copper lines were 0.1 mm and the diagonal lines were 0.07 mm, the minimum Cu etch dimension that the circuit board manufacturers advertise. However it still proved to be very challenging to find circuit board companies that would bid this design. Some initiated work and then stopped. Also there were challenges finding a local supplier that could perform both etching and pick and place for our resistors.

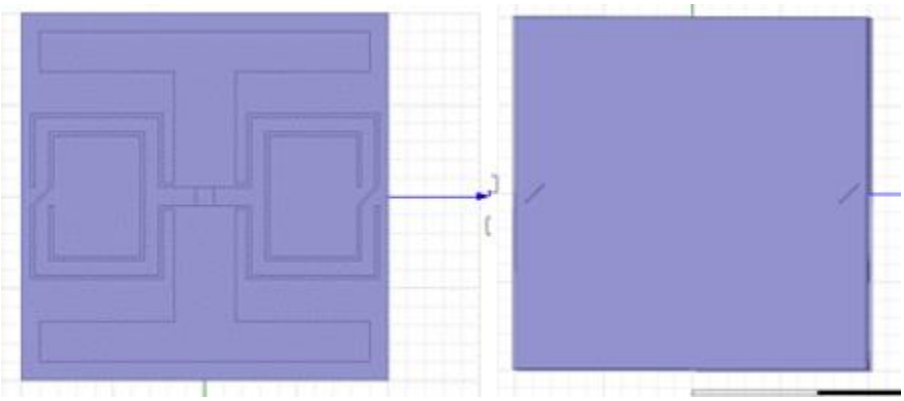

Figure 9-1. Dxf File Front and Back of Duroid Sheet of a Unit Cell.

Since we wanted an approximate 12 inch by 12 inch part to test in the Tunnel for transmission measurements and in the Arch for reflection measurements, we chose the Duroid sheet size available of 12" by 18" to be optimal. We were able to fit approximately 29 unit cells in the vertical direction and 32 unit cells in the horizontal direction.

We were concerned about the mismatch in the coefficient of thermal expansion between the Cu (16-16.7 ppm/^{0}C) and the Duroid 5880 (x=31 and y=48 ppm/^{0}C) of a at least a factor of 2 and the Duroid thermal expansion was anisotropic. Also because most of the copper was going to be etched on the back side of the double copper layer Duroid 5880; we expected the Duroid sheet to curl. To avoid this we maintained a 3 inch by 12 inch un-etched copper area on both sides of the 12 inch panel on the top and bottom of the Duroid to maintain the rigidity of the copper clad Duroid and avoid curling of the Duroid sheet. The Copper was then surface plated with ENIG (Electroless Nickel Imersion Gold) to prevent it from being tarnished.

A 50 ohm resistor by Yageo with miniature dimensions of 1 mm length, 0.5 mm width and 0.32 mm height (0402 packaging) was selected for this application.

The 2 layer copper clad Duroid was etched at Sunstone and the resistors were assembled at Screaming Circuits using solder paste.

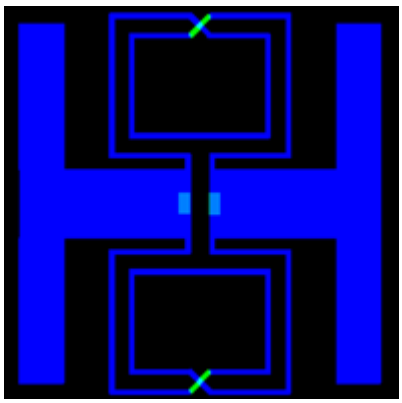

Figure 9-2. Gerber File of Etch Layout with Solder Mask in Light Blue and the Back Side Cu Is in Green.

The final panel is shown in Figure 9-3, Figure 9-4, Figure 9-5, and Figure 9-6.

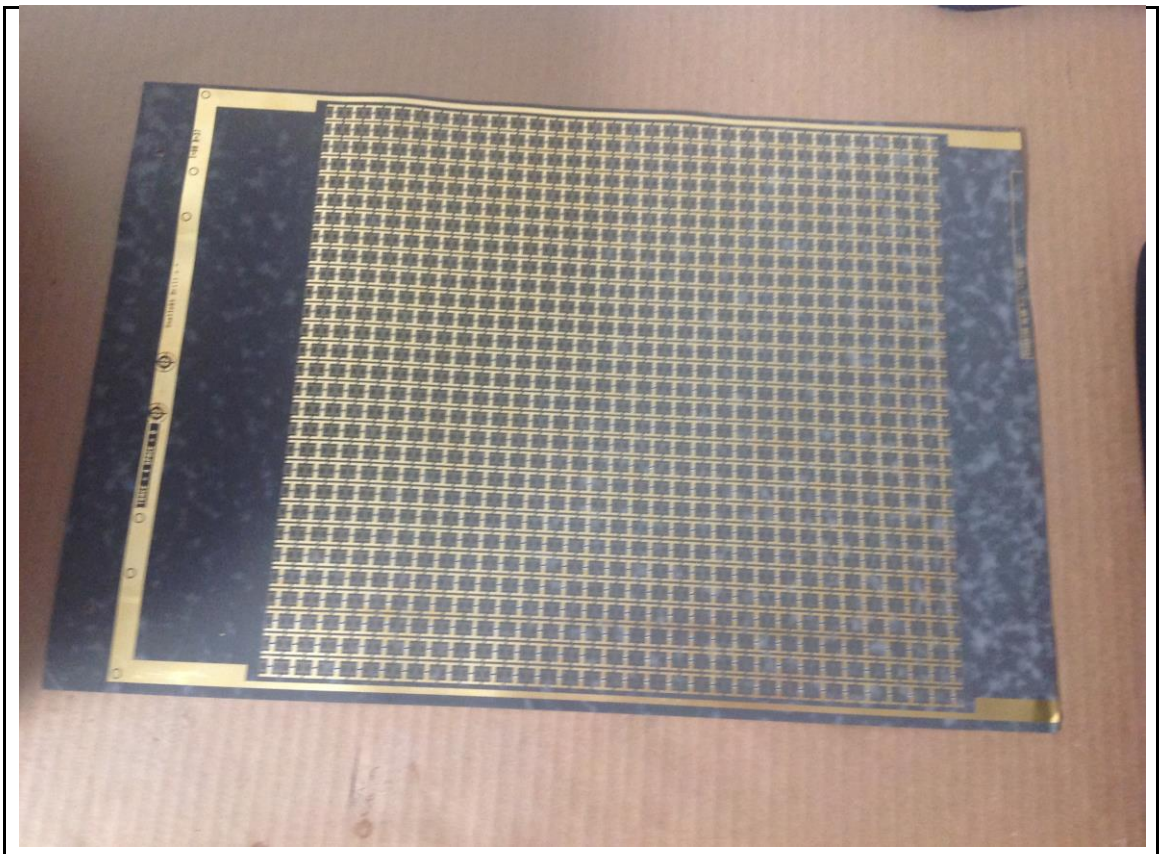

Figure 9-3. I-Beam Zero Circuit Board.

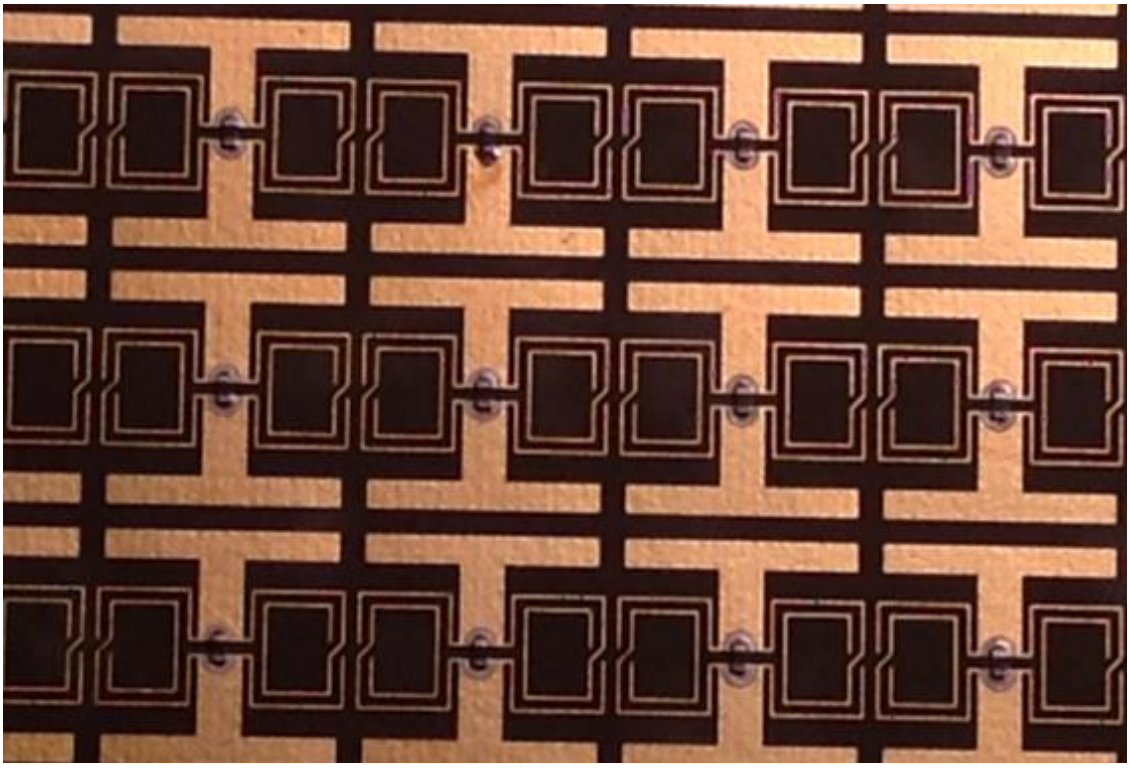

Figure 9-4. Zooming in I-Beam Zero Circuit Board.

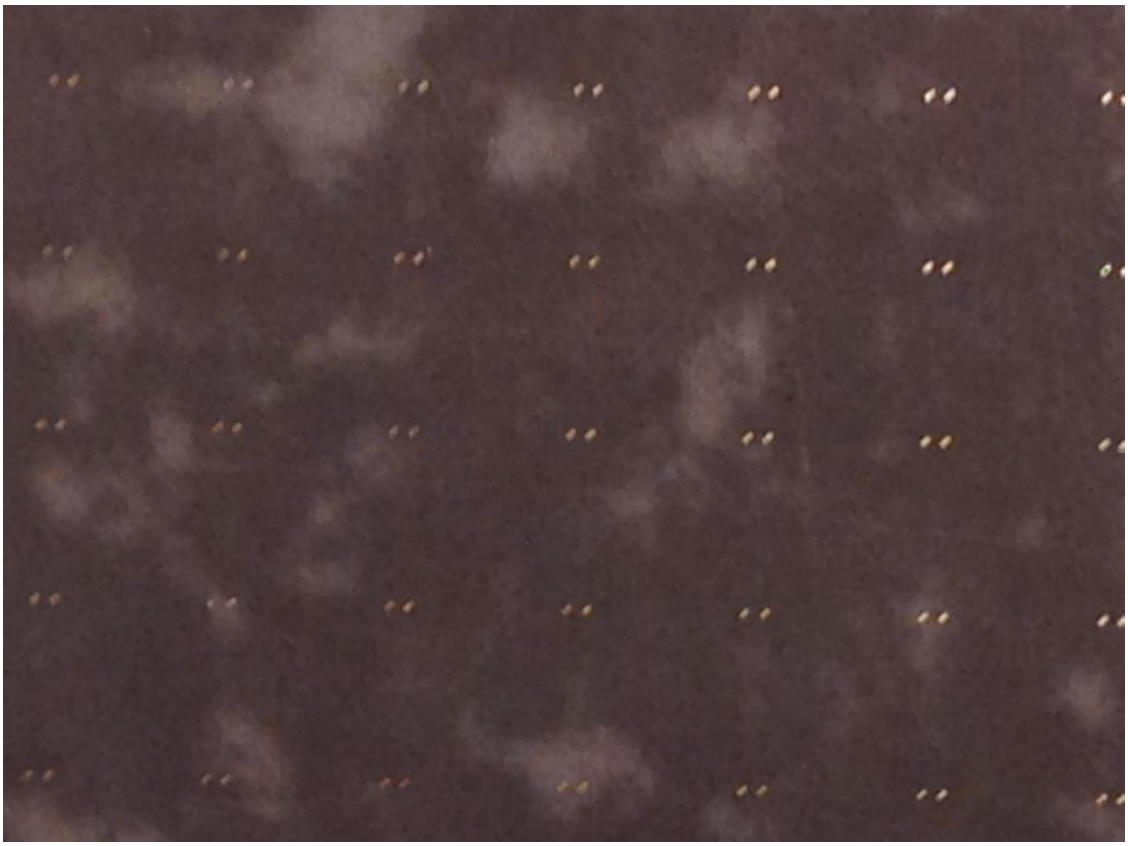

Figure 9-5. Back Side of I-Beam Zero Circuit Board: Capacitive Coupling Across Duroid.

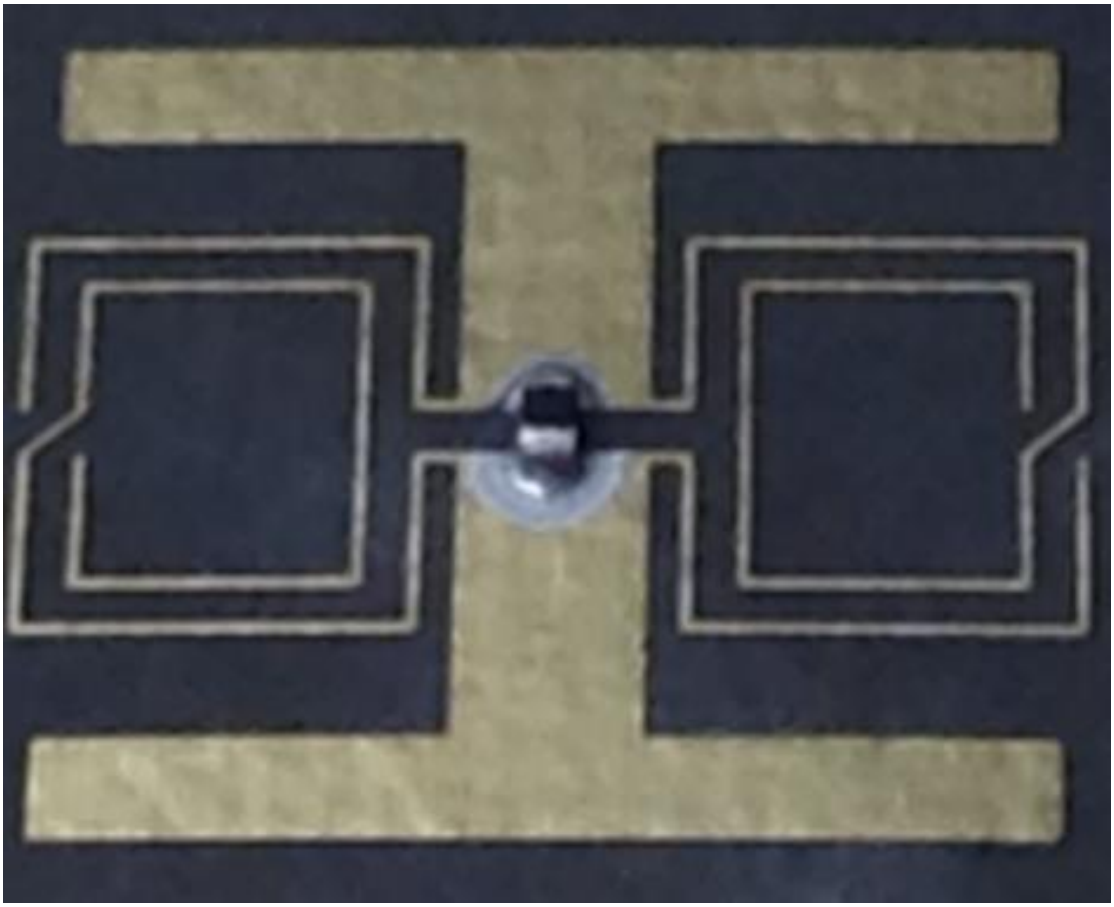

Figure 9-6. I-Beam Zero Circuit Board: Zooming in to a Single Unit Cell with 50 Ohm Resistor at the Center.

Diab H45 foam spacers, 1/8 inch thick were purchased from FiberGlast. Southwest Exhibits machined all our foam with their CNC machines. The matching layers of HDPE high density polyethylene was purchased from Professional Plastics. And Diab Corporation donated the HCP70 foam for our project.

However the costs of manufacturing each panel was prohibitive and since this was a self-funded project we decided to manufacture only one panel. We saw in chapter 7 that a

single panel of the I-beam zero circuit design can clearly demonstrate whether we have a window from transmission or reflection measurements.

Furthermore to mitigate risk and save the cost of building 7 panels we decided to manufacture a single panel for our demonstrator. If we replicate the performance of the HFSS model for a single sheet it is clear we can replicate a stack of these sheets and physically prove our designed window works.

Figure 9-7. Diab HCP70 $\varepsilon_r = 1.39$. Foam Top Matching Layer.

Figure 9-8. HDPE ε_r= 2.33. Second Matching Layer.

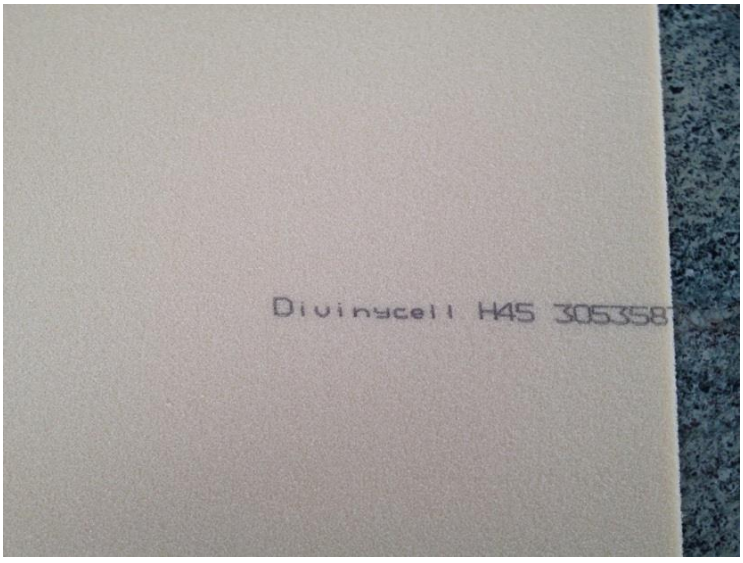

Figure 9-9. Diab H45. ε_r=1.05 Spacers.

Figure 9-10. The I-Beam Stack with Matching Layers and Spacers.

CHAPTER 10

THE TESTING NARROW BAND TRANSPARENCIES AND COMPARING AGAINST HFSS PREDICTIONS

Using a VNA 8720 Agilent Analyzer and a Reflection Arch we measured the I-beam Zero-circuit panel, testing the article both in transmission and reflection.

10.1 Transmission

The VNA 8720 set-up is shown in Figure 10-1 where we tested the I-beam Zero Circuit Panel. Figure 10-2 shows the tunnel iris size and I-beam zero circuit panel placement.

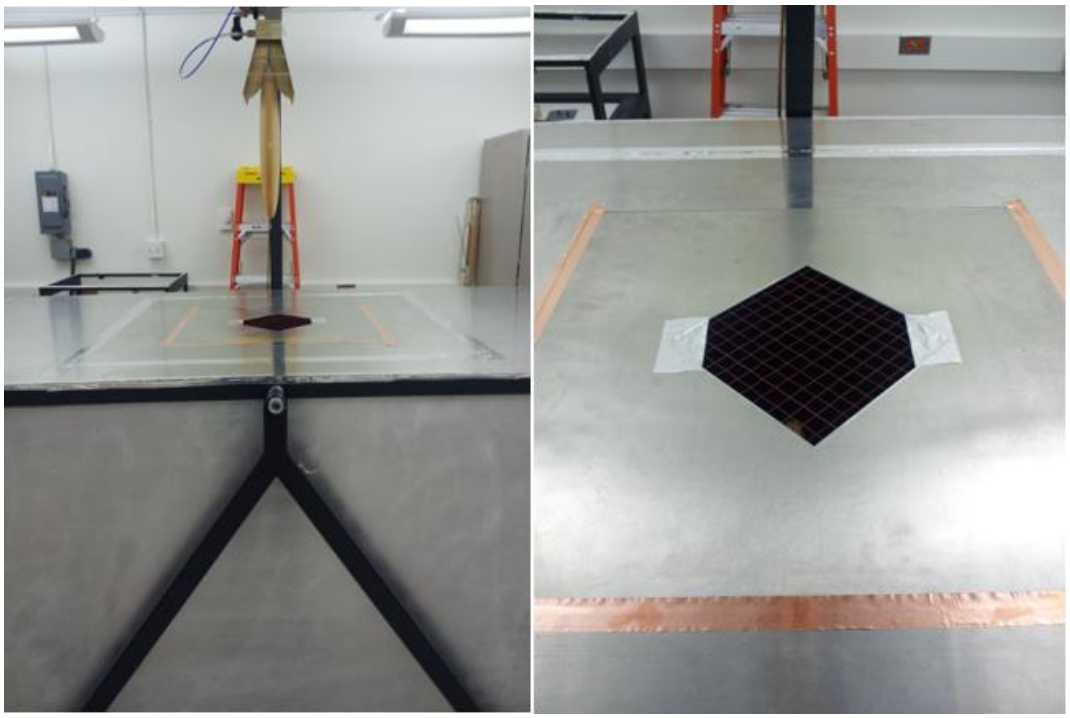

Figure 10-1. Tunnel Set up in Diaz Lab Goldwater.

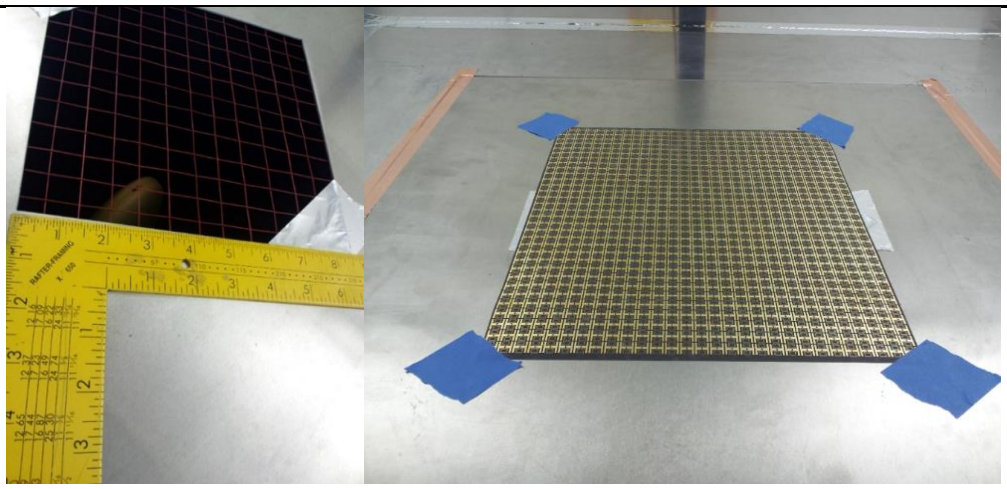

Figure 10-2. Tunnel Iris 8 Inches and I-Beam Zero Circuit Panel in Diaz Lab Gold-water.

Figure 10-3. and Figure 10-4. show the amplitude and phase of the measured properties of the article.

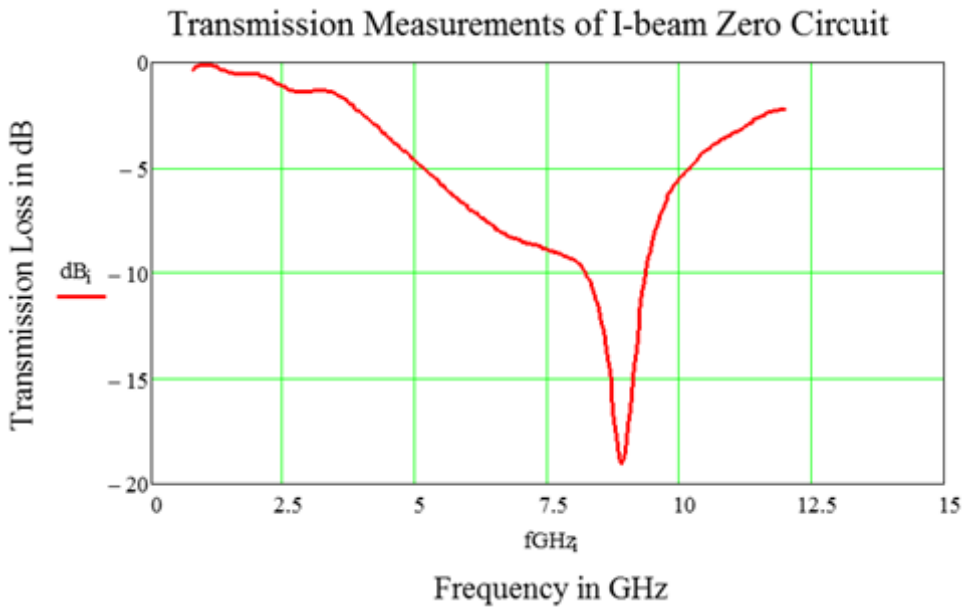

Figure 10-3. I-Beam Zero Transmission Loss in dB.

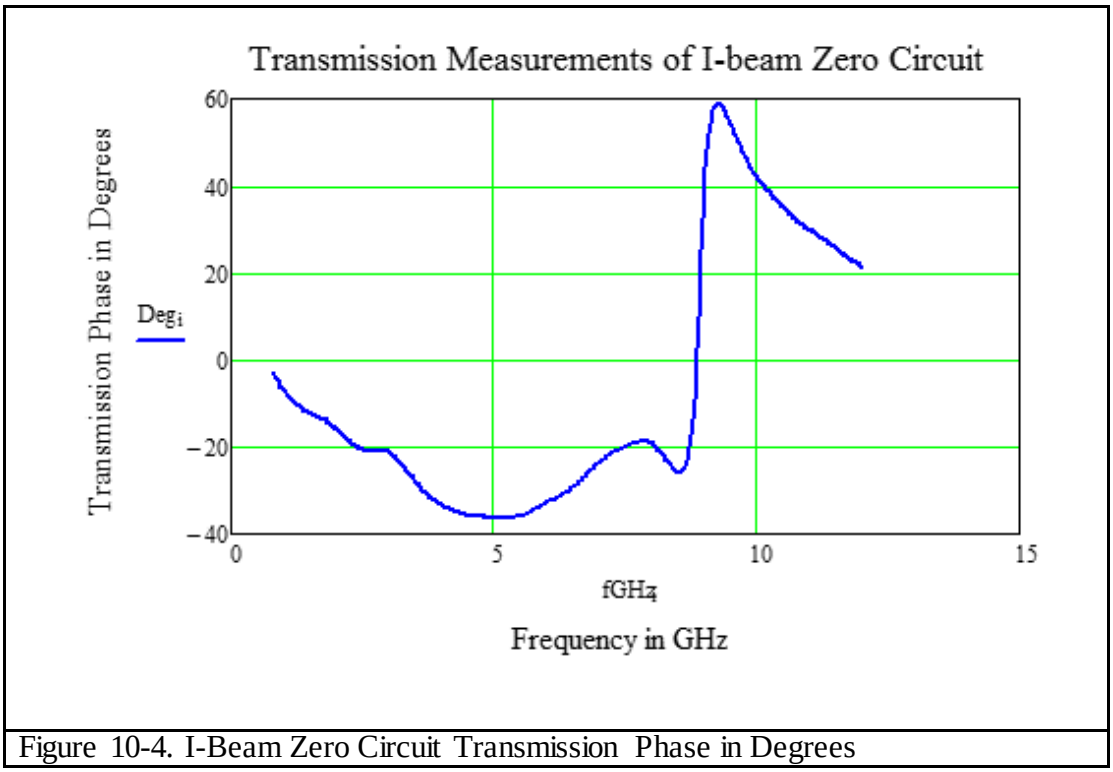

Figure 10-4. I-Beam Zero Circuit Transmission Phase in Degrees

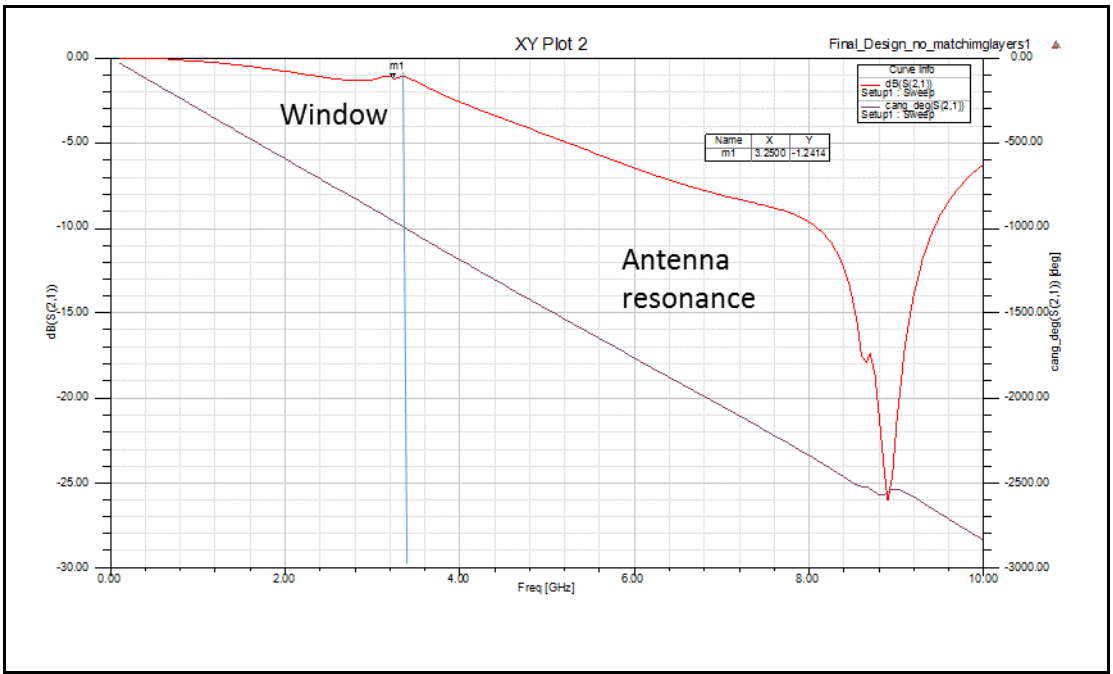

Figure 10-5. I-Beam Zero Circuit Transmission Prediction for a Single Sheet in HFSS.

The HFSS transmission predictions match very closely to the measured article as seen in Figure 10-5.

The sheet capacitance of the I-beam zero circuit was extracted from the measured

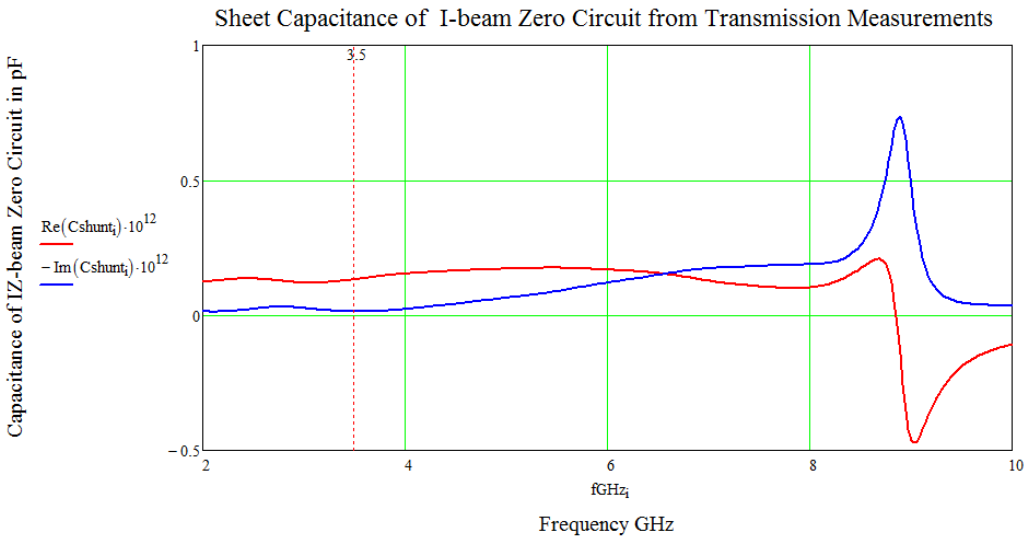

Figure 10-6. Real and Imaginary I-Beam Zero Circuit Capacitance.

transmission data as shown in Figure 10-6 and Figure 10-7. Using the same equations from Chapter 7 we obtained the sheet capacitance from the shunt admittance. Zooming in we see the window is clearly present near 3.4 GHz that was predicted by HFSS.

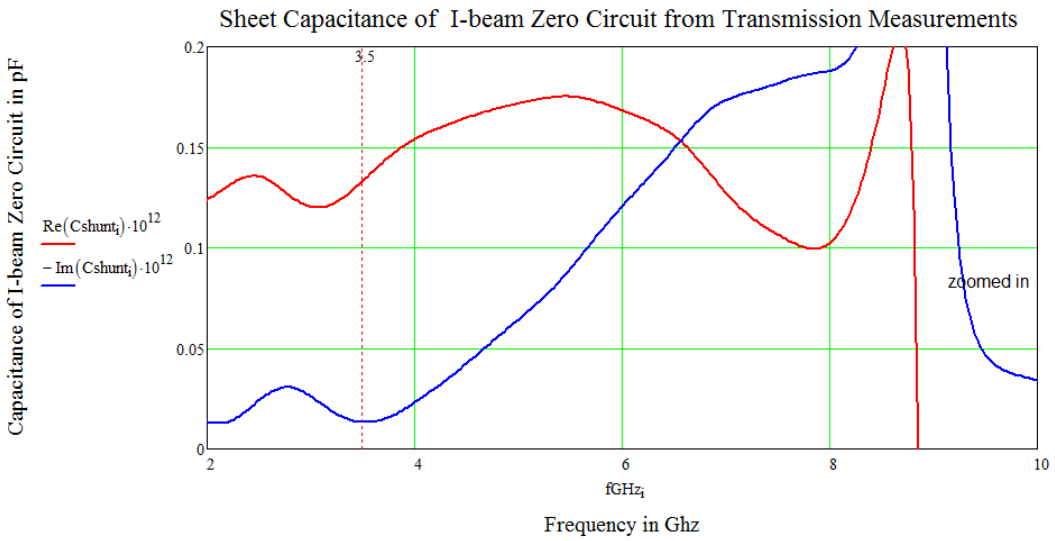

Figure 10-7. Real and Imaginary I-Beam Zero Circuit Capacitance: Zooming In.

$$T_i = 10^{\frac{dB_i}{10}} \exp\left[iDeg_i \frac{\pi}{180}\right]$$

$$Yshunt_i = \frac{2\frac{1}{377}(1 - T_i)}{T_i}$$

$$Cshunt_i = \frac{Yshunt_i}{i2\pi freq_i}$$

Noting that the data is noisy below 2.5 GHz, and that we were using a two nanosecond gate we compared the sheet capacitance extracted from the measured transmission data with our HFSS predictions; we find that the window frequency is very close to 3.4 GHz as predicted and the overall shapes of the curves are similar. The measured window is slightly shallower. The predicted and measured sheet capacitance is shown in Figure 10-8 in a linear frequency scale as all measurements were made in the linear scale. In

Figure 10-9 the sheet capacitance is plotted against log frequency in order to compare with plots in Section 8.3.

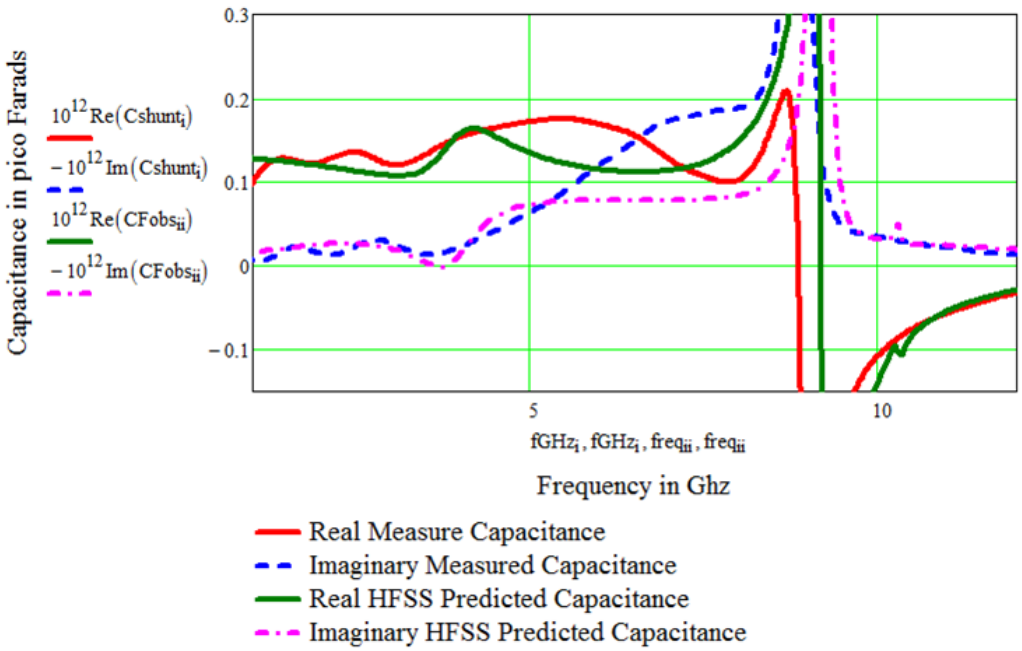

Figure 10-8. Real and Imaginary I-Beam Zero Circuit Capacitance Linear Scale.

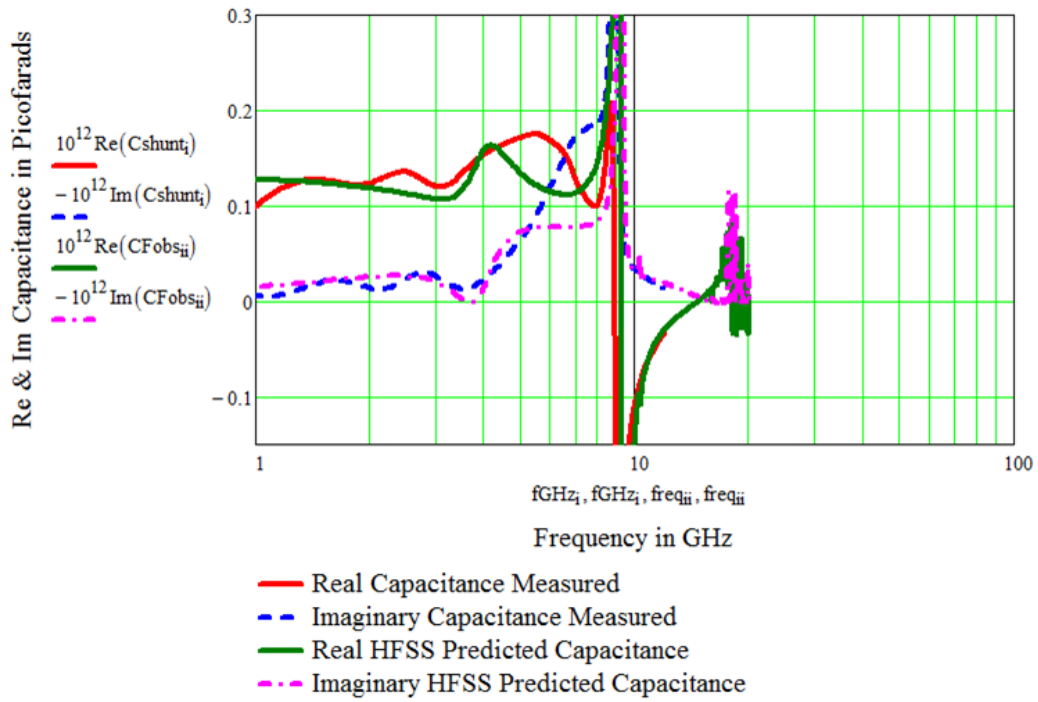

Figure 10-9. Real and Imaginary I-Beam Zero Circuit Capacitance Log Scale.

Zooming into the window we compare the measured results with the HFSS model and Circuit model in Figure 10-10 and both the real kink corresponds with the window as we expect due to the Hilbert relationship.

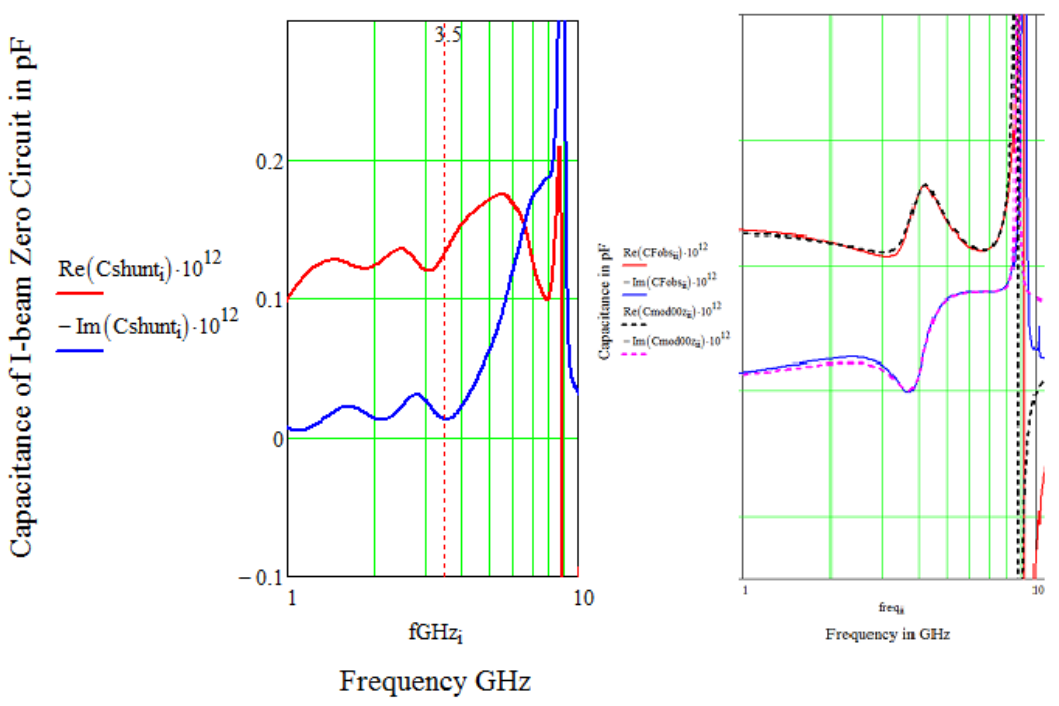

Figure 10-10. Real and Imaginary I-Beam Zero Circuit Capacitance Measured Versus HFSS Pre-Dictions and Circuit Model.

Our final HFSS model and design assumed 7 sheets of the I-beam zero circuit with a separation distance of 6.604 mm. Using the Cohn equation we used in chapter 8.3 we predicted the effective permittivity for such a model. Using the measured sheet capacitance we do the same and compare the measured versus predicted permittivity. The results are shown in Figure 10-11 and Figure 10-12.

The data below 2.5 GHz is clearly noisy and there is a ripple in the data due to the interference between the edges of the iris as the planar wave interacts with it. This makes the measured window in blue appear shallow relative to the theoretical null in

magenta. But if we compare this data with the baseline absorber it is clear even with the noise and interference the measured null is deep relative to the I-beam without the zero circuit as shown in turquoise in Figure 10-13. If we zoom into the imaginary part of the permittivity we see that there is an 8 to 10 dB window relative to the baseline material as shown in Figure 10-14. If we had a smaller spot size for our planar wave or the article was larger with no interference with the iris the null would be even deeper as predicted.

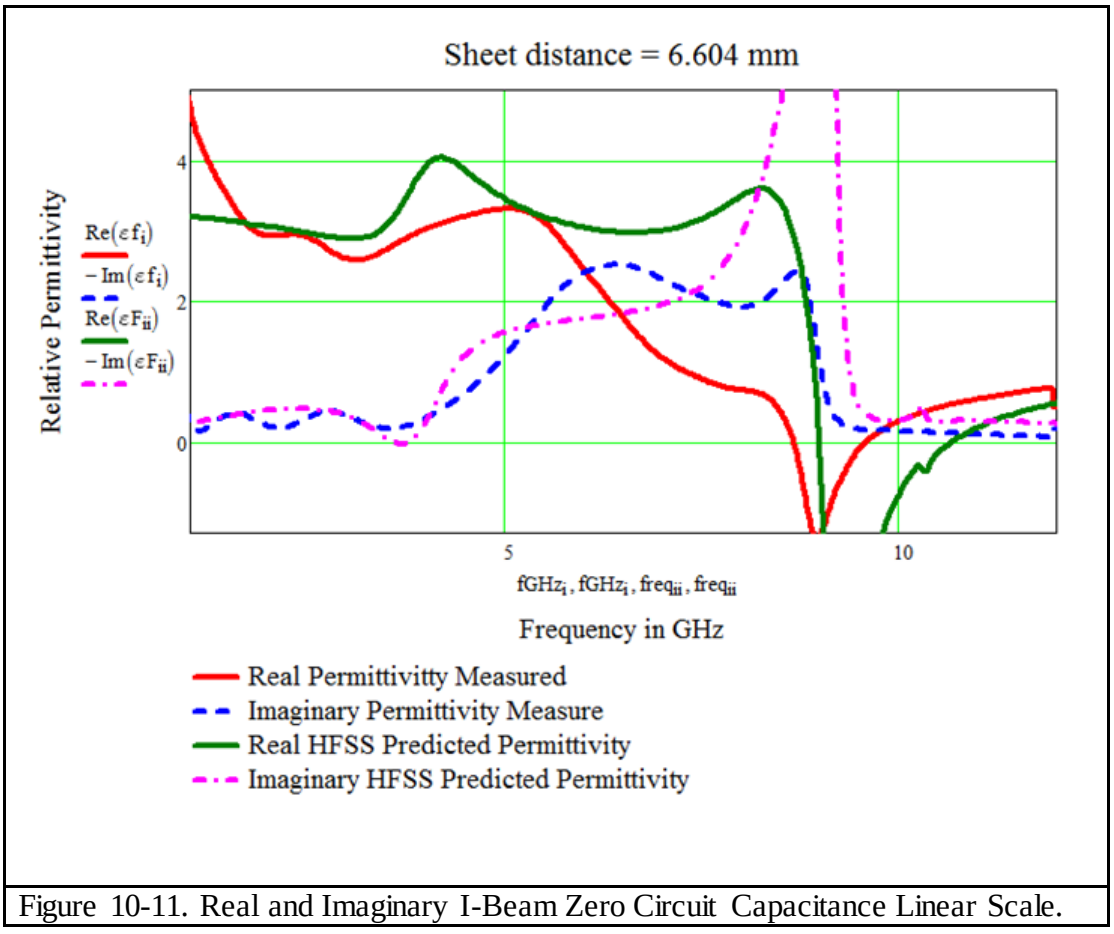

Figure 10-11. Real and Imaginary I-Beam Zero Circuit Capacitance Linear Scale.

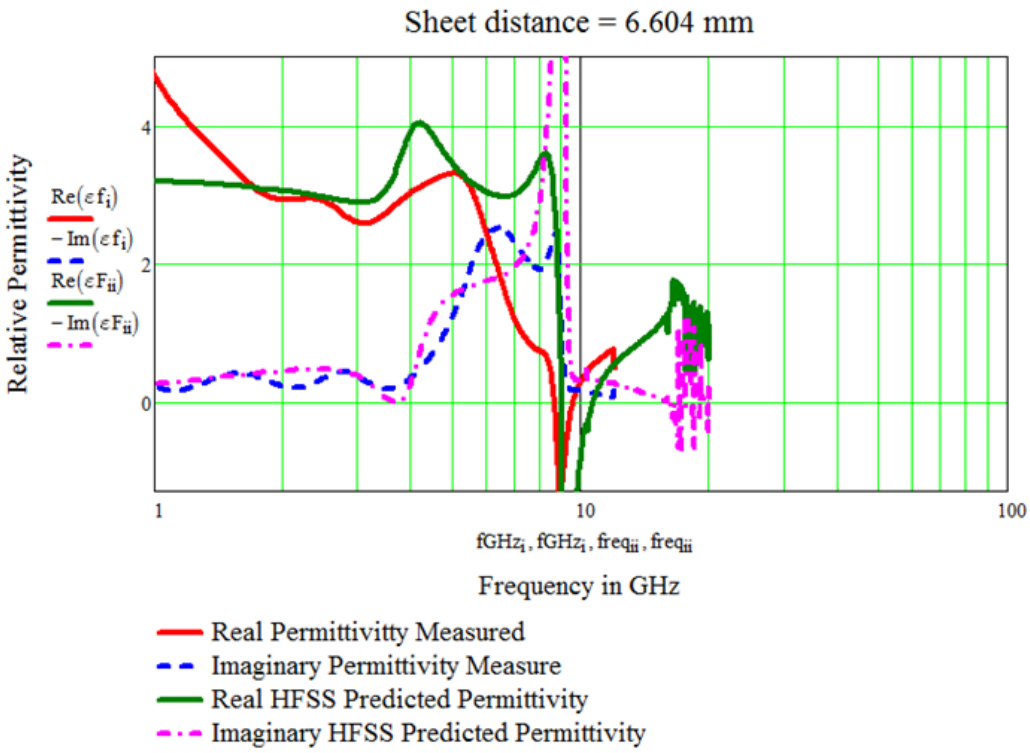

Figure 10-12. Real and Imaginary I-Beam Zero Circuit Capacitance Log Scale.

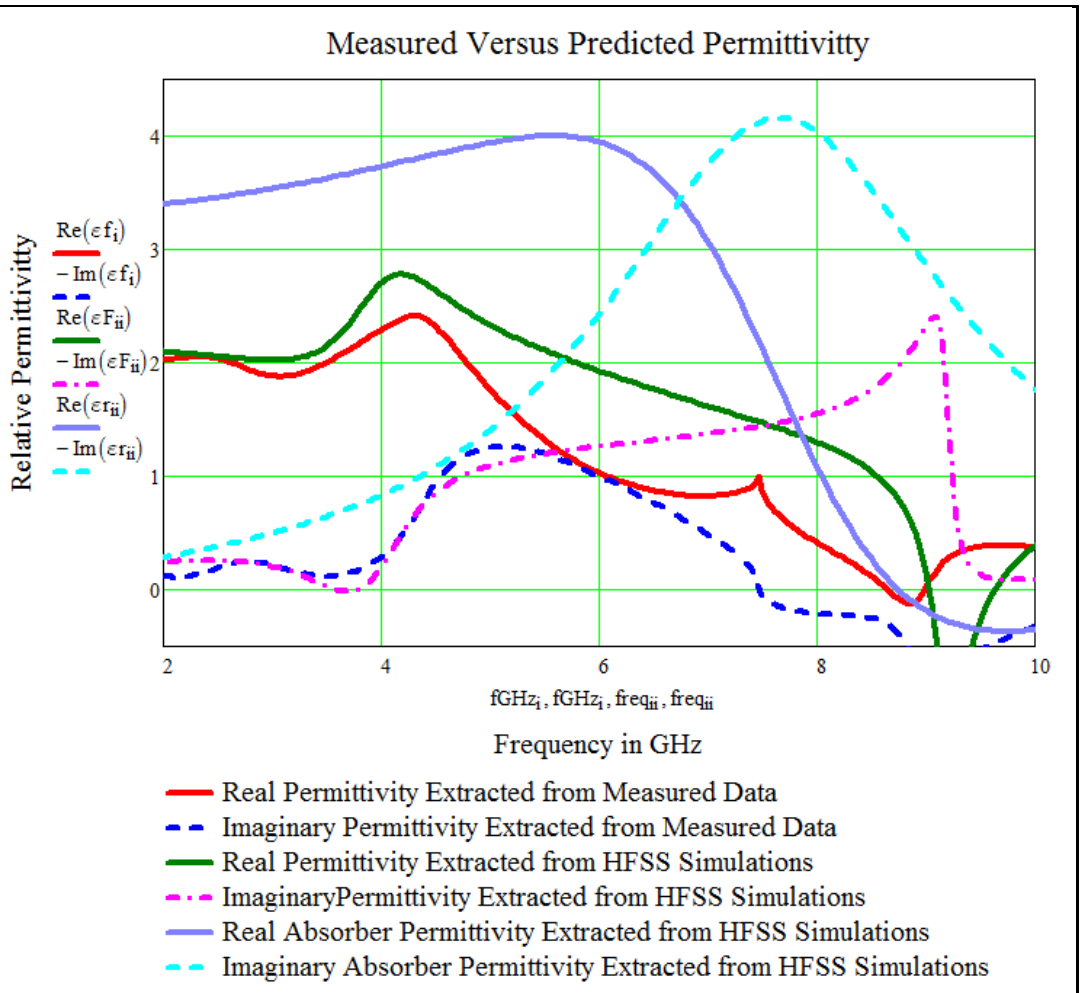

Figure 10-13. Permittivity of a Cascade of these Measured Sheets Relative to the Baseline Absorber and HFSS Predictions.

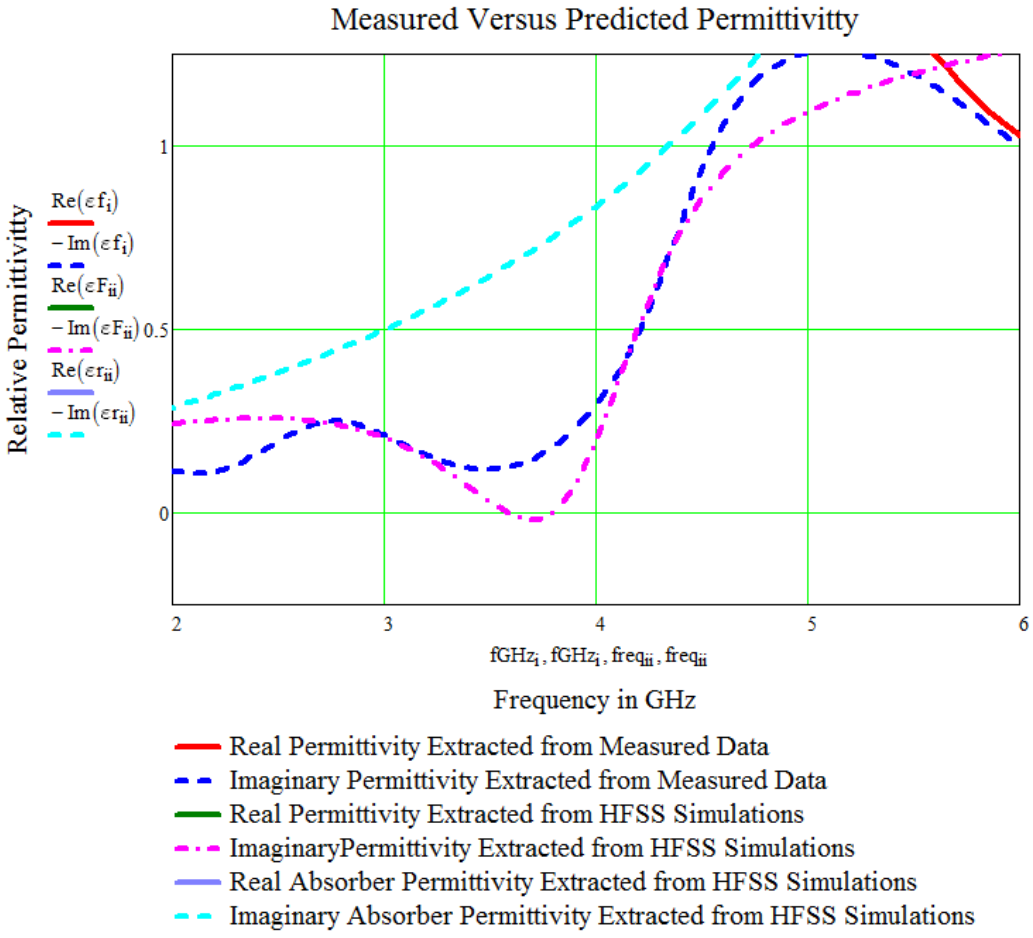

Figure 10-14. Zooming In: Permittivity of a Cascade of these Measured Sheets show a clear Window in the Imaginary Part Relative to the Baseline Absorber.

10.2 Reflection

Using an Arch set-up at a 10 degree angle Jeff Peebles tested the I-beam Zero-circuit panel at the Microwave lab. Figure 10-13 shows the set up. The board was placed on a ground plan separated with 0.125 inch foam. For this test we had to cut off the gold edges to prevent reflection scattering from the arch. This causes the panel to curl which created a distance from the ground plane to panel to be 0.25 inches.

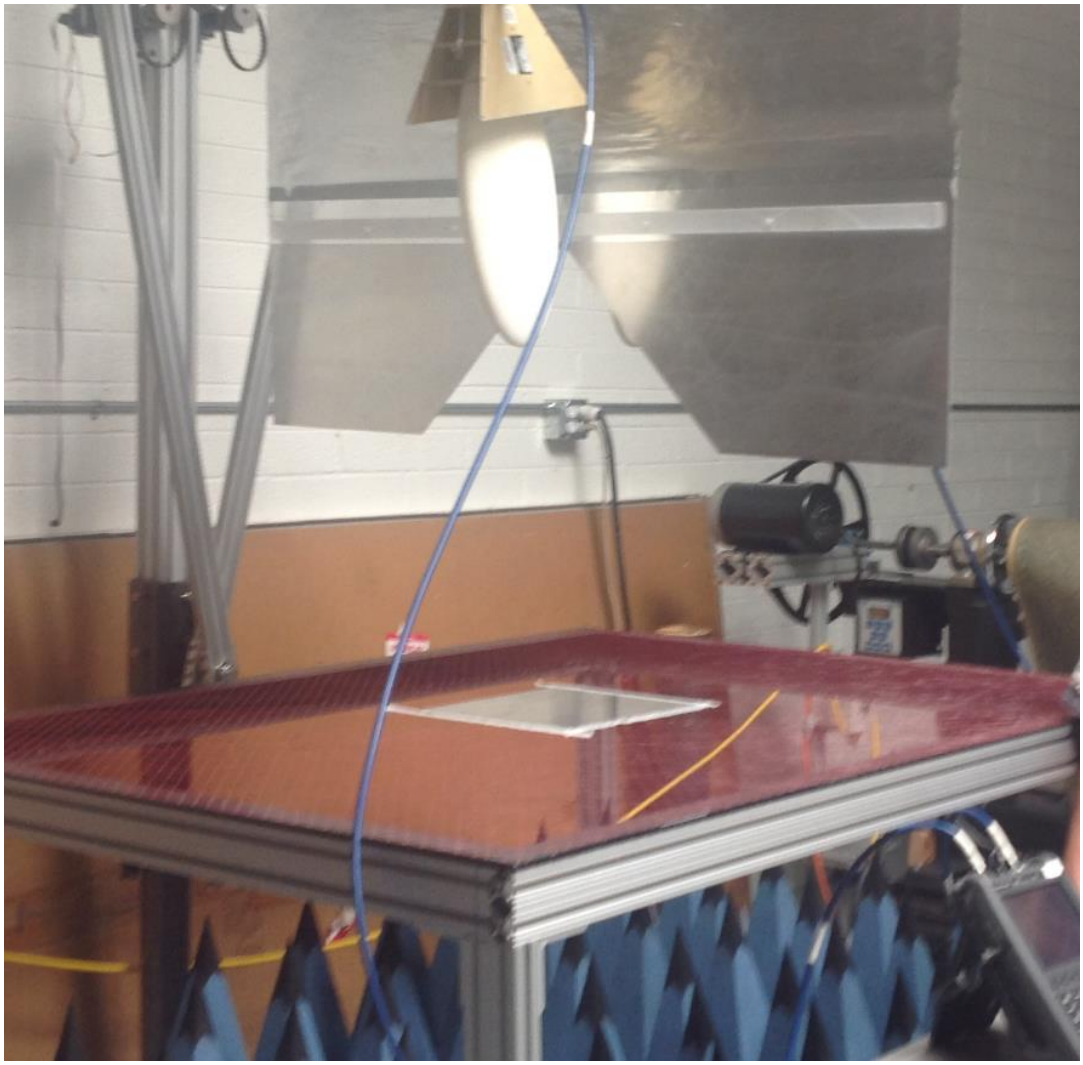

Figure 10-15. Arch Reflection Test Set-Up.

We plotted the S11 reflection data against two data sets. The first data set was using the shunt admittance extracted from the S21 transmission data using the following equations. And the shunt admittance predicted from HFSS using the same equations.

$$Yinput_i = -i\frac{\sqrt{\varepsilon_{air}}}{377}\cot\left(k0_i\sqrt{\varepsilon_{air}}d\right) + Yshunt_i$$

$$\Gamma_i = \frac{\frac{1}{377} - Yinput_i}{\frac{1}{377} + Yinput_i}$$

All three reflection data sets were in reasonable agreement as shown in Figure 10-16.

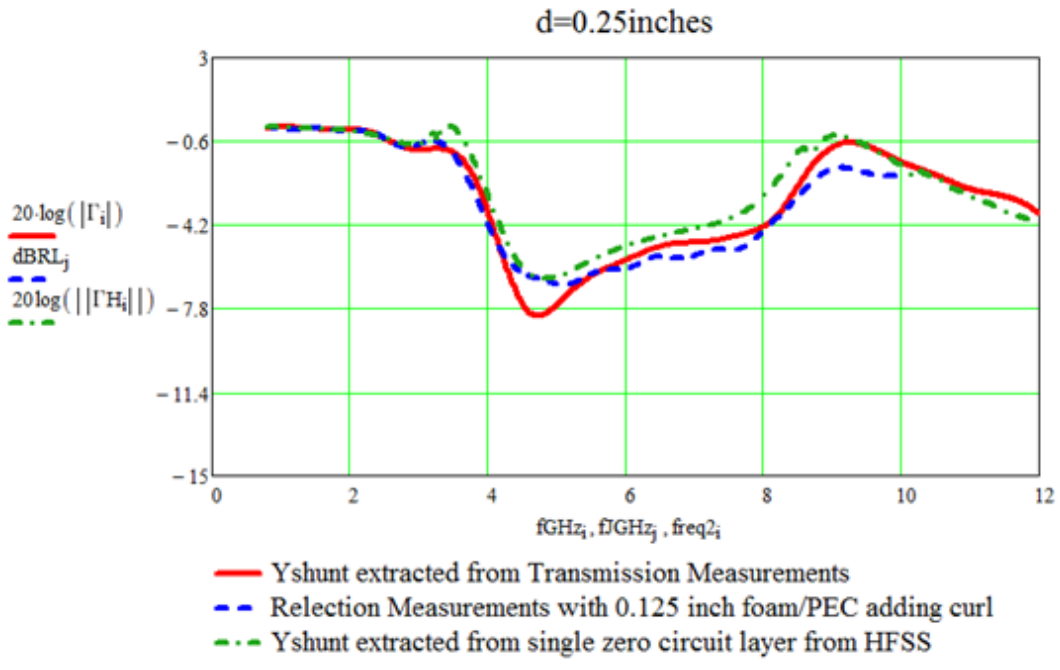

Figure 10-16. Measured Versus Calculated Reflection Performance of I-Beam Zero Circuit for a 0.25 Inch Separation from Ground Plane.

10.3 Sources of Variability

Material Variability

The Duroid materials has anisotropic coefficient of thermal expansion in all three directions. In addition the thermal coefficient of expansion is more than twice that of copper. This causes slight shrinkage of the Duroid and some change in the I-beam unit

cell geometry. There are also tolerances in the variability of the Cu etch width. In addition the 50 ohm resistors vary by +/- 5%. Although resistors were bought from a single reel and lot, all these factors vary from the idealized model we created in HFSS.

Test Variability

There is a lot of noise in the lower frequency data (lower than 2.5 GHz) using VNA 8720. There may be losses in the cables which are not present in the HFSS model.

For the transmission test, the time gate of 2 nanoseconds had to be tweaked to obtain good data. The data is noisy and there is some oscillation. The radiation of the poly rod antenna illuminates the entire iris (sample is finite in size) instead of going through the hole there and there is interaction with the edges. So the origin of this ripple is non-physical and is an artifact of the measurement. This is the combination of the gate and the reflection back and forth of the iris edge - the interaction of the planar wave with the iris. The planar waves from the poly probe sees the iris and it bounces back and forth oscillating and obscuring the depth of the window. So the window appears to be not as deep as the theoretical predictions.

For the reflection measurements there was curl in the panel that added more uncertainty in the distance from the ground plane.

CHAPTER 11

CONCLUSIONS

So we have shown that we can design, model and fabricate an artificial dielectric meta-material with a narrow band transparency and have experimentally demonstrated the window performance for the first time at radio frequencies at a preselected frequency of interest.

These meta-materials do not depend on wavelength dependent cancellation systems due to the periodicity of the structure like FSRs. Rather it relies on the premise that there is a more fundamental model of material that Diaz and Alexopoulos used to model water.

We have now physically validated the zero circuit hypothesis. Experimentally we have shown there is a more generalized universal model of material permittivity than the current models, which although explains most materials, failed to include water. This illustrates there is a more Fundamental model of permittivity that includes the zero circuit and therefore now includes water. The Lorentz in a special case of this Fundamental model when the zero circuit is open which then models all other materials other than water. And the Debye is a special case of the Lorentz model where there is insignificant inductance.

Finally as we discussed in chapter 3 one of the important points of Brillouin's derivation was that the mechanical model exactly maps to an electrical coupled circuit model. This equivalency is a reflection of a deeper symmetry that exists in Physics that allows us to seamlessly transition between systems that share the same differential equations. Our

methodology to make circuits out of materials and materials out of circuits and using meta materials to make a new meta material beautifully illustrates this symmetry and demonstrates a novel creative methodology to construct artificial materials.

In conclusion

- We can design, model and fabricate an artificial dielectric meta-material with a narrow band transparency window
- We have experimentally demonstrated the window performance for the first time at radio frequencies at a preselected frequency of interest.
- This meta-material's transparency window is a bulk property not an interference phenomenon and is independent of angle of incidence.
- The design of this material relies on the premise that there is a more fundamental model of material that Diaz and Alexopoulos used to model water and we have now physically validated their zero circuit hypothesis.
- The circuit model is *not just* a mathematical representation; but is also a template to make the material. The circuit model is equivalent to the material model.
  - Design by a circuit model
  - Fabricated using a circuit model
  - Used circuits to make a material then used materials to make a circuit
- Demonstrated a novel design methodology of a meta-meta material
- This experimentally proves the Fundamental model

To recap we were motivated to study the unique properties of water so we could emulate the sharp optical valley of water where the imaginary permittivity drops eight orders of magnitude at a frequency of $10^{14.73}$ hertz, where water exhibits no loss. We discussed that the optical properties of water are not only unusual; but have significant implications in Material Science. We tried to understand these properties so we could imitate them or engineer them into an artificial material so that all sorts of useful devices could result.

We studied the different models of frequency dependent permittivity to lay a foundation to analyze models of water and showed that the permittivity of water cannot be modeled by a sum of traditional simple harmonic oscillators (Debyes and Lorentzes) that can be used to model all other conventional materials.

We showed that the mathematical model of the simple harmonic oscillator could be used to describe the physical behavior of not only a mass spring dashpot, but also the dielectric properties of the **individual "molecules"** comprising the most **common material behaviors (Lorentz, Debye, and Drüde),** as a sum of simple harmonic oscillators (SHO) and even quantum multi-level systems.

Because all these models arise from a *mechanism* (circuit, quantum mechanical, or purely mechanical) they are equivalent, interchangeable, and equally valid. They all lead to the interpretation that there is only one circuit model, the series LRC (Lorentz or SHO) that by modification can explain Debye (over-damped SHO, the mass goes to zero) or Drüde

(spring constant goes to zero). ***But no combination of SHOs can model the optical transmission window of water.***

Our goal was to understand the role of materials that exhibit true transmission windows in order create a bulk meta-material that behave like a narrow band transparency like water. We applied and analyzed a model of permittivity that assumed windows are fundamental and a necessary part of the harmonic oscillation representation and thereby demonstrate that there is a more universal model that includes the complex permittivity of water.

We surveyed the literature to find causal models of the permittivity of water that could predict water's optical valley. The Fundamental Diaz model was the only causal model we found that could achieve this with their zero shunt circuit.

We showed that the mechanical model exactly maps to an electrical coupled circuit model picture, with the same equations and per Brillion molecular models are equivalent to electrical circuit models. We demonstrated we can represent a Debye or Lorentz material with an electric circuit model and add the zero shunt capacitance to create the narrow band transparency window which we called the Diaz Fundamental model.

We demonstrated how to make a Debye material using Cohn's model which has an exact equation for a shunt capacitor that states what the capacitive obstacle has to look like in terms of geometry to produce an excess capacitance. We used a cascade of these shunt obstacles to make an effective medium. We explored the Cohn metal plate geometry, the

low frequency limit and that if we brought these layers close together, less than the unit cell dimension, they start interacting and start reverberating like a Lorentz. We validated the Cohn model with the Laplace equation and we checked the effective medium outcome by extracting a permittivity from transmission measurements made in HFSS for these constructed effective mediums.

By making these metal Cohn squares resistive we mimicked the RC circuit of a Debye material. We develop a proportionality factor between the resistance of the circuit model and our HFSS model. We tuned our Debye sheet by choosing the excess capacitance and changed the resistance to define our relaxation frequency. We then added the zero circuit to this Debye circuit model by physically making capacitors and inductors as the chip elements were costly and cumbersome and we would have to worry about the self-resonance of the inductors.

Our first set of trials to physically model this in HFSS using double C loop frames on a resistive sheet were unsuccessful because to push the resonance to lower frequencies we had to make the capacitance high and the inductance low. We developed a circuit model for a zero circuit shunt LRC where the requirements for a successful window were high inductance, low capacitance and very low resistance, so the flux would take the shunt path of least resistance.

Our second set of trials was using a bow tie antenna, where we added chip LRC components in shunt. This design was unsuccessful because there were many competing flux

paths from the top and bottom of the bowtie that bypassed the resistor in the center of the antenna.

On our third set of trials we used the same approach as our second trial except that we made an I-beam that had horizontal hats so there was less likelihood of competing flux paths. We show that the I-beam is a Debye/Lorentz like material by representing it with a circuit model. To add the zero circuit we add large Cu loops for high inductance and add overlap on the other side of the substrate to gain very little capacitance for the zero circuit on purpose.

After obtaining the best window using HFSS we backed out the circuit model with the zero circuit shunt and we found it did not fit our assumption of a single shunt LRC in parallel with the Debye resistor of the original Debye series circuit. Instead we found another parallel branch to the original I-beam. This is because even in the I-beam design set-up the inductive loops were close enough to the I-beam hats that there were other flux paths. So we unwittingly added two shunts to the original Debye circuit essentially "coating" the Debye I-beam with a Lorentz and so we were able to achieve a window.

With the reflection data we were able to use the Cohn and Laplace methods to predict the permittivity of a cascade of layers of this I-beam sheet design, demonstrating the window. We fine-tuned the design by using matching layers to reduce the front face reflection and foam separators to construct an article with the minimum number of sheets to save costs.

We added a ground plane half a separation distance away and we simulated full reflection back at the window frequency.

To save costs we constructed one panel of the I-beams on a Cu clad Duroid substrate with 50 ohm resistors. We measured the article in both transmission and reflection and demonstrated the presence of a window at the predicted frequency of interest and showed good agreement with HFSS transmission and reflection data.

CHAPTER 12

RASORBERS AND META MATERIALS

There are a class of materials called rasorbers that at first glance appear to behave like a narrow band meta-material but are not. They are called frequency selective absorbers in three dimensions that we will discuss below.

12.1 Meta-materials

Over the last decade there has been a huge growth in applications of meta-materials. In addition FSS (Frequency Selective Surfaces) and 1 to 3 dimensional EBG (Electromagnetic Band Gap) materials structures as well as AMC (Artificial Magnetic Conductors) are used for many applications especially in the communications industry. These applications which may include frequency selective transmission or reflection, antennas or antenna arrays, and tuneable materials to name a few, all rely on the ability to control electromagnetic wave propagation and radiation. (Yiannis C, August 2014). The ability to realize and optimize features in the most efficient space i.e. within limited real-estate is necessary for both cost considerations and achieving a practical physically realizable solution.

Meta-materials are defined as effective medium material designed by incorporating microscopic elements into scaled up designs to create materials with fundamentally new properties that are not naturally occurring in nature. Unfortunately the term meta-material used is often loosely applied to FSS, EBG and AMC structures as well. AMCs that are effective medium where the unit cell size is much less than the wavelength are considered meta-

materials. However we distinguish meta-materials from the well-known methods to manipulate the electro-magnetic wave like FSS where the principles have been known and introduced by Munk and expanded by others for many years. In an FSS the electrical distance between the layers of element is of the order of half a wavelength so that the wave interference between the layers is a significant part of the design. FSS is not considered an effective medium, a novel meta-material or introducing new principles of material behavior.

12.2 EBG Materials

Once distances between layers are close to ¼ to ½ wavelength we are talking about an EBG material which have been known for a long time to work from1D to 3D. It is not a surprise that such a material could be designed to have pass bands that sidestep loss.

EBG materials also known as PCs (photonic crystals) or PBGs (photonic band gap materials) are a class of materials that can manipulate the propagation of EM waves. Analogous to electron waves propagating in the periodic potential of a crystal lattice separated into different energy bands separated by band gaps we see the same behavior of electromagnetic waves travelling in a medium where the dielectric properties vary in a consistent pattern in space. (Soukoulis, 2006)

The electromagnetic band-gap materials also known as photonic crystals are materials that have a band gap due to the periodicity of the material particularly the alternating dielectric properties of the material as Bragg mirrors.

12.3 Frequency Selective Rasorbers

It is important to point out at his juncture that there are a category of materials called frequency selective rasorbers (FSR) that can be designed to produce a band pass that typically have high reflection at the upper, lower or adjacent frequencies using the same principles described above.

A theoretical paper published by Bo Li and Zhongxiang Shen called the 3D Frequency Selective Rasorbers: Concept, Theory and Design (Bo Li, February 2015)**,** describes FSRs as an application of frequency selective surfaces where there is transmission at the band pass frequency but also reduced reflection i.e. significant absorption at other frequencies. The mechanism of this reduction of reflection is shown as a general equivalent circuit model based on multi-mode resonators. It is a 3D FSR with a periodic array of multi-mode cavities with alternating layers of lossy and lossless resonators. This design provides a band pass filtering response and absorption above and/or below the band pass frequency.

Also Shang et al and the authors of the above paper published a FSR Based on Square-Loop and Cross Dipole Arrays where they went further to illustrate band pass designs that reduce (Yuping Shang, November 2014) reflections around the band pass frequency and fabricated an article.

Because the FSS band pass can have lot of reflection at the adjacent frequencies to the band pass, the authors developed a FSR structure that reduced the reflection around the band pass. The structural design was a lossy layer on top of a low dielectric layer with a dielectric

gap which resided above a slot type lossless FSS. The lossy layers absorbed the non-band pass frequencies just like a Salisbury screen and at the band pass resonance, there was through transmission. In order to reduce transmission loss in the lossy layer it was placed above the slot type lossless layer with an air gap (or low dielectric material) in-between. The pass band frequency of the lossless and lossy FSS layers were made the same to achieve good transmission or low insertion loss. Their design and circuit model is shown below where the dielectric spacer between the loss and lossless layer is h1= ¼ wavelength at the transmission frequency, f1, the lossy layer Z_{F1} and Z_{F2} is the lossless layer and Z_0 and Z_1 are the characteristic impedances of free space and the dielectric respectively.

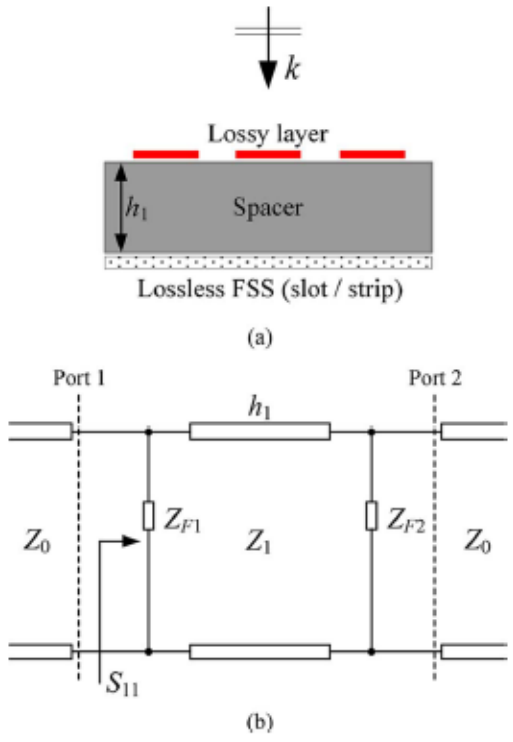

Fig. 1. (a) Side-view of reported rasorber designs with one lossy layer and (b) its equivalent circuit.

Figure 12-1. FSR Structure and Circuit Model by Shang et al.

The circuit model was designed and calculated based on absorptions at frequencies f1 and f3 and transmission at f2. The impedances were calculated by constraints on the transmission and reflection coefficients and the individual LRC components shown in Figure 2 were determined.

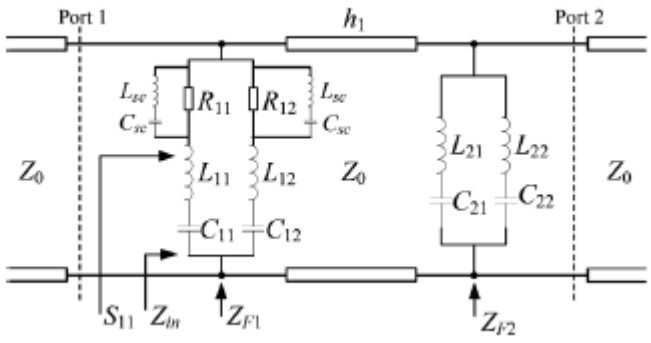

Figure 12-2 Equivalent Circuit Model of the Proposed Absorber by Shang et al.

The short circuit L and C component values were chosen such that the LC resonated at the band pass frequency f2 and the other components were calculated based on the dielectric spacer height defined as the ¼ wavelength at f2 while other constraints on the absorption bands were imposed on the adjacent frequencies to the band pass. It was determined that $Z_0 = Z_1$, so the dielectric layer was air. The results are shown in Figure 3 where f2 shows the band pass transmission and there is high absorption at f1 and f3.

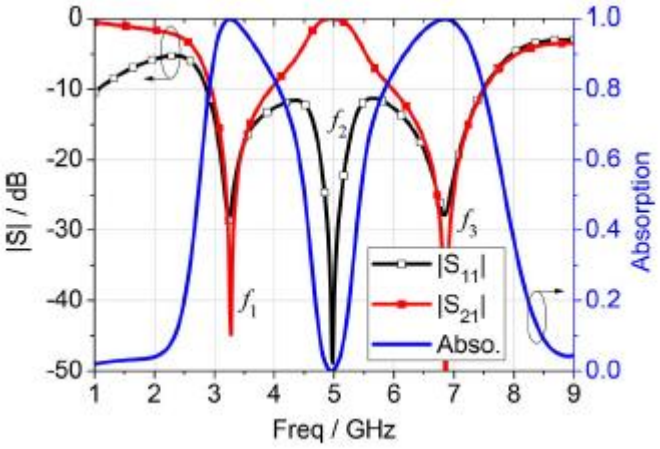

Fig. 4. Reflection, transmission and absorption of the rasorber calculated from the equivalent circuit model.

Figure 12-3. FSR Results from Shang et al.

At first glance it appears to be very similar to the narrow band transmission window we created in our meta-material at 3.2 GHz and where it is lossy in the surrounding frequency band. The mathematics as expected for an LC resonator would be similar to our calculations. But there is a fundamental physical difference how they are obtaining a narrow transmission band by creating conditions for band pass filters primarily by cancelling reflections via the interaction of layers judicially placed ¼ wavelength apart. This is evident by the fact that if their substrates are not placed ¼ wavelength of the band pass frequency – the FSR will not work. In fact the "window" will move as a function of angle of incidence due to the change in path length.

This is because their material structure is an FSS where as our construction is a bulk meta-material.

The Air force definition of a meta-material is when the unit cell is much smaller than the wave length. An FSS or an EBG is not a meta-material. Many of the same FSS materials developed by Munk and others years ago now have been re-branded as a meta-material as if it is something new. FSS is and old concept which is not an effective medium material and therefore not a meta-material.

For a meta-material the periodic unit cell in principle must be much smaller than the wave-length. For our narrow band window we can chose to construct the unit cell to be very tiny or large depending on our manufacturing and testing constraints; as long as it still is an effective medium. But nothing in the design is dependent on the layer separation distance to allow it to perform as a meta-material. So when we can reduce our design to an effective medium which follows the rules of an effective medium like the Laplace capacitive model; or the Cohn square model where there is no interaction between the layers; if we measure its intrinsic unit cell properties in isolation (HFSS: PEC and PMC boundary conditions) they apply to the entire volume. Properties do not depend on the interference, separation distance, and interaction of the layers which is essential to the design of an FSS.

We are making a meta-material whereas the FSR developers are fabricating electromag-netic band gap structures.

The key difference between their band-pass FSR and our narrow band window meta-ma-terial is that they are totally relying on the separation ¼ wave physical separation distance between their layers for their design to work. ***Just like photonic band gaps in a lattice***

structure where the physical periodicity of the lattice constant a, determines the band gap, this is also the case for these FSRs where the physical separation distance determine the band pass.

The essential difference between the meta-material and the FSR becomes clearer when we take it to the limit. Theoretically if we can make our design as small as possible (barring current manufacturing limitations) and we could obtain the window at the same frequency as before.

However in the FSR design they cannot shrink their design to be arbitrarily small. In fact it is ***physically impossible*** for them because they need the ¼ wavelength separation.

12.4 Limitations and Consequences of FSRs

This becomes particularly challenging if we want to create a band pass at low frequencies where the wavelength is large.

For instance if we chose to make a band pass at 300 MHz or 0.30 GHz and we are limited to a real estate of 3 inches it becomes very challenging in fact impossible to use the EBG material to make this material. For a pass band at 0.3 GHz we are talking about a wavelength of 1 meter. This means the dielectric spacer needs to be ¼ wave apart; which means a single dielectric layer alone needs to be 25 centimeters which is almost 10 inches. The FSR cannot achieve this within three inches.

12.5 Narrow Band Meta-Material

For our meta-material if we keep the unit cell size at least 1/10 of the wavelength to be an effective medium; it would mean a unit cell dimension could be a maximum of 10 centimeters. But in reality we could maintain the unit cell to be 1 cm at 1/100 the wavelength as chosen in our design. It would still very much be an effective medium. We would change the zero circuit LC parameters by increasing L or C or both to reduce the resonant frequency of the zero circuit to 300 MHz; remembering from our analysis that it is necessary for L>>C for the zero circuit to function. In our current design the layer separation is 6.6 mm with seven layers which equates to a distance of 4.6 centimeters or 1.8 inches. If we choose our unit cell to be larger, 1 cm cubed; we could still create this band-pass in 7 centimeters or 2.75 inches which is less than the 3 inches required. Our meta-material does not rely on the ¼ wave spacing like an FSR.

This is the difference between these well-established EBG materials and our narrow band transmission meta-material.

This is the closest the latest research has gotten but as we illustrated it is not the same thing. It is rebranding FSS materials demonstrated in the 1940's that have a very limited realm of application that is a function of the wavelength. Our meta-material is an effective medium material independent of the wavelength, a truly new concept and as is the first time it has been fabricated into a real material.

CHAPTER 13

FUTURE WORK

The first logical next step would be to fabricate the six other sheets and construct the complete configuration with separators, and matching layers if we obtain funding.

Another step would be to create a window at a different frequency and demonstrate this methodology for its ability to tune the window to a desired frequency of application.

Even more practical would be to explore different applications, for instance a radome and create a narrow band transparency for the frequencies that the antenna within the radome would potentially operate.

Also we could use this concept to make 3D oriented I-beams that would not depend on the angle of incidence like a FSS absorber; but a true 3D meta material.

Finally we could further explore other cheaper manufacturing alternatives like 3D printing to take the cost and labor out of this product. For instance remove the foams and create a 3D printed framed to hold I-beam samples in place.

Utilize this meta-meta-material design methodology and approach to construct novel applications we have not discussed here. We can use the circuit model not only to design materials; but also use circuits to make materials and materials to make circuits.

REFERENCES

1 Biology, Shmoop. n.d. *Special Properties of Water*. Accessed July 23, 2015. http://www.shmoop.com/biomolecules/properties-water.html.

2 Bo Li, Zhongxiang Shen. February 2015. "3D Frequency Selective Rasorber: Concept Theory and Design." *IEEE* 978-1-4799-8767.

3 Brillouin, Leon. 1953. *Wave Propagation in Periodic Structures* . New York: Dover Publications Inc.

4 Chryssoula A. Kyriazidou, Member, IEEE,, Rodolfo E. Diaz, and Nicólaos G. Alexópoulos, Fellow, IEEE. JANUARY 2000. "Novel Material with Narrow-Band Transparency." *IEEE TRANSACTIONS ON ANTENNAS AND PROPAGATION, VOL. 48, NO. 1,* 107-116.

5 Cohn, S. B. 1948. "Analysis of the Metal-Strip Delay Structure for Microwave Lenses." *Journal of Applied Physics* 258 - 262.

6 Corinne Yee (UCD), Desiree Rozzi (UCD). 2015. *Unusual Properties of Water*. Accessed July 23rd, 2015. http://chemwiki.ucdavis.edu/Physica_Chemistry?Physical_Properties_of_Matter/Bulk_Properties.

7 Diaz, Rudolfo E. 2002. Frequency Selective Microwave Devices Using Narrowband Metal Materials. USA/Arizona Patent 6473048 B1. October 29. Accessed August 3, 2015.

8 Diaz, Rudolfo E. 1992. *The Analytic Continuation Method for the analysis and Design of dispersive Materials*. Dissertation, University of California, Los Angelos, UMI.

9 Edward J. Rothwell1, *, Jonathan L. Frasch1, Sean M. Ellison1,. 2016. "Analysis of the Nicolson-Ross-Weir Method for Characterizing." *Progress In Electromagnetics Research, Vol. 157, 31–47,* 31-46.

10 Fannin, P C, A Mlina, and SW Charles. 1993. "On the generation of complex susceptibility data through the use of the Hilbert transform." *Journal of Physics D: Applied Physics* (Journal of Physics) 26 (Number 11): 2.

11 Griffith, David J. 2007. *Physics Pages: Frequency Dependence of Electric Permittovity*. Accessed August 21, 2015.

http:/physicspages.com/2014/09/20/frequency-dependence-of-electric-permittivity/.

12 Hasted, J. B. 1973. *Aqueous Dielectrics* . London : Chapman & Hall.

13 Hippel, Arthur von. 1995. *Dielectrics and Waves*. Boston London : Artech House.

14 Hummel, Rolf E. 2011. *Electronic Properties of Materials*. 4. New York, New York: Springer. Accessed August 21, 2015.

15 Hyperphysics. n.d. *Physical Properties of Water*. Accessed August 2, 2015. http://hyperphysics.phy-astr.gsu.edu/hbase/chemical/watercon.html#c1.

16 —. n.d. *Quantum Properties of Light*. Accessed September 9, 2015. http://hyperphysics.phy-astr.gsu.edu/hbase/optmod/qualig.html.

17 Jackson, David R. 2013. "ECE 6340 Intermediate EM Waves." *http://www0.egr.uh.edu/courses/ece*. Fall. Accessed August 25, 2015. http://www0.egr.uh.edu/courses/ece/ece6340/sectionjackson/Class%20Notes/notes%204%206340%20Models%20of%20Permittivity.pptx.

18 Johnson, D. W. 1975. "A Fourier Series Method for Numerical Kramers-Kronig Analysis." *J. Physics A: Math Gen* 8 (4): 8 490.

19 Kao, Kwan Chi. 2004. *Dielectric Phenomena in Solids*. San Diego , California: Elsevier Academic Press. Accessed August 21, 2015.

20 ocw.mit.edu/courses. n.d. *ocw.mit.edu/courses/mechanical.../2-58j.../chap6_solid_prop.pdf*. ocw.mit.edu/courses/mechanical.../2-58j.../chap6_solid_prop.pdf.

21 OpenCourseWare, MIT. 2011. "ocw.mit.edu/courses/mechanical.../2-58j.../chap6_solid_prop.pdfCachedSimilar." Spring. Accessed August 2015. http://ocw.mit.edu.

22 n.d. *Permittivity*. Accessed August 23, 2015. http://en.wikipedia.org/wiki/Permittivity.

23 Physics, Hyper. n.d. *Transparancy of Water in the Visible Range*. Accessed November 2013. http://hyperphysics.phy-astr.gsu.edu/hbase/chemical/watabs.html.

24 Puthoff, R. H Pantell & H. E. 1969. *Fundamentals of Quantum Electronics*. New York London Sydney Toronto : Wiley.

25 Shiles, Sasaky, Inokuti & Smith. 1980. "Self Consistency and sum-rule tests in the Kramer-Kronig Analysis of Optical Data: Applications to aluminum. ." *Physical Review B*.

26 Shimoda, Koichi. 1984. *Introduction to Laser Physics*. Berlin Heidelberg New York Tokyo: Springer Verlag. Accessed September 9, 2015.

27 —. 1984. *Introductions to Lasers*. Berlin Heidelberg New York Tokyo: Springer Verlag. Accessed September 9th, 2015.

28 Soukoulis, Maria Kafesaki and Costas M. 2006. "Historical Perspectiv and Review of Fundamental Principles in Modeling Three Dimensional Periodic Structures with Emphasis on Volumetric EBGs." In *Metamaterials Physics and Engineering Explorations*, by Nader Engheta and Richard W. Ziolkowski, 215. Iscatayaw New Jersey: Wiley Interscience.

29 Toll, J. S. 1956. "Causality and the Dispersion Relation: Logical Foundations." *Physics Review vol 104* 1760-1770.

30 U, Bergman, Di Cicco A, Wernet P, Principi E, Glatzel P, and Nilsson A. 2007. "Nearest Neibor oxygen distances in liquid water and ice observed by x-ray Raman based extended x-ray absorption fine structure." *Journal Chem Phys* Abstract.

31 Wikipedia. 2015. *Kramers-Kronig Relations*. October 28th. Accessed December 27, 2015. wikipedia.org/wiki/Kramers-Kronig_relations.

32 Wikipedia. n.d. "Salisbury Screen."

33 —. n.d. *Simple Harmonic Motion* . Accessed August 25, 20015. http:/en.wikipedia.org/wiki/Simple_harmonic_motion.

34 Yiannis C, Vardaxoglou. August 2014. "Metamaterial Arrays and Applications: FSS, EBG & AMC Structures." *IEEE* 978-1-4799-2329.

35 Yuping Shang, Zhongxiang Shen, Senior Member, IEEE, and Shaoquiu Xiao, Member IEEE. November 2014. "Frequency-Selective Rasorber Based on Square-Loop and Cross-Dipole Arrays." *IEEE Transactions on Antennas and Propogation, VOL 62 No. 11* 5581-5589.

SHUBITIDZE AND OSTERBERG MATLAB PROGRAM

Shubitidze and Osterberg MATLAB Program

```
clear All

yy_n=load('Read_actual_data.dat');


%%%%%%%%%%%%%  Resonance # 3

i=1;

Dn(i)=6;

Nn(i)=5;



D(i, 1)=complex(    0.476809954333578E-08,   -0.173232046937905E-17);

D(i, 2)=complex(   -0.719099595872712E-06,    0.122081819893495E-15);

D(i, 3)=complex(    0.477692820332839E-04,   -0.137524195542974E-14);

D(i, 4)=complex(   -0.163009397116141E-02,   -0.475945490194174E-13);

D(i, 5)=complex(    0.296319139300348E-01,    0.107802192241306E-11);

D(i, 6)=complex(   -0.272411400873583E+00,   -0.621655670276182E-11);


N(i, 1)=complex(    0.182974540514735E-17,    0.436532247091081E-08);

N(i, 2)=complex(    0.492148609773319E-15,    0.807839120418427E-07);

N(i, 3)=complex(   -0.460976537790477E-13,   -0.960987981913376E-05);

N(i, 4)=complex(    0.108052354980312E-11,    0.152531943801301E-03);

N(i, 5)=complex(   -0.673990376677299E-11,    0.815016650912784E-05);


N(i, 1:5)=0.6*N(i, 1:5);
```

```
i=2;
Dn(i)=6;
Nn(i)=5;

D(i, 1)=complex(   0.241131336175290E-04,   -0.164268975137902E-14);
D(i, 2)=complex(   -0.836903227940087E-03,   0.970762542481097E-14);
D(i, 3)=complex(   0.122375268871338E-01,   0.259036024827046E-12);
D(i, 4)=complex(   -0.961697606072290E-01,   -0.327596108637332E-11);
D(i, 5)=complex(   0.426987493310241E+00,   0.135950654483177E-10);
D(i, 6)=complex(   -0.101266213409972E+01,   -0.193957599129896E-10);
N(i, 1)=complex(   0.141642275416902E-13,   0.117849098290432E-04);
N(i, 2)=complex(   -0.298662873436138E-12,   -0.256993512248829E-03);
N(i, 3)=complex(   0.235195240084723E-11,   0.209849712989052E-02);
N(i, 4)=complex(   -0.819755381538116E-11,   -0.760599149713317E-02);
N(i, 5)=complex(   0.106714990884535E-10,   0.103299148881628E-01);

N(i, 1:5)=0.8*N(i, 1:5);


i=3;
Dn(i)=6;
Nn(i)=5;

D(i, 1)=complex(   0.130017472062263E-02,   0.896125240401395E-14);
D(i, 2)=complex(   -0.236305125856654E-01,   -0.134586302375215E-12);
```

```
D(i, 3)=complex(   0.178892671097471E+00,   0.808218895777117E-12);
D(i, 4)=complex(  -0.722071179402915E+00,  -0.242590958103592E-11);
D(i, 5)=complex(   0.163896035202330E+01,   0.363953905923064E-11);
D(i, 6)=complex(  -0.198354687663382E+01,  -0.218343743306747E-11);
N(i, 1)=complex(   0.225776302560162E-13,   0.297597838715721E-05);
N(i, 2)=complex(  -0.280698824713530E-12,  -0.493018161633052E-04);
N(i, 3)=complex(   0.130530641713520E-11,   0.313377301298601E-03);
N(i, 4)=complex(  -0.269087427816112E-11,  -0.876523213775654E-03);
N(i, 5)=complex(   0.207502384573184E-11,   0.897778616453127E-03);



i=4;
Dn(i)=8;
Nn(i)=3;

D(i, 1)=complex(   0.155735966726143E-01,   0.212617232756609E-11);
D(i, 2)=complex(  -0.218232732023098E+00,  -0.238102244371992E-10);
D(i, 3)=complex(   0.132274747175931E+01,   0.112370398234050E-09);
D(i, 4)=complex(  -0.452882728330265E+01,  -0.289769844491498E-09);
D(i, 5)=complex(   0.957932878800585E+01,   0.440944443584403E-09);
D(i, 6)=complex(  -0.128181082133538E+02,  -0.395885288313788E-09);
D(i, 7)=complex(   0.105969227296838E+02,   0.194122288709777E-09);
D(i, 8)=complex(  -0.494924884090296E+01,  -0.400965673243015E-10);
```

```
N(i, 1)=complex(   0.276732348106894E-14,   0.365818723726163E-06);
N(i, 2)=complex(  -0.951405243058516E-14,  -0.137179627633014E-05);
N(i, 3)=complex(   0.821058224250961E-14,   0.138190735082626E-05);


i=5;
Dn(i)=8;
Nn(i)=3;

D(i, 1)=complex(   0.202460765781801E+02,   0.535186835448412E-08);
D(i, 2)=complex(  -0.114183858317919E+03,  -0.253929363072498E-07);
D(i, 3)=complex(   0.279606928228480E+03,   0.512629329092922E-07);
D(i, 4)=complex(  -0.388286960790323E+03,  -0.570939401885430E-07);
D(i, 5)=complex(   0.334462529770788E+03,   0.378919439430284E-07);
D(i, 6)=complex(  -0.183000258194299E+03,  -0.149856626963725E-07);
D(i, 7)=complex(   0.621145890179884E+02,   0.326985131023317E-08);
D(i, 8)=complex(  -0.119588738487024E+02,  -0.303664602717245E-09);
N(i, 1)=complex(   0.127343414569749E-11,   0.110150555057169E-03);
N(i, 2)=complex(  -0.190745404345165E-11,  -0.165691205763030E-03);
N(i, 3)=complex(   0.717626083163194E-12,   0.631681186214675E-04);


i=6;
Dn(i)=12;
Nn(i)=3;
```

```
D(i, 1)=complex(  -0.108878585945448E+07,   0.139529046502617E-03);
D(i, 2)=complex(   0.165401894507161E+04,  -0.254728044905815E-04);
D(i, 3)=complex(   0.491000361056760E+07,  -0.465818254481910E-03);
D(i, 4)=complex(  -0.852263407934120E+07,   0.749032697650696E-03);
D(i, 5)=complex(   0.746324485698593E+07,  -0.581882248965049E-03);
D(i, 6)=complex(  -0.411692810485142E+07,   0.276816322398357E-03);
D(i, 7)=complex(   0.154704195985514E+07,  -0.871105313272165E-04);
D(i, 8)=complex(  -0.408576204542642E+06,   0.185890724589496E-04);
D(i, 9)=complex(   0.762227429601001E+05,  -0.267041614636237E-05);
D(i,10)=complex(  -0.986994440748875E+04,   0.247758154739893E-06);
D(i,11)=complex(   0.846128929909977E+03,  -0.134187114889155E-07);
D(i,12)=complex(  -0.432614383723785E+02,   0.322173542013347E-09);
N(i, 1)=complex(  -0.466034743567454E-05,   0.470185088300228E+03);
N(i, 2)=complex(   0.285210102956482E-05,  -0.396482545039419E+03);
N(i, 3)=complex(  -0.372812008661821E-06,   0.578527956264391E+02);



i=7;
Dn(i)=12;
Nn(i)=3;

D(i, 1)=complex(   0.803005744541716E+09,   0.121377235016101E+00);
D(i, 2)=complex(  -0.656169794501136E+04,  -0.170705164288651E-02);
```

```
D(i, 3)=complex(    0.173526744337001E+07,    0.934001079097131E-01);
D(i, 4)=complex(   -0.403324409742438E+09,   -0.150835526011787E+00);
D(i, 5)=complex(    0.354957921050070E+09,    0.886570277056129E-01);
D(i, 6)=complex(   -0.147833304290869E+09,   -0.285232247781373E-01);
D(i, 7)=complex(    0.373113801747888E+08,    0.572571491380883E-02);
D(i, 8)=complex(   -0.620892733735174E+07,   -0.753102083919981E-03);
D(i, 9)=complex(    0.701129374961377E+06,    0.652800115013268E-04);
D(i,10)=complex(   -0.534654524138770E+05,   -0.360694458661981E-05);
D(i,11)=complex(    0.264614121429424E+04,    0.115479854079454E-06);
D(i,12)=complex(   -0.769490483116168E+02,   -0.163403257806549E-08);
N(i, 1)=complex(   -0.187536896786991E-04,    0.215376481837741E+03);
N(i, 2)=complex(    0.555747591734941E-05,   -0.101365402220132E+03);
N(i, 3)=complex(   -0.407824254637021E-06,    0.112457765722161E+02);



i=8;
Dn(i)=10;
Nn(i)=3;



D(i, 1)=complex(   -0.894578315069949E+16,   -0.204116377664408E+07);
D(i, 2)=complex(   -0.228039873886267E+11,   -0.345985653273340E+01);
D(i, 3)=complex(    0.211988152149394E+15,    0.139826580977095E+05);
D(i, 4)=complex(   -0.250464654847871E+14,   -0.737352998830355E+03);
```

```
D(i, 5)=complex(    0.140236215802872E+13,    0.212892609702946E+02);
D(i, 6)=complex(   -0.463557565191333E+11,   -0.390585363145073E+00);
D(i, 7)=complex(    0.966305113030240E+09,    0.456272265440882E-02);
D(i, 8)=complex(   -0.128646157525605E+08,   -0.329648621158009E-04);
D(i, 9)=complex(    0.106214487648793E+06,    0.134217358382534E-06);
D(i,10)=complex(   -0.495751414292685E+03,   -0.235610588323351E-09);
N(i, 1)=complex(    0.265717800281251E+07,   -0.104445524697657E+16);
N(i, 2)=complex(   -0.171144144134818E+06,    0.753419010249941E+14);
N(i, 3)=complex(    0.171419528179475E+04,   -0.265261899658379E+13);


%%%!!!!!!!!!!!!!!!!!1111111reallll

i=9;
Dn(i)=8;
Nn(i)=3;

D(i, 1)=complex(    0.149019866683351E-17,   -0.122271135472144E-27);
D(i, 2)=complex(   -0.124957795120504E-14,   -0.982136497307247E-25);
D(i, 3)=complex(    0.229172602244895E-11,   -0.800241262779948E-22);
D(i, 4)=complex(   -0.838253461819030E-09,    0.103351991558314E-19);
D(i, 5)=complex(    0.183290973858022E-06,   -0.121352834043285E-18);
D(i, 6)=complex(   -0.237343732278274E-04,    0.160710666703582E-17);
D(i, 7)=complex(    0.173476115067901E-02,   -0.300174170921429E-14);
D(i, 8)=complex(   -0.656704860904070E-01,    0.146060356989103E-12);
```

```
N(i, 1)=complex(   -0.235790443468372E-19,    0.109002749580609E-28);
N(i, 2)=complex(    0.696667500461018E-15,   -0.115779728104005E-24);
N(i, 3)=complex(   -0.313729673946882E-13,    0.921628159981826E-23);

 %%%!!!!!!!!!!!!!!!!1111111reallll

i=10;
Dn(i)=-8;
Nn(i)=-3;

D(i, 1)=complex(    0.178809247227920E-17,   -0.175284368007891E-27);
D(i, 2)=complex(   -0.267255639603626E-14,   -0.170286304219136E-24);
D(i, 3)=complex(    0.312869505635337E-11,   -0.105785044354370E-21);
D(i, 4)=complex(   -0.118495273918795E-08,    0.648534483140379E-20);
D(i, 5)=complex(    0.247960248087857E-06,    0.118249690754574E-17);
D(i, 6)=complex(   -0.297217070827536E-04,   -0.114446435744309E-15);
D(i, 7)=complex(    0.200503231992348E-02,    0.124279100112695E-14);
D(i, 8)=complex(   -0.704384451157339E-01,    0.804176399041238E-13);
N(i, 1)=complex(    0.231485323666048E-19,    0.162830578428740E-28);
N(i, 2)=complex(    0.463538768577934E-15,   -0.173860802216102E-24);
N(i, 3)=complex(   -0.226738613227731E-13,    0.998169043270983E-23);
```

```
 i=11;
Dn(i)=8;
Nn(i)=3;

D(i, 1)=complex(    0.204912166854986E-09,    0.740946483161539E-21);
D(i, 2)=complex(   -0.300723722967368E-07,    0.121225361345385E-18);
D(i, 3)=complex(    0.185939189671353E-05,   -0.167487214880736E-16);
D(i, 4)=complex(   -0.632461441341890E-04,    0.715518183086192E-15);
D(i, 5)=complex(    0.129760826259057E-02,   -0.149710415180957E-13);
D(i, 6)=complex(   -0.164872427141606E-01,    0.167085292100706E-12);
D(i, 7)=complex(    0.127071217403121E+00,   -0.949953869968032E-12);
D(i, 8)=complex(   -0.544988200106952E+00,    0.213641761478217E-11);
N(i, 1)=complex(   -0.276390114210373E-12,    0.618241519954187E-22);
N(i, 2)=complex(    0.148091770152658E-10,   -0.341791265290408E-20);
N(i, 3)=complex(   -0.182538556631705E-09,    0.471709115833368E-19);
```

```
 i=12;
Dn(i)=12;
Nn(i)=3;

D(i, 1)=complex(    0.299628414550434E+10,   -0.334110360137443E-01);
D(i, 2)=complex(    0.145690563402376E+07,   -0.148975086720719E-04);
D(i, 3)=complex(    0.710909694842852E+09,    0.220421605989130E-01);
D(i, 4)=complex(   -0.184063965144037E+10,   -0.144383852876144E-01);
D(i, 5)=complex(    0.121371874606673E+10,    0.472215851784406E-02);
D(i, 6)=complex(   -0.417870056901506E+09,   -0.959668372370581E-03);
D(i, 7)=complex(    0.895729407618336E+08,    0.130440605503809E-03);
D(i, 8)=complex(   -0.127965692123849E+08,   -0.121443867271552E-04);
D(i, 9)=complex(    0.124679945840470E+07,    0.768767506880346E-06);
D(i,10)=complex(   -0.822377579508378E+05,   -0.317564857190269E-07);
D(i,11)=complex(    0.352476589406243E+04,    0.774324213282137E-09);
D(i,12)=complex(   -0.888073935742613E+02,   -0.847262890687834E-11);
N(i, 1)=complex(    0.272214752606561E+05,    0.148991756260095E-05);
N(i, 2)=complex(   -0.862450002489323E+04,   -0.411780972780551E-06);
N(i, 3)=complex(    0.669203005970406E+03,    0.284544146142263E-07);


 i=13;
Dn(i)=12;
Nn(i)=5;
D(i, 1)=complex(    0.224199656690788E-06,   -0.122076571674529E-16);
```

```
D(i, 2)=complex(  -0.102964281021972E-04,   0.486228296276323E-15);
D(i, 3)=complex(   0.214080281848989E-03,  -0.867919275863108E-14);
D(i, 4)=complex(  -0.266445928043494E-02,   0.916004042487220E-13);
D(i, 5)=complex(   0.221095210138599E-01,  -0.634742608372072E-12);
D(i, 6)=complex(  -0.128872922172256E+00,   0.303073109904809E-11);
D(i, 7)=complex(   0.541142844180795E+00,  -0.101711590989598E-10);
D(i, 8)=complex(  -0.164966299011010E+01,   0.239878141188707E-10);
D(i, 9)=complex(   0.362435984839570E+01,  -0.389597603979899E-10);
D(i,10)=complex(  -0.559809399336247E+01,   0.415031002544452E-10);
D(i,11)=complex(   0.577171759884929E+01,  -0.261020665612764E-10);
D(i,12)=complex(  -0.356747456162304E+01,   0.734320582787060E-11);
N(i, 1)=complex(   0.153533665065256E-10,  -0.104634484118712E-19);
N(i, 2)=complex(  -0.264256220921621E-09,   0.190269669907308E-18);
N(i, 3)=complex(   0.164389800782089E-08,  -0.123901837111523E-17);
N(i, 4)=complex(  -0.435961876036075E-08,   0.340326127817120E-17);
N(i, 5)=complex(   0.417910289059908E-08,  -0.334814804589455E-17);


  i=14;
Dn(i)=12;
Nn(i)=2;

D(i, 1)=complex(   0.341093568369667E+04,  -0.510460492874808E-03);
D(i, 2)=complex(  -0.239828324873696E+05,   0.114166183344234E-02);
D(i, 3)=complex(   0.760675085649523E+05,  -0.202039291374953E-02);
```

```
D(i, 4)=complex(  -0.140672773341506E+06,   0.260118786129950E-02);
D(i, 5)=complex(   0.170839532080944E+06,  -0.225261076196367E-02);
D(i, 6)=complex(  -0.143551845627351E+06,   0.138730917218846E-02);
D(i, 7)=complex(   0.856203252973933E+05,  -0.625423008479579E-03);
D(i, 8)=complex(  -0.365563664270621E+05,   0.206975294778838E-03);
D(i, 9)=complex(   0.111014926075174E+05,  -0.490972809165942E-04);
D(i,10)=complex(  -0.234146538646201E+04,   0.788549298186779E-05);
D(i,11)=complex(   0.325993884152267E+03,  -0.764282384936678E-06);
D(i,12)=complex(  -0.269347765388244E+02,   0.335667647269352E-07);
N(i, 1)=complex(  -0.173516177369559E+02,  -0.980122702424710E-04);
N(i, 2)=complex(   0.927970308968244E+02,   0.614408926035496E-04);
```

```
   i=15;
Dn(i)=12;
Nn(i)=4;

D(i, 1)=complex(   0.238335596359778E+07,  -0.133154831632230E+00);
D(i, 2)=complex(   0.391449227591339E+04,   0.214205025642204E-03);
D(i, 3)=complex(   0.837374868764651E+06,   0.324001933626814E-01);
D(i, 4)=complex(  -0.661443215505139E+07,   0.144912904620094E+00);
```

```
D(i, 5)=complex(    0.851291556047272E+07,   -0.207927740986336E+00);
D(i, 6)=complex(   -0.550435667011906E+07,    0.126616847570447E+00);
D(i, 7)=complex(    0.219368084346928E+07,   -0.448098242819989E-01);
D(i, 8)=complex(   -0.580873356841553E+06,    0.100828044082053E-01);
D(i, 9)=complex(    0.104841358043345E+06,   -0.147214587241373E-02);
D(i,10)=complex(   -0.128172737596404E+05,    0.135781993842008E-03);
D(i,11)=complex(    0.101934594834842E+04,   -0.721584496852315E-05);
D(i,12)=complex(   -0.477210963496044E+02,    0.168848958419613E-06);
N(i, 1)=complex(    0.198345596413140E+04,    0.510830645059674E-03);
N(i, 2)=complex(   -0.105991917521582E+04,   -0.268357297744296E-03);
N(i, 3)=complex(    0.188830571272145E+03,    0.469692453990141E-04);
N(i, 4)=complex(   -0.112155666428697E+02,   -0.273885087933284E-05);




Kw=1261;
omega_min=log(1e+7);
dw=(log(1e+16)-omega_min)/(Kw-1);


for  k=1 :Kw
%        omega=exp((omega_min+dw*(k-1)))/1e14;
omega=yy_n(k,1)/3e14; %exp(omega);


 Part=complex(0.0);
```

```
for i=1:15

Eps_test_d=complex(omega^Dn(i));
    for id=0:Dn(i)-1
Eps_test_d=Eps_test_d+D(i,id+1)*(omega^id);
    end

Eps_test_N=complex(0.0);
    for in=0:Nn(i)-1
Eps_test_N=Eps_test_N+N(i,in+1)*(omega^in);
    end
Part=Part+Eps_test_N/Eps_test_d;
end

Freq(k)=omega;
N_omega(k)=Part;

end



%% Bose_Ein. Distribution

H=6.62*1e-34; % Plank
K=1.38e-23;   % Boltzman
A_u=0.37122e-9; %%%
```

```
B_u=0.3628e-9; %%%
T=273+20;      %% Tem in Kelvin
Me=9.31e-31;   % El mass
Freq_n=Freq*1e+14;  %%% Freq

r=sqrt(H/Me)./sqrt(Freq_n(:)*pi*pi*2); %% Rad as a fubctioin of Freq

for i=1:length(r)
    rt6=(A_u/(r(i)))^6;
   rt12=(B_u/(r(i)))^12;
r06(i)=rt6;
r12(i)=rt12;
end
Alpha=1;
Epot=-Alpha*(r12-r06);
Ekin=H*(Freq_n(:))/(1.5*K*T);
E=2./(exp(Ekin+Epot')+1);
% end Bose_Einst
%% Lorentz and Debye models

Wl=3.0e+15;          %% Lorentz
sigma=2*3*1.198e+15; %%% Damping
EP_s=2.5;            %%% Lorentz
Ep_inf=1.0;          %% Lorentz
```

```
 xo=7.4;tau1=0.25*1e-10; tau2=3*0.1e-9; %% Debye parameters


for i=1:length(r)


ow=Freq_n(i);

ow2=Freq_n(i)*Freq_n(i);


cm=complex(0,1);

Debye(i)=xo*(1-1/log(tau2/tau1)*log((cm*ow*tau2+1)./(cm*ow*tau1+1)))*sqrt(E(i));

Lorentz(i)=(Debye(i))+sqrt(Ep_inf-Wl*Wl*(EP_s-Ep_inf)/(ow2*9-2*com-
plex(0,1)*sigma*ow-Wl*Wl)*E(i));


Data_new_real(i)=(1+real(N_omega(i)))*real(Lorentz(i));

Data_new_imag(i)=(imag(N_omega(i)))*imag(-Lorentz(i));

Z_mat(i)=complex(Data_new_real(i),Data_new_imag(i));

end



figure(3)

d_imag=loglog(Freq_n,real(Data_new_imag),'r',yy_n(:,1)/3,yy_n(:,3)); zoom on;

set(d_imag,'LineWidth',4)

title ('Imaginary part of n(w)');

   xlabel('Frequency [Hz]');

   ylabel('Imag n(w)');
```

```
    legend('Predicted', 'Data','Error');
figure(4)
dd_r=loglog(Freq_n,real(Data_new_real),'r',yy_n(:,1)/3,yy_n(:,2)); zoom on;
set(dd_r,'LineWidth',4)
title ('Real part of n(w)');
    xlabel('Frequency [Hz]');
    ylabel('Real n(w)');
 legend('Predicted', 'Data','Error');
```

APPENDIX B

HILBERT FROM REAL TO IMAGINARY MATHCAD PROGRAM

Hilbert from Real to Imaginary MathCAD Program

$i := 0..1000$

$w_i := \frac{i}{1000} \cdot 10 \cdot 10^9 + 10^6$

$w1 := 0.8 \cdot 10^9$

$w2 := 1 \cdot 10^9$

$w3 := 2 \cdot 10^9$

$mp_i := 1 + Deb_i + Lor_i$

$Deb_i := \frac{60}{1 + i \cdot \frac{w_i}{w1}}$

$Lor_i := \frac{10}{1 + i \cdot \frac{w_i}{w3} \cdot \frac{1}{3} - \left(\frac{w_i}{w3}\right)^2}$

$RD_i := Re(mp_i) - 1$

$YD_i := Im(mp_i)$

$RD_i := Re(efake_i) - 1$

$YD_i := Im(efake_i)$

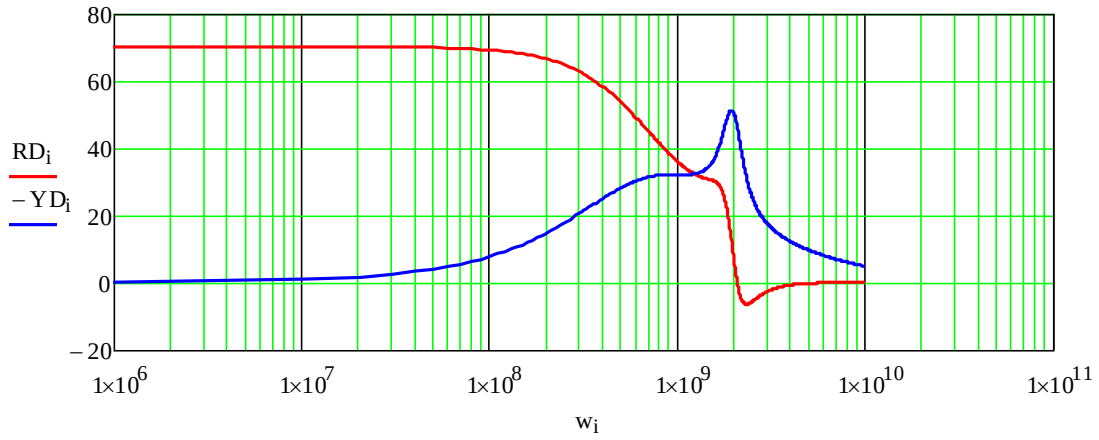

Here RD and YD are renamed to use the fake definition of Shubitidze and Osterberg

First we define the indices of Debye and Lorentz

The fake way

$roL_i := \sqrt{Lor_i}$

$roD_i := \sqrt{Deb_i}$

$reFk_i := Re((roD_i)) \cdot Re((roL_i))$

$imFk_i := Im((roD_i)) \cdot Im((roL_i))$

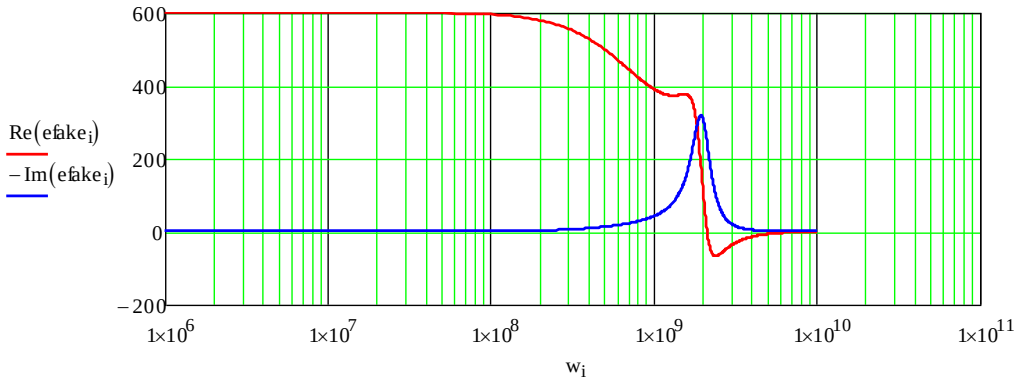

This function is supposed to exist at negative frequencies too...
To use the complex FFT I will create cyclic data from the "measured data"
For instance let's use the imaginary part

$N := 2^{12}$

$2^{12} = 4.096 \times 10^3$

$j := 0..N-1$

Fill the array with zeros first

$om_j := 0$

$Q_j := 0$

$Q_0 := RD_0$

$jj := 1..1000$

$Q_{jj} := RD_{jj}$

$Q_{N-jj} := RD_{jj}$

$om_{jj} := w_{jj}$

$om_{N-jj} := -w_{jj}$

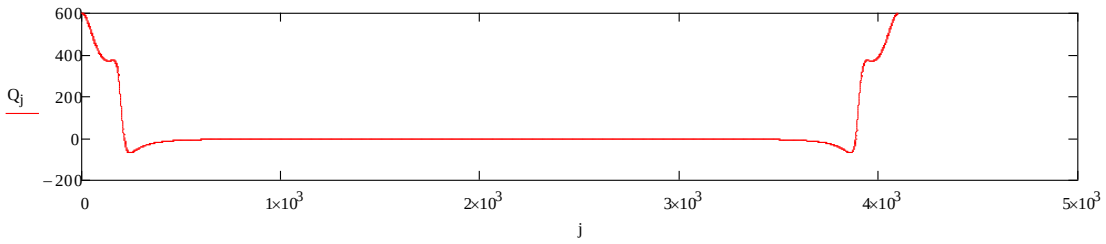

$Tra := ICFFT(Q)$

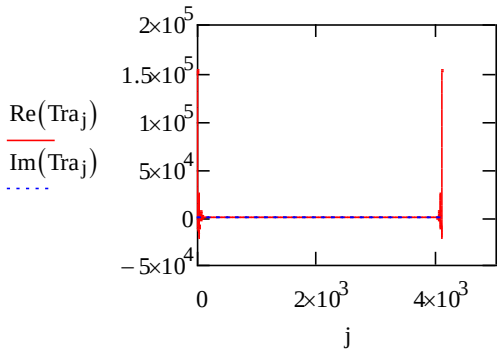

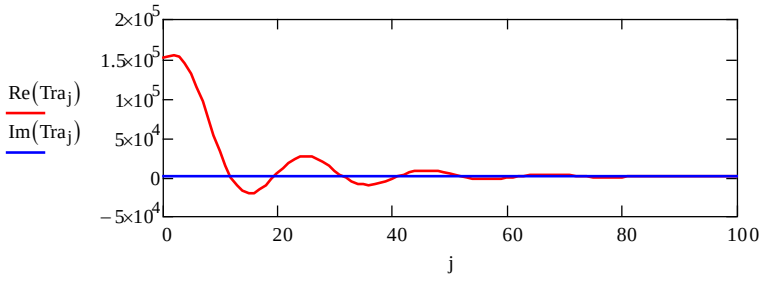

Now multiplying by signum simply means flipping the sign of the last half

$STra_0 := 0$

Diditwork:= CFFT(STra)

$jk := 1 .. \frac{N}{2}$

$STra_{jk} := Re(Tra_{jk})$

$jk := \frac{N}{2} + 1 .. N - 1$

$STra_{jk} := -Re(Tra_{jk})$

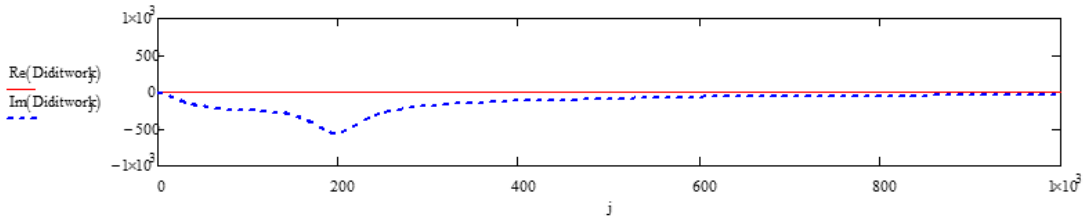

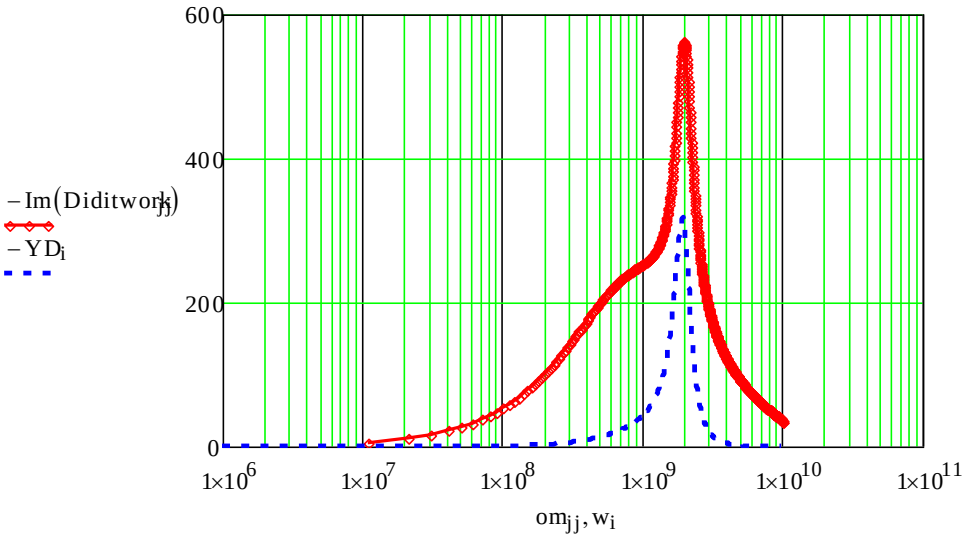

Of course it doesn't work

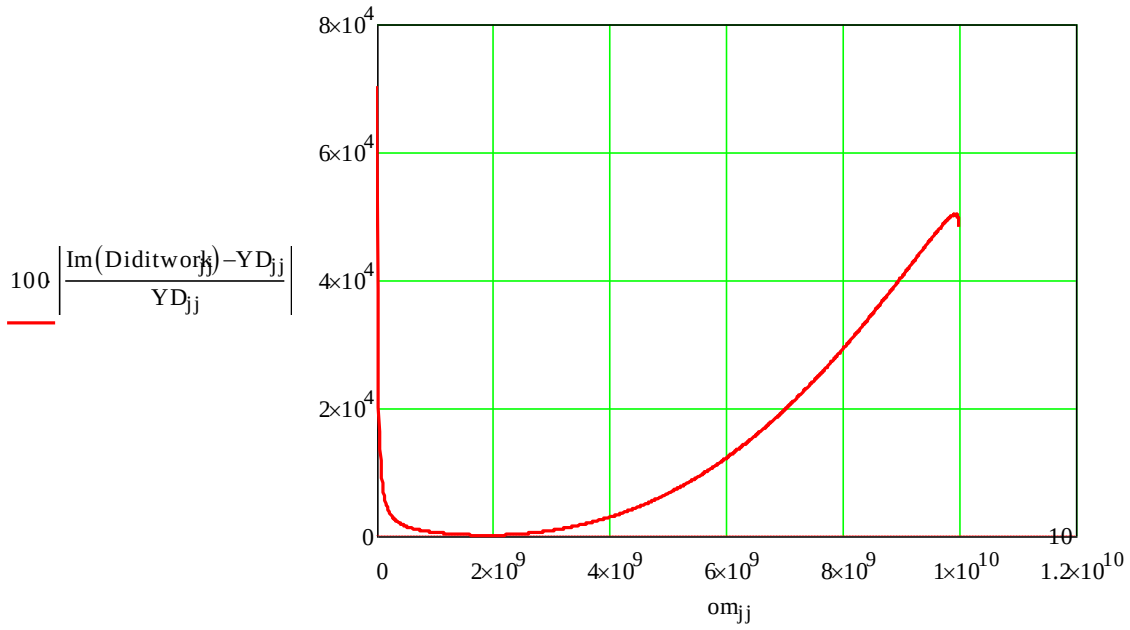

$roD_i := \sqrt{Deb_i}$

$roL_i := \sqrt{Lor_i}$

The only thing that makes sense is to take square root before multiplying

$reFk_i := Re\left[\sqrt{(roD_i)}\right]\cdot Re\left[\sqrt{(roL_i)}\right]$

$imFk_i := Im\left[\sqrt{(roD_i)}\right]\cdot Im\left[\sqrt{(roL_i)}\right]$

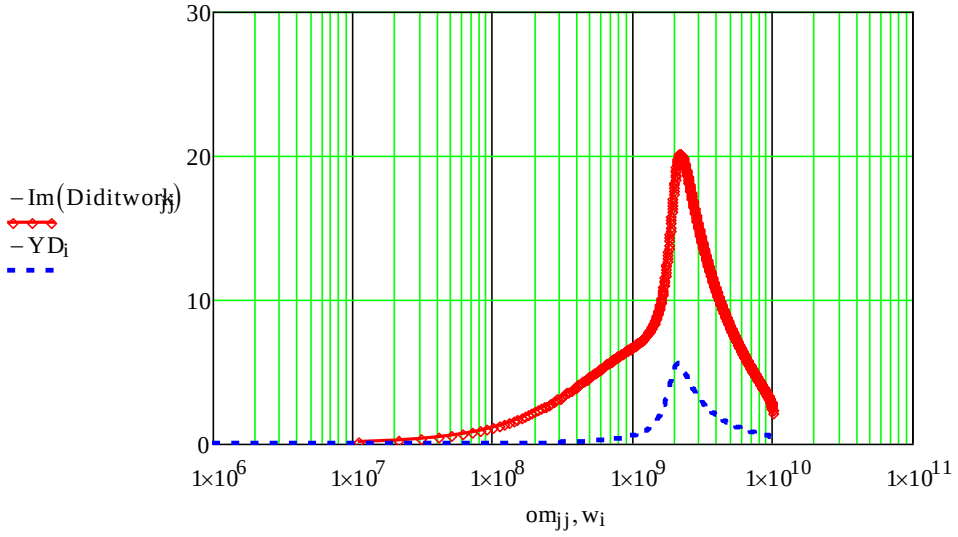

This doesn't work also

$$100 \left| \frac{\mathrm{Im}(\mathrm{Diditworks}_{jj}) - \mathrm{YD}_{jj}}{\mathrm{YD}_{jj}} \right|$$

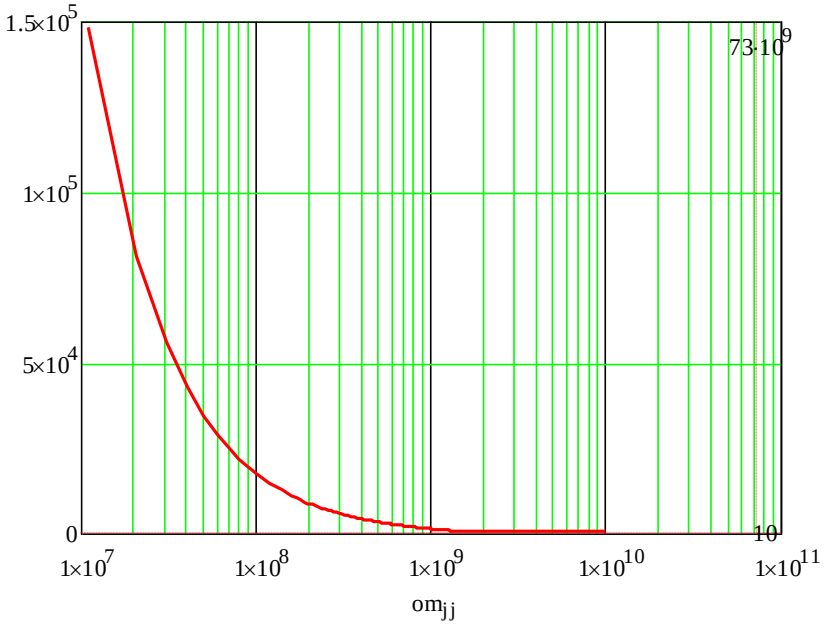

BIOGRAPHICAL SKETCH

Education
PhD in Material Science & Engineering at ASU, Tempe, AZ, 2017
Executive MBA at W.P. Carey ASU, Tempe, AZ 2007
M. S. Material Science & Engineering, minor EE, at ASU, Tempe, AZ, 1999
B. S. Chemical Engineering, minor in Pre-Med, Chemistry, Creative Psychology, Middle Eastern Studies, and Bengali at University of Wisconsin, Madison, WI, 1984
West High School Madison,Wisconsin
Holy Cross High School Dhaka, Bangladesh
Hopewll High School Ottowa, Canada
Born in Dhaka, Bangladesh
Experience
Technical Fellow, Program Manager BR&T, BDS, BCA Boeing Mesa AZ, 1996- Present
Engineering Specialist, Northrup Grumman, Chandler, AZ, 1994-1996
Product Development Engineer, Hexcel Advanced Products, Chandler, AZ, 1992-1994
Sr. Materials & Processing Engineer General Dynamics, San Diego, CA, 1990-1992
Technology Specialist ICI Wilton Material Research Centre, U.K., 1988-1990
Research & Development Engineer, ICI Fiberite, Tempe, AZ, Winona MN, 1984-1988
Research Engineer, Tectonics Research Inc. Minneapolis, MN, 1983-1984
Patents
2016 Brake Health Indicators Using Input and Output Indicators *(pending)*
2016 Acoustically Tunable Foam Core: C-Foam
2016 Thermodynamic Efficiency as a Maintenance Predictor Parts A and B *(pending)*
2014 Fused Porogen Process for Acoustic Core Septa Fabrication *(pending)*
2004 Screen Printed Film Carrier & Electrically Modulated Devise Using Same
2002 High Performance Matched Absorber Using Magneto-Dielectrics
2002 Process of Making Synthetic Magneto-Dielectric with Controlled Off-Normal TE & TM Response
2001 R-Foam & Method of Manufacturing
2000 Continuous Honeycomb Lay-Up
2000 High-Performance Matched Absorber Using Magneto-Dielectrics
2000 Synthetic Magneto-Dielectric with Controlled Off-Normal TE & TM response
1999 Method of Making & Bonding a Screen Printed Ink Film Carrier to an Electric Device
Publications
2016 BTEC Conference Bellevue, WA: A Hybrid Prognostic Approach: 777 FCV & ECV
2014 BTEC Conference St. Louis, MO: "Right Data at the Right Time"
2013 BTEC Conference Seattle, WA: Condition Based Maintenance (CBM) Capability
2000 SAMPE publication: "Why a Cyanate Ester Part Blistered?"
1989 SAMPE publication: "Printing on Unidirectional Tape"